UNIVERSITY OF CALIFORNIA,
IRVINE

Elucidating the Role of Beta-Hairpins in Amyloid-Beta Oligomerization and Toxicity

DISSERTATION

submitted in partial satisfaction of the requirements
for the degree of

DOCTOR OF PHILOSOPHY

in Chemistry

by

Sarah Megan Ruttenberg

Dissertation Committee:
Distinguished Professor James Nowick, Chair
Professor David Van Vranken
Assistant Professor Elizabeth Bess

2024

DEDICATION

To

my mom and dad, my grandparents, and everyone who has supported me through the making of this dissertation.

"There is a theory which states that if ever anyone discovers exactly what the universe is for and why it is here, it will instantly disappear and be replaced by something even more bizarre and inexplicable. There is another theory which states that this has already happened."

—Douglas Adams, *Hitchhikers' Guide to the Galaxy*

TABLE OF CONTENTS

LIST OF FIGURES

LIST OF TABLES

ACKNOWLEDGEMENTS

I would like to thank my advisor, Professor James Nowick for his mentorship over the past five years. You have always supported my many endeavors and you gave me the tools I needed to develop as a scientist and writer. I want to thank Drs. Adam Kreutzer, Chelsea Parrocha, Gretchen Guaglianone, and Xingyue Li for all their mentorship and guidance throughout my research projects. I want to thank all my lab mates over the past five years for their friendship and support. All of you helped me grow as a scientist and as a person, thank you.

I want to thank my managers at AbbVie, Executive Director Joshua Rowe and Dr. Alireza Abdolvahabi, for giving me a refreshing break from grad school and for being such kind and encouraging mentors. Thank you both for giving me the chance to learn more about ocular proteomics, bioanalysis, and the pharmaceutical industry.

I want to thank Ben Katz and Felix Grunn at the mass spectrometry facility for their help and support in my experiments and in getting our laboratory's LC-MS system up and running. I also want to thank Ben for always being a friendly and enthusiastic face every time I saw him.

I want to thank the Sue and Bill Gross stem cell research center, especially Christina Tu, Professor Matthew Blurton-Jones, Zahara Keulen, and Pooja Sakthivel for their help in learning how to culture and differentiate iPSCs which has been invaluable to my Ph.D. research.

For my friends, I cannot express how much you all have helped get me through these dark years. Annie, Bianca, Chelsea, Nadia, Naomi, Rochelle, Shannon, Sophie, Wyatt thank you for giving me a place in California where I could be myself and feel safe and appreciated. Thank you, Alex, Ashley, Erika, Mario, Rob, and Stefanie for being wonderful friends and for always making the time to see me when we're in the same city. Thank you, Annette (and Cole), Emily, Haley, Lorena, Nick, Tiffany, Tina (and Karif and Gwen); even though you all were dozens to thousands of miles away, you made sure I didn't feel alone, and I will never ever forget that. My friends, who are really the family I chose, I love you so very much, thank you for loving me back <3

Thank you to my cousins, Micaela and Sarah for taking on the weight of being my only family in California. I love you both so much and am so grateful I got to come out here and spend time with you both.

Thank you, Kevin and Noah, for making some of the hardest times of my life more bearable. I will always be grateful that I met you.

For my family, I left you all behind to pursue my dreams and you all supported me every step of the way. Three-thousand miles is nothing when you have the kind of love my family gives. Thank you to my grandfather, Alan Borenstein, for inspiring my passion in neuroscience and for always being proud of me. Thank you to my grandmothers, Judi and

Carol who have been the best grandmothers my whole life and who I am so glad are around to see me accomplish this. To all my grandparents and great-grandparents, Neil, Dotty, Molly, and Murray, and those I never got to meet, you all are the reason I have had the privilege to accomplish this degree.

For my Aunt Debbie, thank you for being like another mother to me. Thank you for visiting me and for taking care of my grandparents, I appreciate you endlessly. Uncle Todd and Aunt Michelle, thank you for always treating me like your family. Thank you for coming to every graduation and always being there for me, like a true aunt and uncle. Thank you, Uncle Jason, Aunt Shayne, Uncle Michael, Aunt Michelle, and Uncle David for your advice and support.

For Kathryn, the best stepmother and grand goddess of gift-giving that anyone could ever ask for. Thank you for being a third parent to me. You have inspired me in so many ways, and I love you.

For my father. You are half of me. You gave me this drive. You gave me the ability to put myself out there and bring people together. You taught me to count and to multiply. You taught me how to argue passionately and stand by my principles while still being open-minded. You taught me to work hard and party harder. You taught me that I could accomplish anything. Thank you, Dad, I love you.

For my mom. Mommy, no one has grounded me and supported me as much as you have. I accomplished this because I had you. You gave me empathy and a love for reading and learning and teaching. Most importantly, you gave me unconditional love and support every single day for 27 years. I love you immensely.

And finally, for my cats, Maybe and Kiwi. My life is so much brighter because you two are my babies. You may never read this, but you were integral to me getting to this point and I love you forever and ever.

Chapter 1 of this dissertation is a reprint of the material as it appears in "A turn for the worse: Aβ β-hairpins in Alzheimer's disease" in *Bioorganic & Medicinal Chemistry*, used with permission from *Elsevier Ltd*. (CC-BY 4.0). James S. Nowick, the coauthor listed in this publication, supervised and edited this chapter.

Chapter 2 of this dissertation is a reprint of the material as it appears in "β-Hairpin Alignment Alters Oligomer Formation in Aβ-Derived Peptides" in *Biochemistry*, used with permission from the *American Chemical Society* (CC-BY 4.0). The coauthors listed in this publication are Adam G. Kreutzer, Nicholas L. Truex, and James S. Nowick. James S. Nowick directed and supervised the research described in this chapter and edited the chapter.

Financial support for the research detailed in chapters one through four was provided by the National Institutes of Health, National Institute on Aging (grants AG072587 and AG062296). Financial support for the research detailed in chapter five was provided by AbbVie.

VITA

Sarah Megan Ruttenberg

EDUCATION

University of California, Irvine 2019–2024
Ph.D. Chemistry
Specialization: Chemical Biology

University of Miami 2015–2019
B.S. Chemistry
Minors: Microbiology and Immunology, Spanish

PROFESSIONAL SKILLS

- Peptide synthesis and purification
- Mammalian and iPSC cell culture
- Cell viability and cytotoxicity assays
- Scientific writing and editing
- Teaching and mentorship
- Fluorescence microscopy
- ELISA and immunocytochemistry
- Quadrupole (single and triple) LC-MS
- Targeted proteomics of biofluids
- Pymol molecular modeling
- SDS-PAGE
- Spectroscopy of biomolecules

PROFESSIONAL EXPERIENCE

University of California – Irvine 2019–2024
Ph. D. Candidate, Graduate Student Researcher, Teaching Assistant
James Nowick Laboratory, Department of Chemistry

The Loh Down on Science Podcast
Managing Editor, New Writer Mentor, Writer 2022-2024

UCI Chemistry TA Mentorship Program 2021–2024
Head TA Mentor

AbbVie 2023
Bioanalytical Intern
Local Delivery and Translation Sciences

The Miami Project to Cure Paralysis 2018–2019
Undergraduate Researcher
Jacquelin Sagan Laboratory, University of Miami Miller School of Medicine

University of Miami 2016–2018
Undergraduate Researcher
Roger LeBlanc Laboratory and Angel Kaifer Laboratory, Department of Chemistry

PUBLICATIONS

Ruttenberg, S.M.; Nowick, J.S. A Turn for the Worse: Aβ β-Hairpins in Alzheimer's Disease. *Bioorg. Med. Chem.* **2024**, *105*, 117715, DOI:10.1016/j.bmc.2024.117715.

Ruttenberg, S.M.; Kreutzer, A.G.; Truex, N.L.; Nowick, J.S. β-Hairpin Alignment Alters Oligomer Formation in Aβ-Derived Peptides. *Biochem.* **2024**, 63 (2), 212-218, DOI:10.1021/acs.biochem.3c00526.

Kreutzer, A.G.; Guaglianone, G.; Yoo, S.; Parrocha, C. M. T.; **Ruttenberg, S.M**.; Malonis, R. J.; Tong, K.; Lin, Y.-F.; Nguyen, J. T.; Howitz, W. J.; Diab, M. N.; Hamza, I. L.; Lai, J. R.; Wysocki, V. H.; Nowick, J.S. Probing Differences Among Aβ Oligomers: Two Triangular Trimers Derived from Aβ Exhibit Different Biophysical and Biological Properties. *PNAS*. **2023**, 120 (22), DOI:10.1073/pnas.2219216120.

ABSTRACT OF THE DISSERTATION

Elucidating the Role of β-Hairpins in Amyloid-β Oligomer Toxicity

by

Sarah Megan Ruttenberg

Doctor of Philosophy in Chemistry

University of California, Irvine, 2024

Professor James S. Nowick, Chair

Amyloid-β (Aβ) oligomers are a major cause of neurodegeneration in Alzheimer's disease (AD). These soluble aggregates of the Aβ peptide have proven difficult to study due to their inherent metastability and heterogeneity. Strategies to isolate and stabilize homogenous Aβ oligomer populations have emerged such as mutations, covalent cross-linking, and protein fusions. These strategies along with molecular dynamics simulations have provided a variety of proposed structures of Aβ oligomers, many of which consist of molecules of Aβ in β-hairpin conformations. β-Hairpins are intramolecular antiparallel β-sheets composed of two β-strands connected by a loop or turn. Chapter 1 details three decades of research that suggests Aβ peptides form several different β-hairpin conformations, some of which are building blocks of toxic Aβ oligomers.

β-Hairpins of Aβ can adopt a variety of alignments, but the role that β-hairpin alignment plays in the formation and heterogeneity of Aβ oligomers is poorly understood. Chapter 2 details an exploration of the effect of β-hairpin alignment on the oligomerization of Aβ peptides in which we designed and studied two model peptides with two different β-hairpin alignments. Peptides $A\beta m_{17-36}$ and $A\beta m_{17-35}$ mimic two different β-hairpins that Aβ

can form, the $A\beta_{17-36}$ and $A\beta_{17-35}$ β-hairpins, respectively. In this chapter, I explain how these hairpins are similar in composition but differ in hairpin alignment, altering the facial arrangements of the side chains of the residues they contain. X-ray crystallography and SDS-PAGE demonstrate that the difference in facial arrangement between these peptides leads to distinct oligomer formation.

Our laboratory has synthesized and elucidated the high-resolution structures of a variety of Aβ β-hairpin peptide mimics. These structures have informed the design and synthesis of covalently stabilized β-hairpin oligomer mimics, some of which we have elucidated high-resolution structures of. The insights from these studies and others like it are currently being used to design anti-Aβ antibodies and vaccines to treat AD. Research suggests that antibody therapies designed to target oligomeric Aβ may be more successful at treating AD than antibodies designed to target linear epitopes of Aβ or fibrillar Aβ. Aβ β-hairpins are good epitopes to use in antibody development to selectively target oligomeric Aβ.

We recently reported the generation of a polyclonal antibody, $pAb_{2AT\text{-}L}$ raised against one of our stabilized Aβ β-hairpin trimer mimics. $pAb_{2AT\text{-}L}$ is moderately selective for oligomeric Aβ over monomeric and fibrillar Aβ and stains the diffuse Aβ on the peripheries of Aβ plaques in AD human and mouse brain tissue but does not bind the dense fibrillar plaque cores. Chapter 3 details an investigation into whether $pAb_{2AT\text{-}L}$ is neuroprotective against toxic aggregates of Aβ and whether $pAb_{2AT\text{-}L}$ can inhibit Aβ aggregation. In this chapter, I detail how $pAb_{2AT\text{-}L}$ prevents the toxic effects of $A\beta_{42}$ on iPSC-derived neurons and HMC3 microglia and inhibits $A\beta_{42}$ fibrillization at sub-stoichiometric ratios of antibody to $A\beta_{42}$.

Chapter 4 is a guide to working with human iPSC-derived neurons for new-comers to iPSC culture. In this chapter, I review methods for generating, transfecting, and differentiating human iPSCs with an emphasis on neuronal differentiation, and I highlight how human iPSC-derived are crucial for disease-modelling. This chapter also includes detailed protocols that I used to culture and differentiate iPSCs — these are the methods I used to differentiate the neurons described in chapter 3 — and insights I have gained from performing these protocols.

Finally, chapter 5 describes the research I performed while working at AbbVie during the summer of 2023 as a bioanalytical intern. The project I completed was quantifying hydrolytic enzymes in human and animal vitreous humors using LC-MS/MS-based targeted proteomics. The vitreous humor is a highly hydrated, viscoelastic, gelatinous fluid that occupies the posterior compartment of the eye between the lens and the retina. Intravitreal injections are a common route of administration for back of the eye diseases but are relatively invasive procedures. To avoid repeating these procedures, biodegradable intravitreal implants have become a popular strategy for achieving sustained drug delivery to the back of the eye. Because these implants are degraded through hydrolysis, hydrolytic enzymes have been hypothesized to play a role in their degradation, but limited information is currently available regarding the abundance of hydrolytic enzymes in the vitreous humor. Quantifying these enzymes is necessary to design accurate models of intravitreal biodegradable implant degradation for drug development. Chapter 5 details the identification and quantification of selected hydrolytic enzymes in the human vitreous humor using liquid chromatography triple quadrupole tandem mass spectrometry.

CHAPTER 1[a]

A Turn for the Worse: Aβ β-Hairpins in Alzheimer's Disease

1.1 Preface to chapter 1

Chapter one is a review of the scientific literature regarding Aβ β-hairpins and their role in Alzheimer's disease (AD) pathogenesis.[A] This review is the culmination of three decades of studies detailing the presence of β-hairpins in Aβ peptides with a focus on their presence in Aβ oligomers. My perspective on this research as detailed in this chapter is that β-hairpins are an ideal epitope for the development of antibody immunotherapies. The significance of β-hairpins in AD pathogenesis is the core principle of AD research in our laboratory. This principle is the foundation of the research presented in chapters two and three. Chapter one was written with my advisor, James Nowick for a special issue of *Bioorganic and Medicinal Chemistry* entitled "New Strategies for Amyloid-Targeted Therapies." We thank Dr. Adam Kreutzer for suggesting that we write this article and providing helpful feedback. We thank Pollard and coworkers and *Cell Press* for use of their image in Figure 1.2A.

[a] This chapter is adapted from Ruttenberg, S.M.; Nowick, J.S. A Turn for the Worse: Aβ β-Hairpins in Alzheimer's Disease. *Bioorg. Med. Chem.* **2024**, *105*, 117715, DOI:10.1016/j.bmc.2024.117715.

1.2 Introduction

The Amyloid-β peptide (Aβ) is now a validated target for treating Alzheimer's disease (AD), but questions remain about how best to target it.[1-4] As an intrinsically disordered peptide, Aβ can present a multitude of epitopes that vary in chemical composition, conformation, and assembly.[3-8] Several of these epitopes have been targeted or used in the development of anti-Aβ antibody therapies or vaccines.[1,3,4,6,8-11] Two disease-modifying treatments of AD have garnered FDA approval thus far — both monoclonal antibodies generated against Aβ.[1,4,6]

These antibodies, Aducanumab and Lecanumab, preferentially bind fibrils and protofibrils of Aβ, respectively.[4,6] Donanumab, another anti-Aβ monoclonal antibody, is expected to receive FDA approval in 2024 and binds Aβ plaques.[4,6] These antibody therapies all significantly lower Aβ plaque load in AD patients, but only mildly slow cognitive decline and can cause edema and microhemorrhages of the brain (ARIA-E and ARIA-H) as major side-effects.[1,3,4,12,13] These side-effects are believed to be caused by the disruption of fibrillar Aβ plaques and vascular deposits through antibody binding.[1,3,12,13] Antibody therapies that bind monomeric Aβ have also entered clinical trials, but the trials were ended due to inefficacy and high incidences of negative side-effects.[3,4,6]

Aducanumab, Lecanumab, and Donanumab are a promising start in the development of anti-Aβ treatments but can cause life-threatening side-effects and are not effective enough to substantially improve the quality of life of those living with AD.[3,6,8] Targeting toxic soluble oligomers of Aβ may lead to safer and more efficacious antibody therapies for AD.[1-3,8-11,13,14] Aducanumab, Lecanumab, and Donanumab do not selectively

target oligomeric Aβ, but current evidence suggests that antibodies that selectively bind oligomeric forms of Aβ are less likely to cause ARIAs and may be more effective at slowing cognitive decline than those that bind monomeric or fibrillar forms.[3,6,8] Oligomers have been identified as the most toxic form of Aβ (although not all oligomers of Aβ are toxic), [2,8-11,14-18] but the significant heterogeneity of Aβ oligomer populations makes it particularly difficult to identify and selectively target epitopes that are both disease-relevant and unique to oligomers.[2,8,9,11,14,16,17]

Aβ β-Hairpins are promising epitopes for the design of antibodies that selectively target Aβ oligomers. β-Hairpins consist of two antiparallel β-strands that are connected by a loop or turn region and are hydrogen bonded to one another (Figure 1).[19-22] Aβ peptides have been observed to form a variety of β-hairpins. These β-hairpins can differ in the number of residues in the turn, the number of residues in the strands, the specific residues encompassed by the β-hairpin, and the alignment of the residues within the β-hairpin. Multiple types and alignments of Aβ β-hairpins have been reported or proposed to form oligomers, but very few have been observed in Aβ fibrils. [5,7,23-26]

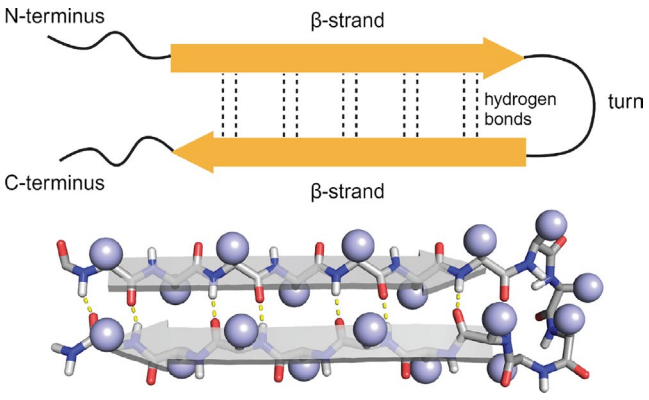

Figure 1.1 Cartoon and molecular model of a β-hairpin. Hydrogen bonds are represented as dashed lines. Side chains are represented spheres in the molecular model.

In this review, we summarize three decades of research surrounding β-hairpins in Aβ peptides. We present evidence that Aβ peptides form a variety of β-hairpins, at least some of which are present in Aβ oligomers and fibrils. We describe how stabilizing some of these β-hairpins affects peptide assembly and toxicity. Finally, we discuss the role that β-hairpins play in AD pathogenesis and the opportunities this knowledge can provide for developing improved therapies for AD.

1.3 Aβ Can Adopt β-Hairpin Conformations

High-resolution structures of Aβ fibrils have been elucidated by solid-state NMR spectroscopy, CryoEM, and X-ray fiber diffraction.[7,23-25] It has been almost impossible to determine high-resolution structures of soluble native Aβ assemblies (oligomers) in solution because of their heterogeneity and high propensity for aggregation.[7,9,11,14,16,17,24,26,27] Structural information about Aβ oligomers comes from a combination of molecular dynamics simulations, low-resolution structural data, and a handful of high-resolution structures of Aβ oligomers that have been stabilized covalently or through interactions with detergents.[7,11,16-18,23,24,26,27] Here we present the current evidence gained from these techniques indicating that Aβ forms β-hairpins.

1.3.1 The discovery of Aβ β-hairpins. Aβ was first explicitly predicted to form a β-hairpin in 1994 by Pollard and coworkers who used molecular modeling to suggest that the first 13 residues of Aβ40 form an amphipathic β-hairpin that assembles to form ion channels in lipid bilayers (Figure 2A).[28] Subsequent molecular modeling studies around this time described the formation of β-hairpins involving the central and C-terminal regions of Aβ,

with a turn located around residues 25–28.[29-31] Although the authors did not explicitly use the term β-hairpin, they describe the folding as such.[32]

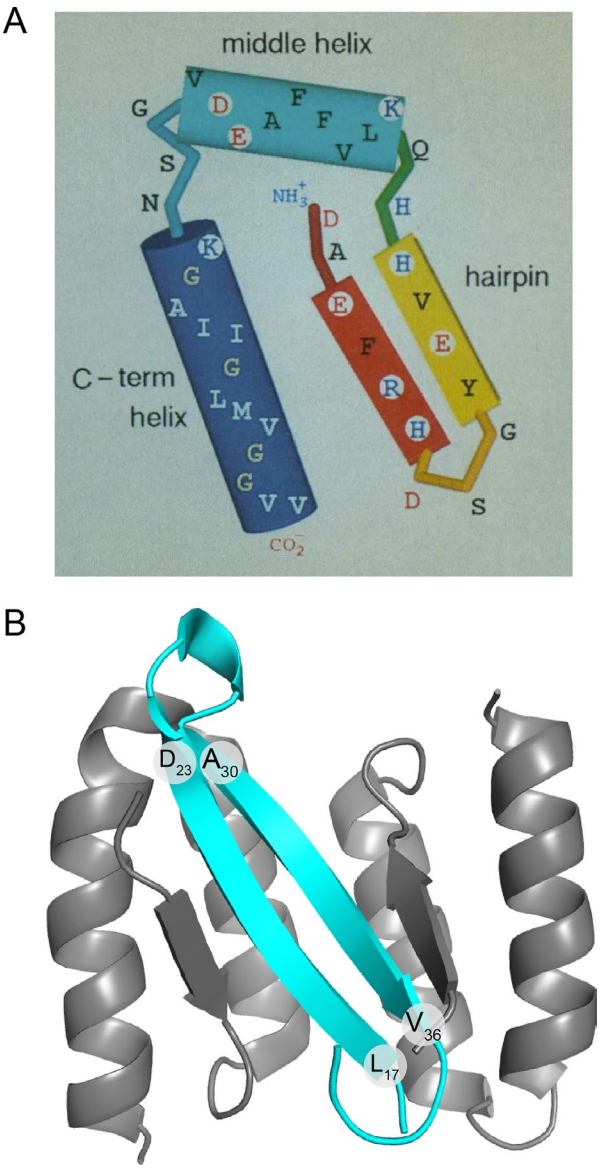

Figure 1.2. (A) Model of Aβ40 in which residues 2 through 13 form a β-hairpin.[28] (B) NMR structure of Aβ40 bound in an affibody in which residues 17 through 36 of Aβ40 form a β-hairpin (PDB: 2OTK).[33]

In 2009, the first experimentally determined β-hairpin structure for Aβ was reported by Hard and coworkers in the solution-phase NMR structure of Aβ40 in complex with an affibody protein (Figure 2B).[33] The β-hairpin consists of residues 17–36, with a

turn region at residues 24–29. Over the following decade, other experimental studies have included this hairpin in their proposed structures of Aβ.[34-37] Concurrently, several molecular dynamics simulations have predicted that Aβ peptides have a propensity to form a variety of β-hairpins consisting of residues ranging the entire peptide (Figure 3).[38-51] The formation of many of these β-hairpin conformations (or similar ones) by Aβ peptides has been supported empirically, with a few studies reporting high-resolution structures of these hairpins.[52-55] Most of the studies that did not report high-resolution structures used NMR data to propose structures of Aβ containing β-hairpins.[27,56-60]

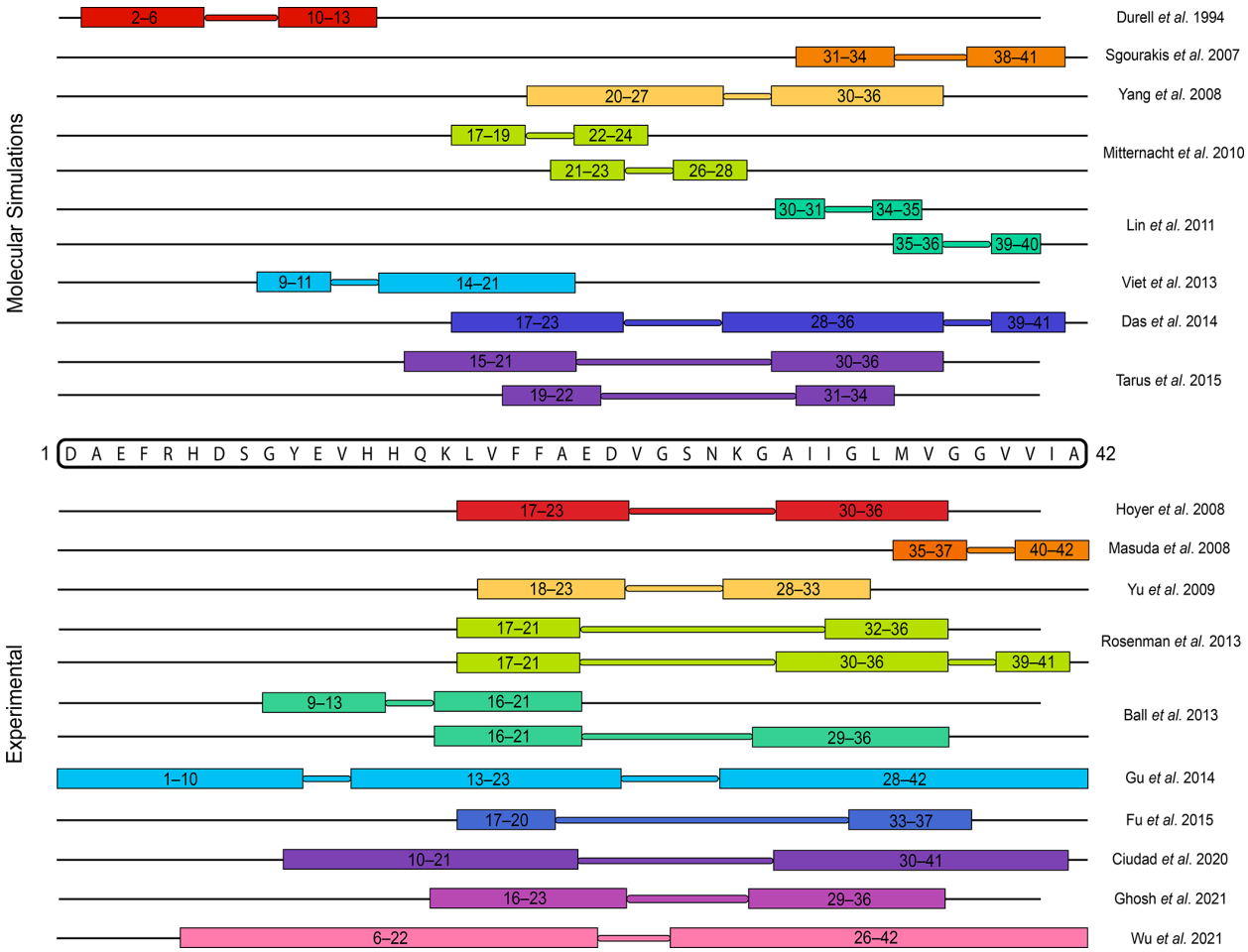

Figure 1.3. Regions of Aβ40 and Aβ42 proposed or reported to form β-hairpins. The top section shows β-hairpins from models proposed using molecular simulations.[28,40,42,44,47,49-51] The bottom section shows β-hairpins from structures proposed or elucidated from experimental observations.[33,52,53,55-60,84]

Structures composed of two β-strands connected by a turn can describe either a β-hairpin or another protein conformation called a *β-arch* (Figure 4). β-Arches are also a common motif observed in Aβ assemblies.[5,7,23-25,53,61] While the β-strands in a β-hairpin are adjacent and hydrogen bond to one another, the β-strands in a β-arch are in different planes and are not hydrogen bonded to one another.[20,25,61] β-Arches are sometimes described as a *U-shape,* misnamed as hairpins, or just not named. β-Arches do not typically exist as isolated entities, but rather form intermolecular hydrogen bonds with β-strands from other β-arches, forming β-sheets.[7,20,23,61] β-Hairpins can also hydrogen bond to one another to form extended β-sheets, but each strand is only available to form one set of intermolecular hydrogen bonds while maintaining the intramolecular hydrogen bonds within the hairpin.

An important distinction between the β-sheets formed by β-hairpins and those formed by β-arches involves the orientation of the β-strands. In a β-hairpin, the component β-strands are inherently antiparallel, running in opposite directions. Conversely, the component β-strands of β-arches typically assemble to form parallel β-sheets.[20,61] Though these distinctions between β-hairpins and β-arches are not always clear in the literature, they are significant. β-Hairpins and β-arches are also not the only peptide conformations that can form β-sheets; individual peptides can contribute singular β-strands to β-sheets as well.[52,61] The differences in the conformation and orientation of the β-strands within β-sheets lead to the formation of different assemblies.[20,61]

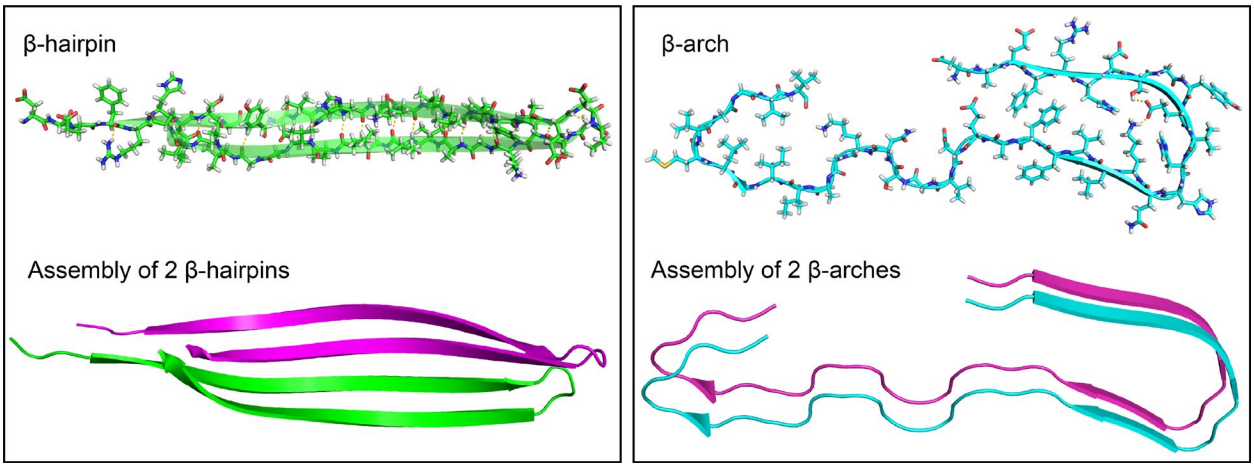

Figure 1.4. Comparison between a β-hairpin and a β-arch and their relative assemblies. The β-hairpin is from the cryoEM structure of Aβ42 grafted into the oligomer-forming domain of α-hemolysin toxin (PDB 7O1Q).[55] The β-arch is from a cryoEM structure of an Aβ40 fibril extracted from the meningeal tissue of a patient with AD (PDB 6SHS).[158]

1.3.2 Aβ β-hairpins in fibrils. A wealth of structures of Aβ fibrils have now emerged through NMR spectroscopy and more recently, cryoEM.[5,7,25,61] Almost all these structures consist of parallel in-register β-sheets connected by β-arches.[5,7,23-25,61] Nevertheless, a couple of structures of Aβ fibrils containing β-hairpins have been described.[53,62] Fraser and coworkers proposed a structure of Aβ fibrils containing β-hairpins.[62] Their proposed structure was based on X-ray fiber diffraction data of fibrils of $A\beta_{11-25}$ and was composed of an extended sheet of β-hairpins. To our knowledge, this is the only proposed structure of Aβ fibrils that consists entirely of β-hairpins. Tycko and coworkers published a cryoEM structure of Aβ40 fibrils in which the exterior of the primary core is decorated by β-hairpins (Figure 5).[53] The core itself consists of Aβ40 molecules in extended parallel β-sheets. The structure was derived from cortical tissue of an AD patient seeded by fibril growth and was corroborated with ssNMR data.

The fibril structure reported by Tycko and coworkers is consistent with the theory that β-hairpins play a role in fibril growth by binding to the edge of a β-sheet and recruiting

subsequent monomers. This theory has been suggested by several research groups,[7,63,64] and may be disease-relevant, but no published structures of Aβ fibrils extracted from AD patients have contained β-hairpins.[25] The predominant theory regarding the role of β-hairpins in the formation of Aβ fibrils is that they are a conformation that Aβ peptides adopt before converting into the β-arches observed in fibrils.[7,18,34,36,59,65-67]

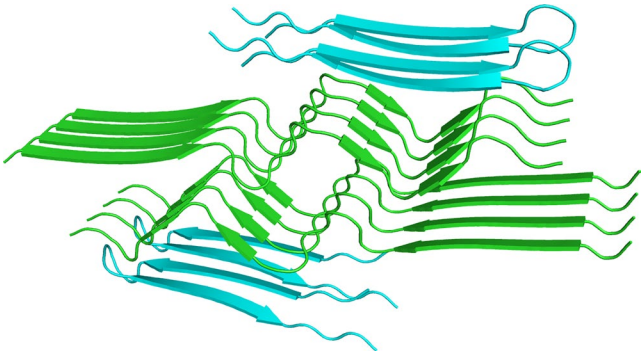

Figure 1.5. Proposed structure of Aβ40 fibrils seeded from cortical tissue of an AD.[57] The structure consists of networks of parallel in-register β-sheets (green) with bound β-hairpins (cyan). The structure is based on cryoEM and ssNMR data.

1.3.3 Aβ β-hairpins in oligomers. Much less is known about the structures of Aβ oligomers than fibrils. While fibrils of Aβ are stable and homogenous, oligomers of Aβ are metastable and heterogeneous.[9,11,14,16,18] Several strategies have emerged to isolate and stabilize oligomers of Aβ to better enable their characterization. Several structures of Aβ oligomers have been proposed using these strategies, [5,7,16-18] but further validation is necessary to determine which of these structures are biologically relevant.[2,5,9,11,14,16,18]

Most proposed structures of Aβ oligomers consist of molecules of Aβ in β-hairpin or β-arch conformations.[5,7,10,18,23] β-Hairpins are preorganized to self-assemble into oligomers because they present hydrophobic surfaces that can participate in hydrophobic interactions and edges that display alternating patterns of hydrogen bond donors and acceptors that are able to participate in hydrogen-bonding interactions.[19,21] Many of the β-

hairpins believed to form Aβ oligomers contain the hydrophobic central region of Aβ composed of residues 17–21 (LVFFA).[34-36,52,59,60,66-72] Several groups have stabilized β-hairpins in this and other regions of Aβ and observed increased oligomer formation.[73-76] Our research group has extensively studied the formation of oligomers from stabilized β-hairpins derived from this region of Aβ.[24,26,77,78]

1.3.3.1 Dimers and tetramers. Several studies have reported the formation of dimers made up of two Aβ peptides in a β-hairpin conformation.[60,75,76,79,80] Hard and coworkers demonstrated that the β-hairpin they observed by NMR (Figure 2B) forms dimers when stabilized with an intramolecular disulfide bond at residues 21 and 30.[75] This peptide assembles into SDS-stable dimers, among other species, but does not fibrillize. Molecular dynamics simulations of Aβ peptides have also proposed the presence of this β-hairpin conformation in dimers of Aβ.[43,49,81-83] Our laboratory has engineered a recombinant Aβ42 peptide containing an N-terminal methionine and an intramolecular disulfide bond between residues 18 and 33 to encourage the formation of a β-hairpin consisting of residues 15–36. This peptide forms SDS-stable dimers and does not aggregate to form fibrils (Figure 6A).[76] Our lab has also observed dimer formation from a cyclic Aβ β-hairpin mimic of the 16–36 by X-ray crystallography and SDS-PAGE.[80]

Olejniczak and coworkers reported a different type of β-hairpin dimer for Aβ42 containing an N-terminal methionine (Figure 6B).[60] Their NMR structure revealed soluble oligomers of Aβ42 that contain β-hairpins consisting of residues 18–33, with residues 24–27 forming the loop region. These oligomers are made up of dimer subunits in which both molecules of Aβ form a β-hairpin. The two β-hairpins do not appear to be in direct contact with each other, but the N-terminal amino acids of each molecule form a 2-stranded

parallel β-sheet with one another. Dadlez and coworkers later reported that this structure was consistent with ion mobility spectrometry mass spectrometry (IM-MS) and molecular modeling of Aβ40 oligomers.[69]

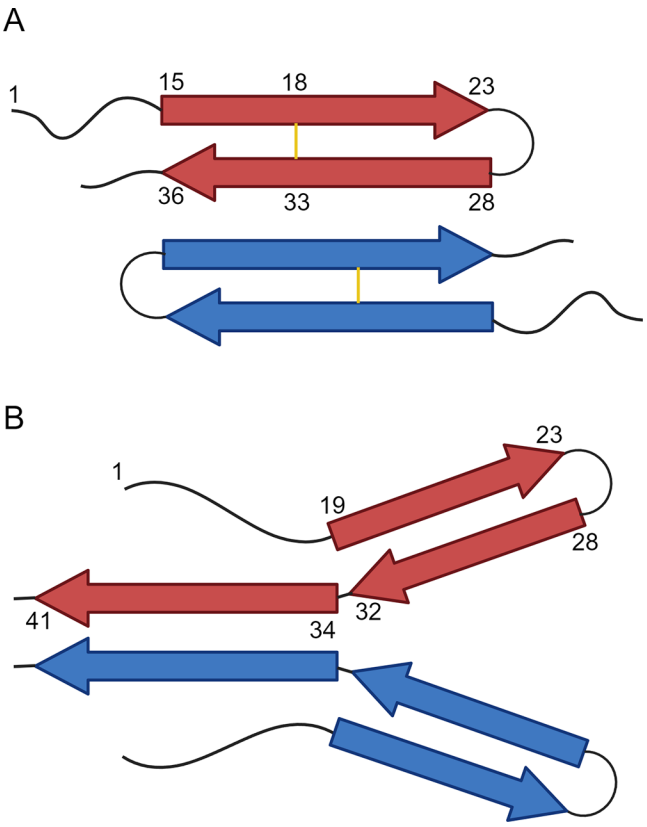

Figure 1.6. (A) Cartoon of a dimer structure of Aβ42 with an intramolecular disulfide bond between residues 18 and 33.[76] (B) Cartoon of a dimer structure of Aβ42 based on NMR data.[60]

Tetramer structures of Aβ containing β-hairpins have also been reported by multiple groups.[52,54,77,78,80,84] One Aβ42 tetramer structure was proposed by Guo and coworkers based on site-directed spin labeling with electron paramagnetic resonance spectroscopy and X-ray powder diffraction.[84] The tetramer was generated by Aβ42 as part of a fusion protein with GroES and ubiquitin, which was designed to encourage ordered oligomer formation without fibrillization. In the proposed structure, each molecule of Aβ forms a triple-stranded antiparallel β-sheet, sometimes called a β-meander (two hairpins

that share a common central strand). The three β-strands consist of residues 1–10, 13–23, and 28–42. Two of these intramolecular antiparallel β-sheets hydrogen bond edge to edge to form a flat dimer, and two of these dimers sandwich together to form the tetramer. Using molecular modeling, four of these tetramers were predicted to further assemble to form a 16-mer.

Another tetramer structure was reported in the crystal structure of a chimera of Aβ and a shark Ig new antigen receptor (IgNAR) (Figure 7A).[54] This chimera incorporates residues 18–41 of Aβ into the CDR3 loop region of IgNAR where they form a triple-stranded intramolecular antiparallel β-sheet (but not a β-meander). The three β-strands consist of residues 18–20, 30–35, and 39–41. This β-sheet contains a β-hairpin composed of residues 32–41 — only residues 32–35 of the second β-strand contribute to the hairpin. The first β-strand (18–20) does not contribute to a β-hairpin, but instead hydrogen bonds to the third β-strand (39–41). These intramolecular β-sheets form sandwich-like dimers that further dimerize by hydrogen bonding at their edges to form two six stranded β-sheets in a sandwich-like tetramer.

Our laboratory has also reported several X-ray crystallographic structures at atomic resolution of cyclic peptides mimicking Aβ β-hairpins that assemble into tetramers. One peptide mimicking a β-hairpin composed of Aβ residues 16–36 forms twisted β-sheet tetramers and sandwich-like tetramers in the crystal state.[80] Two other β-hairpin peptides mimicking β-hairpins formed by Aβ residues 17–35 and 12–30, respectively, both form tetrameric β-barrels in the crystal state.[77,78]

Carulla and coworkers published a structure of a flat Aβ42 tetramer.[52] This NMR structure consists of a six-stranded antiparallel β-sheet in which two of the molecules in

the tetramer are β-hairpins consisting of residues 10–41. The other two molecules contribute singular β-strands to the tetramer structure (Figure 7B). Two tetramers were observed to further assemble through hydrophobic packing to form a sandwich-like octamer. This structure is especially noteworthy because it is the only atomic resolution structure of an oligomer of unmodified full-length Aβ42.

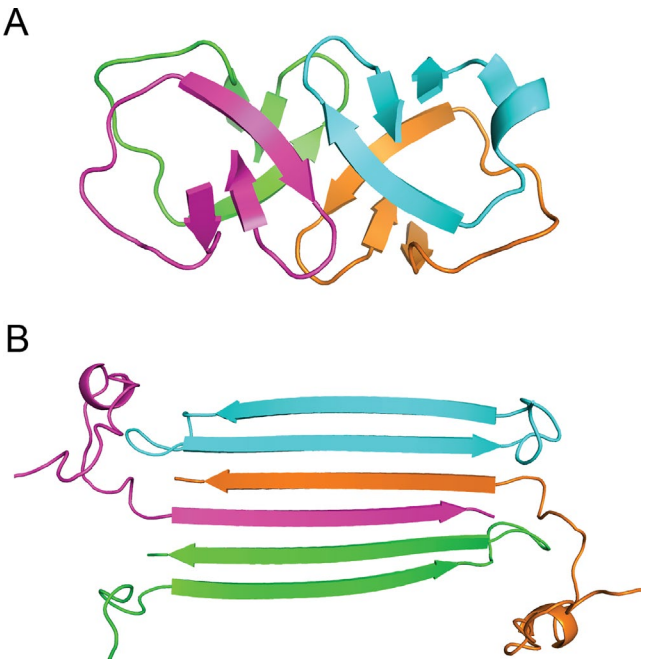

Figure 1.7. (A) Tetramer of Aβ18–41 from the X-ray crystallographic structure of IgNAR-Aβ chimera (PDB 3MOQ).[54] (B) NMR structure of a tetramer of Aβ42 (PDB 6RHY).[52]

1.3.3.2 β-Barrels and other pore-like assemblies. While β-hairpins have been observed in a variety of Aβ oligomers, one of the most studied is the β-barrel. β-Barrels are assemblies of β-strands hydrogen-bonded to create a cylindrical structure resembling an open-ended barrel.[86] These structures of Aβ are heavily studied because some can insert into lipid bilayers — a proposed mechanism of Aβ oligomer toxicity.[5,28,35,68,85-89] β-Barrels and other amyloid oligomers can also be part of annular pores — larger donut-shaped structures named for their ability to form pores in cellular membranes.[28,87,88] Not all β-

barrels and annular pores of Aβ peptides consist of β-hairpins — several consist of β-arches or individual β-strands. Nevertheless, several studies have reported or proposed β-barrel structures where some or all molecules of Aβ contain a β-hairpin.[28,35,55,68,70,72,77,78,86-90]

The first Aβ β-hairpin ever reported, the 2–13 β-hairpin (Figure 2A), was predicted to form a β-barrel.[28,86] Since then, the authors of this work have spent three decades developing molecular models of β-barrels and annular pores of Aβ based on electron microscopy images. Several of these proposed models (though not all) contain β-hairpins.[87,88] The models vary in size from low molecular weight oligomers (fewer than a dozen molecules of Aβ) to annular pores composed of dozens of molecules of Aβ. The β-hairpins within the models also vary, but most form in the N-terminal region of Aβ.

In most Aβ β-barrel structures that contain β-hairpins, the β-hairpins are composed of central and C-terminal residues of Aβ. Hard and coworkers showed that their 17–36 β-hairpin forms hexameric β-barrels when stabilized with an intramolecular disulfide bond.[70] NMR data suggested that every peptide in the β-barrel adopted an identical β-hairpin conformation. A similar structure of Aβ42 oligomers was proposed by Gräslund and coworkers using native IM-MS.[35] The same β-hairpin was also observed in molecular dynamics simulations of Aβ40 by Wolynes and coworkers and was found to be stabilized by assembly into trimeric and tetrameric β-barrels.[72]

Our laboratory has observed annular pore formation from a cyclic peptide mimicking the Hard 17–36 Aβ β-hairpin.[91] X-ray crystallography revealed that the peptide assembles into dodecamers in the crystal state, five of which assemble to form an annular pore (Figure 8A). We have also observed β-barrel formation from our cyclic peptides that

mimic the 17–35 and 12–30 β-hairpins. Both peptides form tetrameric β-barrels in the crystal state.[77,78]

Luo and coworkers observed a longer β-barrel composed of β-hairpins spanning residues 16–42 of Aβ.[55] This cryoEM structure was part of a chimera of Aβ42 and α-hemolysin toxin in which Aβ42 was fused to the oligomerizing soluble domain of the α-hemolysin toxin. They observed by cryoEM that the region consisting of Aβ42 assembled into heptameric β-barrels (Figure 8B) formed by β-hairpins consisting of residues 16–42. Carulla and coworkers have also proposed β-barrels composed of β-hairpins to explain the NMR, CD, SDS-PAGE, and electrical conductance behavior of Aβ42 in lipid bilayers.[89] Their model did not specify the alignments of the β-hairpins or how many molecules of Aβ formed the β-barrel.

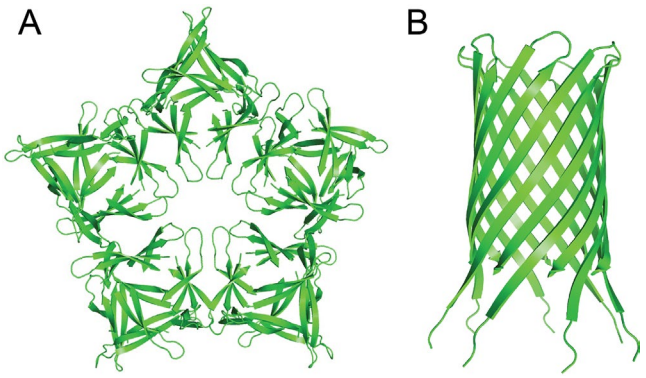

Figure 1.8. (A) Crystal structure of an annular pore formed from a cyclic peptide mimic of a β-hairpin consisting of residues 17–36 of Aβ (PDB 5HOX).[91] (B) CryoEM structure of a β-barrel formed by Aβ42 grafted onto the oligomer-forming domain of α-hemolysin toxin (PDB 7O1Q).[55] The hairpin consists of residues 16–42, seven of which form the β-barrel.

Several other studies have suggested that Aβ peptides form β-barrels made up of β-hairpin units, although they note that alternative structures are plausible, such as a flat antiparallel β-sheets made up of β-hairpins,[68,92] or a β-barrel with β-arches stacked

together in a fibril-like manner.[65,93,94] These structures range in the number of molecules they contain, typically from four to ten.

1.3.3.3 Other soluble oligomers. While dimers, tetramers, and β-barrels may be the most studied Aβ oligomers, they are not the only structures reported or proposed to contain β-hairpins.[26,73,74,95,96] Our laboratory has observed the formation of triangular trimers from several cyclic β-hairpin peptides derived from Aβ.[26] We elucidated the structures of these assemblies by X-ray crystallography and were the first to observe this type of assembly. The trimers further assemble into larger oligomers in the crystal state and by SDS-PAGE (Figure 9).[77,91,97-103]

Hard and coworkers also observed the formation of SDS-stable trimers (in addition to dimers) from their Aβ42 peptide with an intramolecular disulfide linkage between residues 21 and 30.[74] Teplow and coworkers synthesized Aβ40 and Aβ42 containing G33V, V36P, and G38V mutations designed to stabilize the formation of a C-terminal β-hairpin spanning residues 31–40 or 42.[28] These Aβ40- and Aβ42-VPV mutants form SDS-stable hexamers and nonamers after crosslinking by PICUP. Pentamers of Aβ42 have also been observed and analyzed by a variety of methods, some of which are proposed to be made up of β-hairpins, while other are proposed to be made up of β-arches.[95,96,104]

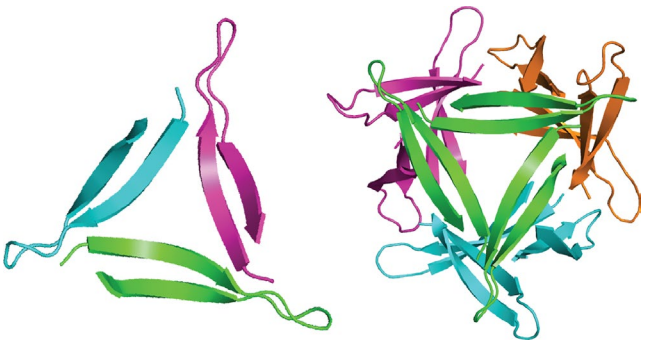

Figure 1.9. Crystal structure of a trimer and dodecamer of a cyclic peptide mimic of a β-hairpin consisting of residues 17–36 of Aβ (PDB 5HOX).[91]

1.4 Aβ β-Hairpins in Disease

The extensive observations of β-hairpins *in vitro* and *in silico* suggest that β-hairpins are relevant in Alzheimer's disease, even though Aβ β-hairpins have not been observed in the brain. To our knowledge, no exact conformations of individual molecules in Aβ oligomers extracted from AD tissue have been determined.[11,15] Although soluble Aβ can be extracted and isolated from brain tissue, the current techniques available to characterize the structures of soluble Aβ assemblies formed *in vivo* (from AD patients or AD mouse models) — or those formed *in vitro* — are limited.[7,9,11,14-18] These techniques can ascertain assembly size (various types of microscopy, mass spectrometry, SEC, gel electrophoresis) and β-sheet content (FTIR and CD spectroscopies) but cannot identify the exact conformations of individual molecules.[7,11,15-18]

Conformation-specific antibodies have also been used to garner structural information about soluble Aβ assemblies and identify toxic species.[2,10,14,16-18,105] Antibodies that are designed to selectively bind β-hairpin epitopes have been shown to stain AD tissue, but the exact epitopes of endogenous Aβ bound by these antibodies have not been confirmed due to the challenges of characterizing Aβ oligomers from tissue.[16] The limitations associated with characterizing toxic Aβ oligomers have thus far precluded establishing a relationship between the formation of Aβ β-hairpins and AD pathogenesis. High-resolution structural data have been obtained for stabilized (non-native) Aβ β-hairpins and oligomers.[27,33,52,54,55,60] Some of these structures are similar in size and shape to oligomers isolated from AD brain tissue, but similarities at the atomic level cannot be determined.[11,75,105] Here, we discuss the current evidence correlating β-hairpin formation with Aβ oligomer-mediated toxicity in AD.

1.4.1 Aβ β-hairpins form toxic oligomers. Several studies have suggested that β-hairpins are building blocks of toxic Aβ oligomers.[5,23,52,60,66,75,94,106] Raussens and coworkers were among the first to propose that Aβ oligomers containing β-hairpins are toxic. They prepared Aβ42 oligomers and fibrils and observed by IR spectroscopy (FTIR) that the oligomers contained antiparallel β-sheets, while the fibrils contained parallel β-sheets.[65] Their proposed model of these oligomers is composed of β-hairpins. Aβ42 oligomers prepared in the same manner previously were shown to cause greater mitochondrial dysfunction than Aβ42 fibrils in cortical neurons and glia harvested from mice.[107] Raussens and coworkers further proposed that the antiparallel β-sheet conformation is responsible for the greater neurotoxicity of Aβ42 oligomers.

More recently, Ding and coworkers proposed structures of toxic Aβ42 oligomers that consist of β-hairpins arranged in β-barrels.[94] They performed extensive molecular dynamics simulations of early-stage oligomerization of Aβ42 and observed the formation of small β-barrels composed of three to six molecules of Aβ42 all in β-hairpin conformations. Subsequent TEM imaging of Aβ42 oligomers formed *in vitro* showed larger barrel-like structures (~9 nm). The study did not discuss the discrepancy between the size of the simulated structures and those observed *in vitro*. These oligomers exhibited greater toxicity toward SH-SY5Y neuroblastoma cells than Aβ42 monomers or fibrils, as measured by propidium iodide staining. The oligomers also elicited increased markers of inflammation, apoptosis, and autophagy when injected into the brains of mice.

The region of Aβ containing residues 17 through 35 has specifically been identified to play a pivotal role in the toxicity and β-sheet content of Aβ peptides.[108] Several studies have reported that stabilizing β-hairpins in this region leads to increased formation of toxic

oligomers. Hard and coworkers stabilized their Aβ 17–36 β-hairpin with an intramolecular disulfide bond and observed the formation of oligomers and protofibrils similar in morphology to those extracted from AD brain tissue.[75] The oligomers induced substantial apoptosis in SH-SY5Y cells under conditions in which Aβ42 fibrils and monomers did not. Other Aβ peptides containing intramolecular disulfide bonds in the same region have also been shown to exhibit greater toxicity than their native counterparts.[76,109]

Two of our cyclic model peptides mimicking the 17–36 and 16–36 β-hairpins form trimers that cause apoptosis, membrane permeability, and mitochondrial dysfunction in SH-SY5Y cells and iPSC-derived cortical neurons at micromolar concentrations (unpublished results).[99] Another of our peptides, which mimics a β-hairpin spanning Aβ residues 12–40, also causes apoptosis and membrane permeability in SH-SY5Y cells.[78] In the crystal state this peptide forms tetrameric β-barrels composed of β-hairpins.

The Aβ42-VPV mutant prepared by Teplow and coworkers exhibited increased oligomer formation compared to wild-type Aβ42. These oligomers had different morphology from wild-type oligomers of Aβ42 but similar toxicity towards rat primary hippocampal and cortical neurons. Aβ40-VPV exhibited similar oligomerization to Aβ42-VPV and significantly increased toxicity compared to wild-type Aβ40.[74]

One explanation for the increased toxicity of some oligomers of Aβ over fibrils is that the toxic Aβ oligomers can disrupt cellular membranes while Aβ fibrils cannot.[7,11,110,111] The ability of toxic Aβ oligomers to disrupt cellular membranes may be related to the presence of antiparallel β-sheets which are often found in Aβ oligomers, but rarely observed in Aβ fibrils.[5,7,11,65,112,113] Several studies have predicted or observed the formation of oligomers of Aβ that contain β-hairpins and can form pores in lipid

bilayers.[7,35,52,55,68,89,114] The first study to predict that an Aβ peptide would form a β-hairpin also predicted that the β-hairpins would form pores in membranes.[28] Other simulations of Aβ peptides in lipid bilayers have predicted the formation of β-hairpin oligomers that can penetrate lipid bilayers.[90,115-118]

Experimentally determined structures of Aβ oligomers formed in lipid environments have contained β-hairpins as well. Maiti and coworkers proposed that Aβ40 forms β-hairpin β-barrels in lipid bilayers based on ssNMR and surface-enhanced Raman spectroscopy.[68] Graslund and coworkers found by native IM-MS that Aβ42 formed hexameric β-barrels containing β-hairpins in membrane mimicking micelles.[35] The Aβ42 tetramer reported by Carulla *et al*, though not a β-barrel, was also observed to form in a membrane mimicking environment where it formed pores.[50] Other studies have demonstrated that oligomers of Aβ made up of antiparallel β-sheets perturb lipid bilayer membranes and cause neurotoxicity, but the authors were unable to specify if the individual molecules form β-hairpins.[112,113,119-121]

Some researchers have proposed that the greater toxicity of Aβ42 compared to Aβ40 is due to a greater ability of Aβ42 to form β-hairpins and insert in lipid bilayers. Carulla and coworkers theorized that the absence of I41 and A42 in Aβ40 may alter a C-terminal β-hairpin spanning residues 10–41, making it too short to span the hydrophobic portion of the lipid bilayer.[52] Kanaya and coworkers have suggested that the absence of I41 and A42 may prevent

the formation of a C-terminal β-hairpin spanning residues 35–42 that stabilizes an S-oxidized radical cation at M35, causing oxidative stress, and that the reduced toxicity of Aβ40 can be explained by an inability to form this β-hairpin.[57] Although these explanations

for the greater toxicity of Aβ42 are related to β-hairpin formation, there are several other reasonable explanations unrelated to β-hairpin formation.[5,6,11] Regardless of which explanations are most accurate, there is significant evidence that residues 41 and 42 promote β-hairpin and β-sheet formation.[42,56,58,66,77,122-126] Concurrently, and perhaps consequently, Aβ40 and Aβ42 also assemble differently.[5,11,58,66,125]

1.4.2 Aβ β-hairpins in FAD. Although most cases of AD are sporadic, a small subset of the population has mutations that are associated with familial AD (FAD) and result in the certain onset of AD at a younger age than most sporadic AD cases (Figure 10).[127-132] Some Aβ mutants linked to FAD adopt β-hairpin conformations more readily than wild-type Aβ and exhibit increased oligomer formation and neurotoxicity.[32,40,44,45,50,123,124,133-138] These properties suggest a correlation between β-hairpin formation and toxicity of the peptide. The properties of these mutants also highlight how certain residues are particularly consequential to β-hairpin formation and peptide assembly.

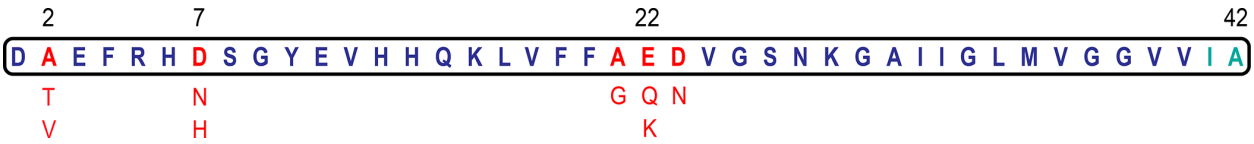

Figure 1.10. Aβ42 sequence with common familial mutations (red) and residues 41 and 42 (teal) highlighted.

Several FAD-related mutations occur at E22, a residue that has been identified as a contributor to Aβ oligomer stability.[139] The Dutch mutant (E22Q) swaps the negatively charged glutamic acid with a neutral glutamine, the Italian mutant (E22K) swaps the glutamic acid with a positively charged lysine, the Arctic mutant (E22G) has no sidechain at position 22, and the Osaka mutant (E22Δ) has a deletion at position 22.[127,129,140] The Dutch and Arctic mutants both form β-hairpins more readily than wild-type Aβ and exhibit increased oligomer formation and toxicity.[124,133,134,137,138] The Osaka mutation has also been

shown to increase oligomer formation and toxicity of the peptide,[140] but to our knowledge its propensity to form a β-hairpin has not been explicitly studied. The Italian mutant has a similar propensity to form β-hairpins compared to wild-type Aβ but may be more prone to forming toxic assemblies.[42,114]

Mutation at D23 can also cause FAD, and this residue has been identified to be important in stabilizing β-hairpins and β-arches through salt-bridge formation with K28.[46] Like the Dutch mutant, the Iowa mutant (D23N) swaps a negatively charged amino acid (aspartic acid) for a neutral one (asparagine). Despite losing the conformation-stabilizing salt bridge between D23 and K28, this mutant also more readily forms β-hairpins than wild-type Aβ.[63,123,133,134] *In vitro* evidence suggests that the Dutch and Iowa mutants aggregate more quickly than wild-type Aβ, but still form the same transient β-hairpin before transitioning to fibrillization.[34] This change in aggregation kinetics may reflect differences in the rates of β-hairpin formation and transition from a β-hairpin to a β-arch.[63,123,133,134]

Another residue that has multiple FAD-related mutations is D7.[132,141] The Taiwanese mutant (D7H) exhibits a prolonged oligomer state and increased neurotoxicity compared to wild-type Aβ.[141] The Tottori mutant (D7N) exhibits accelerated fibrillization and forms larger and more neurotoxic oligomers than wild-type Aβ.[136,142] These differences in aggregation have been explained by a decrease in β-content in the Taiwanese mutant,[143] and an increased tendency to form a β-hairpin in the Tottori mutant.[50,94,136] A neighboring mutation, the English mutation (H6R), also accelerates fibril formation[142] and produces larger and more toxic β-sheet rich oligomers than the wild-type.[136] While the secondary

structures in the English and Tottori oligomers may or may not be β-hairpins, molecular dynamics simulations suggest that this is a significant possibility.[50,144]

A2V is an FAD-related mutation that exhibits an increased propensity for N-terminal β-hairpin formation and oligomer formation compared to wild-type Aβ.[40,45,131,145] Conversely, A2T is a neuroprotective Aβ mutation that reduces the propensity for N-terminal β-hairpin formation.[40] Belfort and coworkers theorize that the differences in aggregation between A2V, A2T, and wild-type Aβ can be attributed to valine increasing hydrophobic clustering and threonine participating in long-range electrostatic interactions with the C-terminus that do not occur in wild-type Aβ.[40]

Although many FAD-related mutants exhibit an increased propensity to form β-hairpins, other properties of mutant Aβ peptides likely contribute to FAD pathogenesis. These properties can include increased propensity to form β-sheets, enhanced ability to disrupt lipid bilayers, and altered aggregation kinetics prolonged oligo (faster nuecleation or prolonged oligomer state), among others.[7,134,136,138,146,147] The effects of any single mutation on Aβ folding and aggregation can likely be attributed to altered charge, hydrophobicity, and size of the mutated residue.[138,146,147]

1.4.3 Aβ β-hairpins in immunotherapy and vaccines. Monoclonal antibodies and vaccines are the main therapies currently being developed to ameliorate the toxic effects of Aβ.[1,3,4,148] Although vaccines containing fragments or assemblies of Aβ are currently being tested in clinical trials to treat AD, none have yet gained FDA approval.[4,148] On the other hand, two monoclonal IgG antibodies targeting Aβ have received FDA approval, and additional monoclonal antibodies are likely to follow.[1,4,6] Monoclonal antibodies target a single epitope and have the potential to be selective for individual conformations of that epitope,

such as a β-hairpin.[2,3,10,11,148] This level of selectivity cannot be achieved in vaccines because the antibodies elicited are heterogeneous. For this reason, monoclonal antibodies may have a greater potential for efficacy.[3,4,10,148]

Anti-Aβ antibodies can reduce the neurotoxic effects of Aβ through multiple mechanisms.[1,8,10,12,148] Antibodies circulating in the blood bind Aβ and may facilitate efflux of Aβ from the brain and prevent re-entry.[1,3,4,8,10,12] Circulating antibodies enter the brain with limited efficacy and sequester toxic Aβ assemblies, preventing them from causing neurodegeneration.[1,6,8,148] Generally, these antibodies mark Aβ assemblies for recognition by microglia, which subsequently degrade the assemblies through phagocytosis.[1,4,10,12,13,17,148] Some anti-Aβ antibodies solubilize fibrils, disaggregate oligomers, or prevent monomeric Aβ from aggregating into toxic assemblies.[1,6,12,13,17,148] These antibody mechanisms can have negative effects, however, like causing inflammation in the brain, disrupting the physiological function of monomeric Aβ, or increasing the presence of toxic soluble oligomers.[1,3,6,8,12,13,105,148]

Although there have been important advances in the development of anti-Aβ immunotherapies to treat AD, the benefits of the immunotherapies developed thus far are limited and further advances are needed. One strategy to develop improved anti-Aβ immunotherapies is targeting conformational epitopes of toxic Aβ oligomers.[2,3,8,10,11,15,149,150] Several monoclonal antibodies have been developed that selectively bind oligomers of Aβ, but the exact conformations of the epitopes they bind are often unknown.[10,16] Many of these antibodies offer neuroprotective effects in both *in vitro* and *in vivo* models of AD, but only one, ACU193, has made it to clinical trials thus far.[3,151] Though the exact epitope of ACU193 is unknown, it is over 650-fold more selective for

oligomers than for monomers, exhibits minimal plaque-binding, and binds to a range of oligomers.[152] This antibody was able to reverse memory deficits in 6-month-old 5xFAD mice to the point that cognitive function was indistinguishable from wild-type mice a month after treatment.[153]

A few studies have reported monoclonal antibodies that selectively bind defined β-hairpin epitopes.[106,154,155] Bayer and coworkers identified a murine antibody, TAP01, that binds a β-hairpin formed by N-truncated pyroglutamate Aβ3–42 (AβpE3).[154] This variant of Aβ has an increased propensity to form toxic oligomers and is associated with AD pathology but not normal APP processing.[14,154] Through an X-ray co-crystallographic structure with TAP01, the researchers found that AβpE3–14 forms a β-hairpin-like conformation consisting of residues 3–12 with a turn containing residues 5–9 (Figure 11).[154] TAP01 and its humanized equivalent, TAP01-04, both bind this hairpin but do not bind fibrils of Aβ. Immunotherapy with TAP01-04 reduced Aβ plaque load, improved memory, and reduced neuron loss in AD mouse models. Vaccination with a cyclized version of Aβ1-14 that is designed to adopt this conformation exhibited similar neuroprotective effects.[154] While the soon-to-be-FDA-approved monoclonal antibody Donanemab also targets AβpE3, it does not bind the β-hairpin conformation characterized by Bayer and coworkers.[154]

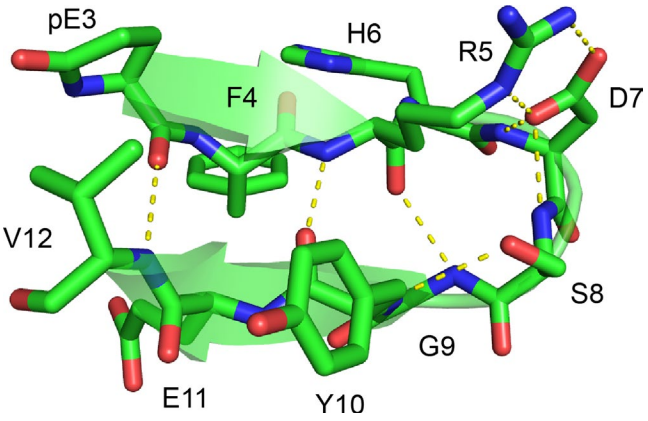

Figure 1.11. Crystal structure of a fragment of N-truncated pyroglutamate Aβ that forms a β-hairpin that is bound by TAP01 (PDB 7OW1).[154]

Ebert and coworkers generated oligomer-specific monoclonal antibodies against Aβ20–42 "globulomers" which were generated by proteolysis of globular oligomers formed from the Aβ42 dimers shown in Figure 6A.[60,106] The most promising antibody, A-887755, bound the β-hairpin conformation reported by Olejeniczak and coworkers (Figure 6A) and selectively bound soluble Aβ oligomers in brain tissue extracts from AD patients and APP transgenic mice. A-887755 also improved synaptic transmission in rat brain slices treated with Aβ oligomers. When APP/L transgenic mice were vaccinated with Aβ20–42 globulomers or given immunotherapy with A-887755 they exhibited cognitive function akin to wild-type mice.[106] Although these results are promising, another anti-Aβ antibody generated by Ebert and coworkers was not conformationally selective for oligomers and exhibited similar protective effects.

Our laboratory has also begun developing antibodies that bind Aβ β-hairpins.[100,155] Currently, we have developed polyclonal and monoclonal antibodies against covalently stabilized trimer models consisting of central and C-terminal regions of Aβ in β-hairpin conformations. The structures of these trimers have been elucidated by X-ray

crystallography, and their assembly and toxicity have been thoroughly characterized.[99,100,155] The most promising antibodies thus far were developed against a neurotoxic trimer known as 2AT-L. These polyclonal antibodies, pAb2AT-L, recognize unique pathological features in Aβ plaques from both mouse and human brain tissue. Immunostaining studies revealed pAb2AT-L recognizes only diffuse Aβ outside of the plaque cores (in burned-out plaques there is minimal pAb2AT-L staining).[100] Additionally, these antibodies protect iPSC-derived neurons from Aβ42 toxicity and inhibit Aβ42 fibrillization (unpublished results).

We have performed similar studies with monoclonal antibodies derived against two of our trimer models.[155] Although these antibodies selectively bound conformationally defined aggregates of Aβ *in vitro*, they did not recognize biogenic Aβ species in immunostaining studies with brain slices from 5xFAD mice. These results suggest that the targeted epitopes were either absent or not exposed in the brain tissue. Alternatively, these epitopes may be present in earlier stages of disease, and then change conformation as the disease progresses. We are continuing to study these antibodies, as well as antibodies generated against other conformationally defined oligomers containing Aβ β-hairpins.

Although monoclonal antibodies have been the most successful therapies thus far, vaccines continue to be developed to treat AD. One vaccine meant to target soluble oligomers of Aβ is currently undergoing clinical trials and contains an Aβ β-hairpin; AZL-101 contains the stabilized β-hairpin designed by Hard and coworkers. Few other details about the vaccine are public knowledge.[4,75] We are aware of five other vaccines containing fragments of Aβ that are currently undergoing clinical trials as well (ABvac40, AV-1959D, ACI-24, UB-311, and ALZN002).[4,156]

The protective effects of Aβ vaccines and non-specific anti-Aβ antibodies in mouse models are often similar to those elicited by oligomer-specific anti-Aβ antibodies.[1,106,141,157] These results, and the failure of several anti-Aβ treatments in clinical trials suggest that preclinical studies in mouse models may not translate to humans.[1,4,157] Although the benefits of selectively targeting Aβ oligomers may not be obvious in mouse models, the results from clinical trials suggest that this is currently the most promising avenue for anti-Aβ drug development.[1-3,8-11,13,14]

Even though the Aβ epitopes being targeted are important, many aspects of clinical trials affect the success of immunotherapies and vaccines. Treatment timeline (stage of disease, frequency of treatment) and dosage as well as the subjects being treated (type of AD, age, sex, other conditions) can significantly affect the outcomes of clinical trials.[1,3,4,15] Earlier treatment has been identified as especially important for future clinical trials to prevent disease progression and should enable better targeting of toxic oligomers of Aβ that are likely more prevalent before plaque formation.[1,3,4,8,11,14,15] Much of the research presented here can also be applied to early detection of AD for the same reason.[10,11,14,15,17] While these aspects of clinical trials can and likely will be optimized to improve drug performance, it is important to continue creating better and safer AD treatments.

1.5 Conclusions and Perspective

The literature describing the conformations and assembly of Aβ is extensive, and a single uniform picture has not emerged. Nevertheless, some properties of Aβ are certain. Aβ peptides can adopt a wide range of conformations and follow several different aggregation pathways.[3-8] In AD, Aβ mostly assembles to form various types of β-sheets.[5,7,25,61,85,112] Fibrils are one of these β-sheet assemblies and the final product of most

Aβ aggregation pathways.[61,67,85] As a result, fibrils are the most abundant form of Aβ in AD pathogenesis,[9,16,65] but fibrillar Aβ itself is not believed to cause significant neurotoxicity, and clearance of Aβ fibrils from the brain has not been very successful at treating AD.[1,3,4,6,8] Instead, oligomers of Aβ, which form before fibrillar Aβ or upon disaggregation of fibrillar Aβ, are believed to be the most neurotoxic form of Aβ. [2,8-11,14-16,18] We believe the most promising targets for drugs to treat AD are epitopes unique to oligomeric Aβ.[2,3,8,10,11,15,149]

The most successful type of anti-Aβ drugs so far are monoclonal antibodies. Oligomer-targeting antibodies must have high selectivity for oligomeric Aβ to be effective because Aβ oligomers are much less abundant in the brain than Aβ fibrils and monomers.[9,6,150] Selectivity for oligomeric Aβ should also minimize the negative side-effects that have been observed upon treatment with antibodies targeting fibrillar or monomeric Aβ.[1,3,4,6] To achieve selective targeting of oligomeric Aβ, antibodies need to bind conformational epitopes that are unique to oligomers. Structural characterization of Aβ oligomers is necessary to identify epitopes for antibody development. Defining these epitopes should also benefit vaccine development and the development of other types of anti-Aβ drugs like β-sheet or β-hairpin breakers that prevent Aβ aggregation.[4,17]

Identifying conformational epitopes of Aβ oligomers has proven difficult thus far because most experimental studies of Aβ oligomers have not been able to achieve high-resolution structural characterization. Often, the best that can be ascertained about the structures of Aβ oligomers is their size and their degree of β-sheet content.[5,7,11,16,17,65,67] This type of low-resolution structural data combined with extensive molecular dynamics simulations have provided a significant amount of knowledge about these elusive oligomers, but these techniques by themselves are not enough to clearly define epitopes of

Aβ for drug development. This limitation has led researchers to create stabilized Aβ oligomers that are amenable to high-resolution structural analysis. Structures of these oligomers are highlighted in this review and have provided evidence that Aβ oligomers often consist of β-hairpins.

The studies described throughout this review support the significance of Aβ β-hairpins in AD pathogenesis. These studies also suggest that Aβ β-hairpins occur predominantly in oligomeric Aβ, making them an ideal target for antibody therapy. Preclinical studies on antibodies that selectively bind β-hairpins show that they exhibit selectivity for oligomers of Aβ *in vitro* and exhibit neuroprotective effects in mouse models of AD.[106,154] We anticipate that further studies of antibodies of this kind will yield more effective AD drugs.

1.6 References and Notes

A. Ruttenberg, S.M.; Nowick, J.S. A Turn for the Worse: Aβ β-Hairpins in Alzheimer's Disease. *Bioorg. Med. Chem.* **2024**, *105*, 117715, https://doi.org/10.1016/j.bmc.2024.117715.

1. Lian, Y.; Jia, Y.-J.; Wong, J.; Zhou, X.-F.; Song, W.; Guo, J.; Masters, C. L.; Wang, Y.-J. Clarity on the Blazing Trail: Clearing the Way for Amyloid-Removing Therapies for Alzheimer's Disease. *Molecular Psychiatry* **2023**, 1–9. https://doi.org/10.1038/s41380-023-02324-4.
2. Song, C.; Zhang, T.; Zhang, Y. Conformational Essentials Responsible for Neurotoxicity of Aβ42 Aggregates Revealed by Antibodies against Oligomeric Aβ42. *Molecules* **2022**, *27* (19), 6751. https://doi.org/10.3390/molecules27196751.
3. van Dyck, C. H. Anti-Amyloid-β Monoclonal Antibodies for Alzheimer's Disease: Pitfalls and Promise. *Biological Psychiatry* **2018**, *83* (4), 311–319. https://doi.org/10.1016/j.biopsych.2017.08.010.
4. Zhang, Y.; Chen, H.; Li, R.; Sterling, K.; Song, W. Amyloid β-Based Therapy for Alzheimer's Disease: Challenges, Successes and Future. *Signal Transduction and Targeted Therapy* **2023**, *8* (1), 1–26. https://doi.org/10.1038/s41392-023-01484-7.
5. Aleksis, R.; Oleskovs, F.; Jaudzems, K.; Pahnke, J.; Biverstål, H. Structural Studies of Amyloid-β Peptides: Unlocking the Mechanism of Aggregation and the Associated Toxicity. *Biochimie* **2017**, *140*, 176–192. https://doi.org/10.1016/j.biochi.2017.07.011.

6. Imbimbo, B. P.; Ippati, S.; Watling, M.; Imbimbo, C. Role of Monomeric Amyloid-β in Cognitive Performance in Alzheimer's Disease: Insights from Clinical Trials with Secretase Inhibitors and Monoclonal Antibodies. *Pharmacological Research* **2023**, *187*, 106631. https://doi.org/10.1016/j.phrs.2022.106631.
7. Nasica-Labouze, J.; Nguyen, P. H.; Sterpone, F.; Berthoumieu, O.; Buchete, N.-V.; Coté, S.; De Simone, A.; Doig, A. J.; Faller, P.; Garcia, A.; Laio, A.; Li, M. S.; Melchionna, S.; Mousseau, N.; Mu, Y.; Paravastu, A.; Pasquali, S.; Rosenman, D. J.; Strodel, B.; Tarus, B. Amyloid β Protein and Alzheimer's Disease: When Computer Simulations Complement Experimental Studies. *Chemical Reviews* **2015**, *115* (9), 3518–3563. https://doi.org/10.1021/cr500638n.
8. Sengupta, U.; Nilson, A. N.; Kayed, R. The Role of Amyloid-β Oligomers in Toxicity, Propagation, and Immunotherapy. *EBioMedicine* **2016**, *6*, 42–49. https://doi.org/10.1016/j.ebiom.2016.03.035.
9. Goure, W. F.; Krafft, G. A.; Jerecic, J.; Hefti, F. Targeting the Proper Amyloid-Beta Neuronal Toxins: A Path Forward for Alzheimer's Disease Immunotherapeutics. *Alzheimer's Research & Therapy* **2014**, *6* (4), 42. https://doi.org/10.1186/alzrt272.
10. Murakami, K. Conformation-Specific Antibodies to Target Amyloid β Oligomers and Their Application to Immunotherapy for Alzheimer's Disease. *Bioscience, Biotechnology, and Biochemistry* **2014**, *78* (8), 1293–1305. https://doi.org/10.1080/09168451.2014.940275.
11. Shea, D.; Daggett, V. Amyloid-β Oligomers: Multiple Moving Targets. *Biophysica* **2022**, *2* (2), 91–110. https://doi.org/10.3390/biophysica2020010.
12. Agarwal, A. K.; Gupta, V.; Brahmbhatt, P.; Desai, A.; Vibhute, P.; Joseph-Mathurin, N.; Bathla, G. Amyloid-Related Imaging Abnormalities in Alzheimer Disease Treated with Anti–Amyloid-β Therapy. *Radiographics* **2023**, *43* (9). https://doi.org/10.1148/rg.230009.
13. Hampel, H.; Elhage, A.; Cho, M.; Apostolova, L. G.; Nicoll, J.; Atri, A. Amyloid-Related Imaging Abnormalities (ARIA): Radiological, Biological and Clinical Characteristics. *Brain* **2023**. https://doi.org/10.1093/brain/awad188.
14. Cline, E. N.; Bicca, M. A.; Viola, K. L.; Klein, W. L. The Amyloid-β Oligomer Hypothesis: Beginning of the Third Decade. *Journal of Alzheimer's Disease* **2018**, *64* (s1), S567–S610. https://doi.org/10.3233/jad-179941.
15. Viola, K. L.; Klein, W. L. Amyloid β Oligomers in Alzheimer's Disease Pathogenesis, Treatment, and Diagnosis. *Acta Neuropathologica* **2015**, *129* (2), 183–206. https://doi.org/10.1007/s00401-015-1386-3.
16. Hayden, E. Y.; Teplow, D. B. Amyloid β-Protein Oligomers and Alzheimer's Disease. *Alzheimer's Research & Therapy* **2013**, *5* (6), 60. https://doi.org/10.1186/alzrt226.
17. Wang, Y.; Chen, J.; Gao, F.; Hu, M.; Wang, X. Recent Developments in the Chemical Biology of Amyloid-β Oligomer Targeting. *Organic and Biomolecular Chemistry* **2023**, *21* (22), 4540–4552. https://doi.org/10.1039/d3ob00509g.
18. Nagel-Steger, L.; Owen, M. C.; Strodel, B. An Account of Amyloid Oligomers: Facts and Figures Obtained from Experiments and Simulations. *ChemBioChem* **2016**, *17* (8), 657–676. https://doi.org/10.1002/cbic.201500623.

19. DuPai, C. D.; Davies, B. W.; Wilke, C. O. A Systematic Analysis of the Beta Hairpin Motif in the Protein Data Bank. *Protein Science* **2021**, *30* (3), 613–623. https://doi.org/10.1002/pro.4020.
20. Hennetin, J.; Jullian, B.; Steven, A. C.; Kajava, A. V. Standard Conformations of β-Arches in β-Solenoid Proteins. *Journal of Molecular Biology* **2006**, *358* (4), 1094–1105. https://doi.org/10.1016/j.jmb.2006.02.039.
21. Ptitsyn, A.; Finkelstein, P.; Falk (bendzko. *PRINCIPAL FOLDING PATHWAY and TOPOLOGY of ALL-P PROTEINS*; 1979. https://core.ac.uk/download/pdf/82015124.pdf (accessed 2024-02-12).
22. Sibanda, B. L.; Thornton, J. M. β-Hairpin Families in Globular Proteins. *Nature* **1985**, *316* (6024), 170–174. https://doi.org/10.1038/316170a0.
23. Abelein, A.; Abrahams, J. A.; Danielsson, J.; Gräslund, A.; Jarvet, J.; Luo, J.; Tiiman, A.; Wärmländer, S.K.T.S. The Hairpin Conformation of the Amyloid β Peptide Is an Important Structural Motif along the Aggregation Pathway. *Journal of Biological Inorganic Chemistry* **2014**, *19* (4-5), 623–634. https://doi.org/10.1007/s00775-014-1131-8.
24. Kreutzer, A. G.; Nowick, J. S. Elucidating the Structures of Amyloid Oligomers with Macrocyclic β-Hairpin Peptides: Insights into Alzheimer's Disease and Other Amyloid Diseases. *Accounts of Chemical Research* **2018**, *51* (3), 706–718. https://doi.org/10.1021/acs.accounts.7b00554.
25. Sawaya, M. R.; Hughes, M.; Rodriguez, J. A.; Riek, R.; Eisenberg, D. The Expanding Amyloid Family: Structure, Stability, Function, and Pathogenesis. *Cell* **2021**, *184* (19), 4857–4873. https://doi.org/10.1016/j.cell.2021.08.013.
26. Samdin, T. D.; Kreutzer, A. G.; Nowick, J. S. Exploring Amyloid Oligomers with Peptide Model Systems. *Current Opinion in Chemical Biology* **2021**, *64*, 106–115. https://doi.org/10.1016/j.cbpa.2021.05.004.
27. Jeon, J.; Yau, W.-M.; Tycko, R. Early Events in Amyloid-β Self-Assembly Probed by Time-Resolved Solid State NMR and Light Scattering. *Nature communications* **2023**, *14* (1). https://doi.org/10.1038/s41467-023-38494-6.
28. Durell, S. R.; Guy, H. R.; Arispe, N.; Rojas, E.; Pollard, H. B. Theoretical Models of the Ion Channel Structure of Amyloid Beta-Protein. *Biophysical Journal* **1994**, *67* (6), 2137–2145. https://doi.org/10.1016/s0006-3495(94)80717-9.
29. George, A.R. and Howlett, D.R. Computationally derived structural models of the β-amyloid found in Alzheimer's disease plaques and the interaction with possible aggregation inhibitors. *Biopolymers* **1999**, *50*, 733-741. https://doi.org/10.1002/(SICI)1097-0282(199912)50:7<733::AID-BIP6>3.0.CO;2-7
30. Li, L.; Darden, T. A.; Bartolotti, L.; Kominos, D.; Pedersen, L. G. An Atomic Model for the Pleated β-Sheet Structure of Aβ Amyloid Protofilaments. *Biophysical Journal* **1999**, *76* (6), 2871–2878. https://doi.org/10.1016/s0006-3495(99)77442-4.
31. Tjernberg, L. O.; Callaway, D. J. E.; Tjernberg, A.; Hahne, S.; Lilliehöök, C.; Terenius, L.; Thyberg, J.; Nordstedt, C.. A Molecular Model of Alzheimer Amyloid β-Peptide Fibril Formation. *Journal of Biological Chemistry* **1999**, *274* (18), 12619–12625. https://doi.org/10.1074/jbc.274.18.12619.

32. Tycko and coworkers later referred to the folding of Aβ described in references 31-33 as β-hairpins [Petkova, A. T.; Ishii, Y.; Balbach, J. J.; Antzutkin, O. N.; Leapman, R. D.; Delaglio, F.; Tycko, R. A Structural Model for Alzheimer's β-Amyloid Fibrils Based on Experimental Constraints from Solid State NMR. *Proceedings of the National Academy of Sciences* **2002**, *99* (26), 16742–16747. https://doi.org/10.1073/pnas.262663499.]
33. Hoyer, W.; Grönwall, C.; Jonsson, A.; Ståhl, S.; Härd, T. Stabilization of a β-Hairpin in Monomeric Alzheimer's Amyloid-β Peptide Inhibits Amyloid Formation. *Proceedings of the National Academy of Sciences* **2008**, *105* (13), 5099–5104. https://doi.org/10.1073/pnas.0711731105.
34. Fu, Z.; Van, W. E.; Smith, S. O. Anti-Parallel β-Hairpin Structure in Soluble Aβ Oligomers of Aβ40-Dutch and Aβ40-Iowa. *International Journal of Molecular Sciences* **2021**, *22* (3), 1225–1225. https://doi.org/10.3390/ijms22031225.
35. Österlund, N.; Moons, R.; Ilag, L. L.; Sobott, F.; Gräslund, A. Native Ion Mobility-Mass Spectrometry Reveals the Formation of β-Barrel Shaped Amyloid-β Hexamers in a Membrane-Mimicking Environment. *Journal of the American Chemical Society* **2019**, *141* (26), 10440–10450. https://doi.org/10.1021/jacs.9b04596.
36. Scheidt, H. A.; Morgado, I.; Huster, D. Solid-State NMR Reveals a Close Structural Relationship between Amyloid-β Protofibrils and Oligomers. *Journal of Biological Chemistry* **2012**, *287* (27), 22822–22826. https://doi.org/10.1074/jbc.m112.367474.
37. Yamaguchi, T.; Matsuzaki, K.; Hoshino, M. Transient Formation of Intermediate Conformational States of Amyloid-β Peptide Revealed by Heteronuclear Magnetic Resonance Spectroscopy. *FEBS Letters* **2011**, *585* (7), 1097–1102. https://doi.org/10.1016/j.febslet.2011.03.014.
38. Chebaro, Y.; Mousseau, N.; Derreumaux, P. Structures and Thermodynamics of Alzheimer's Amyloid-β Aβ(16−35) Monomer and Dimer by Replica Exchange Molecular Dynamics Simulations: Implication for Full-Length Aβ Fibrillation. *The Journal of Physical Chemistry B* **2009**, *113* (21), 7668–7675. https://doi.org/10.1021/jp900425e.
39. Daidone, I.; Simona, F.; Roccatano, D.; Broglia, R. A.; Tiana, G.; Colombo, G.; Di Nola, A. β-Hairpin Conformation of Fibrillogenic Peptides: Structure and α-β Transition Mechanism Revealed by Molecular Dynamics Simulations. *Proteins: Structure, Function, and Bioinformatics* **2004**, *57* (1), 198–204. https://doi.org/10.1002/prot.20178.
40. Das, P.; Murray, B.; Belfort, G. Alzheimer's Protective A2T Mutation Changes the Conformational Landscape of the Aβ1–42 Monomer Differently than Does the A2V Mutation. *Biophysical Journal* **2015**, *108* (3), 738–747. https://doi.org/10.1016/j.bpj.2014.12.013.
41. Larini, L.; Shea, J.-E. Role of β-Hairpin Formation in Aggregation: The Self-Assembly of the Amyloid-β(25–35) Peptide. *Biophysical Journal* **2012**, *103* (3), 576–586. https://doi.org/10.1016/j.bpj.2012.06.027.
42. Lin, Y.-S.; Bowman, G. R.; Beauchamp, K. A.; Pande, V. S. Investigating How Peptide Length and a Pathogenic Mutation Modify the Structural Ensemble of Amyloid Beta Monomer. *Biophysical Journal* **2012**, *102* (2), 315–324. https://doi.org/10.1016/j.bpj.2011.12.002.

43. Man, V. H.; Nguyen, P. H.; Derreumaux, P. High-Resolution Structures of the Amyloid-β 1–42 Dimers from the Comparison of Four Atomistic Force Fields. *The Journal of Physical Chemistry B* **2017**, *121* (24), 5977–5987. https://doi.org/10.1021/acs.jpcb.7b04689.
44. Mitternacht, S.; Staneva, I.; Härd, T.; Irbäck, A. Comparing the Folding Free-Energy Landscapes of Aβ42 Variants with Different Aggregation Properties. *Proteins: Structure, Function, and Bioinformatics* **2010**, n/a-n/a. https://doi.org/10.1002/prot.22775.
45. Nguyen, P. H.; Tarus, B.; Derreumaux, P. Familial Alzheimer A2 v Mutation Reduces the Intrinsic Disorder and Completely Changes the Free Energy Landscape of the Aβ1–28 Monomer. *The Journal of Physical Chemistry B* **2014**, *118* (2), 501–510. https://doi.org/10.1021/jp4115404.
46. Reddy, G.; Straub, J. E.; Thirumalai, D. Influence of Preformed Asp23–Lys28 Salt Bridge on the Conformational Fluctuations of Monomers and Dimers of Aβ Peptides with Implications for Rates of Fibril Formation. *The Journal of Physical Chemistry B* **2009**, *113* (4), 1162–1172. https://doi.org/10.1021/jp808914c.
47. Sgourakis, N. G.; Yan, Y.; McCallum, S.; Wang, C.; Garcia, A. E. The Alzheimer's Peptides Aβ40 and 42 Adopt Distinct Conformations in Water: A Combined MD / NMR Study. *Journal of molecular biology* **2007**, *368* (5), 1448–1457. https://doi.org/10.1016/j.jmb.2007.02.093.
48. Song, W.; Wang, Y.; Colletier, J.-P.; Yang, H.; Xu, Y. Varied Probability of Staying Collapsed/Extended at the Conformational Equilibrium of Monomeric Aβ40 and Aβ42. *Scientific Reports* **2015**, *5* (1). https://doi.org/10.1038/srep11024.
49. Tarus, B.; Tran, T. T.; Nasica-Labouze, J.; Sterpone, F.; Nguyen, P. H.; Derreumaux, P. Structures of the Alzheimer's Wild-Type Aβ1-40 Dimer from Atomistic Simulations. *Journal of Physical Chemistry B* **2015**, *119* (33), 10478–10487. https://doi.org/10.1021/acs.jpcb.5b05593.
50. Viet, M. H.; Nguyen, P. H.; Ngo, S. T.; Li, M. S.; Derreumaux, P. Effect of the Tottori Familial Disease Mutation (D7N) on the Monomers and Dimers of $A\beta_{40}$ and $A\beta_{42}$. **2013**, *4* (11), 1446–1457. https://doi.org/10.1021/cn400110d.
51. Yang, M.; Teplow, D. B. Amyloid β-Protein Monomer Folding: Free Energy Surfaces Reveal Alloform Specific Differences. *Journal of molecular biology* **2008**, *384* (2), 450–464. https://doi.org/10.1016/j.jmb.2008.09.039.
52. Ciudad, S.; Puig, E.; Botzanowski, T.; Meigooni, M.; Arango, A. S.; Do, J.; Mayzel, M.; Bayoumi, M.; Chaignepain, S.; Maglia, G.; Cianferani, S.; Orekhov, V.; Tajkhorshid, E.; Bardiaux, B.; Carulla, N. Aβ(1-42) Tetramer and Octamer Structures Reveal Edge Conductivity Pores as a Mechanism for Membrane Damage. *Nature Communications* **2020**, *11* (1), 3014. https://doi.org/10.1038/s41467-020-16566-1.
53. Ghosh, U.; Thurber, K. R.; Yau, W.-M.; Tycko, R. Molecular Structure of a Prevalent Amyloid-β Fibril Polymorph from Alzheimer's Disease Brain Tissue. *Proceedings of the National Academy of Sciences* **2021**, *118* (4), e2023089118. https://doi.org/10.1073/pnas.2023089118.
54. Streltsov, V. A.; Varghese, J. N.; Masters, C. L.; Nuttall, S. D. Crystal Structure of the Amyloid-β P3 Fragment Provides a Model for Oligomer Formation in Alzheimer's

Disease. *The Journal of Neuroscience* **2011**, *31* (4), 1419–1426. https://doi.org/10.1523/jneurosci.4259-10.2011.
55. Wu, J.; Blum, T. B.; Farrell, D. P.; DiMaio, F.; Abrahams, J. P.; Luo, J. Cryo-Electron Microscopy Imaging of Alzheimer's Amyloid-Beta 42 Oligomer Displayed on a Functionally and Structurally Relevant Scaffold. *Angewandte Chemie* **2021**, *60* (34), 18680–18687. https://doi.org/10.1002/anie.202104497.
56. Ball, K. A.; Phillips, A. H.; Wemmer, D. E.; Head-Gordon, T. Differences in β-Strand Populations of Monomeric Aβ40 and Aβ42. *Biophysical Journal* **2013**, *104* (12), 2714–2724. https://doi.org/10.1016/j.bpj.2013.04.056.
57. Masuda, Y.; Uemura, S.; Nakanishi, A.; Ohashi, R.; K. Takegoshi; Shimizu, T.; Takuji Shirasawa; Irie, K. Verification of the C-Terminal Intramolecular β-Sheet in Aβ42 Aggregates Using Solid-State NMR: Implications for Potent Neurotoxicity through the Formation of Radicals. *Bioorganic & Medicinal Chemistry Letters* **2008**, *18* (11), 3206–3210. https://doi.org/10.1016/j.bmcl.2008.04.060.
58. Rosenman, D. J.; Connors, C. D.; Chen, W.; Wang, C.; Garcia, A. E. Aβ Monomers Transiently Sample Oligomer and Fibril-like Configurations: Ensemble Characterization Using a Combined MD/NMR Approach. *Journal of Molecular Biology* **2013**, *425* (18), 3338–3359. https://doi.org/10.1016/j.jmb.2013.06.021.
59. Fu, Z.; Aucoin, D.; Davis, J.; Van, W. E.; Smith, S. O. Mechanism of Nucleated Conformational Conversion of Aβ42. *Biochemistry* **2015**, *54* (27), 4197–4207. https://doi.org/10.1021/acs.biochem.5b00467.
60. Yu, L.; Edalji, R.; Harlan, J. E.; Holzman, T. F.; Lopez, A. P.; Labkovsky, B.; Hillen, H.; Barghorn, S.; Ebert, U.; Richardson, P. L.; Miesbauer, L. R.; Solomon, L. R.; Bartley, D. M.; Walter, K. A.; Johnson, R. W.; Hajduk, P. J.; Olejniczak, E. T. Structural Characterization of a Soluble Amyloid β-Peptide Oligomer. *Biochemistry* **2009**, *48* (9), 1870–1877. https://doi.org/10.1021/bi802046n.
61. Tycko, R. Amyloid Polymorphism: Structural Basis and Neurobiological Relevance. *Neuron* **2015**, *86* (3), 632–645. https://doi.org/10.1016/j.neuron.2015.03.017.
62. Serpell, L. C.; Blake, C. C. F.; Fraser, P. E. Molecular Structure of a Fibrillar Alzheimer's Aβ Fragment†. *Biochemistry* **2000**, *39* (43), 13269–13275. https://doi.org/10.1021/bi000637v.
63. Han, M.; Ulrich, H. E. H. Replica Exchange Molecular Dynamics of the Thermodynamics of Fibril Growth of Alzheimer's Aβ42 Peptide. *The Journal of Chemical Physics* **2011**, *135* (6). https://doi.org/10.1063/1.3617250.
64. Larini, L.; Shea, J.-E. Role of β-Hairpin Formation in Aggregation: The Self-Assembly of the Amyloid-β(25–35) Peptide. *Biophysical Journal* **2012**, *103* (3), 576–586. https://doi.org/10.1016/j.bpj.2012.06.027.
65. Cerf, E.; Sarroukh, R.; Tamamizu-Kato, S.; Breydo, L.; Derclaye, S.; Dufrêne, Y. F.; Narayanaswami, V.; Goormaghtigh, E.; Ruysschaert, J.-M.; Raussens, V. Antiparallel β-Sheet: A Signature Structure of the Oligomeric Amyloid β-Peptide. *Biochemical Journal* **2009**, *421* (3), 415–423. https://doi.org/10.1042/bj20090379.
66. Khaled, M.; Rönnbäck, I.; Ilag, L. L.; Gräslund, A.; Strodel, B.; Österlund, N. A Hairpin Motif in the Amyloid-β Peptide Is Important for Formation of Disease-Related

Oligomers. *Journal of the American Chemical Society* **2023**, *145* (33), 18340–18354. https://doi.org/10.1021/jacs.3c03980.
67. Sarroukh, R.; Cerf, E.; Derclaye, S.; Dufrêne, Y. F.; Goormaghtigh, E.; Ruysschaert, J. M.; Raussens, V. Transformation of Amyloid β(1–40) Oligomers into Fibrils Is Characterized by a Major Change in Secondary Structure. **2011**, *68* (8), 1429–1438. https://doi.org/10.1007/s00018-010-0529-x.
68. Bhowmik, D.; Mote, K. R.; MacLaughlin, C. M.; Biswas, N.; Chandra, B.; Basu, J. K.; Walker, G. C.; Madhu, P. K.; Maiti, S. Cell-Membrane-Mimicking Lipid-Coated Nanoparticles Confer Raman Enhancement to Membrane Proteins and Reveal Membrane-Attached Amyloid-β Conformation. *ACS Nano* **2015**, *9* (9), 9070–9077. https://doi.org/10.1021/acsnano.5b03175.
69. Kłoniecki, M; Jabłonowska, A.; Poznański, J.; Langridge, J.; Hughes, C.; Campuzano, I.; Giles, K.; Dadlez, M. Ion Mobility Separation Coupled with MS Detects Two Structural States of Alzheimer's Disease Aβ1–40 Peptide Oligomers. *Journal of Molecular Biology* **2011**, *407* (1), 110–124. https://doi.org/10.1016/j.jmb.2011.01.012.
70. Lendel, C.; Bjerring, M.; Dubnovitsky, A.; Kelly, R. T.; Filippov, A.; Antzutkin, O. N.; Nielsen, N. Chr.; Härd, T. A Hexameric Peptide Barrel as Building Block of Amyloid-β Protofibrils. *Angewandte Chemie International Edition* **2014**, *53* (47), 12756–12760. https://doi.org/10.1002/anie.201406357.
71. Mastrangelo, I. A.; Ahmed, M.; Sato, T.; Liu, W.; Wang, C.; Hough, P.; Smith, S. O. High-Resolution Atomic Force Microscopy of Soluble Aβ42 Oligomers. *Journal of Molecular Biology* **2006**, *358* (1), 106–119. https://doi.org/10.1016/j.jmb.2006.01.042.
72. Zheng, W.; Tsai, M.-Y.; Chen, M.; Wolynes, P. G. Exploring the Aggregation Free Energy Landscape of the Amyloid-β Protein (1–40). *Proceedings of the National Academy of Sciences of the United States of America* **2016**, *113* (42), 11835–11840. https://doi.org/10.1073/pnas.1612362113.
73. Maity, S.; Hashemi, M.; Lyubchenko, Y. L. Nano-Assembly of Amyloid β Peptide: Role of the Hairpin Fold. *Scientific Reports* **2017**, *7* (1). https://doi.org/10.1038/s41598-017-02454-0.
74. Roychaudhuri, R.; Yang, M.; Deshpande, A.; Cole, G. M.; Frautschy, S. A.; Lomakin, A.; Benedek, G. B.; Teplow, D. B. C-Terminal Turn Stability Determines Assembly Differences between Aβ40 and Aβ42. *Journal of Molecular Biology* **2013**, *425* (2), 292–308. https://doi.org/10.1016/j.jmb.2012.11.006.
75. Sandberg, A.; Luheshi, L. M.; Söllvander, S.; de Barros, P. T.; Macao, B.; Knowles, T. P. J.; Biverstål, H.; Lendel, C.; Ekholm-Petterson, F.; Dubnovitsky, A.; Lannfelt, L.; Dobson, C. M.; Härd, T. Stabilization of Neurotoxic Alzheimer Amyloid-β Oligomers by Protein Engineering. *Proceedings of the National Academy of Sciences* **2010**, *107* (35), 15595–15600. https://doi.org/10.1073/pnas.1001740107.
76. Zhang, S.; Yoo, S.; Snyder, D. T.; Katz, B. B.; Henrickson, A.; Demeler, B; Wysocki, V. H.; Kreutzer, A. G.; Nowick, J. S. A Disulfide-Stabilized Aβ That Forms Dimers but Does Not Form Fibrils. *Biochemistry* **2022**, *61* (4), 252–264. https://doi.org/10.1021/acs.biochem.1c00739.
77. Ruttenberg, S. M.; Kreutzer, A. G.; Truex, N. L.; Nowick, J. S. β-Hairpin Alignment Alters Oligomer Formation in Aβ-Derived Peptides. *Biochemistry* **2024**. https://doi.org/10.1021/acs.biochem.3c00526.

78. Samdin, T. D.; Jones, C. R.; Guaglianone, G.; Kreutzer, A. G.; Freites, J. A.; Wierzbicki, M.; Nowick, J. S. A β-Barrel-like Tetramer Formed by a β-Hairpin Derived from Aβ. *Chemical Science* **2024**, *15* (1), 285–297. https://doi.org/10.1039/d3sc05185d.
79. Kim, B. H.; Palermo, N. Y.; Lovas, S.; Zaikova, T.; Keana, J. F. W.; Lyubchenko, Y. L. Single-Molecule Atomic Force Microscopy Force Spectroscopy Study of Aβ-40 Interactions. *Biochemistry* **2011**, *50* (23), 5154–5162. https://doi.org/10.1021/bi200147a.
80. Kreutzer, A. G.; Samdin, T. D.; Guaglianone, G.; Spencer, R. K.; Nowick, J. S. X-Ray Crystallography Reveals Parallel and Antiparallel β-Sheet Dimers of a β-Hairpin Derived from $A\beta_{16-36}$ That Assemble to Form Different Tetramers. *ACS Chemical Neuroscience* **2020**, *11* (15), 2340–2347. https://doi.org/10.1021/acschemneuro.0c00290.
81. Itoh, S. G.; Yagi-Utsumi, M.; Kato, K.; Okumura, H. Key Residue for Aggregation of Amyloid-β Peptides. *ACS Chemical Neuroscience* **2022**, *13* (22), 3139–3151. https://doi.org/10.1021/acschemneuro.2c00358.\
82. Sun, Y.; Qian, Z.; Wei, G. The Inhibitory Mechanism of a Fullerene Derivative against Amyloid-β Peptide Aggregation: An Atomistic Simulation Study. *Physical Chemistry Chemical Physics* **2016**, *18* (18), 12582–12591. https://doi.org/10.1039/c6cp01014h.
83. Urbanc, B.; Cruz, L.; Ding, F.; Sammond, D. W.; Khare, S. D.; Buldyrev, S. V.; Stanley, H. E.; Dokholyan, N. V. Molecular Dynamics Simulation of Amyloid β Dimer Formation. **2004**, *87* (4), 2310–2321. https://doi.org/10.1529/biophysj.104.040980.
84. Gu, L.; Liu, C.; Stroud, J. C.; Ngo, S.; Jiang, L.; Guo, Z. Antiparallel Triple-Strand Architecture for Prefibrillar Aβ42 Oligomers. *Journal of Biological Chemistry* **2014**, *289* (39), 27300–27313. https://doi.org/10.1074/jbc.m114.569004.
85. Sulatskaya, A. I.; Kosolapova, A. O.; Bobylev, A. G.; Belousov, M. V.; Antonets, K. S.; Sulatsky, M. I.; Kuznetsova, I. M.; Turoverov, K. K.; Stepanenko, O. V.; Nizhnikov, A. A. β-Barrels and Amyloids: Structural Transitions, Biological Functions, and Pathogenesis. *International Journal of Molecular Sciences* **2021**, *22* (21), 11316–11316. https://doi.org/10.3390/ijms222111316.
86. Arispe, N. Architecture of the Alzheimer?S AβP Ion Channel Pore. *Journal of Membrane Biology* **2004**, *197* (1), 33–48. https://doi.org/10.1007/s00232-003-0638-7.
87. Durell, S. R.; Kayed, R.; Guy, H. R. The Amyloid Concentric β-Barrel Hypothesis: Models of Amyloid Beta 42 Oligomers and Annular Protofibrils. *Proteins: Structure, Function, and Bioinformatics* **2022**. https://doi.org/10.1002/prot.26301.
88. Guy, H. R.; Durell, S. R.; Kayed, R. Theory of Concentric β-Barrel Structures: Models of Amyloid Beta 42 Oligomers, Annular Protofibrils, and Transmembrane Channels. *bioRxiv (Cold Spring Harbor Laboratory)* **2018**. https://doi.org/10.1101/499061.
89. Serra-Batiste, M.; Ninot-Pedrosa, M.; Bayoumi, M.; Gairí, M.; Maglia, G.; Carulla, N. Aβ42 Assembles into Specific β-Barrel Pore-Forming Oligomers in Membrane-Mimicking Environments. *Proceedings of the National Academy of Sciences of the*

United States of America **2016**, *113* (39), 10866–10871. https://doi.org/10.1073/pnas.1605104113.
90. Nguyen, P. H.; Campanera, J. M.; Ngo, S. T.; Loquet, A.; Derreumaux, P. Tetrameric Aβ40 and Aβ42 β-Barrel Structures by Extensive Atomistic Simulations. I. In a Bilayer Mimicking a Neuronal Membrane. *The Journal of Physical Chemistry B* **2019**, *123* (17), 3643–3648. https://doi.org/10.1021/acs.jpcb.9b01206.
91. Kreutzer, A. G.; Hamza, I. L.; Spencer, R. K.; Nowick, J. S. X-Ray Crystallographic Structures of a Trimer, Dodecamer, and Annular Pore Formed by an $A\beta_{17-36}$ β-Hairpin. *Journal of the American Chemical Society* **2016**, *138* (13), 4634–4642. https://doi.org/10.1021/jacs.6b01332.
92. Baronio, C. M.; Baldassarre, M.; Barth, A. Insight into the Internal Structure of Amyloid-β Oligomers by Isotope-Edited Fourier Transform Infrared Spectroscopy. *Physical Chemistry Chemical Physics* **2019**, *21* (16), 8587–8597. https://doi.org/10.1039/c9cp00717b.
93. Pan, J.; Han, J.; Borchers, C. H.; Konermann, L. Structure and Dynamics of Small Soluble Aβ(1–40) Oligomers Studied by Top-down Hydrogen Exchange Mass Spectrometry. *Biochemistry* **2012**, *51* (17), 3694–3703. https://doi.org/10.1021/bi3002049.
94. Sun, Y.; Kakinen, A.; Wan, X.; Moriarty, N.; Hunt, C. P. J.; Li, Y.; Andrikopoulos, N.; Nandakumar, A.; Davis, T. P.; Parish, C. L.; Song, Y.; Ke, P. C.; Ding, F. Spontaneous Formation of β-Sheet Nano-Barrels during the Early Aggregation of Alzheimer's Amyloid Beta. *Nano Today* **2021**, *38*, 101125. https://doi.org/10.1016/j.nantod.2021.101125.
95. Ma, B.; Nussinov, R. Polymorphic Triple β-Sheet Structures Contribute to Amide Hydrogen/Deuterium (H/D) Exchange Protection in the Alzheimer Amyloid β42 Peptide. *Journal of Biological Chemistry* **2011**, *286* (39), 34244–34253. https://doi.org/10.1074/jbc.m111.241141.
96. Xing, X.; Zhao, W.; Hu, D.; Kang, B.; Shi, H.; Lee, J. Y.; Ai, H. Tautomerization Effect of Histidines on Oligomer Aggregation of β-Amyloid(1–40/42) during the Early Stage: Tautomerism Hypothesis for Misfolding Protein Aggregation. *ACS Chemical Neuroscience* **2019**, *10* (5), 2602–2608. https://doi.org/10.1021/acschemneuro.9b00094.
97. Kreutzer, A. G.; Spencer, R. K.; McKnelly, K. J.; Yoo, S.; Hamza, I. L.; Salveson, P. J.; Nowick, J. S. A Hexamer of a Peptide Derived from Aβ16–36. *Biochemistry* **2017**, *56* (45), 6061–6071. https://doi.org/10.1021/acs.biochem.7b00831.
98. Kreutzer, A. G.; Yoo, S.; Spencer, R. K.; Nowick, J. S. Stabilization, Assembly, and Toxicity of Trimers Derived from Aβ. *Journal of the American Chemical Society* **2017**, *139* (2), 966–975. https://doi.org/10.1021/jacs.6b11748.
99. Kreutzer, A. G.; Guaglianone, G.; Yoo, S.; Marie, C.; Ruttenberg, S. M.; Malonis, R. J.; Tong, K.; Lin, Y.-F.; Nguyen, J. T.; Howitz, W. J.; Diab, M. N.; Hamza, I. L.; Lai, J. R.; Wysocki, V. H.; Nowick, J. S. Probing Differences among Aβ Oligomers with Two Triangular Trimers Derived from Aβ. **2023**, *120* (22). https://doi.org/10.1073/pnas.2219216120.
100. Kreutzer, A. G.; Marie, C.; Haerianardakani, S.; Guaglianone, G.; Nguyen, J.; Diab, M. N.; Yong, W. H.; Perez-Rosendahl, M.; Head, E.; Nowick, J. S. Antibodies

Raised against an Aβ Oligomer Mimic Recognize Pathological Features in Alzheimer's Disease and Associated Amyloid-Disease Brain Tissue. *ACS Central Science* **2023**. https://doi.org/10.1021/acscentsci.3c00592.
101. Salveson, P. J.; Spencer, R. K.; Kreutzer, A. G.; Nowick, J. S. X-Ray Crystallographic Structure of a Compact Dodecamer from a Peptide Derived from $A\beta_{16-36}$. *Organic Letters* **2017**, *19* (13), 3462–3465. https://doi.org/10.1021/acs.orglett.7b01445.
102. Samdin, T. D.; Wierzbicki, M.; Kreutzer, A. G.; Howitz, W. J.; Valenzuela, M.; Smith, A.; Sahrai, V.; Truex, N. L.; Klun, M.; Nowick, J. S. Effects of N-Terminal Residues on the Assembly of Constrained β-Hairpin Peptides Derived from Aβ. *Journal of the American Chemical Society* **2020**, *142* (26), 11593–11601. https://doi.org/10.1021/jacs.0c05186.
103. Spencer, R. K.; Li, H.; Nowick, J. S. X-Ray Crystallographic Structures of Trimers and Higher-Order Oligomeric Assemblies of a Peptide Derived from $A\beta_{17-36}$. *Journal of the American Chemical Society* **2014**, *136* (15), 5595–5598. https://doi.org/10.1021/ja5017409.
104. Ahmed, M.; Davis, J.; Aucoin, D.; Sato, T.; Ahuja, S.; Aimoto, S.; Elliott, J. I.; Van Nostrand, W. E.; Smith, S. O. Structural Conversion of Neurotoxic Amyloid-β1–42 Oligomers to Fibrils. *Nature Structural & Molecular Biology* **2010**, *17* (5), 561–567. https://doi.org/10.1038/nsmb.1799.
105. Yang, T.; Li, S.; Xu, H.; Walsh, D. M.; Selkoe, D. J. Large Soluble Oligomers of Amyloid β-Protein from Alzheimer Brain Are Far Less Neuroactive than the Smaller Oligomers to Which They Dissociate. *The Journal of Neuroscience* **2016**, *37* (1), 152–163. https://doi.org/10.1523/jneurosci.1698-16.2016.
106. Hillen, H.; Barghorn, S.; Striebinger, A.; Labkovsky, B.; Müller, R.; Nimmrich, V.; Nolte, M. W.; Perez-Cruz, C.; van der Auwera, I.; Van Leuven, F.; van Gaalen, M.; Bespalov, A. Y.; Schoemaker, H.; Sullivan, J. P.; Ebert, U. Generation and Therapeutic Efficacy of Highly Oligomer-Specific β-Amyloid Antibodies. *The Journal of Neuroscience* **2010**, *30* (31), 10369–10379. https://doi.org/10.1523/jneurosci.5721-09.2010.
107. Manelli, A. M.; Bulfinch, L.; Sullivan, P. M.; LaDu, M. J.. Aβ42 Neurotoxicity in Primary Co-Cultures: Effect of ApoE Isoform and Aβ Conformation. *Neurobiology of Aging* **2007**, *28* (8), 1139–1147. https://doi.org/10.1016/j.neurobiolaging.2006.05.024.
108. Liao, M. Q.; Tzeng, Y. J.; Chang, L. Y. X.; Huang, H. B.; Lin, T. H.; Chyan, C. L.; Chen, Y. C. The Correlation between Neurotoxicity, Aggregative Ability and Secondary Structure Studied by Sequence Truncated Aβ Peptides. *FEBS Letters* **2007**, *581* (6), 1161–1165. https://doi.org/10.1016/j.febslet.2007.02.026.
109. Matsushima, Y.; Yanagita, R. C.; Irie, K. Control of the Toxic Conformation of Amyloid β42 by Intramolecular Disulfide Bond Formation. *Chemical Communications* **2020**, *56* (29), 4118–4121. https://doi.org/10.1039/d0cc01053g.
110. Bode, D. C.; Freeley, M.; Nield, J.; Palma, M.; Viles, J. H. Amyloid-β Oligomers Have a Profound Detergent-like Effect on Lipid Membrane Bilayers, Imaged by Atomic Force and Electron Microscopy. *Journal of Biological Chemistry* **2019**, *294* (19), 7566–7572. https://doi.org/10.1074/jbc.ac118.007195.

111. Mrdenovic, D.; Pieta, I. S.; Nowakowski, R.; Kutner, W.; Lipkowski, J.; Pieta, P. Amyloid β Interaction with Model Cell Membranes – What Are the Toxicity-Defining Properties of Amyloid β? *International Journal of Biological Macromolecules* **2022**, *200*, 520–531. https://doi.org/10.1016/j.ijbiomac.2022.01.117.
112. Liu, P.; Reed, M. N.; Kotilinek, L. A.; Grant, M. K. O.; Forster, C. L.; Qiang, W.; Shapiro, S. L.; Reichl, J. H.; Chiang, A. C. A.; Jankowsky, J. L.; Wilmot, C. M.; Cleary, J. P.; Zahs, K. R.; Ashe, K. H. Quaternary Structure Defines a Large Class of Amyloid-β Oligomers Neutralized by Sequestration. *Cell Reports* **2015**, *11* (11), 1760–1771. https://doi.org/10.1016/j.celrep.2015.05.021.
113. Madhu, P.; Das, D.; Mukhopadhyay, S. Conformation-Specific Perturbation of Membrane Dynamics by Structurally Distinct Oligomers of Alzheimer's Amyloid-β Peptide. *Physical Chemistry Chemical Physics* **2021**, *23* (16), 9686–9694. https://doi.org/10.1039/d0cp06456d.
114. McKnelly, K. J.; Kreutzer, A. G.; Howitz, W. J.; Haduong, K.; Yoo, S.; Hart, C.; Nowick, J. S. Effects of Familial Alzheimer's Disease Mutations on the Assembly of a β-Hairpin Peptide Derived from $A\beta_{16-36}$. *Biochemistry* **2022**, *61* (6), 446–454. https://doi.org/10.1021/acs.biochem.1c00664.
115. Ngo, S. T.; Nguyen, P. H.; Derreumaux, P. Stability of Aβ11–40 Trimers with Parallel and Antiparallel β-Sheet Organizations in a Membrane-Mimicking Environment by Replica Exchange Molecular Dynamics Simulation. *The Journal of Physical Chemistry B* **2020**, *124* (4), 617–626. https://doi.org/10.1021/acs.jpcb.9b10982.
116. Press-Sandler, O.; Miller, Y. Molecular Insights into the Primary Nucleation of Polymorphic Amyloid β Dimers in DOPC Lipid Bilayer Membrane. *Protein Science* **2022**, *31* (5). https://doi.org/10.1002/pro.4283.
117. Sepehri, A.; Lazaridis, T. Putative Structures of Membrane-Embedded Amyloid β Oligomers. *ACS Chemical Neuroscience* **2022**, *14* (1), 99–110. https://doi.org/10.1021/acschemneuro.2c00535.
118. Strodel, B.; Lee, J. W. L.; Whittleston, C. S.; Wales, D. J. Transmembrane Structures for Alzheimer's $A\beta_{1-42}$ Oligomers. *Journal of the American Chemical Society* **2010**, *132* (38), 13300–13312. https://doi.org/10.1021/ja103725c.
119. Henry, S.; Vignaud, H.; Bobo, C.; Decossas, M.; Lambert, O.; Harte, E.; Alves, I. D.; Cullin, C.; Lecomte, S. Interaction of Aβ(1-42) Amyloids with Lipids Promotes "Off-Pathway" Oligomerization and Membrane Damage. *Biomacromolecules* **2015**, *16* (3), 944–950. https://doi.org/10.1021/bm501837w.
120. Ladiwala, A. R. A.; Litt, J.; Kane, R. S.; Aucoin, D.; Smith, S. O.; Ranjan, S.; Davis, J. E.; Van, W. E.; Tessier, P. M. Conformational Differences between Two Amyloid β Oligomers of Similar Size and Dissimilar Toxicity. *Journal of Biological Chemistry* **2012**, *287* (29), 24765–24773. https://doi.org/10.1074/jbc.m111.329763.
121. Morel, B.; Carrasco, M. P.; Jurado, S.; Marco, C.; Conejero-Lara, F. Dynamic Micellar Oligomers of Amyloid Beta Peptides Play a Crucial Role in Their Aggregation Mechanisms. *Physical Chemistry Chemical Physics* **2018**, *20* (31), 20597–20614. https://doi.org/10.1039/C8CP02685H.

122. Takano, K.; Endo, S.; Mukaiyama, A.; Chon, H.; Matsumura, H.; Koga, Y.; Kanaya, S. Structure of Amyloid Beta Fragments in Aqueous Environments. *FEBS Journal* **2006**, *273* (1), 150–158. https://doi.org/10.1111/j.1742-4658.2005.05051.x.
123. Côté, S.; Derreumaux, P.; Mousseau, N. Distinct Morphologies for Amyloid Beta Protein Monomer: Aβ1–40, Aβ1–42, and Aβ1–40(D23N). *Journal of Chemical Theory and Computation* **2011**, *7* (8), 2584–2592. https://doi.org/10.1021/ct1006967.
124. Lam, A. R.; Teplow, D. B.; Stanley, H. E.; B. Urbanc. Effects of the Arctic ($E^{22}\rightarrow G$) Mutation on Amyloid β-Protein Folding: Discrete Molecular Dynamics Study. *Journal of the American Chemical Society* **2008**, *130* (51), 17413–17422. https://doi.org/10.1021/ja804984h.
125. Lv, Z.; Roychaudhuri, R.; Condron, M. M.; Teplow, D. B.; Lyubchenko, Y. L. Mechanism of Amyloid β−Protein Dimerization Determined Using Single−Molecule AFM Force Spectroscopy. *Scientific Reports* **2013**, *3* (1). https://doi.org/10.1038/srep02880.
126. Morimoto, A.; Irie, K.; Murakami, K.; Masuda, Y.; Ohigashi, H.; Nagao, M.; Fukuda, H.; Shimizu, T.; Shirasawa, T. Analysis of the Secondary Structure of β-Amyloid (Aβ42) Fibrils by Systematic Proline Replacement. *Journal of Biological Chemistry* **2004**, *279* (50), 52781–52788. https://doi.org/10.1074/jbc.m406262200.
127. Bugiani, O.; Giaccone, G.; Rossi, G.; Mangieri, M.; Capobianco, R.; Morbin, M.; Mazzoleni, G.; Cupidi, C.; Marcon, G.; Giovagnoli, A.; Bizzi, A.; Di Fede, G.; Puoti, G.; Carella, F.; Salmaggi, A.; Romorini, A.; Patruno, G. M.; Magoni, M.; Padovani, A.; Tagliavini, F. Hereditary Cerebral Hemorrhage with Amyloidosis Associated with the E693K Mutation of APP. *Archives of Neurology* **2010**, *67* (8). https://doi.org/10.1001/archneurol.2010.178.
128. Grabowski, T. J.; Cho, H. S.; Vonsattel, J. P.; Rebeck, G. W.; Greenberg, S. M. Novel amyloid precursor protein mutation in an Iowa family with dementia and severe cerebral amyloid angiopathy *Annals of Neurology* **2001**, 49, 697– 705. https://doi.org/10.1002/ana.1009.
129. Kamino, K.; Orr, H. T.; Payami, H.; Wijman, E. M.; Pulst, S. M.; Anderson, L.; O'dahl, S.; Nemens, E.; White, J. A.1992, Linkage and mutational analysis of familial Alzheimer disease kindreds for the APP gene region Am. J. Hum. Genet. 51, 998– 1014
130. Levy, E., Carman, M. D., Fernandez-Madrid, I. J., Power, M. D., Lieberburg, I., van Duinen, S. G., Bots, G. T. A. M., Luyendijk, W., and Frangione, B. Mutation of the Alzheimer's disease amyloid gene in hereditary cerebral hemorrhage, Dutch type Science 1, *Science* **1990**, 1124– 1126. https://www.science.org/doi/10.1126/science.2111584.
131. Messa, M.; Colombo, L.; Del Favero, E.; Cantù, L.; Stoilova, T.; Cagnotto, A.; Rossi, A.; Morbin, M.; Di Fede, G.; Tagliavini, F.; Salmona, M. The Peculiar Role of the A2V Mutation in Amyloid-β (Aβ) 1–42 Molecular Assembly. **2014**, *289* (35), 24143–24152. https://doi.org/10.1074/jbc.m114.576256.
132. Wakutani, Y. Novel Amyloid Precursor Protein Gene Missense Mutation (D678N) in Probable Familial Alzheimer's Disease. *Journal of Neurology,*

Neurosurgery & Psychiatry **2004**, *75* (7), 1039–1042. https://doi.org/10.1136/jnnp.2003.010611.
133. Cruz, L.; Rao, J. S.; Teplow, D. B.; B. Urbanc. Dynamics of Metastable β-Hairpin Structures in the Folding Nucleus of Amyloid β-Protein. *The Journal of Physical Chemistry B* **2012**, *116* (22), 6311–6325. https://doi.org/10.1021/jp301619v.
134. Rajpoot, J.; Crooks, E. J.; Irizarry, B. A.; Amundson, A.; Van Nostrand, W. E.; Smith, S. O. Insights into Cerebral Amyloid Angiopathy Type 1 and Type 2 from Comparisons of the Fibrillar Assembly and Stability of the Aβ40-Iowa and Aβ40-Dutch Peptides. *Biochemistry* **2022**, *61* (12), 1181–1198. https://doi.org/10.1021/acs.biochem.1c00781.
135. Kalimo, H.; Lalowski, M.; Bogdanovic, N.; Philipson, O.; Bird, T. D.; Nochlin, D.; Schellenberg, G. D.; Brundin, R.; Olofsson, T.; Soliymani, R.; Baumann, M.; Wirths, O.; Bayer, T. A.; Nilsson, L.; Basun, H.; Lannfelt, L.; Ingelsson, M. The Arctic AβPP Mutation Leads to Alzheimer's Disease Pathology with Highly Variable Topographic Deposition of Differentially Truncated Aβ. *Acta neuropathologica communications* **2013**, *1* (1). https://doi.org/10.1186/2051-5960-1-60.
136. Ono, K.; Condron, M. M.; Teplow, D. B. Effects of the English (H6R) and Tottori (D7N) Familial Alzheimer Disease Mutations on Amyloid β-Protein Assembly and Toxicity. *Journal of Biological Chemistry* **2010**, *285* (30), 23186–23197. https://doi.org/10.1074/jbc.m109.086496.
137. Whalen, B. M.; Selkoe, D. J.; Hartley, D. M. Small Non-Fibrillar Assemblies of Amyloid β-Protein Bearing the Arctic Mutation Induce Rapid Neuritic Degeneration. *Neurobiology of Disease* **2005**, *20* (2), 254–266. https://doi.org/10.1016/j.nbd.2005.03.007.
138. Yang, X.; Meisl, G.; Frohm, B.; Thulin, E.; Knowles, T. P. J.; Linse, S. On the Role of Sidechain Size and Charge in the Aggregation of a *β* 42 with Familial Mutations. *Proceedings of the National Academy of Sciences of the United States of America* **2018**, *115* (26). https://doi.org/10.1073/pnas.1803539115.
139. Firouzi, R.; Noohi, B. Identification of Key Stabilizing Interactions of Amyloid-*β* Oligomers Based on Fragment Molecular Orbital Calculations on Macrocyclic *β*-Hairpin Peptides. *Proteins: Structure, Function, and Bioinformatics* **2021**, *90* (1), 229–238. https://doi.org/10.1002/prot.26212.
140. Nishitsuji, K.; Tomiyama, T.; Ishibashi, K.; Ito, K.; Teraoka, R.; Lambert, M. P.; Klein, W. L.; Mori, H. The E693Δ Mutation in Amyloid Precursor Protein Increases Intracellular Accumulation of Amyloid β Oligomers and Causes Endoplasmic Reticulum Stress-Induced Apoptosis in Cultured Cells. *The American Journal of Pathology* **2009**, *174* (3), 957–969. https://doi.org/10.2353/ajpath.2009.080480.
141. Chen, W. T.; Chen, H.; Lin, Y. T.; Chang, W. H.; Huang, H. T.; Liao, J. Y.; Chang, Y.; Hsieh, Y. F.; Cheng, C. Y.; Liu, H. C.; Chen, Y.; Cheng, I. H. Amyloid-Beta (Aβ) D7H Mutation Increases Oligomeric Aβ42 and Alters Properties of Aβ-Zinc/Copper Assemblies. *PLOS ONE* **2012**, *7* (4), e35807–e35807. https://doi.org/10.1371/journal.pone.0035807.
142. Hori, Y.; Hashimoto, T.; Wakutani, Y.; Urakami, K.; Nakashima, K.; Condron, M. M.; Tsubuki, S.; Saido, T. C.; Teplow, D. B.; Iwatsubo, T. The Tottori (D7N) and English (H6R) Familial Alzheimer Disease Mutations Accelerate Aβ Fibril Formation

without Increasing Protofibril Formation. *Journal of Biological Chemistry* **2006**, *282* (7), 4916–4923. https://doi.org/10.1074/jbc.m608220200.
143. Truong, P. M.; Viet, M. H.; Nguyen, P. H.; Hu, C.-K.; Li, M. S.. Effect of Taiwan Mutation (D7H) on Structures of Amyloid-β Peptides: Replica Exchange Molecular Dynamics Study. *The Journal of Physical Chemistry B* **2014**, *118* (30), 8972–8981. https://doi.org/10.1021/jp503652s.
144. Shi, H.; Wang, L.; Yao, Z.; Lee, J. Y.; Guo, W. Role of the English (H6R) Mutation on the Structural Properties of Aβ40 and Aβ42 Owing to the Histidine Tautomeric Effect. *ACS Chemical Neuroscience* **2021**, *12* (14), 2705–2711. https://doi.org/10.1021/acschemneuro.1c00355.
145. Diomede, L.; Di Fede, G.; Romeo, M.; Bagnati, R.; Ghidoni, R.; Fiordaliso, F; Salio, M.; Rossi, A.; Catania, M.; Paterlini, A.; Benussi, L.; Bastone, A.; Stravalaci, M.; Gobbi, M.; Tagliavini, F.; Salmona, M. Expression of A2V-Mutated Aβ in Caenorhabditis Elegans Results in Oligomer Formation and Toxicity. *Neurobiology of Disease* **2014**, *62*, 521–532. https://doi.org/10.1016/j.nbd.2013.10.024.
146. Howitz, W. J.; Guaglianone, G.; McKnelly, K. J.; Haduong, K.; Ashby, S. N.; Laayouni, M.; Nowick, J. S. Macrocyclic Peptides Derived from Familial Alzheimer's Disease Mutants Show Charge-Dependent Oligomeric Assembly and Toxicity. *ACS Chemical Neuroscience* **2022**, *13* (6), 714–720. https://doi.org/10.1021/acschemneuro.1c00833.
147. Seuma, M.; Lehner, B.; Bolognesi, B. An Atlas of Amyloid Aggregation: The Impact of Substitutions, Insertions, Deletions and Truncations on Amyloid Beta Fibril Nucleation. *Nature Communications* **2022**, *13* (1). https://doi.org/10.1038/s41467-022-34742-3.
148. Mantile, F.; Prisco, A. Vaccination against β-Amyloid as a Strategy for the Prevention of Alzheimer's Disease. *Biology* **2020**, *9* (12), 425. https://doi.org/10.3390/biology9120425.
149. Bitencourt, A. L. B.; Campos, R. M.; Cline, E. N.; Klein, W. L.; Sebollela, A. Antibody Fragments as Tools for Elucidating Structure-Toxicity Relationships and for Diagnostic/Therapeutic Targeting of Neurotoxic Amyloid Oligomers. *International Journal of Molecular Sciences* **2020**, *21* (23), 8920. https://doi.org/10.3390/ijms21238920.
150. Hong, W.; Wang, Z.; Liu, W.; O'Malley, T. T.; Jin, M.; Willem, M.; Haass, C.; Frosch, M. P.; Walsh, D. M. Diffusible, Highly Bioactive Oligomers Represent a Critical Minority of Soluble Aβ in Alzheimer's Disease Brain. *Acta Neuropathologica* **2018**, *136* (1), 19–40. https://doi.org/10.1007/s00401-018-1846-7.
151. Lacorte, E.; Ancidoni, A.; Zaccaria, V.; Remoli, G.; Tariciotti, L.; Bellomo, G.; Sciancalepore, F.; Corbo, M.; Lombardo, F. L.; Bacigalupo, I.; Canevelli, M.; Piscopo, P.; Vanacore, N. Safety and Efficacy of Monoclonal Antibodies for Alzheimer's Disease: A Systematic Review and Meta-Analysis of Published and Unpublished Clinical Trials. *Journal of Alzheimer's Disease* **2022**, *87* (1), 101–129. https://doi.org/10.3233/JAD-220046.
152. Krafft, G. A.; Jerecic, J.; Siemers, E.; Cline, E. N. ACU193: An Immunotherapeutic Poised to Test the Amyloid β Oligomer Hypothesis of

Alzheimer's Disease. *Frontiers in Neuroscience* **2022**, *16*. https://doi.org/10.3389/fnins.2022.848215.
153. Viola, K. L.; Bicca, M. A.; Bebenek, A. M.; Kranz, D. F.; Nandwana, V.; Waters, E. A.; Haney, C. R.; Lee, M. P.; Gupta, A.; Brahmbhatt, Z.; Huang, W.; Chang, T.-T.; Peck, A.; Valdez, C.; Dravid, V. P.; William. The Therapeutic and Diagnostic Potential of Amyloid β Oligomers Selective Antibodies to Treat Alzheimer's Disease. **2022**, *15*. https://doi.org/10.3389/fnins.2021.768646.
154. Bakrania, P.; Hall, G.; Bouter, Y.; Bouter, C.; Beindorff, N.; Cowan, R.; Davies, S.; Price, J.; Mpamhanga, C.; Love, E.; Matthews, D.; Carr, M. D.; Bayer, T. A. Discovery of a Novel Pseudo β-Hairpin Structure of N-Truncated Amyloid-β for Use as a Vaccine against Alzheimer's Disease. *Molecular Psychiatry* **2021**. https://doi.org/10.1038/s41380-021-01385-7
155. Kreutzer, A. G.; Malonis, R. J.; Marie, C.; Tong, K.; Guaglianone, G.; Nguyen, J. T.; Diab, M. N.; Lai, J. R.; Nowick, J. S. Generation and Study of Antibodies against Two Triangular Trimers Derived from Aβ. *Peptide Science* **2023**. https://doi.org/10.1002/pep2.24333.
156. Yu, H. J.; Dickson, S. P.; Wang, P.; Chiu, M.; Huang, C.; Chang, C.; Liu, H.; Hendrix, S.; Dodart, J-C.; Verma, A.; Wang, C. Y.; Cummings, J. L. Safety, Tolerability, Immunogenicity, and Efficacy of UB-311 in Participants with Mild Alzheimer's Disease: A Randomised, Double-Blind, Placebo-Controlled, Phase 2a Study. *EBioMedicine* **2023**, *94*, 104665–104665. https://doi.org/10.1016/j.ebiom.2023.104665.
157. Zhai, Z.; Kong, F.; Zhu, Z.; Dai, J.; Cai, J.; Xie, D.; Shen, Y.; Xu, Y.; Sun, T. Effect and Potential Mechanism of Immunotherapy on Cognitive Deficits in Animal Models of Alzheimer's Disease: A Systematic Review and Meta-Analysis. *The American Journal of Geriatric Psychiatry* **2023**. https://doi.org/10.1016/j.jagp.2023.11.011.
158. Kollmer, M.; Close, W.; Funk, L.; Rasmussen, J.; Bsoul, A.; Schierhorn, A.; Schmidt, M.; Sigurdson, C. J.; Jucker, M.; Fändrich, M. Cryo-EM Structure and Polymorphism of Aβ Amyloid Fibrils Purified from Alzheimer's Brain Tissue. *Nature Communications* **2019**, *10* (1). https://doi.org/10.1038/s41467-019-12683-8.

Chapter 2[a]

β-Hairpin Alignment Alters Oligomer Formation in Aβ-Derived Peptides

2.1 Preface to Chapter 2

Chapter 2 describes the design, synthesis, and oligomerization of two cyclic β-hairpin peptides designed to mimic Aβ β-hairpins spanning Aβ residues 17–36 and 17–35, respectively.[A] This chapter is a comparison of these two peptides, Aβm$_{17–36}$ and Aβm$_{17–35}$, that demonstrates how β-hairpin alignment can affect oligomerization. The results presented in this chapter suggest that the adoption of a variety of β-hairpin conformations by Aβ peptides could contribute to the observed heterogeneity among Aβ oligomer populations. This chapter was written alongside my advisor Professor James Nowick and contains research performed by myself, Dr. Adam Kreutzer, and Professor Nicholas Truex. We thank The Advanced Light Source for allowing the acquisition of crystallographic data. Beamline 5.0.2 of the Advanced Light Source, a DOE Office of Science User Facility under Contract No. DE-AC02-05CH11231, is supported in part by the ALS-ENABLE program funded by the National Institutes of Health, National Institute of General Medical Sciences, grant P30 GM124169-01. We also thank the National Institutes of Health (NIH), National Institute on Aging (NIA) for funding this research through grant AG072587 afforded to James Nowick.

[a] This chapter is adapted from Ruttenberg, S.M.; Kreutzer, A.G.; Truex, N.L.; Nowick, J.S. β-Hairpin Alignment Alters Oligomer Formation in Aβ-Derived Peptides. *Biochem.*, **2024**, 63 (2), 212-218, DOI:10.1021/acs.biochem.3c00526.

2.2 Introduction

Amyloid-β (Aβ) is intrinsically disordered and can adopt myriad conformations, including β-sheets, α-helices, and a variety of β-hairpins.[1-18] These secondary structures can direct the formation of toxic Aβ assemblies implicated in Alzheimer's disease (AD).[4,6,9,11,12,15-18] Several studies have demonstrated that toxic Aβ oligomers consist of β-hairpin building blocks.[4,6,9,12,19] Multiple β-hairpins have been reported for Aβ that differ in the alignment of the β-strands and the residues they contain.[1,4,6-13,18,19] The role that β-hairpin alignment plays in the formation and heterogeneity of oligomers of Aβ is poorly understood. Atomic-level analysis of these oligomers is necessary to better understand the molecular basis of AD, but the transience of Aβ oligomers makes characterization difficult.

To better study these elusive Aβ oligomers, our laboratory has developed peptide model systems consisting of conformationally constrained β-hairpin peptides derived from Aβ.[20-27] These model systems have provided a variety of high-resolution structures of oligomeric assemblies that cannot be achieved from oligomers formed by Aβ itself. In the current study, we use two similar model peptides to explore the effect of β-hairpin alignment on the assembly of peptides derived from Aβ. Aβm$_{17–36}$ and Aβm$_{17–35}$ mimic two different β-hairpins that Aβ can form, the Aβ$_{17–36}$ and Aβ$_{17–35}$ β-hairpins, respectively.[13,18,19]

Aβm$_{17–36}$ and Aβm$_{17–35}$ differ in the alignment of the β-strands that comprise each peptide. In both peptides, residues 17–23 constitute one of the β-strands. In Aβm$_{17–36}$, residues 30–36 constitute the other β-strand, while in Aβm$_{17–35}$, residues 29–35 constitute the other β-strand (Figure 1). This difference results in a different alignment of the peptide strands, with the bottom strand of Aβm$_{17–36}$ shifted by one amino acid toward the C-terminus in comparison to Aβm$_{17–35}$. Thus, Leu$_{17}$ is across from Val$_{36}$ in Aβm$_{17–36}$, while

Leu$_{17}$ is across from Met$_{35}$ in Aβm$_{17-35}$. This shift changes the hydrogen-bonded pairs of the residues within the hairpin as well as the surface on which the side chains are displayed. The change in facial arrangement is illustrated by Figure 1, with the even-numbered side chains (green) being displayed on the "top" face in Aβm$_{17-36}$ and the "bottom" face in Aβm$_{17-35}$.

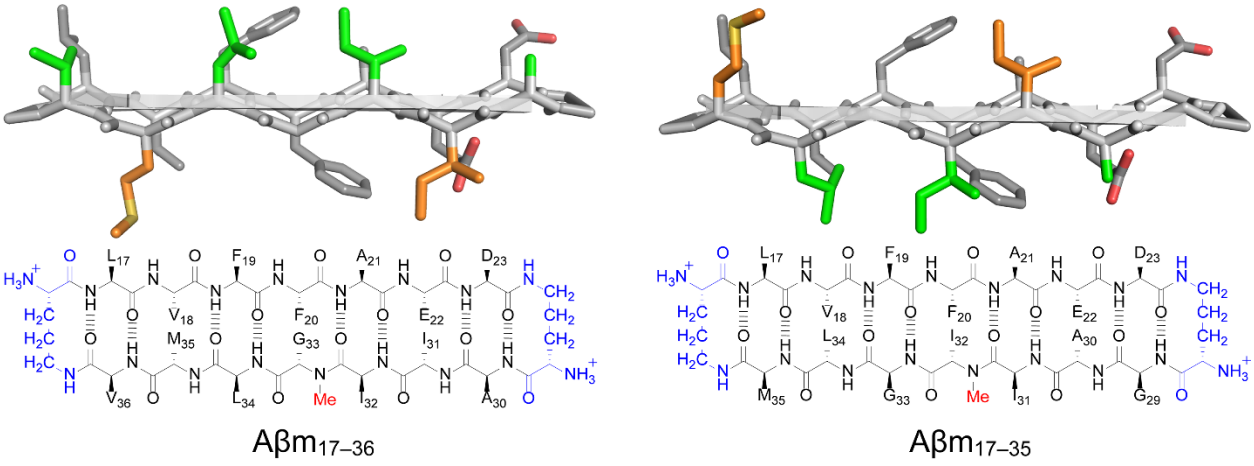

Figure 2.1. Chemical drawings (bottom) and cartoon representations (top) of Aβm$_{17-36}$ and Aβm$_{17-35}$. In the chemical drawings, the δ-linked ornithine turn units are shown in blue and the *N*-methyl group is shown in red. In the cartoon representations, the residues in Aβm$_{17-35}$ are colored to match those in Aβm$_{17-36}$, indicating the differences between the faces of Aβm$_{17-36}$ and Aβm$_{17-35}$.

Notably, the chemical compositions of Aβm$_{17-36}$ and Aβm$_{17-35}$ are almost identical — Aβm$_{17-36}$ contains Val$_{36}$ whereas Aβm$_{17-35}$ contains Gly$_{29}$. The similarity of Aβm$_{17-36}$ and Aβm$_{17-35}$ makes them good candidates for exploring how β-hairpin alignment, and thus the facial arrangement of residues, affects oligomeric assembly. In this study, we compare Aβm$_{17-36}$ and Aβm$_{17-35}$ and demonstrate that the alignment of the β-hairpin can affect the assembly of peptides derived from Aβ.

2.3 Design of the Model System

Aβm$_{17–36}$ and Aβm$_{17–35}$ are cyclic hexadecapeptides consisting of two heptapeptide β-strands (Aβ$_{17–23}$ and Aβ$_{30–36}$ or Aβ$_{29–35}$) connected by two δ-linked ornithine turn units that promote a β-hairpin-like conformation. The peptides also contain an *N*-methyl group on Gly$_{33}$ (Aβm$_{17–36}$) or Ile$_{32}$ (Aβm$_{17–35}$) to attenuate aggregation through intermolecular hydrogen bond formation. These features facilitate the formation of well-defined oligomers that, unlike oligomers of full-length Aβ, are amenable to high-resolution structural characterization through X-ray crystallography.

Aβm$_{17–36}$ is designed to display the side chains of Val$_{36}$, Leu$_{34}$, Ile$_{32}$, and Ala$_{30}$ on the same face of the β-hairpin as the side chains of Leu$_{17}$, Phe$_{19}$, Ala$_{21}$, and Asp$_{23}$ (the LFAD face). The side chains of Met$_{35}$, *N*-methyl-Gly$_{33}$, and Ile$_{31}$, as well as the side chains of Val$_{18}$, Phe$_{20}$, and Glu$_{22}$, are in turn, displayed on the opposite face (the VFE face). Aβm$_{17–35}$ is designed to display the side chains of Met$_{35}$, Gly$_{33}$, Ile$_{31}$, and Gly$_{29}$ on the LFAD face and the side chains of Leu$_{34}$, *N*-methyl-Ile$_{32}$, and Ala$_{30}$ on the VFE face. Figure 1 illustrates these differences through the colors of the side chains (green and orange). While both peptides primarily consist of hydrophobic residues, the differences between the faces of Aβm$_{17–36}$ and Aβm$_{17–35}$ lead to the formation of different oligomeric assemblies.

2.4 Assembly by SDS-PAGE

Aβm$_{17–36}$ and Aβm$_{17–35}$ were subjected to sodium dodecyl sulfate-polyacrylamide gel electrophoresis (SDS-PAGE) to evaluate their propensity to oligomerize. When a 200 μM solution of Aβm$_{17–36}$ is subjected to SDS-PAGE and visualized by silver staining, a ladder of seven bands is observed (Figure 2). The bands appear to be evenly separated by about 2 kDa, which is consistent with the molecular weight of the monomer (1.76 kDa). The lowest

molecular weight band corresponds to either monomer or dimer, and the subsequent bands correspond to either dimer through heptamer, or trimer through octamer. The ladderlike appearance suggests that the oligomers are formed by sequential addition of $A\beta m_{17-36}$ monomers. The intensities of the bands indicate that the smallest species (monomer or dimer) predominates, and that the oligomers corresponding to the second, fourth, fifth, and sixth bands may be more stable than those corresponding to the third. Fewer bands are observed with decreasing concentration, suggesting that oligomer formation is concentration dependent. Alternatively, the larger oligomers may still be present at lower concentrations, but not abundant enough to reach the sensitivity limit of the silver stain.

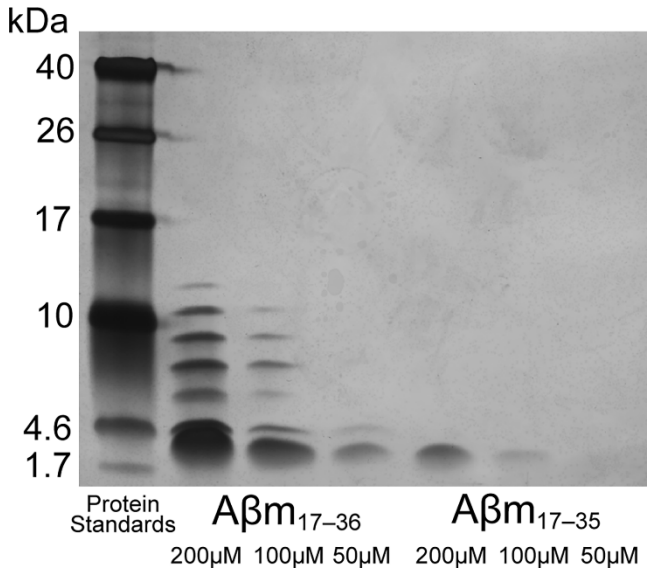

Figure 2.2. Silver-stained SDS-PAGE gel of $A\beta m_{17-36}$ and $A\beta m_{17-35}$.

To our knowledge, the periodic ladderlike oligomerization exhibited by $A\beta m_{17-36}$ has not been observed for other Aβ peptides in SDS-PAGE. $A\beta_{1-42}$ typically exhibits prominent monomer, trimer, and tetramer bands in SDS-PAGE, while $A\beta_{1-40}$ typically exhibits predominantly a monomer band.[28-30] Ladders of oligomers are observed in SDS-

PAGE when $A\beta_{1-40}$ or $A\beta_{1-42}$ are subjected to photo-induced cross-linking of unmodified proteins (PICUP).[28-29] Our laboratory has also observed a ladder of oligomers upon TCEP treatment of an $A\beta_{1-42}$ peptide containing an intramolecular disulfide bond.[31,32]

In contrast to $A\beta m_{17-36}$, $A\beta m_{17-35}$ migrates as a single diffuse band at molecular weights consistent with monomer or dimer in SDS-PAGE (Figure 2). $A\beta m_{17-35}$ exhibits fainter bands than $A\beta m_{17-36}$ at the same concentrations. Staining with Bio-Rad fluorescent stains Flamingo and Oriole also showed slightly weaker bands for $A\beta m_{17-35}$ compared to $A\beta m_{17-36}$ (data not shown). The decreased intensity of $A\beta m_{17-35}$ with both silver staining and fluorescent stains might reflect a greater propensity of $A\beta m_{17-35}$ to diffuse out of the gel during the staining process or lower solubility of $A\beta m_{17-35}$ leading to poorer penetration into the gel.

2.5 X-ray Crystallography

$A\beta m_{17-36}$ and $A\beta m_{17-35}$ both proved amenable to structural elucidation by X-ray crystallography (Figure 3). $A\beta m_{17-36}$ afforded crystals under conditions used previously for a homologue containing ornithine in place of Met_{35} (HEPES buffer and Jeffamine M-600).[33] $A\beta m_{17-35}$ afforded crystals from a buffer consisting of bicine and Trisma and a mixture of ethylene glycol oligomers. Diffraction data for crystals of $A\beta m_{17-36}$ were collected to 2.05 Å in-house on a Rigaku Micromax-007HF X-ray diffractometer equipped with a copper anode. Diffraction data for crystals of $A\beta m_{17-35}$ were collected to 1.52 Å on the synchrotron at the Advanced Light Source at Lawrence Berkeley National Laboratory. The X-ray crystallographic phases of $A\beta m_{17-36}$ were solved by soaking the crystals in potassium iodide to incorporate iodide ions into the crystal lattice, and then performing single-wavelength anomalous diffraction (SAD) phasing. The X-ray crystallographic phases of

Aβm$_{17-35}$ were solved using molecular replacement with an all-alanine model of a related β-hairpin peptide as a search model (PDB 5W4H).[34]

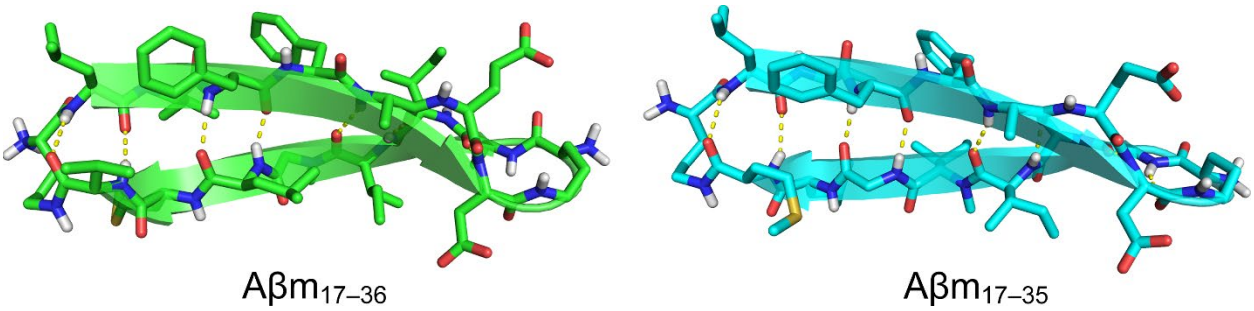

Figure 2.3. X-ray crystallographic structures of representative monomers of Aβm$_{17-36}$ and Aβm$_{17-35}$ (PDB 8GJD and 8GJC). Aβm$_{17-36}$ contains 16 unique molecules in the asymmetric unit; Aβm$_{17-35}$ contains 2 unique molecules in the asymmetric unit.

Aβm$_{17-36}$ and Aβm$_{17-35}$ form different oligomers in the crystal state. The X-ray crystallographic structure of Aβm$_{17-36}$ contains sixteen molecules of Aβm$_{17-36}$ in the asymmetric unit. Each of the molecules folds to form a twisted β-hairpin, and variation between monomers is minimal, consisting mainly of Met$_{35}$ and Leu$_{34}$ rotamers. In the crystal lattice, Aβm$_{17-36}$ assembles to form trimers which loosely pack into hexamers (Figure 4A). The X-ray crystallographic structure of Aβm$_{17-35}$ contains two molecules of Aβm$_{17-35}$ in the asymmetric unit. Both molecules fold to form twisted β-hairpins, and variation between the two monomers is minimal, consisting mainly of Met$_{35}$ rotamers. The different Met$_{35}$ rotamers likely aid in maximizing hydrophobic packing within the crystal lattice. In the crystal lattice, both molecules of Aβm$_{17-35}$ assemble to form tetrameric β-barrels, or cylindrins[35] (Figure 4B).

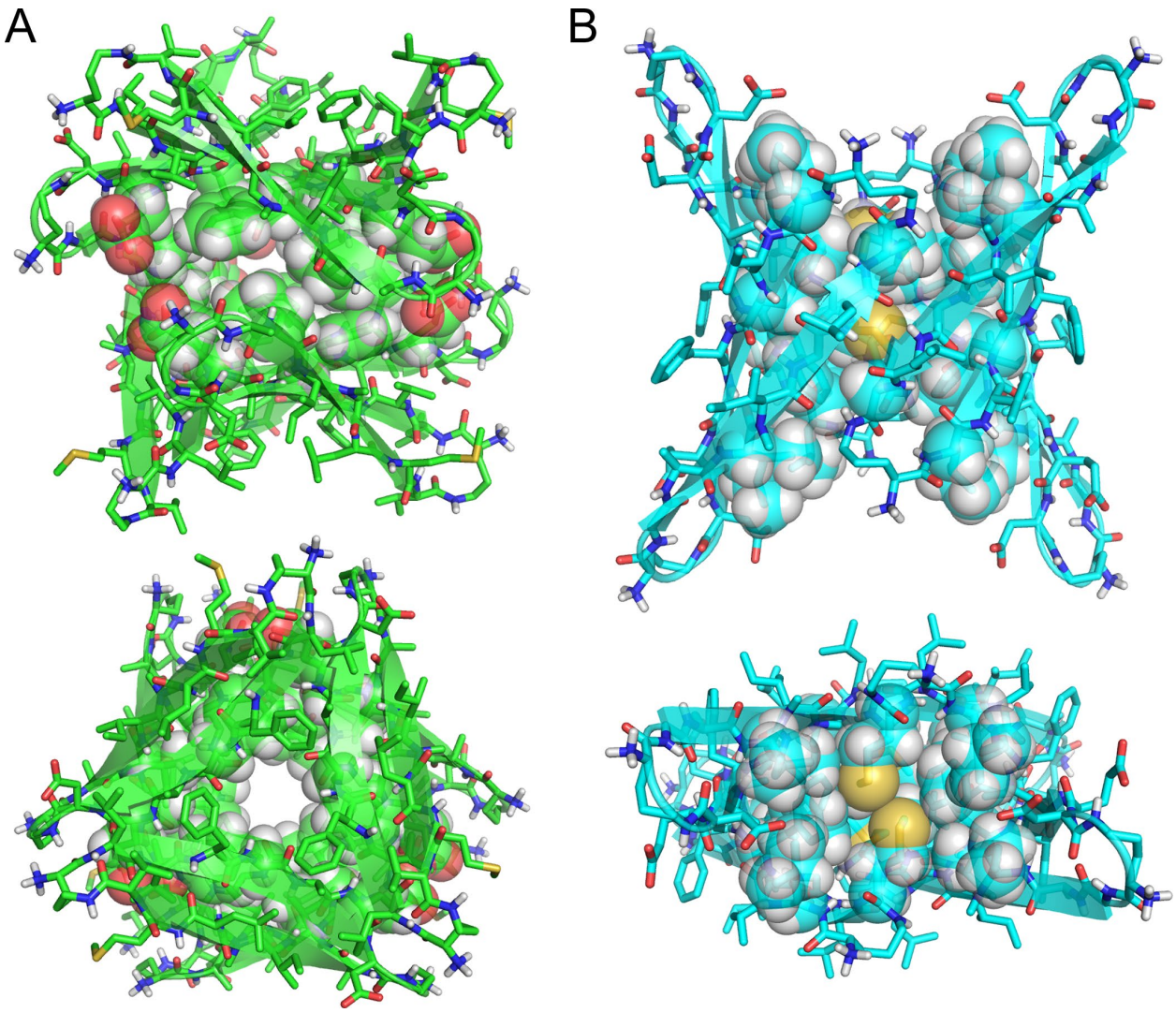

Figure 2.4. X-ray crystallographic structure of (A) the hexamer formed by Aβm$_{17-36}$ and (B) the tetramer formed by Aβm$_{17-35}$. Side chains of residues in the hydrophobic cores of the assemblies are shown as spheres to illustrate packing. Assemblies are shown from a "side" view (top), then rotated 90˚ to show a "top" view (bottom).

The trimers formed by Aβm$_{17-36}$ consist of three β-hairpins in a triangular assembly with a cavity at the center of the triangle (Figure 5A). Phe$_{20}$ and Phe$_{19}$ sit on opposite faces at the center of the trimer, surrounding this cavity. The trimer is stabilized by hydrophobic packing of residues on both faces and by intermolecular hydrogen bonding between the backbones of Val$_{18}$ and Glu$_{22}$ at each corner. Two trimers further pack together on the VFE face to form a hexamer. Although the hexamer is not stabilized by hydrogen bonds between

the component trimers, it is stabilized by bridging water molecules that hydrogen bond to both trimers. The side chains of residues Phe_{20}, Glu_{22}, and Ile_{31} form the hydrophobic core of the hexamer, with the carboxyl groups of Glu_{22} sitting at the corners. Although Met_{35} and Gly_{33} also sit on the VFE face of $A\beta m_{17-36}$, neither appears to contribute to the packing of the trimer or hexamer.[36] The remaining side chains sit outside of the hydrophobic core of the hexamer.

The tetramers formed by $A\beta m_{17-35}$ consist of four β-hairpins arranged around a central axis to form a β-barrel. The tetramer can be viewed as a dimer of dimers, in which two monomers assemble to form an antiparallel dimer (Figure 5B) and two antiparallel dimers further assemble to form the tetramer. The hydrophobic side chains of the LFAD face comprise the core of the tetramer. The side chains of Phe_{19} and Met_{35} lie at the center of the hydrophobic core and are buttressed by the side chains of Leu_{17}, Ala_{21}, and Ile_{31}. The absence of a side chain at Gly_{33} facilitates the tight packing of these hydrophobic side chains, in a fashion similar to that previously reported for a cylindrin comprising three β-hairpins from αB crystallin.[35] The charged residues Glu_{22} and Asp_{23} sit on the solvent-exposed ends of the $A\beta m_{17-35}$ cylindrin, away from the hydrophobic core. Intermolecular hydrogen bonds between the monomer subunits further stabilize the tetramer. The backbones of the Phe_{20} residues hydrogen bond to each other at the interfaces between monomers within the dimers. The backbones of the Leu_{34} residues hydrogen bond to each other at the interfaces between the dimers.

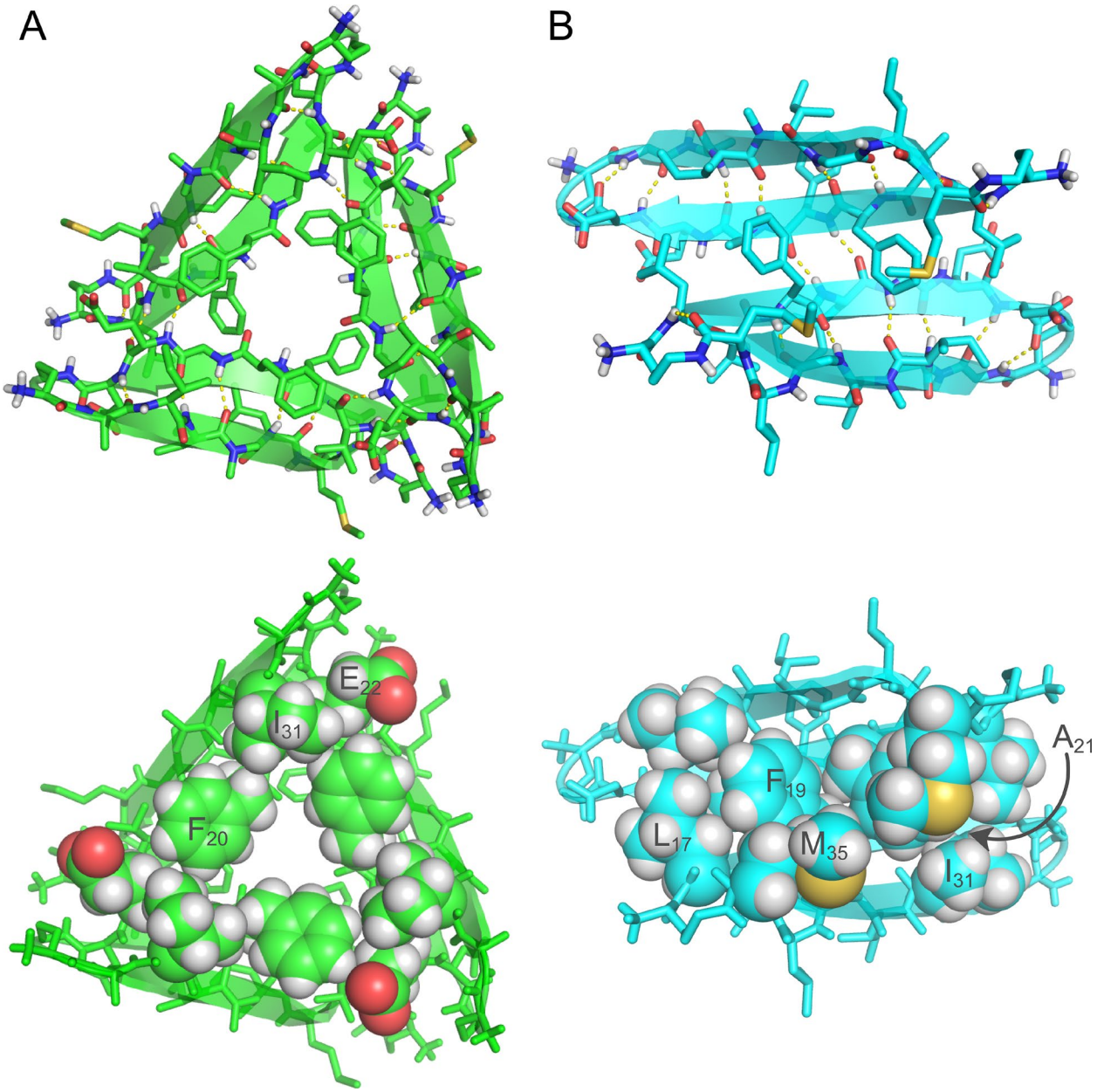

Figure 2.5. X-ray crystallographic structures of (A) a trimer formed by Aβm$_{17-36}$ and (B) an antiparallel dimer formed by Aβm$_{17-35}$. Hydrogen bonds within the structures are shown by yellow dashed lines (top). The side chains of residues that pack into the hydrophobic core of the hexamer formed by Aβm$_{17-36}$ and the tetramer formed by Aβm$_{17-35}$ are shown as spheres (bottom). These residues are labelled on one monomer within each structure. Ala$_{21}$ in the dimer of Aβm$_{17-35}$ is mostly hidden behind Phe$_{19}$ and Met$_{35}$ of the adjacent molecule of Aβm$_{17-35}$.

Although both the hexamer of Aβm$_{17-36}$ and the tetramer of Aβm$_{17-35}$ are stabilized by hydrophobic packing, this packing occurs on opposite faces of the peptides. The hexamer of Aβm$_{17-36}$ packs on the VFE face, even though the LFAD face displays three more hydrophobic side chains (Val$_{18}$, Phe$_{20}$, Ile$_{31}$, and Met$_{35}$ *vs.* Leu$_{17}$, Phe$_{19}$, Ala$_{21}$, Ala$_{30}$, Ile$_{32}$, Leu$_{34}$, and Val$_{36}$). Additional intermolecular contacts in the lattice involving Leu$_{17}$ and Val$_{36}$ may promote packing of the trimers on the less hydrophobic VFE face. The relatively loose packing of the trimers within the hexamer suggests that the trimer is the primary oligomeric building block in the crystal lattice. To this end, the trimer is stabilized by extensive packing of three sets of hydrophobic side chains in its center (Leu$_{17}$, Phe$_{19}$ Phe$_{20}$, Ala$_{21}$, Ile$_{31}$, and Leu$_{34}$).

The Aβm$_{17-35}$ tetramer packs on the LFAD face, rather than the VFE face. The two faces each display the same number of hydrophobic side chains (Leu$_{17}$, Phe$_{19}$, Ala$_{21}$, Ile$_{31}$, and Met$_{35}$ *vs.* Val$_{18}$, Phe$_{20}$, Ala$_{30}$, Ile$_{32}$, and Leu$_{34}$). Packing on the LFAD face may result from better self-complementarity of this face, permitting tighter hydrophobic packing. No major hydrophobic interactions are observed between the tetramers in the lattice, despite the exterior of each tetramer presenting multiple hydrophobic side chains. Although the tetramers pack together in the lattice, the packing interactions do not appear to lead to well-defined higher-order assemblies.

2.6 Discussion and Conclusions

The assemblies observed for Aβm$_{17-36}$ and Aβm$_{17-35}$ in the crystal state do not match the assemblies observed in SDS-PAGE. These differences likely result from the different experimental conditions required for SDS-PAGE and crystallization. SDS-PAGE is run at micromolar concentrations in a pH 6.8 Tris loading buffer containing 2% glycerol.

Crystallization occurs at millimolar concentrations at pH 6.75 and pH 8.5 for Aβm$_{17–36}$ and Aβm$_{17–35}$, respectively. The varied behaviors of Aβm$_{17–36}$ and Aβm$_{17–35}$ across different techniques is reminiscent of that of full-length Aβ peptides, for which assembly is highly dependent on experimental conditions.[37-52] Peptide concentration, the presence of detergents or lipids, pH, and temperature, among other factors, can direct, alter, induce, or inhibit assembly in full-length Aβ peptides. [37-52]

Aβm$_{17–36}$ and Aβm$_{17–35}$ mimic just two of the many conformations that full-length Aβ can form. In this manuscript, X-ray crystallography and SDS-PAGE demonstrate that the alignment of the β-strands within an Aβ-derived β-hairpin affects how the peptide oligomerizes. The range of assemblies Aβm$_{17–36}$ and Aβm$_{17–35}$ form under different conditions exemplifies how β-hairpin assembly can be affected by environment and provides insight into the factors that drive the oligomerization of Aβ peptides. The current study provides evidence that β-hairpin formation, along with environmental variation, can contribute to Aβ oligomer heterogeneity. While the heterogeneity of Aβ oligomers is still an obstacle to understanding the molecular basis of AD, this study illustrates how small changes in the folding of the component Aβ monomer subunits can have profound effects upon Aβ oligomer structure and assembly.

2.7 References and Notes

A. Ruttenberg, S.M.; Kreutzer, A.G.; Truex, N.L.; Nowick, J.S. β-Hairpin Alignment Alters Oligomer Formation in Aβ-Derived Peptides. *Biochem.*, **2024**, 63 (2), 212-218, https://doi.org/10.1021/acs.biochem.3c00526.

1. Maity, S., Hashemi, M., Lyubchenko, Y. L. (2017). Nano-Assembly of Amyloid β Peptide: Role of the Hairpin Fold. *Scientific Reports 7* (1). 10.1038/s41598-017-02454-0.
2. Rasmussen, J., Mahler, J., Beschorner, N., Kaeser, S. A., Häsler, L. M., Baumann, F., Nyström, S., Portelius, E., Blennow, K., Lashley, T., et al. (2017). Amyloid

polymorphisms constitute distinct clouds of conformational variants in different etiological subtypes of Alzheimer's disease. *Proceedings of the National Academy of Sciences of the United States of America*, *114*(49), 13018–13023. 10.1073/pnas.1713215114.
3. Tycko, R. Amyloid Polymorphism: Structural Basis and Neurobiological Relevance. (2015). *Neuron. 86* (3), 632–645. 10.1016/j.neuron.2015.03.017.
4. Abelein, A., Abrahams, J. P., Danielsson, J., Gräslund, A., Jarvet, J., Luo, J., Tiiman, A., Wärmländer, S. K. (2014). The Hairpin Conformation of the Amyloid β Peptide Is an Important Structural Motif along the Aggregation Pathway. *JBIC Journal of Biological Inorganic Chemistry. 19* (4-5), 623–634. 10.1007/s00775-014-1131-8.
5. Ono, K., Condron, M. M., Teplow, D. B. (2009). Structure–Neurotoxicity Relationships of Amyloid β-Protein Oligomers. *Proceedings of the National Academy of Sciences*. *106* (35), 14745–14750. 10.1073/pnas.0905127106.
6. Miller, Y., Ma, B., Nussinov, R. (2010). Polymorphism in Alzheimer AB Amyloid Organization Reflects Conformational Selection in a Rugged Energy Landscape. *Chemical Reviews*. *110* (8), 4820–4838. 10.1021/cr900377t.
7. Lührs, T., Ritter, C., Adrian, M., Riek-Loher, D., Bohrmann, B., Döbeli, H., Schubert, D., Riek, R. (2005). 3D Structure of Alzheimer's Amyloid-β(1–42) Fibrils. *Proceedings of the National Academy of Sciences. 102* (48), 17342–17347. 10.1073/pnas.0506723102.
8. Petkova, A. T., Yau, W.-M.; Tycko, R. (2005). Experimental Constraints on Quaternary Structure in Alzheimer's β-Amyloid Fibrils. *Biochemistry*. *45* (2), 498–512. 10.1021/bi051952q.
9. Ciudad, S., Puig, E., Botzanowski, T., Meigooni, M., Arango, A. S., Do, J., Mayzel, M., Bayoumi, M., Chaignepain, S., Maglia, G., Cianferani, S., Orekhov, V., Tajkhorshid, E., Bardiaux, B., Carulla, N. (2020). AB(1-42) Tetramer and Octamer Structures Reveal Edge Conductivity Pores as a Mechanism for Membrane Damage. *Nature Communications*. *11* (1). 10.1038/s41467-020-16566-1.
10. Wu, J., Blum, T. B., Farrell, D. P., DiMaio, F., Abrahams, J. P., Luo, J. (2021). Cryo-Electron Microscopy Imaging of Alzheimer's Amyloid-Beta 42 Oligomer Displayed on a Functionally and Structurally Relevant Scaffold. *Angewandte Chemie International Edition*. *60* (34), 18680–18687. 10.1002/anie.202104497.
11. Morimoto, A., Irie, K., Murakami, K., Masuda, Y., Ohigashi, H., Nagao, M., Fukuda, H., Shimizu, T., Shirasawa, T. (2004). Analysis of the Secondary Structure of β-Amyloid (AB42) Fibrils by Systematic Proline Replacement. *Journal of Biological Chemistry*. *279* (50), 52781–52788. 10.1074/jbc.M406262200.
12. Masuda, Y., Uemura, S., Ohashi, R., Nakanishi, A., Takegoshi, K., Shimizu, T., Shirasawa, T., Irie, K. (2009). Identification of Physiological and Toxic Conformations in AB42 Aggregates. *ChemBioChem. 10* (2), 287–295. 10.1002/cbic.200800411.
13. Hoyer, W., Grönwall, C., Jonsson, A., Ståhl, S., Härd, T. (2008). Stabilization of a β-Hairpin in Monomeric Alzheimer's Amyloid-β Peptide Inhibits Amyloid Formation. *Proceedings of the National Academy of Sciences*. *105* (13), 5099–5104. 10.1073/pnas.0711731105.

14. Sonar, K., Mancera, R. L. (2022). Characterization of the Conformations of Amyloid Beta 42 in Solution That May Mediate Its Initial Hydrophobic Aggregation. *The Journal of Physical Chemistry B*. *126* (40), 7916–7933. 10.1021/acs.jpcb.2c04743.
15. Liu, P., Reed, M. N., Kotilinek, L. A., Grant, M. K. O., Forster, C. L., Qiang, W., Shapiro, S. L., Reichl, J. H., Chiang, A. C. A., Jankowsky, J. L., Wilmot, C. M., Cleary, J. P., Zahs, K. R., Ashe, K. H. (2015). Quaternary Structure Defines a Large Class of Amyloid-β Oligomers Neutralized by Sequestration. *Cell Reports. 11* (11), 1760–1771. 10.1016/j.celrep.2015.05.021.
16. Benilova, I., Karran, E., De Strooper, B. (2012). The Toxic AB Oligomer and Alzheimer's Disease: An Emperor in Need of Clothes. *Nature Neuroscience*. *15* (3), 349–357. 10.1038/nn.3028.
17. Cline, E. N., Bicca, M. A., Viola, K. L., Klein, W. L. (2018). The Amyloid-β Oligomer Hypothesis: Beginning of the Third Decade. *Journal of Alzheimer's Disease. 64* (s1). 10.3233/JAD-179941.
18. Lendel, C., Bjerring, M., Dubnovitsky, A., Kelly, R. T., Filippov, A., Antzutkin, O. N., Nielsen, N. C., and Härd, T. (2014). A hexameric peptide barrel as building block of amyloid-β Protofibrils. *Angewandte Chemie International Edition 53*, 12756–12760. **10.1002/anie.201406357**.
19. Sandberg, A., Luheshi, L. M., Söllvander, S., Pereira de Barros, T., Macao, B., Knowles, T. P., Biverstål, H., Lendel, C., Ekholm-Petterson, F., Dubnovitsky, A., Lannfelt, L., Dobson, C. M., Härd, T. (2010). Stabilization of Neurotoxic Alzheimer Amyloid-β Oligomers by Protein Engineering. *Proceedings of the National Academy of Sciences*. *107* (35), 15595–15600. 10.1073/pnas.1001740107.
20. Wang, Y., Truex, N. L., Vo, N. D. P., Nowick, J. S. (2018). Effects of Charge and Hydrophobicity on the Oligomerization of Peptides Derived from IAPP. *Bioorganic & Medicinal Chemistry*. *26* (6), 1151–1156. 10.1016/j.bmc.2017.10.001.
21. Kreutzer, A. G., Nowick, J. S. (2018). Elucidating the Structures of Amyloid Oligomers with Macrocyclic β-Hairpin Peptides: Insights into Alzheimer's Disease and Other Amyloid Diseases. *Accounts of Chemical Research*. *51* (3), 706–718. 10.1021/acs.accounts.7b00554.
22. Samdin, T. D., Wierzbicki, M., Kreutzer, A. G., Howitz, W. J., Valenzuela, M.; Smith, A., Sahrai, V., Truex, N. L., Klun, M., Nowick, J. S. (2020). Effects of N-Terminal Residues on the Assembly of Constrained β-Hairpin Peptides Derived from AB. *Journal of the American Chemical Society*. *142* (26), 11593–11601. 10.1021/jacs.0c05186.
23. Guaglianone, G., Kreutzer, A. G., Nowick, J. S. (2021). Synthesis and Study of Macrocyclic β-Hairpin Peptides for Investigating Amyloid Oligomers. *Synthetic and Enzymatic Modifications of the Peptide Backbone*. 123–168. 10.1016/bs.mie.2021.04.023.
24. Samdin, T. D., Kreutzer, A. G., Nowick, J. S. (2021). Exploring Amyloid Oligomers with Peptide Model Systems. *Current Opinion in Chemical Biology*. *64*, 106–115. 10.1016/j.cbpa.2021.05.004.
25. Howitz, W. J., Guaglianone, G., McKnelly, K. J., Haduong, K., Ashby, S. N., Laayouni, M., Nowick, J. S. (2022). Macrocyclic Peptides Derived from Familial Alzheimer's Disease Mutants Show Charge-Dependent Oligomeric Assembly and Toxicity. *ACS Chemical Neuroscience*. *13* (6), 714–720. 0.1021/acschemneuro.1c00833.

26. McKnelly, K. J., Kreutzer, A. G., Howitz, W. J., Haduong, K., Yoo, S., Hart, C., Nowick, J. S. (2022). Effects of Familial Alzheimer's Disease Mutations on the Assembly of a β-Hairpin Peptide Derived from AB16–36. *Biochemistry*. *61* (6), 446–454. 10.1021/acs.biochem.1c00664.
27. Liu, C., Sawaya, M. R., Cheng, P.-N., Zheng, J., Nowick, J. S., Eisenberg, D. (2011). Characteristics of Amyloid-Related Oligomers Revealed by Crystal Structures of Macrocyclic β-Sheet Mimics. *Journal of the American Chemical Society*. *133* (17), 6736–6744. 10.1021/ja200222n.
28. Bitan, G., Kirkitadze, M. D., Lomakin, A., Vollers, S. S., Benedek, G. B., Teplow, D. B. (2002). Amyloid β-Protein (AB) Assembly: AB40 and AB42 Oligomerize through Distinct Pathways. *Proceedings of the National Academy of Sciences*. *100* (1), 330–335. 10.1073/pnas.222681699.
29. Pujol-Pina, R., Vilaprinyó-Pascual, S., Mazzucato, R., Arcella, A., Vilaseca, M., Orozco, M., Carulla, N. (2015). SDS-PAGE Analysis of AB Oligomers Is Disserving Research into Alzheimer´s Disease: Appealing for ESI-Im-MS. *Scientific Reports*. *5* (1). 10.1038/srep14809.
30. Kreutzer, A. G., Samdin, T. D., Guaglianone, G., Spencer, R. K., Nowick, J. S. (2020). X-Ray Crystallography Reveals Parallel and Antiparallel β-Sheet Dimers of a β-Hairpin Derived from AB16–36 That Assemble to Form Different Tetramers. *ACS Chemical Neuroscience*. *11* (15), 2340–2347. 10.1021/acschemneuro.0c00290.
31. Zhang, S., Yoo, S., Snyder, D. T., Katz, B. B., Henrickson, A., Demeler, B., Wysocki, V. H., Kreutzer, A. G., Nowick, J. S. (2022) A Disulfide-Stabilized Aβ That Forms Dimers but Does Not Form Fibrils. *Biochemistry*. *61* (4), 252–264. 10.1021/acs.biochem.1c00739.
32. We believe that this treatment leads to the transient formation of covalently bonded oligomers HS-Aβ-S-(PR_3-S-Aβ-S)$_n$-Aβ-SH.
33. Kreutzer, A. G., Yoo, S., Spencer, R. K., Nowick, J. S. (2017). Stabilization, Assembly, and Toxicity of Trimers Derived from AB. *Journal of the American Chemical Society*. *139* (2), 966–975. 10.1021/jacs.6b11748.
34. Kreutzer, A. G., Spencer, R. K., McKnelly, K. J., Yoo, S., Hamza, I. L., Salveson, P. J., Nowick, J. S. (2017). A hexamer of a peptide derived from AB16–36. *Biochemistry*, *56*(45), 6061–6071. 10.1021/acs.biochem.7b00831
35. Laganowsky, A., Liu, C., Sawaya, M. R., Whitelegge, J. P., Park, J., Zhao, M., Pensalfini, A., Soriaga, A. B., Landau, M., Teng, P. K., et al. (2012). Atomic View of a Toxic Amyloid Small Oligomer. *Science*. *335* (6073), 1228–1231. 10.1126/science.1213151.
36. The crystal structure of peptide 1a which contains the mutation M35O, further emphasizes the lack of involvement of residue 35 in this assembly (figure S#). Trimers and hexamers formed by peptides 1 and 1a are almost identical — the α-linked ornithine residue is situated similarly to the methionine it replaces, and neither contributes to the hydrophobic packing at the core of the hexamers.
37. Shao, H., Jao, S.-chuan, Ma, K., Zagorski, M. G. (1999). Solution Structures of Micelle-Bound Amyloid β-(1-40) and β-(1-42) Peptides of Alzheimer's Disease 1 1edited by P. E. Wright. *Journal of Molecular Biology*. *285* (2), 755–773. 10.1006/jmbi.1998.2348.

38. Jarvet, J., Danielsson, J., Damberg, P., Oleszczuk, M., Gräslund, A. (2007). Positioning of the Alzheimer AB(1–40) Peptide in SDS Micelles Using NMR and Paramagnetic Probes. *Journal of Biomolecular NMR*. *39* (1), 63–72. 10.1007/s10858-007-9176-4.
39. Mandal, P. K., Pettegrew, J. W. (2004). Alzheimer's Disease: Soluble Oligomeric aβ(1-40) Peptide in Membrane Mimic Environment from Solution NMR and Circular Dichroism Studies. *Neurochemical Research*. *29* (12), 2267–2272. 10.1007/s11064-004-7035-1.
40. Terzi, E., Hölzemann, G., Seelig, J. (1997). Interaction of Alzheimer β-Amyloid Peptide(1–40) with Lipid Membranes. *Biochemistry*. *36* (48), 14845–14852. 10.1021/bi971843e.
41. de Planque, M. R. R., Raussens, V., Contera, S. A., Rijkers, D. T. S., Liskamp, R. M. J., Ruysschaert, J.-M.; Ryan, J. F., Separovic, F., Watts, A. (2007). B-Sheet Structured β-Amyloid(1-40) Perturbs Phosphatidylcholine Model Membranes. *Journal of Molecular Biology*. *368* (4), 982–997. 10.1016/j.jmb.2007.02.063.
42. Lau, T.-L.; Ambroggio, E. E.; Tew, D. J.; Cappai, R.; Masters, C. L.; Fidelio, G. D.; Barnham, K. J.; Separovic, F. (2006) Amyloid-β Peptide Disruption of Lipid Membranes and the Effect of Metal Ions. *Journal of Molecular Biology*. *356* (3), 759–770. 10.1016/j.jmb.2005.11.091.
43. Dahse, K.; Garvey, M.; Kovermann, M.; Vogel, A.; Balbach, J.; Fändrich, M.; Fahr, A. (2010) DHPC Strongly Affects the Structure and Oligomerization Propensity of Alzheimer's AB(1–40) Peptide. *Journal of Molecular Biology*. *403* (4), 643–659. 10.1016/j.jmb.2010.09.021.
44. Rangachari, V.; Reed, D. K.; Moore, B. D.; Rosenberry, T. L. (2006) Secondary Structure and Interfacial Aggregation of Amyloid-β(1–40) on Sodium Dodecyl Sulfate Micelles. *Biochemistry*. *45* (28), 8639–8648. 10.1021/bi060323t.
45. Lindberg, D. J.; Wesén, E.; Björkeroth, J.; Rocha, S.; Esbjörner, E. K. (2017) Lipid Membranes Catalyse the Fibril Formation of the Amyloid-β (1–42) Peptide through Lipid-Fibril Interactions That Reinforce Secondary Pathways. *Biochimica et Biophysica Acta (BBA) – Biomembranes*. *1859* (10), 1921–1929. 10.1016/j.bbamem.2017.05.012.
46. Petkova, A. T.; Buntkowsky, G.; Dyda, F.; Leapman, R. D.; Yau, W.-M.; Tycko, R. (2004) Solid State NMR Reveals a Ph-Dependent Antiparallel β-Sheet Registry in Fibrils Formed by a β-Amyloid Peptide. *Journal of Molecular Biology*. *335* (1), 247–260. 0.1016/j.jmb.2003.10.044.
47. Kusumoto, Y.; Lomakin, A.; Teplow, D. B.; Benedek, G. B. (1998) Temperature Dependence of Amyloid β-Protein Fibrillization. *Proceedings of the National Academy of Sciences*. *95* (21), 12277–12282. 10.1073/pnas.95.21.12277.
48. Niu, Z., Zhang, Z., Zhao, W., Yang, J. (2018). Interactions between Amyloid β Peptide and Lipid Membranes. *Biochimica et Biophysica Acta (BBA) – Biomembranes*. *1860* (9), 1663–1669. 10.1016/j.bbamem.2018.04.004.
49. Rangachari, V., Moore, B. D., Reed, D. K., Sonoda, L. K., Bridges, A. W., Conboy, E., Hartigan, D., Rosenberry, T. L. (2007). Amyloid-β(1–42) Rapidly Forms Protofibrils and Oligomers by Distinct Pathways in Low Concentrations of Sodium Dodecylsulfate. *Biochemistry*. *46* (43), 12451–12462. 10.1021/bi701213s.
50. Rangachari, V., Dean, D. N., Rana, P., Vaidya, A., Ghosh, P. (2018). Cause and Consequence of AB – Lipid Interactions in Alzheimer Disease Pathogenesis.

Biochimica et Biophysica Acta (BBA) – Biomembranes. *1860* (9), 1652–1662. 10.1016/j.bbamem.2018.03.004.
51. Ege, C., Lee, K. Y. (2004). Insertion of Alzheimer's AB40 Peptide into Lipid Monolayers. *Biophysical Journal*. *87* (3), 1732–1740. 10.1529/biophysj.104.043265.
52. Analytical ultracentrifugation (AUC), circular dichroism (CD) spectroscopy, ion-mobility mass spectrometry (IM-MS), and size-exclusion chromatography (SEC) were attempted to explore and compare the effects of some of these factors on the assembly of Aβm$_{17–36}$ and Aβm$_{17–35}$. AUC and SEC did not provide clear data on the assembly states of the peptides. CD did not provide reliable data due to the poor solubility of the peptides in buffers suitable for CD. In IM-MS, the peptides remained monomeric in both the presence and absence of a non-ionic detergent.
53. iPSC-derived cortical neurons were treated with up to 50 μM of either peptide for 72 hours. Neither peptide exhibited toxicity by Promega assays CellTiter-Glo® Luminescent Cell Viability Assay and CytoTox-Glo Cytotoxicity Assay (data not shown).

CHAPTER 3

Antibodies Raised Against a Structurally Defined Aβ Oligomer Mimic Protect Human iPSC Neurons from Aβ Toxicity at Sub-stoichiometric Concentrations

3.1 Preface to chapter 3

Chapter 3 is adapted from a manuscript that will be submitted for publication this year and is a continuation of a study on a polyclonal antibody developed by the Nowick Laboratory called $pAb_{2AT\text{-}L}$. Initial characterization of this antibody was previously reported in *ACS Central Science*.[13] This chapter further characterizes how $pAb_{2AT\text{-}L}$ interacts with Aβ *in vitro* and demonstrates that at sub-stoichiometric concentrations, $pAb_{2AT\text{-}L}$ protects against $A\beta_{42}$-mediated toxicity and inhibits $A\beta_{42}$ fibrillization. The protective effects of this antibody are significantly larger than the protective effects afforded by most reported Aβ antibodies. This work was pioneered by Dr. Adam Kreutzer who authored the first report of this antibody in *ACS Central Science* and performed the thioflavin T assay reported in this chapter. My advisor, Professor James Nowick wrote this chapter with me. $pAb_{2AT\text{-}L}$ was generated by Pacific Immunology. We would like to thank Christina Tu and the Blurton-Jones Laboratory at the UCI Sue and Bill Gross Stem Cell Research Center for providing us with Ngn2 iPSCs and the guidance used to generate the neurons used for the research described in this chapter. We would like to thank Dr. Li Xing and Dr. Rakia Dhaoui for their help performing TEM experiments. Finally, we would like to thank the National Institutes of Health (NIH) National Institute on Aging (NIA) for funding (grants AG062296 and AG072587).

3.2 Introduction

Research over the past two decades has identified oligomers as the most toxic form of Aβ.[1-6] Identifying and targeting these species in Alzheimer's disease (AD) pathogenesis has proven difficult because of the heterogeneity and metastability of Aβ oligomer populations and the low abundance of oligomers in AD pathology compared to monomeric and fibrillar Aβ.[1-5,7,8] Although methods exist to isolate oligomers from AD brain tissue, these methods cannot provide high-resolution structural data and can potentially alter the structures of the oligomers during the isolation or characterization processes.[1,2,5,8] No high-resolution structures of Aβ oligomers isolated from AD brain tissue have been elucidated. Techniques have emerged to stabilize Aβ oligomers formed *in vitro*, some of which have provided high-resolution structures, but the biological relevance of these structures remains to be determined.[4,5,7,9,10]

Anti-Aβ antibodies can be a valuable tool for determining the relevance of certain Aβ oligomer structures in AD pathology and are used in many aspects of AD research. Hundreds of antibodies have been raised against various fragments and species of Aβ. Some target linear epitopes – specific residues of Aβ, while others target conformational epitopes present in oligomeric, or fibrillar Aβ. These antibodies have been used for biomarker detection, characterization or isolation of Aβ aggregates, studies on the relationship between Aβ structure and toxicity, and a few have been approved for use as AD therapeutics.[1-5,11] Although some antibodies have been developed that target oligomeric Aβ, most do not have defined conformational epitopes. Antibodies developed against homogenous, structurally defined Aβ oligomers can provide stronger evidence for the relevance of certain oligomer structures in AD pathogenesis.[2-4,6,11]

To this end, our laboratory has synthesized and elucidated high-resolution structures of covalently stabilized Aβ oligomer mimics and used them to develop antibodies.[4,10,12,13] These oligomer mimics are composed of peptides designed to mimic β-hairpin conformations present in toxic Aβ oligomers. β-hairpins are molecules of Aβ folded to form two β-strands hydrogen bonded to one another, connected by a loop or turn region.[4,14-17] This conformation is prone to oligomerization and is distinctly different from the parallel β-sheets that make up fibrils of Aβ.[4,15,18] We recently reported the high-resolution structure of one of our Aβ oligomer mimics, 2AT-L (**Figure 3.1**). 2AT-L is a toxic trimer composed of three β-hairpins arranged in a triangular fashion and covalently stabilized with three disulfide bonds.[13]

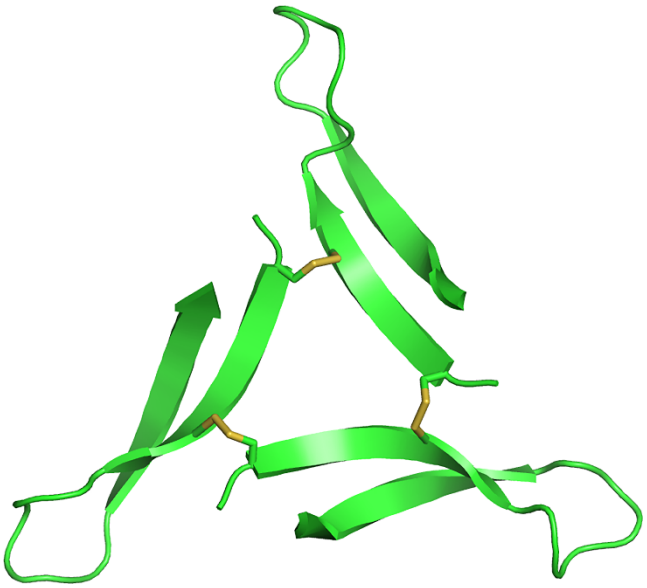

Figure 3.1. X-ray crystallographic structure of 2AT-L.

We recently reported the generation of a polyclonal antibody raised against 2AT-L, $pAb_{2AT\text{-}L}$, and the subsequent study of the binding of this antibody.[13] These studies revealed that $pAb_{2AT\text{-}L}$ is moderately selective for oligomeric Aβ over monomeric and fibrillar Aβ and stains the diffuse peripheries of Aβ plaques in AD human and mouse brain tissue but does

not bind the dense fibrillar plaque cores. The staining of $pAb_{2AT\text{-}L}$ in AD tissue suggests that 2AT-L shares structural similarities with assemblies of Aβ present in AD pathology.

In the current study, we set out to determine if $pAb_{2AT\text{-}L}$ is neuroprotective against toxic aggregates of Aβ. We chose to use human iPSC-derived neurons for these experiments because they are a better model for the human neurons affected by AD than immortalized mammalian cell lines or primary rodent neurons.[19] I thus examined the effects of $Aβ_{42}$ on iPSC-derived neurons in the presence of various concentrations of $pAb_{2AT\text{-}L}$. I further studied the ability of $pAb_{2AT\text{-}L}$ to mediate the toxic effects of $Aβ_{42}$ on pro-inflammatory cytokine production in an immortalized human-derived microglia cell line, HMC3, because microglia-induced inflammation can exacerbate AD pathology. Finally, we examined the effects of $pAb_{2AT\text{-}L}$ on $Aβ_{42}$ aggregation through Thioflavin T (ThT) assays and transmission electron microscopy (TEM).

3.3 Results

3.3.1 $pAb_{2AT\text{-}L}$ protects human iPSC-derived neurons from $Aβ_{42}$ toxicity in cell culture

Human iPSC-derived neurons are increasingly being used to study neurodegenerative diseases. Simple methods for generating iPSC-derived neurons have recently emerged, making the use of human neurons in research more accessible.[20] To investigate whether $pAb_{2AT\text{-}L}$ can mitigate the neurotoxicity of Aβ, I studied the effect of recombinant $Aβ_{42}$ on i^3Neurons in the presence and absence of $pAb_{2AT\text{-}L}$. i^3Neurons (i^3 = integrated, inducible, and isogenic) are glutamatergic cortical neurons that are differentiated from human Ngn2 iPSCs which contain a doxycycline-inducible neurogenin 2 transgene.[21,22] Treatment with doxycycline causes overexpression of Ngn2 which rapidly

converts iPSCs to neurons.[21,22] These iPSCs were designed for use in AD research[22], but to our knowledge, the toxicity of recombinant Aβ on i^{3}Neurons has not been studied.

I generated i^{3}Neurons by differentiating Ngn2 iPSCs following the protocols of Gan and coworkers[21] and measured their viability using two metrics — ATP production (metabolic activity) and LDH release (membrane integrity). Cellular ATP production was measured using the Promega™ CellTiter-Glo® 2.0 assay and LDH release was measured using the CyQuant™ LDH assay. Initially, i^{3}Neurons were treated with recombinant $A\beta_{42}$ at concentrations ranging from 25 μM to 98 nM and assayed for viability after 48 hours. In AD, concentrations of Aβ in the brain can vary significantly. In plaques, the concentration of Aβ is in the high millimolar range, but earlier in disease pathogenesis it is likely lower.[23] The IC50 of $A\beta_{42}$ is in the micromolar range, and this is the range that researchers commonly treat cells with to induce neurotoxicity, so this is the range I used.[24,25]

Treatment with $A\beta_{42}$ reduced ATP production and increased LDH release at a minimum concentration of 400 nM in i^{3}Neurons. Toxicity increased in a concentration-dependent manner up to the highest concentration tested, 25 μM (Figure B1). At 25 μM the cells appear to be almost entirely dead, exhibiting almost no ATP production, significant LDH release, and morphological changes. Based on these assays, 5 μM appeared to be a good approximation of the lowest concentration of $A\beta_{42}$ exhibiting significant toxicity by both metrics within 48 hours. This was the concentration of $A\beta_{42}$ I used in subsequent cell assays with $pAb_{2AT\text{-}L}$. It was later determined that peak LDH release at this concentration occurred closer to 72 hours. This was the time point I chose for subsequent assays.

i^{3}Neurons were treated with 5 μM $A\beta_{42}$ and $pAb_{2AT\text{-}L}$ at concentrations ranging from approximately 200 to 6 nM (because polyclonal antibodies are heterogeneous, the

concentration is approximate). A positive control of 5 μM $A\beta_{42}$ without $pAb_{2AT\text{-}L}$ and a negative control of just phosphate buffered saline pH 7.4 (PBS), the vehicle for $pAb_{2AT\text{-}L}$ and $A\beta_{42}$ were also included. After 72 hours of treatment, I measured the relative amounts of ATP and LDH produced by the neurons. $pAb_{2AT\text{-}L}$ exhibited significant protective effects on the i^3Neurons at or above 50 nM (a 100:1 ratio of Aβ to antibody) (**Figure 3.2**). The protective effects of $pAb_{2AT\text{-}L}$ are concentration dependent with 200 nM, the highest concentration tested, appearing to almost completely rescue the cells from $A\beta_{42}$-mediated toxicity (a 25:1 ratio of Aβ to antibody) (Figure 2). ATP production was restored to levels consistent with the negative control at 200 nM $pAb_{2AT\text{-}L}$ (**Figure 3.2A**). LDH release was reduced to just above the negative control at 200 nM $pAb_{2AT\text{-}L}$ (**Figure 3.2B**).

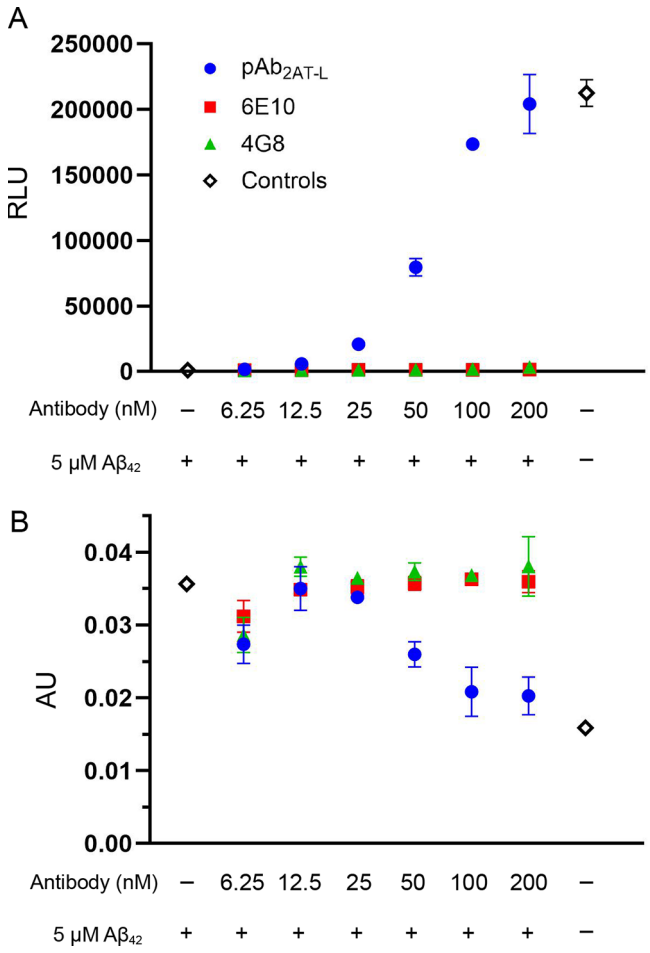

Figure 3.2. Graphs demonstrating (A) the change in ATP production by i^{3}Neurons in the presence of $A\beta_{42}$ with varying concentrations of $pAb_{2AT\text{-}L}$ measured by the luminescent CellTiter-Glo® 2.0 assay (B) the change in LDH release by i^{3}Neurons in the presence of $A\beta_{42}$ with varying concentrations of $pAb_{2AT\text{-}L}$ measured by the CyQuant™ LDH assay.

I compared the protective effects of $pAb_{2AT\text{-}L}$ to those of the commercially available anti-Aβ antibodies 6E10 and 4G8; these antibodies are the most widely used in AD research.[26] 6E10 is a monoclonal antibody that targets residues 1–16 of Aβ and has previously been shown to disaggregate Aβ fibrils and increase Aβ neurotoxicity against SH-SY5Y neuroblastoma cells.[27,28] 4G8 is a monoclonal antibody that targets residues 17–24 of Aβ and, in the same study, did not affect cell viability of SH-SY5Y cells treated with Aβ nor did it alter the amount of Aβ fibrils or oligomers present.[27.28] 6E10 and 4G8 have been shown to bind monomeric, oligomeric, and fibrillar Aβ, with 6E10 having some preference

for monomeric and oligomeric over fibrillar. To my knowledge, the protective effects of either of these antibodies against $A\beta_{42}$ have not been studied in iPSC-derived neurons.

In i^3Neurons treated with 5uM $A\beta_{42}$, 6E10 and 4G8 were unable to protect against the neurotoxic effects of recombinant $A\beta_{42}$ at the concentrations tested. ATP production was not restored, nor were the levels of LDH reduced at any concentrations tested of these antibodies (200 nM – 6.25 nM). This is consistent with previous studies of 6E10 and 4G8 in SH-SY5Y cells.[29] To confirm that the protective effects exhibited by $pAb_{2AT\text{-}L}$ were not a result of being generated in rabbits, I performed the same experiment with a generic rabbit IgG antibody. The generic antibody did not have any protective effects against $A\beta_{42}$ in i^3Neurons (Figure B2).

To confirm that this effect was not unique to iPSC-derived neurons, I also tested the ability of $pAb_{2AT\text{-}L}$ to inhibit $A\beta_{42}$-induced pro-inflammatory cytokine production by HMC3 microglia. HMC3 microglia are an immortalized human-derived cell line, and treatment with Aβ causes HMC3 microglia to produce the pro-inflammatory cytokine IL-6 (Figure B3).[30-32] Il-6 is also upregulated in AD animal models and human AD patients.[33] I tested the ability of $pAb_{2AT\text{-}L}$ to reduce IL-6 production and cytotoxicity in HMC3 cells after 72 hours of treatment with $A\beta_{42}$. $pAb_{2AT\text{-}L}$ was able to dose-dependently decrease IL-6 production and reduce toxicity caused by $A\beta_{42}$ at the same concentrations tested in iPSC-derived neurons (Figure B3).

3.3.2 ThT assay of $A\beta_{42}$ with $pAb_{2AT\text{-}L}$

To investigate the effects of $pAb_{2AT\text{-}L}$ on $A\beta_{42}$ aggregation, Dr. Adam Kreutzer monitored the fibrilization of 3 μM recombinant $A\beta_{42}$ using thioflavin T in the presence and absence of $pAb_{2AT\text{-}L}$. In the absence of $pAb_{2AT\text{-}L}$, the ThT signal began to increase after one

hour in solution, plateauing after 2 hours (**Figure 3.3**). In the presence of $pAb_{2AT\text{-}L}$, $A\beta_{42}$ fibrillization kinetics were altered. 3 μM $A\beta_{42}$ was incubated with a range of concentrations of $pAb_{2AT\text{-}L}$ varying from approximately 800 to 210 nM. At 800 nM $pAb_{2AT\text{-}L}$, ThT-positive aggregates of $A\beta_{42}$ did not appear to form until after 5 hours in solution, indicating that the antibody delayed fibrillization by about four hours. At the lowest concentration tested, 210 nM, fibrillization was delayed by about an hour, with ThT-positive aggregates of $A\beta_{42}$ forming after about two hours in solution.

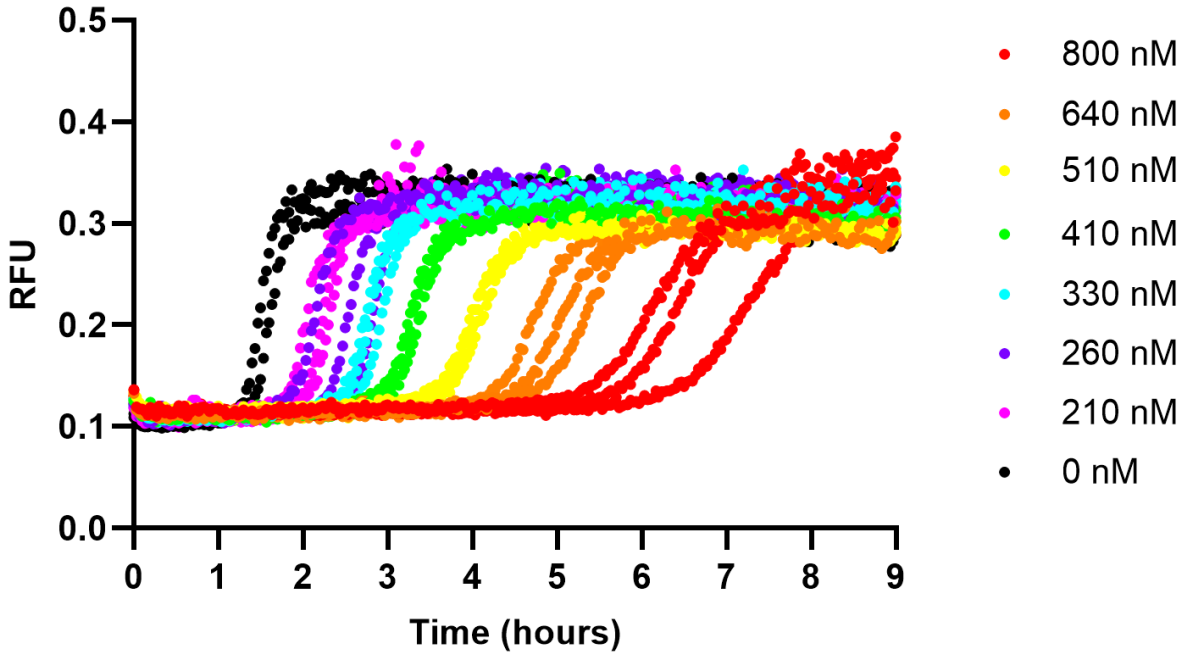

Figure 3.3. ThT assay of $A\beta_{42}$ in the presence of varying concentrations of $pAb_{2AT\text{-}L}$.

3.3.3 TEM of $A\beta_{42}$ with $pAb_{2AT\text{-}L}$

To further investigate how $pAb_{2AT\text{-}L}$ impacts $A\beta_{42}$ aggregation, Rakia Dhaoui and I performed transmission electron microscopy on $A\beta_{42}$ in the presence and absence of $pAb_{2AT\text{-}L}$. Recombinant lyophilized $A\beta_{42}$ was dissolved in PBS to create a 3 μM solution in the presence and absence of 800 nM $pAb_{2AT\text{-}L}$. After incubating for four hours at room

temperature, samples were deposited on carbon-copper mesh grids and stained with one percent uranyl acetate. In the absence of $pAb_{2AT\text{-}L}$, $A\beta_{42}$ formed bundles of fibrillar structures. The protofibrils making up the bundles appeared to be approximately 200 nm to 1 μm in length and were often observed in the presence of spherical or amorphous aggregates (**Figure 3.4**). In the presence of $pAb_{2AT\text{-}L}$ under the same conditions, neither of these fibrillar structures were observed by TEM for $A\beta_{42}$. Instead, amorphous aggregates resembling those observed in the just $A\beta_{42}$ sample were present without any fibrillar structures. In the sample of just $pAb_{2AT\text{-}L}$ alone no fibrils or spherical aggregates were observed. All samples exhibited some crystalline and amorphous structures including a sample containing just a generic rabbit IgG (Figure B4).

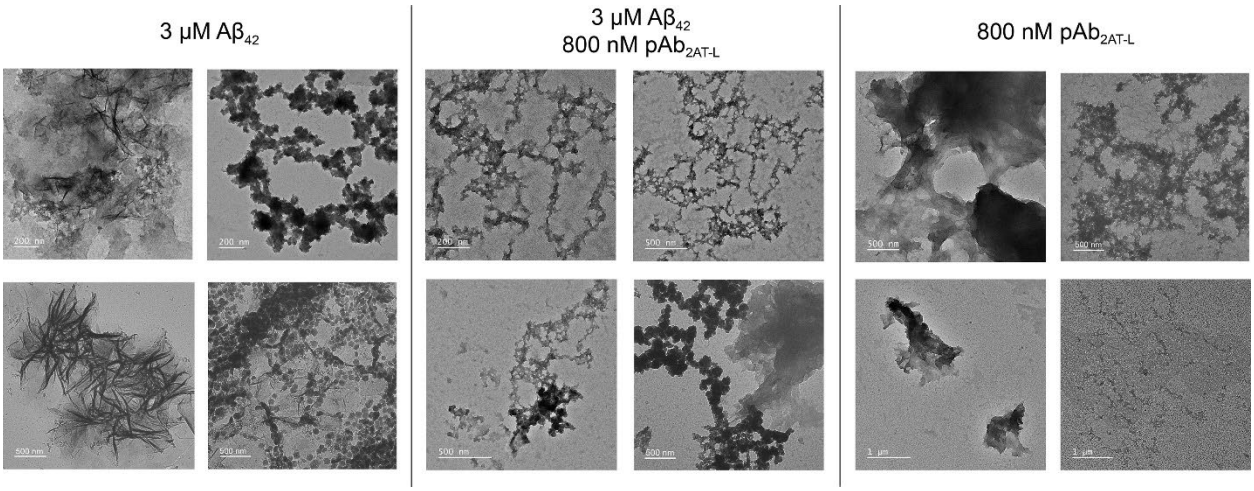

Figure 3.4. Representative TEM images of 3 μM $A\beta_{42}$ (left), 3 μM $A\beta_{42}$ and 800 nM $pAb_{2AT\text{-}L}$ (middle), and 800 nM $pAb_{2AT\text{-}L}$ (right). After three hours of incubation in PBS, samples were applied to carbon mesh copper grids and stained with 1 % uranyl acetate before imaging.

3.4 Discussion and Conclusions

A11 and OC are the main polyclonal antibodies commonly used in AD research. While OC binds fibrils and fibrillar oligomers of Aβ, A11 binds high-molecular weight (~40 kDa or larger) non-fibrillar oligomers of Aβ, as well as a variety of other amyloid

oligomers.[34,35] Glabe and coworkers originally generated A11 against $A\beta_{40}$ oligomers stabilized by conjugation to gold nanoparticles.[34] At equimolar concentrations or more, A11 protects SH-SY5Y cells from the toxicity of A11-positive $A\beta_{40}$ and $A\beta_{42}$ oligomers, but at lower concentrations A11 exhibits minimal inhibition of Aβ oligomer-mediated toxicity.[34,36,37]

It is noteworthy that $pAb_{2AT\text{-}L}$ at nanomolar concentrations substantially alters the toxicity and aggregation of Aβ at micromolar concentrations. There are few reports of antibodies affording significant neuroprotective effects at such low ratios of antibody to Aβ. To our knowledge, the only antibodies that exhibit significant protective effects in cell culture at less than equimolar concentrations of antibody to Aβ, are single-chain variable domain antibody fragments.[38-43] The most effective of these fragments come from Zhang and coworkers whose fragments exhibited protective effects on SH-SY5Y cells at ratios of antibody to $A\beta_{42}$ oligomers as low as 1:100 in some cases.[40] Other oligomer-specific anti-Aβ antibodies and antibody fragments reportedly do not exhibit significant protective effects on cells at less than equimolar concentrations of antibody to $A\beta_{42}$ or the protective effects at specific ratios of antibody to $A\beta_{42}$ have not been reported.[37,44-50]

The sub-stoichiometric activity of $pAb_{2AT\text{-}L}$ against the toxicity and aggregation of $A\beta_{42}$ suggests that the antibody binds toxic $A\beta_{42}$ oligomers and does not simply sequester monomeric $A\beta_{42}$ and prevent its aggregation. If $pAb_{2AT\text{-}L}$ was binding monomeric $A\beta_{42}$, only a small fraction of $A\beta_{42}$ would be sequestered at the concentrations of $pAb_{2AT\text{-}L}$ that were tested, and this would not result in the significant reduction of $A\beta_{42}$-mediated toxicity. The binding of monomer would also not result in substantial delays of fibril formation in the ThT assay. Although the data presented here do not definitively confirm that $pAb_{2AT\text{-}L}$ does

not bind fibrillar $A\beta_{42}$, the ThT and TEM data show that fibrillar $A\beta_{42}$ is not present in the first four hours of incubation with $pAb_{2AT\text{-}L}$, suggesting that there is significant binding of $A\beta_{42}$ species by $pAb_{2AT\text{-}L}$ before fibril formation. We previously showed that $pAb_{2AT\text{-}L}$ has a moderate preference for binding oligomeric $A\beta_{42}$ over fibrillar and monomeric,[13] and the data presented here support that conclusion.

The apparent selectivity of $pAb_{2AT\text{-}L}$ for oligomeric Aβ and the protective effect it affords against $A\beta_{42}$-mediated toxicity may reflect that the 2AT-L Aβ oligomer mimic was used as the antigen to generate $pAb_{2AT\text{-}L}$. Generating a polyclonal antibody against a well-defined oligomer mimic that lacks the N-terminus of Aβ has the advantage of limiting the epitopes of Aβ that can act as antigens, while still creating a heterogeneous set of antibodies. 2AT-L displays three molecules of central and C-terminal regions of Aβ (residues 17–36) in β-hairpin conformations. β-Hairpins are the building blocks of several reported and proposed structures of toxic Aβ oligomers[4,7,13,51-57] but are not present in structures of Aβ fibrils extracted from AD patients.[18] The results presented here support the idea that β-hairpins are a conformation present in toxic oligomers of Aβ that are absent or less prevalent in fibrils.

Alternatively, the selectivity of $pAb_{2AT\text{-}L}$ for oligomeric Aβ could reflect the residues of Aβ it binds. $pAb_{2AT\text{-}L}$ likely does not bind significantly to residues 1 through 16 or 37 through 42 of Aβ since they were not present in the species used to generate $pAb_{2AT\text{-}L}$. Residues 17–36 of Aβ may buried in the interior of Aβ fibrils, preventing binding in this region. This explanation for the selectivity of $pAb_{2AT\text{-}L}$ is less likely because it would not explain the increased affinity of $pAb_{2AT\text{-}L}$ for oligomeric Aβ over monomeric.

The ability of $pAb_{2AT\text{-}L}$ to both alter the fibrillization kinetics of $A\beta_{42}$ and prevent $A\beta_{42}$-mediated neurotoxicity could reflect multiple potential mechanisms of action. $pAb_{2AT\text{-}L}$ may bind toxic $A\beta_{42}$ assemblies and sequester them, preventing them from fibrillizing or exhibiting toxicity. The reduction of $A\beta_{42}$ available to form fibrils in solution would slow the fibrillization process. Alternatively, $pAb_{2AT\text{-}L}$ binding could temporarily sequester the toxic species or alter their conformation in such a way that they can still ultimately convert into fibrils without causing toxicity to the cells. Further study of $pAb_{2AT\text{-}L}$ is needed to clarify its mechanism of action.

Regardless of its mechanism of action, $pAb_{2AT\text{-}L}$ exhibits properties that suggest toxic $A\beta_{42}$ oligomers share conformational similarities with 2AT-L. These similarities may be conformations adopted by the individual molecules, conformations of the assemblies, or both. In either case, the similarities are strong enough to imply that 2AT-L is a realistic model of a toxic Aβ oligomer, and that $pAb_{2AT\text{-}L}$ has the potential to be used to isolate or detect toxic Aβ oligomers in solution. Future AD research could benefit from the use of both the model and the antibody.

3.5 References and Notes

1. Cline, E. N.; Bicca, M. A.; Viola, K. L.; Klein, W. L. The Amyloid-β Oligomer Hypothesis: Beginning of the Third Decade. *Journal of Alzheimer's Disease* **2018**, *64* (s1), S567–S610. https://doi.org/10.3233/jad-179941.
2. Shea, D.; Daggett, V. Amyloid-β Oligomers: Multiple Moving Targets. *Biophysica* **2022**, *2* (2), 91–110. https://doi.org/10.3390/biophysica2020010.
3. Song, C.; Zhang, T.; Zhang, Y. Conformational Essentials Responsible for Neurotoxicity of Aβ42 Aggregates Revealed by Antibodies against Oligomeric Aβ42. *Molecules* **2022**, *27* (19), 6751. https://doi.org/10.3390/molecules27196751.
4. https://doi.org/10.1016/j.bmc.2024.117715 Ruttenberg
5. Wang, Y.; Chen, J.; Gao, F.; Hu, M.; Wang, X. Recent Developments in the Chemical Biology of Amyloid-β Oligomer Targeting. *Organic and Biomolecular*

6. Zhang, Y.; Chen, H.; Li, R.; Sterling, K.; Song, W. Amyloid β-Based Therapy for Alzheimer's Disease: Challenges, Successes and Future. *Signal Transduction and Targeted Therapy* **2023**, *8* (1), 1–26. https://doi.org/10.1038/s41392-023-01484-7.
7. Aleksis, R.; Oleskovs, F.; Jaudzems, K.; Pahnke, J.; Biverstål, H. Structural Studies of Amyloid-β Peptides: Unlocking the Mechanism of Aggregation and the Associated Toxicity. *Biochimie* **2017**, *140*, 176–192. https://doi.org/10.1016/j.biochi.2017.07.011.
8. Hong, W.; Wang, Z.; Liu, W.; O'Malley, T. T.; Jin, M.; Willem, M.; Haass, C.; Frosch, M. P.; Walsh, D. M. Diffusible, Highly Bioactive Oligomers Represent a Critical Minority of Soluble Aβ in Alzheimer's Disease Brain. *Acta Neuropathologica* **2018**, *136* (1), 19–40. https://doi.org/10.1007/s00401-018-1846-7.
9. Jeon, J.; Yau, W.-M.; Tycko, R. Early Events in Amyloid-β Self-Assembly Probed by Time-Resolved Solid-State NMR and Light Scattering. *Nature communications* **2023**, *14* (1). https://doi.org/10.1038/s41467-023-38494-6.
10. Samdin, T. D.; Kreutzer, A. G.; Nowick, J. S. Exploring Amyloid Oligomers with Peptide Model Systems. *Current Opinion in Chemical Biology* **2021**, *64*, 106–115. https://doi.org/10.1016/j.cbpa.2021.05.004.
11. Bitencourt, A. L. B.; Campos, R. M.; Cline, E. N.; Klein, W. L.; Sebollela, A. Antibody Fragments as Tools for Elucidating Structure-Toxicity Relationships and for Diagnostic/Therapeutic Targeting of Neurotoxic Amyloid Oligomers. *International Journal of Molecular Sciences* **2020**, *21* (23), 8920. https://doi.org/10.3390/ijms21238920.
12. Kreutzer, A. G.; Malonis, R. J.; Marie, C.; Tong, K.; Guaglianone, G.; Nguyen, J. T.; Diab, M. N.; Lai, J. R.; Nowick, J. S. Generation and Study of Antibodies against Two Triangular Trimers Derived from Aβ. *Peptide Science* **2023**. https://doi.org/10.1002/pep2.24333.
13. Kreutzer, A. G.; Marie, C.; Sepehr Haerianardakani; Guaglianone, G.; Nguyen, J.; Diab, M. N.; Yong, W. H.; Perez-Rosendahl, M.; Head, E.; Nowick, J. S. Antibodies Raised against an Aβ Oligomer Mimic Recognize Pathological Features in Alzheimer's Disease and Associated Amyloid-Disease Brain Tissue. *ACS Central Science* **2023**. https://doi.org/10.1021/acscentsci.3c00592.
14. DuPai, C. D.; Davies, B. W.; Wilke, C. O. A Systematic Analysis of the Beta Hairpin Motif in the Protein Data Bank. *Protein Science* **2021**, *30* (3), 613–623. https://doi.org/10.1002/pro.4020.
15. Hennetin, J.; Jullian, B.; Steven, A. C.; Kajava, A. V. Standard Conformations of β-Arches in β-Solenoid Proteins. *Journal of Molecular Biology* **2006**, *358* (4), 1094–1105. https://doi.org/10.1016/j.jmb.2006.02.039.
16. Ptitsyn, A.; Finkelstein, P.; Falk (bendzko. *PRINCIPAL FOLDING PATHWAY and TOPOLOGY of ALL-P PROTEINS*; **1979**. https://core.ac.uk/download/pdf/82015124.pdf (accessed 2024-02-12).
17. Sibanda, B. L.; Thornton, J. M. β-Hairpin Families in Globular Proteins. *Nature* **1985**, *316* (6024), 170–174. https://doi.org/10.1038/316170a0.
18. Sawaya, M. R.; Hughes, M.; Rodriguez, J. A.; Riek, R.; Eisenberg, D. The Expanding Amyloid Family: Structure, Stability, Function, and Pathogenesis. *Cell* **2021**, *184* (19), 4857–4873. https://doi.org/10.1016/j.cell.2021.08.013.

19. Dolmetsch, R.; Geschwind, Daniel H. The Human Brain in a Dish: The Promise of IPSC-Derived Neurons. *Cell* **2011**, *145* (6), 831–834. https://doi.org/10.1016/j.cell.2011.05.034.
20. Cetin, S.; Knez, D.; Gobec, S.; Kos, J.; Pišlar, A. Cell Models for Alzheimer's and Parkinson's Disease: At the Interface of Biology and Drug Discovery. *Biomedicine & Pharmacotherapy* **2022**, *149*, 112924. https://doi.org/10.1016/j.biopha.2022.112924.
21. Fernandopulle, M. S.; Prestil, R.; Grunseich, C.; Wang, C.; Gan, L.; Ward, M. E. Transcription Factor-Mediated Differentiation of Human IPSCs into Neurons. *Current Protocols in Cell Biology* **2018**, *79* (1), e51. https://doi.org/10.1002/cpcb.51.
22. Wang, C.; Ward, M. E.; Chen, R.; Liu, K.; Tracy, T. E.; Chen, X.; Xie, M.; Sohn, P. D.; Ludwig, C.; Meyer-Franke, A.; Karch, C. M.; Ding, S.; Gan, L. Scalable Production of IPSC-Derived Human Neurons to Identify Tau-Lowering Compounds by High-Content Screening. *Stem Cell Reports* **2017**, *9* (4), 1221–1233. https://doi.org/10.1016/j.stemcr.2017.08.019.
23. Raskatov, J. A. What Is the "Relevant" Amyloid β42 Concentration?. **2019**, *20* (13), 1725–1726. https://doi.org/10.1002/cbic.201900097.
24. Dutta, S.; Foley, A. R.; Christopher; Zhang, X.; Rolandi, M.; Abrams, B.; Raskatov, J. A. Suppression of Oligomer Formation and Formation of Non-Toxic Fibrils upon Addition of Mirror-Image Aβ42 to the Natural L -Enantiomer. *Angewandte Chemie* **2017**, *56* (38), 11506–11510. https://doi.org/10.1002/anie.201706279.
25. Finder, V. H.; Vodopivec, I.; Nitsch, R. M.; Glockshuber, R. The Recombinant Amyloid-β Peptide Aβ1–42 Aggregates Faster and Is More Neurotoxic than Synthetic Aβ1–42. *Journal of Molecular Biology* **2010**, *396* (1), 9–18. https://doi.org/10.1016/j.jmb.2009.12.016.
26. Hunter, S.; Brayne, C. Do Anti-Amyloid Beta Protein Antibody Cross Reactivities Confound Alzheimer Disease Research? *Journal of Negative Results in BioMedicine* **2017**, *16* (1). https://doi.org/10.1186/s12952-017-0066-3.
27. Hatami, A.; Albay, R.; Monjazeb, S.; Milton, S.; Glabe, C. Monoclonal Antibodies against Aβ42 Fibrils Distinguish Multiple Aggregation State Polymorphismsin Vitroand in Alzheimer Disease Brain. *Journal of Biological Chemistry* **2014**, *289* (46), 32131–32143. https://doi.org/10.1074/jbc.m114.594846.
28. Liu, Y.-H.; Bu, X.-L.; Liang, C.-R.; Wang, Y.-R.; Zhang, T.; Jiao, S.-S.; Zeng, F.; Yao, X.-Q.; Zhou, H.-D.; Deng, J.; Wang, Y.-J. An N-Terminal Antibody Promotes the Transformation of Amyloid Fibrils into Oligomers and Enhances the Neurotoxicity of Amyloid-Beta: The Dust-Raising Effect. *Journal of neuroinflammation* **2015**, *12* (1). https://doi.org/10.1186/s12974-015-0379-4.
29. $pAb_{2AT\text{-}L}$, 6E10, and 4G8 all exhibited significant binding to $A\beta_{42}$ by ELISA. 6E10 and 4G8 exhibited stronger binding than $pAb_{2AT\text{-}L}$ (Figure B#). Before treating the cells, the concentrations of all three antibodies were compared by absorbance at 280 nm using a nanodrop and confirmed to be in the same range, with $pAb_{2AT\text{-}L}$ exhibiting a lower absorbance than 6E10 and 4G8 (Figure B#).
30. Lin, H.; Steven Grant Dixon; Hu, W.; Hamlett, E. D.; Jin, J.; Adviye Ergul; Wang, G. Y. P38 MAPK Is a Major Regulator of Amyloid Beta-Induced IL-6 Expression in Human

Microglia. *Molecular neurobiology* **2022**, *59* (9), 5284–5298. https://doi.org/10.1007/s12035-022-02909-0.
31. Polini, B.; Ricardi, C.; Bertolini, A.; Carnicelli, V.; Rutigliano, G.; Saponaro, F.; Zucchi, R.; Grazia Chiellini. T1AM/TAAR1 System Reduces Inflammatory Response and β-Amyloid Toxicity in Human Microglial HMC3 Cell Line. *International journal of molecular sciences* **2023**, *24* (14), 11569–11569. https://doi.org/10.3390/ijms241411569.
32. Wei, P.-C.; Lee-Chen, G.-J.; Chen, C.-M.; Chen, Y.; Lo, Y.-S.; Chang, K.-H. Isorhamnetin Attenuated the Release of Interleukin-6 from β-Amyloid-Activated Microglia and Mitigated Interleukin-6-Mediated Neurotoxicity. *Oxidative Medicine and Cellular Longevity* **2022**, *2022*, 3652402. https://doi.org/10.1155/2022/3652402.
33. Wang, W.-Y.; Tan, M.-S.; Yu, J.-T.; Tan, L. Role of Pro-Inflammatory Cytokines Released from Microglia in Alzheimer's Disease. *Annals of Translational Medicine* **2015**, *3* (10), 7. https://doi.org/10.3978/j.issn.2305-5839.2015.03.49.
34. Kayed, R. Common Structure of Soluble Amyloid Oligomers Implies Common Mechanism of Pathogenesis. *Science* **2003**, *300* (5618), 486–489. https://doi.org/10.1126/science.1079469.
35. Kayed, R.; Head, E.; Sarsoza, F.; Saing, T.; Cotman, C. W.; Necula, M.; Margol, L.; Wu, J.; Breydo, L.; Thompson, J. L.; Rasool, S.; Gurlo, T.; Butler, P.; Glabe, C. G. Fibril Specific, Conformation Dependent Antibodies Recognize a Generic Epitope Common to Amyloid Fibrils and Fibrillar Oligomers That Is Absent in Prefibrillar Oligomers. *Molecular Neurodegeneration* **2007**, *2* (1), 18. https://doi.org/10.1186/1750-1326-2-18.
36. Bigi, A.; Loffredo, G.; Cascella, R.; Cecchi, C. Targeting Pathological Amyloid Aggregates with Conformation-Sensitive Antibodies. *Current Alzheimer research* **2020**, *17* (8), 722–734. https://doi.org/10.2174/1567205017666201109093848.
37. Bigi, A.; Napolitano, L.; Vadukul, D. M.; Fabrizio Chiti; Cecchi, C.; Aprile, F. A.; Cascella, R. A Single-Domain Antibody Detects and Neutralises Toxic Aβ42 Oligomers in the Alzheimer's Disease CSF. *Alzheimer's research & therapy* **2024**, *16* (1). https://doi.org/10.1186/s13195-023-01361-z.
38. Kasturirangan, S.; Li, L.; Emadi, S.; Boddapati, S.; Schulz, P.; Sierks, M. R. Nanobody Specific for Oligomeric Beta-Amyloid Stabilizes Nontoxic Form. *Neurobiology of Aging* **2012**, *33* (7), 1320–1328. https://doi.org/10.1016/j.neurobiolaging.2010.09.020.
39. Meli, G.; Visintin, M.; Cannistraci, I.; Cattaneo, A. Direct in Vivo Intracellular Selection of Conformation-Sensitive Antibody Domains Targeting Alzheimer's Amyloid-β Oligomers. *Journal of Molecular Biology* **2009**, *387* (3), 584–606. https://doi.org/10.1016/j.jmb.2009.01.061.
40. Song, C.; Li, H.; Zheng, C.; Zhang, T.; Zhang, Y. Dual Efficacy of a Catalytic Anti-Oligomeric Aβ42 ScFv Antibody in Clearing Aβ42 Aggregates and Reducing Aβ Burden in the Brains of Alzheimer's Disease Mice. *Molecular neurobiology* **2023**, *60* (10), 5515–5532. https://doi.org/10.1007/s12035-023-03406-8.
41. Zameer, A.; Kasturirangan, S.; Emadi, S.; Nimmagadda, S. V.; Sierks, M. R. Anti-Oligomeric Aβ Single-Chain Variable Domain Antibody Blocks Aβ-Induced Toxicity against Human Neuroblastoma Cells. *Journal of Molecular Biology* **2008**, *384* (4), 917–928. https://doi.org/10.1016/j.jmb.2008.09.068.

42. Zhang, Y.; Chen, X.; Liu, J.; Zhang, Y. The Protective Effects and Underlying Mechanism of an Anti-Oligomeric Aβ42 Single-Chain Variable Fragment Antibody. *Neuropharmacology* **2015**, *99*, 387–395. https://doi.org/10.1016/j.neuropharm.2015.07.038.
43. Zhang, X.; Yangyang Huai; Cai, J.; Song, C.; Zhang, Y. Novel Antibody against Oligomeric Amyloid-β: Insight into Factors for Effectively Reducing the Aggregation and Cytotoxicity of Amyloid-β Aggregates. *International immunopharmacology* **2019**, *67*, 176–185. https://doi.org/10.1016/j.intimp.2018.12.014.
44. Bodani, R. U.; Sengupta, U.; Castillo-Carranza, D. L.; Guerrero-Muñoz, M. J.; Gerson, J. E.; Jai Rudra; Kayed, R. Antibody against Small Aggregated Peptide Specifically Recognizes Toxic Aβ-42 Oligomers in Alzheimer's Disease. *ACS chemical neuroscience* **2015**, *6* (12), 1981–1989. https://doi.org/10.1021/acschemneuro.5b00231.
45. Gibbs, E.; Silverman, J. M.; Zhao, B.; Peng, X.; Wang, J.; Wellington, C. L.; Mackenzie, I. R.; Plotkin, S. S.; Kaplan, J. M.; Cashman, N. R. A Rationally Designed Humanized Antibody Selective for Amyloid Beta Oligomers in Alzheimer's Disease. *Scientific Reports* **2019**, *9* (1). https://doi.org/10.1038/s41598-019-46306-5.
46. Lee, E. B. Targeting Amyloid-Beta Peptide (Abeta) Oligomers by Passive Immunization with a Conformation-Selective Monoclonal Antibody Improves Learning and Memory in Abeta Precursor Protein (APP) Transgenic Mice. *Journal of Biological Chemistry* **2006**, *281* (7), 4292–4299. https://doi.org/10.1074/jbc.m511018200.
47. Limbocker, R.; Mannini, B.; Cataldi, R.; Chhangur, S.; Wright, A. K.; Kreiser, R. P.; Albright, J. A.; Chia, S.; Habchi, J.; Sormanni, P.; Kumita, J. R.; Ruggeri, F. S.; Dobson, C. M.; Chiti, F.; Aprile, F. A.; Vendruscolo, M. Rationally Designed Antibodies as Research Tools to Study the Structure–Toxicity Relationship of Amyloid-β Oligomers. *International Journal of Molecular Sciences* **2020**, *21* (12), 4542. https://doi.org/10.3390/ijms21124542.
48. Sebollela, A.; Cline, E. N.; Popova, I.; Luo, K.; Sun, X.; Ahn, J.; Barcelos, M. A.; Bezerra, V. N.; Lyra e Silva, N. M.; Patel, J.; Pinheiro, N. R.; Qin, L. A.; Kamel, J. M.; Weng, A.; DiNunno, N.; Bebenek, A. M.; Velasco, P. T.; Viola, K. L.; Lacor, P. N.; Ferreira, S. T. A Human ScFv Antibody That Targets and Neutralizes High Molecular Weight Pathogenic Amyloid-β Oligomers. *Journal of Neurochemistry* **2017**, *142* (6), 934–947. https://doi.org/10.1111/jnc.14118.
49. Stern, A. M.; Liu, L.; Jin, S.; Liu, W.; Meunier, A. L.; Ericsson, M.; Miller, M. B.; Batson, M.; Sun, T.; Kathuria, S.; Reczek, D.; Pradier, L.; Selkoe, D. J. A Calcium-Sensitive Antibody Isolates Soluble Amyloid-β Aggregates and Fibrils from Alzheimer's Disease Brain. *Brain* **2022**. https://doi.org/10.1093/brain/awac023.
50. Wacker, J.; Raik Rönicke; Westermann, M.; Wulff, M.; Reymann, K. G.; Dobson, C. M.; Horn, U.; Crowther, D. C.; Luheshi, L. M.; Fändrich, M. Oligomer-Targeting with a Conformational Antibody Fragment Promotes Toxicity in Aβ-Expressing Flies. *Acta neuropathologica communications* **2014**, *2* (1). https://doi.org/10.1186/2051-5960-2-43.
51. Abelein, A.; Abrahams, J. A.; Danielsson, J.; Gräslund, A.; Jarvet, J.; Luo, J.; Tiiman, A.; Wärmländer, S.K.T.S. The Hairpin Conformation of the Amyloid β Peptide Is an Important Structural Motif along the Aggregation Pathway. *Journal of Biological*

Inorganic Chemistry **2014**, *19* (4-5), 623–634. https://doi.org/10.1007/s00775-014-1131-8.
52. Ciudad, S.; Puig, E.; Botzanowski, T.; Meigooni, M.; Arango, A. S.; Do, J.; Mayzel, M.; Bayoumi, M.; Chaignepain, S.; Maglia, G.; Cianferani, S.; Orekhov, V.; Tajkhorshid, E.; Bardiaux, B.; Carulla, N. Aβ(1-42) Tetramer and Octamer Structures Reveal Edge Conductivity Pores as a Mechanism for Membrane Damage. *Nature Communications* **2020**, *11* (1), 3014. https://doi.org/10.1038/s41467-020-16566-1.
53. Khaled, M.; Rönnbäck, I.; Ilag, L. L.; Gräslund, A.; Strodel, B.; Österlund, N. A Hairpin Motif in the Amyloid-β Peptide Is Important for Formation of Disease-Related Oligomers. *Journal of the American Chemical Society* **2023**, *145* (33), 18340–18354. https://doi.org/10.1021/jacs.3c03980.
54. Kreutzer, A. G.; Guaglianone, G.; Yoo, S.; Marie, C.; Ruttenberg, S. M.; Malonis, R. J.; Tong, K.; Lin, Y.-F.; Nguyen, J. T.; Howitz, W. J.; Diab, M. N.; Hamza, I. L.; Lai, J. R.; Wysocki, V. H.; Nowick, J. S. Probing Differences among Aβ Oligomers with Two Triangular Trimers Derived from Aβ. **2023**, *120* (22). https://doi.org/10.1073/pnas.2219216120.
55. Sandberg, A.; Luheshi, L. M.; Söllvander, S.; de Barros, P. T.; Macao, B.; Knowles, T. P. J.; Biverstål, H.; Lendel, C.; Ekholm-Petterson, F.; Dubnovitsky, A.; Lannfelt, L.; Dobson, C. M.; Härd, T. Stabilization of Neurotoxic Alzheimer Amyloid-β Oligomers by Protein Engineering. *Proceedings of the National Academy of Sciences* **2010**, *107* (35), 15595–15600. https://doi.org/10.1073/pnas.1001740107.
56. Sun, Y.; Kakinen, A.; Wan, X.; Moriarty, N.; Hunt, C. P. J.; Li, Y.; Andrikopoulos, N.; Nandakumar, A.; Davis, T. P.; Parish, C. L.; Song, Y.; Ke, P. C.; Ding, F. Spontaneous Formation of β-Sheet Nano-Barrels during the Early Aggregation of Alzheimer's Amyloid Beta. *Nano Today* **2021**, *38*, 101125. https://doi.org/10.1016/j.nantod.2021.101125.
57. Yu, L.; Edalji, R.; Harlan, J. E.; Holzman, T. F.; Lopez, A. P.; Labkovsky, B.; Hillen, H.; Barghorn, S.; Ebert, U.; Richardson, P. L.; Miesbauer, L. R.; Solomon, L. R.; Bartley, D. M.; Walter, K. A.; Johnson, R. W.; Hajduk, P. J.; Olejniczak, E. T. Structural Characterization of a Soluble Amyloid β-Peptide Oligomer. *Biochemistry* **2009**, *48* (9), 1870–1877.
58. Hölttä, M.; Hansson, O.; Andreasson, U.; Hertze, J.; Minthon, L.; Nägga, K.; Andreasen, N.; Zetterberg, H.; Blennow, K. Evaluating Amyloid-β Oligomers in Cerebrospinal Fluid as a Biomarker for Alzheimer's Disease. *PLoS ONE* **2013**, *8* (6), e66381. https://doi.org/10.1371/journal.pone.0066381.
59. Kulenkampff, K.; Wolf Perez, Adriana-M.; Sormanni, P.; Habchi, J.; Vendruscolo, M. Quantifying Misfolded Protein Oligomers as Drug Targets and Biomarkers in Alzheimer and Parkinson Diseases. *Nature Reviews Chemistry* **2021**, *5* (4), 277–294. https://doi.org/10.1038/s41570-021-00254-9.
60. Scarano, S.; Lisi, S.; Ravelet, C.; Peyrin, E.; Minunni, M. Detecting Alzheimer's Disease Biomarkers: From Antibodies to New Bio-Mimetic Receptors and Their Application to Established and Emerging Bioanalytical Platforms – a Critical Review. **2016**, *940*, 21–37. https://doi.org/10.1016/j.aca.2016.08.008.
61. Ascoli, C. A.; Aggeler, B. Overlooked Benefits of Using Polyclonal Antibodies. *BioTechniques* 2018, *65* (3), 127–136. https://doi.org/10.2144/btn-2018-0065.

62. Bakrania, P.; Hall, G.; Bouter, Y.; Bouter, C.; Beindorff, N.; Cowan, R.; Davies, S.; Price, J.; Mpamhanga, C.; Love, E.; Matthews, D.; Carr, M. D.; Bayer, T. A. Discovery of a Novel Pseudo β-Hairpin Structure of N-Truncated Amyloid-β for Use as a Vaccine against Alzheimer's Disease. *Molecular Psychiatry* **2021**. https://doi.org/10.1038/s41380-021-01385-7
63. Gibbs, E.; Silverman, J. M.; Zhao, B.; Peng, X.; Wang, J.; Wellington, C. L.; Mackenzie, I. R.; Plotkin, S. S.; Kaplan, J. M.; Cashman, N. R. A Rationally Designed Humanized Antibody Selective for Amyloid Beta Oligomers in Alzheimer's Disease. *Scientific Reports* **2019**, *9* (1). https://doi.org/10.1038/s41598-019-46306-5.
64. Hillen, H.; Barghorn, S.; Striebinger, A.; Labkovsky, B.; Müller, R.; Nimmrich, V.; Nolte, M. W.; Perez-Cruz, C.; van der Auwera, I.; Van Leuven, F.; van Gaalen, M.; Bespalov, A. Y.; Schoemaker, H.; Sullivan, J. P.; Ebert, U. Generation and Therapeutic Efficacy of Highly Oligomer-Specific β-Amyloid Antibodies. *The Journal of Neuroscience* **2010**, *30* (31), 10369–10379.
65. Sandberg, A.; Berenjeno-Correa, E.; Rosa Crespo Rodriguez; Axenhus, M.; Sophia Schedin Weiss; Batenburg, K. L.; Jeroen J.M. Hoozemans; Tjernberg, L. O.; Scheper, W. Aβ42 Oligomer-Specific Antibody ALZ-201 Reduces the Neurotoxicity of Alzheimer's Disease Brain Extracts. *Alzheimer's Research & Therapy* **2022**, *14* (1). https://doi.org/10.1186/s13195-022-01141-1.

Chapter 4

A Beginner's Guide to Human iPSC-Derived Neurons

4.1 Preface to chapter 4

Chapter 4 gives an overview of how to use human iPSC-derived neurons in a research setting and is intended for laboratories like mine with no prior experience working with iPSCs. Before initiating the use of iPSCs in our laboratory, I took a two-week iPSC/ESC culturing techniques course at the Gross Stem Cell Research Center, here at UCI. The course was taught by Christina Tu and included lectures from Professors Matthew Blurton-Jones, Peter Donovan, and Aileen Anderson. The course covered coating plates with Matrigel, freezing, passaging, and thawing adult human induced pluripotent stem cells and human embryonic stem cells, and a variety of differentiation protocols for these cells. The course also included trips to the CRIPSR and flow cytometry cores at the center. I would like to thank Christina Tu and the guest lecturers from this course, especially Professor Matthew Blurton-Jones and his lab who aided in the initiation of iPSC culture in our laboratory. The protocols detailed in the methods section are my own protocols adapted from protocols by Christina Tu, the Blurton-Jones laboratory, and Fernandopulle et al.[15] for working with the Ngn2 and ADRC76 hiPSC cell lines, both of which were obtained from the Blurton-Jones laboratory.

4.2 Introduction

Over the last decade, human induced pluripotent stem cells (hiPSCs) have become a staple in disease research and regenerative therapy, replacing the more controversial embryonic stem cells (hESCs) in many capacities.[1-6] hiPSCs are derived from adult somatic cells, and are genetically reprogrammed to obtain a pluripotent state, similar to hESCs.[1,4,6-8] Although immortalized human mammalian cell lines are sufficient models for many types of research, there are many cell types that do not proliferate (remain in a quiescent state or G0 phase) and thus cannot be immortalized for research.[3,9-11] These cell types include fibroblasts, hepatocytes, lymphocytes, oocytes, neurons, cardiomyocytes and various progenitor cells, like hematopoietic, muscle, epithelial, and neural progenitor cells, that can be further differentiated into mature cell types.[10,11] These cell types must instead be differentiated from stem cells as needed for research.

hiPSCs have the potential to be differentiated into a variety of different cell types. Differentiation is the process of stem cells maturing into a specific cell type. This process can be especially useful for the study of disease progression.[3,5,6,9,12] Although immortalized cell lines can be generated from people with diseases, these cells are typically collected after disease pathology has developed. hiPSC lines derived from patients with a specific disease or those from healthy adults which are then modified to include disease-related mutations can both be useful for studying disease progression.[1-3,6,9] Hundreds of hiPSC lines with genetic mutations of interest are available for research use from various organizations.[2,4,13,14] In some cases, these lines are also modified with genetic cassettes that enable easier differentiation of hiPSCs into various cell types.[15-17] These cassettes can be activated by adding a compound designed to induce expression of a gene that directs the

cell to differentiate into a certain lineage. Other growth factors are typically also added to the culture media to help induce or inhibit expression of genes to achieve the differentiation into the desired cell lineage (**Figure 4.1**).[3,15,18,19]

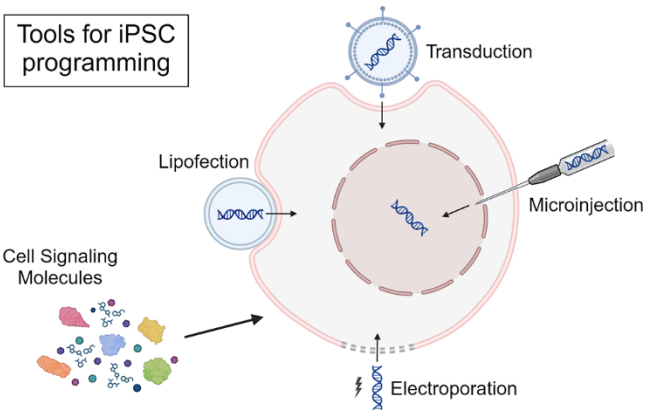

Figure 4.1. Cartoon diagram showing methods of chemical and genetic cell programming.

Neuronal differentiation is one of the most common uses for hiPSCs and this ability was what made them attractive for our research on Alzheimer's disease. For many years we used the human mammalian immortalized neuroblastoma cell line SH-SY5Y as a cell model for our research. Although SH-SY5Y cells are an established cell model for studying neurodegenerative disorders, they have significant differences from the post-mitotic neurons most affected by AD.[6,9,15] hiPSC-derived neurons are a recently established and improved cell model for studying a variety of neurological disorders, and several protocols have emerged for this purpose.[5,9,20-23]

Many laboratories like mine do cell-work but do not have the means to harvest and generate or genetically modify hiPSCs. This guide is intended for these laboratories; in it I cover the basics of culturing and differentiating hiPSCs with an emphasis on neuronal differentiation protocols. I also briefly cover how hiPSCs are made and how they can be genetically modified to create disease-relevant cell-lines. I highlight the hiPSC repositories

that enable laboratories like mine to obtain these cell lines. Finally, I detail my own protocols and give some insights I have acquired from working with them.

4.3 Culturing hiPSCs

4.3.1 Making iPSCs. In 2007, two groups demonstrated that human fibroblasts could be reprogrammed to form pluripotent stem cells by inducing the expression of four transcription factors— two of these transcription factors were common between the two groups, the other two differed.[24,25] Since then, these methods have been optimized for improved efficiency, and multiple combinations of transcription factors have been identified that can be used to generate hiPSCs from fibroblasts, but the overall efficiency of this reprogramming is still very low.[1,6-8,12] Low reprogramming efficiency can be attributed in part to the methods necessary to induce ectopic gene expression. The original methods detailed by Yamanaka and coworkers and Thomson and coworkers both utilized types of viral vector transduction to generate hiPSCs from fibroblasts, retroviral and lentiviral, respectively.[24,25] Today, many methods are used to generate hiPSCs including both integrative and non-integrative methods, but efficiency still remains below 1 %.[1,8,26] Generally, viral vectors are still utilized in these method, but nonviral vectors have also been used for this purpose with lower efficiency.[1,26]

4.3.2 Thawing, passaging, and freezing. iPSCs are generally cultured on Matrigel™-coated plates.[18,27,28] Matrigel™ and similar alternatives are gelatinous protein-rich hydrogels or basement membrane matrices that help stem cells adhere and remain undifferentiated.[18,27,28] These matrices are designed to mimic the extracellular

environment found in healthy tissue.[27,28] Matrigel™ itself is derived from murine Engelbreth-Holm-Swarm sarcoma and is the most commonly used of these matrices.[27,28]

Practices for thawing, passaging, and freezing iPSCs are generally similar to those for immortalized mammalian cell lines. Cells can be thawed in warm media and frozen in media with 10 % DMSO.[15,18] iPSCs are usually washed with PBS before being treated with Accutase™ are other cell dissociation reagents to gently detach them from the plate. Accutase™ is a solution of enzymes that cleave the proteins that adhere cells to plates.[15,29] Following detachment, cells are typically centrifuged to form a pellet and resuspended in fresh media with ROCK inhibitor.[13,29] ROCK inhibitor or Y-27632 is an inhibitor of p160-Rho-associated coiled-coil kinase (ROCK) that helps to prevent apoptosis in iPSCs.[29]

iPSCs generally require daily feeding (replacement of media) and are typically passaged once they have grown to greater than 80 % confluency.[15,18] Passaging frequency is dependent upon plating density, but is typically necessary every two to four days. Plating densities are generally suggested at splitting ratios ranging from 1:3 to 1:12.[15,18] I personally like to count the cells using a cell counter and plate at a density of between two hundred-thousand and 1 million cells per milliliter of media.

4.4 Transfection of iPSCs

The delivery of genetic payloads into hiPSCs is generally performed for one of two purposes: to direct differentiation or to alter the expression of a gene of interest. It is difficult to effectively transfect post-mitotic cells,[30,31] so transfection of hiPSCs before differentiation is preferable. Transfection is the process of introducing foreign oligonucleotides (DNA, RNA, etc) to a host cell (**Figure 4.1**). Often this involves the integration of DNA or RNA into the host genome where it will be replicated as the cells

proliferate. Alternatively, DNA or RNA can be introduced to the host cell in the form of a plasmid or oligonucleotides which will not replicate with the host cell. Generally, these genetic payloads are delivered via either viral vectors or plasmid vectors.[31-33] Each of these methods have risk of mutagenesis and gene disruption, though some have higher risk than others.[30-32] These risks should be evaluated depending on the usage.

4.4.1 Viral transfection. Viral transfection is also known as transduction and is the most common method of transfection in hiPSCs. Retroviruses or lentiviruses are generally used to transfect cells in a non-clinical setting as they provide the most efficient and stable transfection.[30-32] While retroviruses can only transfect dividing cells, lentiviruses can be used to transfect non-dividing cells but are associated with higher risk of infection or mutagenesis.[230-32] Adeno-associated viruses (AAVs) have similar abilities to lentiviruses and exhibit lower immunogenicity and pathogenicity, but they have a smaller packaging capacity; AAVs are the most used method for gene therapy and for introducing the tetracycline-inducible gene expression system (Tet-On) in hiPSCs — a useful tool for the efficient differentiation of hiPSCs.[16,30-32]

4.4.2 Non-viral transfection. Non-viral transfection can be performed via mechanical or chemical methods. The most common method of mechanical transfection is electroporation; electroporation is the application of an electric current to cells to temporarily increase membrane permeability and allow the entry of foreign genetic material into the cell.[31-33] Other physical methods include sonoporation, magnetofection, gene microinjection, and laser irradiation — these methods use ultrasound, magnetic forces, a small needle, and lasers, respectively, to create small holes in cell membranes.[31,32]

Mechanical methods of transfection are generally highly effective but have higher rates of damaging and killing cells.

Chemical transfection is typically performed through lipofection in which charged lipids encapsulate the genetic payload and merge with the phospholipid bilayer to deliver it.[30,31] Other methods include using calcium phosphate, dendrimers, polymers, or nanoparticles to aid in the uptake of genetic payloads into the cell.[31,32] Chemical transfection is generally safer but less efficient than physical or viral transfection. In some instances, chemical methods are used in conjunction with viral vectors to deliver genetic payloads; this is referred to as hybrid transfection.[32]

4.5 Neural Differentiation of iPSCs

Differentiation is controlled by gene expression and can be manipulated *in vitro* through transfection or through treatment with certain signaling molecules.[3,12,18,19,34,35] Treatment with small molecules and proteins that induce changes in gene expression can mimic *in vivo* development, but the process can be time consuming (weeks or months to maturation) and can produce significant variability in the final cell population.[12,35] Transfection of genetic constructs into the cells can create more homogenous populations of mature cells more quickly (days or weeks), but requires the design, synthesis, and genomic integration of these genetic constructs.[12,35] Generally both methods are used synergistically to induce differentiation, and many protocols have been published detailing these methods.[3,12,19,21,22,34,35]

Because of the limited availability of living human brain tissue, one of the most common uses of hiPSCs in research is neuronal differentiation. The majority of protocols for generating neurons from hiPSCs involve stepwise differentiation — the generation of

embryoid bodies, neurospheres, or neural progenitor cells that are then matured into neurons (**Figure 4.2**).[12,21,22,35-37] These protocols generally utilize various transcription factors and signaling molecules to induce differentiation toward certain lineages and inhibit differentiation toward alternative lineages.

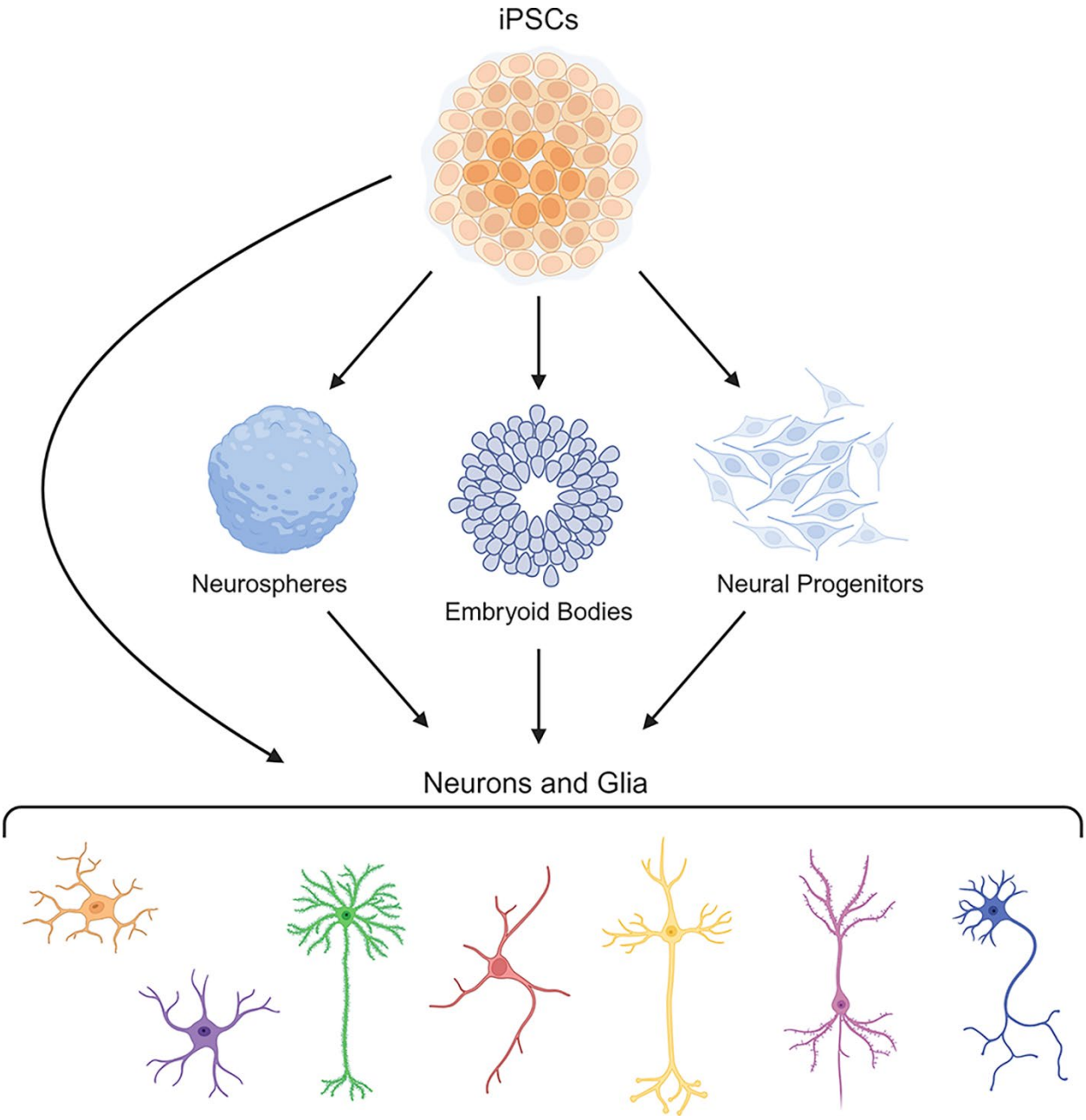

Figure 4.2. Cartoon diagram demonstrating pathways for differentiating neurons and glia.

Today, there are several publicly available hiPSC lines that have genetic expression cassettes incorporated into their genome for simplified neuronal differentiation. These cassettes include regulatory switches that can be triggered by a single molecule to induce gene expression. The most common of these switches is called the Tet-On system.[15,16,30] The system consists of two constructs: 1) a gene of interest fused to the Tet-On promoter which consists of the minimal cytomegalovirus (CMV) promoter fused to repeats of the Tet-operon from E. coli, and 2) the reverse tetracycline transactivator (rtTA) which is a fusion of a mutant tetracycline repressor and the activation domain of the herpes simplex virus virion protein 16.[16,17] When doxycycline is added to cells with these two components, the rtTA binds to the Tet-operon repeats and activates gene expression via the CMV promoter.[16,17] Forced expression of certain genes causes the cells to differentiate toward a specific lineage; for neurons, this gene is usually neurogenein2 (Ngn2).[16,17] Cell lines containing the Tet-On system are typically well characterized by the institution that developed them and provide the user with a simple method to alter gene expression to elicit differentiation.

4.5.1 Neural progenitor cells. hiPSCs are often differentiated into neural progenitor cells (NPCs) prior to neuronal maturation. The entire process often involves three or more sequential cell fate transitions.[38,39] Not all neuronal differentiation protocols require differentiation to NPCs before maturation — the method of differentiation should be chosen based on the research goals. Directly differentiating hiPSCs into mature neurons is faster than going through multiple differentiation steps, but this approach skips or accelerates certain developmental stages that the cell would go through *in vivo*. If these

developmental stages are relevant to the research being performed, stepwise differentiation with NPCs is the better method.[40,41]

NPCs can be of multiple lineages and can be formed in multiple ways. The current protocols for NPC differentiation typically use chemical induction of gene expression for differentiation to mimic the slow development that occurs *in vivo*.[40,42] In some cases, iPSCs are first differentiated into neuroepithelial cells, neural rosettes, or embryoid bodies before proceeding to NPC lineage.[38,39,41,43] In addition to neuronal growth factors and supplments, chemical NPC differentiation often utilizes growth inhibitors to prevent unwanted differentiation into alternative cell lineages. Common inhibitors include bone morphogenic protein inhibitors like dorsmorphin, noggin, or LDN193189 and a transforming growth factor beta-signaling inhibitor called SB43152.[38-42] Both of these inhibitors inhibit the SMAD signaling pathway and their use is commonly referred to as dual-SMAD inhibition.

4.5.2 Glutamatergic neurons. Glutamatergic neurons are excitatory neurons that originate from the dorsal telencephalon.[44,45] These neurons help control cognitive and motor function and make up most of the excitatory networks in the central nervous system. Dysfunction of cortical glutamatergic neurons contributes to several neurodegenerative and neuropsychiatric disorders.[22,44,45]

Differentiation of hiPSCs into cortical glutamatergic neurons is one of the most well studied, and now one of the easiest, hiPSC differentiations. In 2013, Sudhof and coworkers determined that overexpressing Ngn2 alone rapidly converts iPSCs into relatively homogenous excitatory glutamatergic neurons.[46] To simplify and scale up this protocol, Gan and coworkers engineered an iPSC line that contains a doxycycline-inducible mouse

Ngn2 transgene.[15,47] Treating these cells with doxycycline and neuronal growth factors produces a pure population of cortical glutamatergic neurons.

Other protocols have been published that describe different methods to differentiate glutamatergic neurons, but most require NPC differentiation prior to maturation.[44,45] These protocols may be superior for the study of neurodevelopment but are generally more difficult and time-consuming to accomplish than using Ngn2 hiPSCs.

4.5.3 GABAergic neurons GABAergic neurons are inhibitory interneurons that originate from the ventral tenecephalon and regulate neuronal signaling in the brain.[44,45,48-51] Dysfunction of GABAergic neurons causes or affects a variety of neurodevelopmental, neurodegenerative, and neuropsychiatric disorders.[48,50-53] iPSC-derived GABAergic neurons can be purchased commercially, differentiated from NPCs, or differentiated directly from hiPSCs.

Only two methods have been reported that describe the generation of GABAergic neurons directly from hiPSCs. The first describes induced overexpression of five transcription factors in hiPSCs to generate immature neurons with GABAergic fate after just three weeks. The purity of the resulting neuronal population is reportedly low and the functionality of the neurons was only established upon co-culture with hippocampal primary neurons.[49]

An improved protocol for the direct differentiation of GABAergic neurons directly from hiPSCs was published in 2017 by Wernig and coworkers. Their protocol produced highly homogenous and mature GABAergic neurons from hiPSs after five weeks by inducing expression of just two transcription factors, ASCl1 and DLX2.[51] Brennand and coworkers later published an adaption of this protocol that overexpressed these

transcription factors in hiPSC-derived NPCs to minimize variability in the final neuron population.[48] While this adaption may be longer, it produces a purer population of GABAergic neurons.

Other published methods to generate GABAergic neurons also require differentiation into some type of progenitor cell before maturation. Kriegstein and coworkers reported that the generation of medial ganglionic eminence- like progenitors (MGEs) could produce mature GABAergic interneurons after up to seven months of development.[50] This protocol mimics endogenous human neural development. A similar, but faster protocol was reported by Chung and coworkers who produced mature GABAergic neurons from MGEs after 12 weeks.[53] Another protocol produces GABAergic medium spiny neurons (MSN) from a multi-step differentiation procedure involving the generation of hiPSC-derived MSN progenitor cells.[52]

4.5.4 Dopaminergic neurons Dopaminergic neurons are a small population of midbrain neurons that are the main source of dopamine in the central nervous system.[55] Dopaminergic neurons help regulate cognitive and motor functions as well as the reward system that controls many behaviors.[55] The degeneration of dopaminergic neurons is generally associated with Parkinson's disease.[36,37,55,56] In recent years, transcription factors that regulate dopaminergic neurotransmitter selection in neurons have been identified, most notably ASCL1.[36,37] Wernig and coworkers reported that the induced expression of ASCL1 along with five other transcription factors in hiPSCs led to the generation of homogenous dopaminergic neurons within four weeks.[37]

An alternative approach was co-opted by Kriegstein and coworkers who combined the overexpression of Ngn2 pioneered by Sudhof and coworkers with a commercially

available midbrain differentiation kit to produce mature dopaminergic neurons within one month.[46,56] The homogeneity of these neurons is reported to be around 60 %, and the protocol likely needs to be optimized for higher purity. There is potential for this protocol to be simplified by using the isogenic iPSC line made by Gan and coworkers which already contains a doxycycline-inducible Ngn2 cassette. Other protocols for differentiating dopaminergic neurons require initial differentiation into NPCs before maturation.[36,56,57]

4.5.5 lower/spinal motor neurons Spinal or lower motor neurons are cholinergic neurons that extend from the spinal cord into muscles to control motor function.[58-60] hiPSC-derived motor neurons are typically used to study motor function loss in disease and neural injury.[58-63] Motor neurons were first differentiated from hiPSCs in 2008 by Eggan and coworkers who formed embryoid bodies from hiPSCs and then treated them with an agonist of sonic hedgehog signaling and retinoic acid to achieve a mixed culture of neurons, of which about 20 % expressed markers of motor lineage.[64] Most modern protocols for differentiating motor neurons still require initial differentiation into NPCs or the formation of embryoid bodies before maturation, but generally produce a more homogenous culture of motor neurons.[59-62]

A few methods do not require intermediate steps, instead differentiating hiPSCs directly into motor neurons. One of these adds rodent glia to the culture of transcriptionally modified iPSCs to encourage motor neuron differentiation.[63] To my knowledge, only one protocol has been published that describes a method for directly differentiating hiPSCs into motor neurons without the addition of other cell types. This protocol comes from Ward and coworkers and utilizes a modified version of the Ngn2 Tet-On transgene that induces the over-expression of transcription factors Ngn2, ISL1, and

LHX3. The overexpression of these genes produces a highly pure population of mature lower motor neurons in less than two weeks.[15] To my knowledge, the only other protocol that yields greater than 90 % pure lower motor neurons comes from Zhang and coworkers. Their protocol utilizes the generation of motor neuron progenitors and produces mature lower motor neurons in less than a month.[58]

4.5.6 Microglia and astrocytes. Microglia and astrocytes are the two most abundant types of neural immune cells.[65,66] Microglia perform phagocytosis and mediate inflammation in the CNS by secreting cytokines and chemokines.[66,67] Astrocytes aid in neurogenesis, synapse maintenance, and blood-brain barrier integrity.[65,66,68] Both astrocytes and microglia can exhibit multiple morphologies and states depending on their environment and both respond to harmful stimuli in the CNS.[65-68] The neuroinflammation caused by microglia and astrocytes can in some cases damage neurons and exacerbate disease pathogenesis.[65-68]

Current methods to differentiate microglia and astrocytes require stepwise differentiation and generally take a month or more to grow to maturity.[66-72] These protocols range from two growth phases (iPSCs →HPC → mature astrocytes or microglia) to five growth phases (iPSCs → EBs → neural rosettes/neurospheres → NPCs → astrocyte or microglia PCs → mature astrocytes or microglia). Often, these protocols also require co-culture of HPCs with primary neurons and, for microglia, with primary astrocytes.[57,66,70] In some cases, the addition of certain cytokines is sufficient.[66-68,70] The similarities of the glia produced by these methods and naturally occurring human glia vary by protocol.[67,70] It should be noted that many of these protocols refer to the final cell type as *iPSC-derived microglia-like cells*; only some refer to the cells as iPSC-derived microglia.

Reportedly, microglia similar to primary human microglia will innately develop in iPSC-derived cerebral organoids.[70] Both neurons and astrocytes are necessary for the development of mature electrophysiology in these organoids and other neural networks.[73-75] In many cases, murine astrocytes are utilized for this purpose, but murine astrocyte morphology and gene expression can differ dramatically from that of human astrocytes.[73,74] Despite the extra work that might be necessary to generate hiPSC-derived glia, their use ultimately yields more accurate models of the human brain.

4.6 hiPSC-Derived Neurons in Disease Modeling

Human iPSC-derived neurons and glia are becoming a necessity in neurological disease research and drug development. Although human mammalian cell lines and primary rodent neurons and glia can be useful models, these cells are significantly different from the human neurons and glia affected by these diseases.[6,9,15] The high failure rate of drugs for neurological disorders in human clinical trials can be attributed in part to a lack of sufficient human models used in research and development.[5,20,23] hiPSC-derived neurons and glia have begun to help fill this gap while also enabling the observation of disease development during neurogenesis and maturation, which cannot be observed when culturing other mammalian cells or primary rodent cells.[4,5,20]

hiPSCs are also ideal for the development of neural networks and organoids that realistically model the environment and electrophysiology of the human brain.[73-75] These models have the potential to reveal previously unknown aspects of disease pathology and provide an improved platform for drug development.[73-77] hiPSC-derived neural organoids are slowly becoming a standard for studying both normal and disease brain function *in vitro*.

Although ESCs can also be used to generate human neurons and glia, their use in research is still highly controversial and they cannot be used for patient-specific genetic studies. hiPSCs can be generated from a variety of donors to study the genetic basis of disease. Doing these types of studies in a variety of iPSC lines can aid in determining new genes of interest and clarify the causes of differences in disease pathology between people individuals and ethnic groups. For these purposes, many scientific non-profits have developed iPSC banks or repositories that provide researchers with a hundreds of iPSC lines derived from people with different genotypes and phenotypes.[2,4,13,14] Non-disease iPSCs are also available and can be used as controls or to study the genetic basis of disease through genetic engineering.

Non-profit organizations in the United States with large iPSC repositories include the NIH center for Alzheimer's disease and related dementias (CARD), the California institute for regenerative medicine (CIRM), the Coriell institute for medical research, and WiCell research institute. The iPSC lines that come from these organizations are well characterized and standardized for quality assurance.[4,13,14] Many of these cell lines were developed specifically for the study of various neurological disorders and come from patients with a disease of interest or contain genetic modifications relevant to a disease of interest. The most common disease-related iPSC lines are from patients with neurodegenerative disorders like Alzheimer's, Parkinson's, or ALS, but there are iPSC lines in these repositories for most neurological disorders ranging from neuropsychiatric disorders like schizophrenia to neurodevelopmental disorders like Rett syndrome.

4.7 Insights on iPSC-Neurons

iPSC-neurons can be relatively easy to differentiate, especially when using Ngn2 iPSCs, but these cells, like all neurons, have certain limitations. iPSC-derived neurons are one of the most delicate cell-types to work with. Cortical neurons have long, thin dendrites that form interconnected networks with other neurons. These dendrites make up a significant amount of their surface area, so the neurons do not adhere to culture dishes as strongly as many other cell types do and thus do not tolerate multiple changes of media. When performing techniques like fluorescence microscopy with these neurons it is best to minimize changes in media or risk lifting sheets of neurons.

iPSC-derived neurons also require Poly-D-Lysine coated cell culture vessels to successfully adhere.[15] In some cases you can buy these plates pre-coated, but not all plate types can be purchased like this. I was unable to find 96-well plates with PDL coating for purchase, and so I coated them myself, washed them with PBS, and dried them before culturing neurons. In my experience, alternatives like poly-L-lysine or poly-ornithines do not provide a sufficient surface for these neurons to adhere to.

Ultimately, I hoped to generate iPSC-derived microglia and co-culture them with my iPSC-derived neurons. I attempted to differentiate iPSC-derived microglia following the protocol published by Blurton-Jones and coworkers.[73] This protocol requires differentiation to hematopoietic progenitor cells using a commercially available kit from StemDiff™, followed by treatment with cytokines and other supplements to induce microglial lineage. The entire protocol takes about two months. Despite taking advisement from members of the Blurton-Jones lab, I was unable to successfully complete this differentiation after several months of trying. I believed my technique to be consistent with

the protocol, and I believe I successfully made HPCs, but I was unable to differentiate them into microglia. A possible reason for this may be mishandling of the cytokines, as they are very sensitive to their environment.

Although I was unsuccessful at culturing iPSC-derived microglia, I ultimately had a positive experience working with iPSCs and iPSC-derived neurons. These cells are high maintenance and not as robust as most mammalian cells, but they enable the study of diseases in a more comprehensive, realistic, and often ethical manner. I hope this guide encourages those unfamiliar with culturing iPSCs and differentiating iPSC-derived neurons to use these techniques. The growing accessibility of these cells and methods should make these practices available to any research laboratory that does cell work. Good luck!

4.8 Methods

4.8.1 Culturing iPSCs

Table 4.1. Materials for iPSC culture

Name	Catalog #
Essential 8™ Medium (with E8 supplement)	A1517001
mTeSR™1 (or mTeSR/mTeSR Plus/TeSR-E8)	5850
Y-27632 (hydrochloride), ROCK inhibitor	10005583
MATRIGEL™ MATRIX GFR PHENOL RED-FREE 10mL	356231
Knockout DMEM	10829018
Knockout DMEM/F12	12660-012
StemPro® Accutase® Cell Dissociation Reagent	A1110501
DPBS (no Ca or Mg)	14190144
DMEM F12	11320033
6-well, sterile, cell culture-treated, individually wrapped plates	
Cryovials	
Sterile DMSO	

Aliquotting

Matrigel™

Thaw Matrigel™ overnight in ice in deli case, prechill tubes and tips

Aliquot into 500 µL aliquots and store in -80°C

ROCK Inhibitor (RI)
Dissolve in sterile DMSO 10 mM (1000x)
Aliquot into 15 µL aliquots and store in -80°C (up to a year+)

DPBS (no Ca or Mg)
50 mL aliquots in 50 mL conical tubes RT (3 years)

Accutase™
Thaw overnight at 4°C 5 mL aliquots at 4°C for 2 years

Essential 8™ Basal Media (E8)
Thaw E8™ supplement at RT or overnight at 4°C
Remove 10 mL of media, replace with thawed supplement
Store at 4°C 2-4 weeks

StemCell mTeSR™ Media (any variation)
Thaw supplement at RT or overnight at 4°C
Add thawed supplement to media
Store at 4°C 2 weeks, -20°C 6 months

Knockout DMEM
45-50 mL in 50 mL conical tubes in 4°C
(With Matrigel™ can be stored at 4°C for 1 month)

Knockout DMEM F12 and DMEM F12
50ml aliquots store at 4°C

Coating with Matrigel™

1. Take a 45-50 mL aliquot of Knockout DMEM and thaw/add a 500 µL aliquot of Matrigel™ (using the cold media)
2. Add 1 mL per well (6-well plate, half volume)
3. Store plates 1 hour – 2 weeks at RT or in incubator
4. Aspirate immediately before use
5. Store Matrigel at 4°C for one month

Thawing and plating

Note: iPSCs meant for microglial differentiation should use mTeSR™ (not E8™)

1. Prewarm: 9 mL KO DMEM:F12, E8™ or mTeSR™ + RI (2 mL per well, 6 well plate)
2. Thaw cryovial halfway
3. When it is half thawed, Use warmed KO DMEM:F12 to transfer the cells to a 15 mL conical tube(with the rest of the KO DMEM:F12)
4. Centrifuge 3–5 min 200g/750rpm

5. Aspirate supernatant from tube of cells
6. Resuspend in prewarmed E8™ or mTeSR™ +RI
7. Transfer to Matrigel coated plate
8. Gently shake and incubate
9. Next Day: aspirate media and replace with prewarmed E8™ or mTeSR™ (no RI)
10. Change media daily (or every other day if low confluency and add additional media)

Passaging/Splitting

1. Prewarm Accutase™, DPBS, E8™ or mTeSR™ +RI
2. Aspirate Media
3. Wash with 1 mL DPBS (no Ca Mg)
4. Add 1 mL Accutase™ and incubate 5min 37°C
5. Transfer Accutase™ with cells to 15ml conical
6. Add 2 mL DPBS to well then transfer to conical, repeat (should have 5 mL total in the conical)
7. Centrifuge 900 rpm for 4 min
8. Aspirate supernatant
9. Resuspend in prewarmed E8™ or mTeSR™ +RI, gently pipet
10. Aspirate Matrigel™ and plate cells in E8 or mTeSR™ +RI (2 mL per well for a six well plate, seed cells based on density 400,000 – 1million cells per well)
11. Gently rock plate and incubate

Freezing and storing

Prep Freezing Media: DMEM:F12 and 10% DMSO (option: with 20% FBS)
For 1 well of a 6-well plate at 70-80% confluency:

1. Aspirate
2. Wash w/1 mL DPBS
3. Add 1 mL Accutase™
4. Incubate 5 min at 37°C
5. Add 2-4 mL PBS and transfer to 15 mL conical (add PBS, transfer to conical, add more PBS, transfer to conical)
6. Centrifuge at 700-900 rpm for 4 min
7. Aspirate
8. Resuspend in 0.5mls freezing media
9. Transfer to cryovial
10. Put in CoolCell®, put in -80°C for 48 hr
11. Transfer to liquid nitrogen

4.8.2 Differentiating iPSCs into i³Neurons

Table 4.2. Materials for neuronal differentiation

Item	Catalog #
Essential 8™ Medium (with E8 supplement)	A1517001
mTeSR™1	5850
Y-27632 (hydrochloride), ROCK inhibitor	10005583
MATRIGEL™ MATRIX GFR PHENOL RED-FREE 10mL	356231
Knockout DMEM	10829018
MEM Non-Essential Amino Acids Solution (100X) (NEAA)	11140050
Recombinant Human NT-3	450-03
Recombinant Human BDNF	450-02
Knockout DMEM/F12	12660-012
Neurobasal®-A Medium	12349-015
B-27® Supplement (50X), serum free	17504044
N-2 Supplement (100X)	17502-048
Laminin Mouse Protein, Natural (for small batch culture)	23017-015
Doxycycline hyclate	D9891
StemPro® Accutase® Cell Dissociation Reagent	A1110501
GlutaMAX™ Supplement	35050-061
Gibco™ Poly-D-Lysine	A3890401
Recombinant Human NT-3	450-03
Recombinant Human BDNF	450-02
Neurobasal®-A Medium	12349-015
B-27® Supplement (50X), serum free	17504044
N-2 Supplement (100X)	17502-048
Laminin Mouse Protein, Natural	23017-015
Doxycycline hyclate	D9891
6-well, sterile, cell culture-treated, individually wrapped plates	

Aliquoting
Knockout DMEM F12
50 mL aliquots store at 4°C

Neurobasal Media and DMEM F12
Aliquot into 50 mL conicals at a 1:1 ratio (25 mL each)

BDNF 50 µL aliquots of 1000x (10 µg/mL) in 0.1%BSA store in -80°C
NT3 50 µL aliquots of 1000x (10 µg/mL) in 0.1%BSA store in -80°C

Mouse Laminin thaw at 4°C, 50ul aliquots of 1000x (1 mg/mL) store at 5°C to -20°C for six months
Doxycyline 50 µL aliquots of 1000x (2 mg/mL) in PBS at -20°C
N2 thaw overnight at 4°C, 500 µL aliquots of 100x store at -20°C
B27 thaw overnight at 4°C, 500 µL aliquots of 50x store at -20°C
Non-essential amino acids (NEAA) 500 µL aliquots of 100x store in 4°C
Glutamax™ 250 µL aliquots of 100x store in 4°C

Media Preparation
Predifferentiation Media
(Filter after preparation if necessary)
50 mL KO DMEM F12
500 µL 100x N2
500 µL 100x NEAA
50 µL 1000x BDNF
50 µL 1000x NT3
50 µL 1000x mouse laminin
50 µL 1000x doxycycline
50 µL 1000x ROCK Inhibitor*
* After day 1, no ROCK inhibitor

Maturation Media
(filter after preparation if necessary)
25 mL Neurobasal A Media
25 mL DMEM F12
250 µL 100x N2
500 µL 50x B27
500 µL 100x NEAA
250 µL 100x Glutamax™
50 µL 1000x BDNF
50 µL 1000x NT3
50 µL 1000x mouse laminin
50 µL 1000x doxycycline*
*Weeks 2-5 no doxycycline

Coating with Poly-D-Lysine (PDL) (0.1mg/ml)

1. Dilute desired volume in half with DPBS (0.05 mg/mL)
2. Coat plate with half well volume (12 well plate, 0.5 mL per well)
3. Incubate at RT for 1 hr
4. Remove solution

5. Rinse three times with DPBS
6. Let Dry 2 hours
7. Use or store wrapped in parafilm at 4°C for up to a week

Predifferentiation from Ngn2 iPSCs into I³Neurons

1. Aspirate media
2. Rinse with 1 mL DPBS
3. Add 1 mL Accutase™
4. Incubate 5 min at 37°C
5. Add 2–4 mL DPBS and transfer to 15 mL conical (add 2ml PBS, transfer to conical, add more PBS, transfer to conical)
6. Centrifuge at 700-900rpm for 4 min
7. Aspirate
8. Resuspend in 1 mL E8™ or mTeSR™ with RI
9. Seed 1 million cells per well (6-welll plate) in predifferentiation media
10. Incubate overnight
11. Aspirate media
12. Replace with day 2+ media, repeat until morphology starts to change (~ 3 days)

Freezing and storing

Prep freezing media for predifferentiated I³Neurons: KO DMEM F12 with 20% FBS and 10% DMSO

For 1 well of a 6-well plate at 70-80% confluency:

1. Aspirate
2. Wash w/1 mL DPBS
3. Add 1 mL Accutase™
4. Incubate 5 min at 37°C
5. Add 2–4 mL PBS and transfer to 15 mL conical tube (add PBS, transfer to conical, add more PBS, transfer to conical)
6. Centrifuge at 700–900 rpm for 4 min
7. Aspirate
8. Resuspend in 0.5 mL freezing media
9. Transfer to cryovial
10. Put in CoolCell®, put in -80°C for 48 hr then transfer to liquid nitrogen

Maturation

Thawing and plating predifferentiated I³Neurons for maturation

1. Prewarm: 9 mL DMEM:F12, week 1 MM (100 µL per well, 96 well PDL-coated plate)
2. Thaw cryovial halfway

3. When it is half thawed, Use warmed DMEM:F12 to transfer the cells to a 15 mL conical tube (with the rest of the DMEM:F12)
4. Centrifuge 3–5 min 200g/750rpm
5. Aspirate supernatant from tube of cells
6. Resuspend in 1 mL week 1 maturation media
7. Seed 200,000 cells per mL in PDL-coated plate with maturation media
8. Gently shake and incubate

Maturation directly from predifferentiation

1. Aspirate media
2. Rinse with 1 mL DPBS
3. Add 1 mL Accutase™
4. Incubate 5 min at 37°C
5. Add 2–4 mL PBS and transfer to 15 mL conical tube (add PBS, transfer to conical, add more PBS, transfer to conical)
6. Centrifuge at 700–900 rpm for 4 min
7. Aspirate
8. Resuspend in 1 mL maturation media
9. Seed 200,000 cells per ml in PDL-coated plate with maturation media

Maintenance of Mature i^3Neurons

1. After one week, half-media change with week 2–5 maturation media
2. After another week, remove half media, replace with full volume of week 2–5 maturation media
3. After the third week, do the same
4. After the fourth week change 1/3 of the media weekly

Use cells before day 10 for experimentation if possible

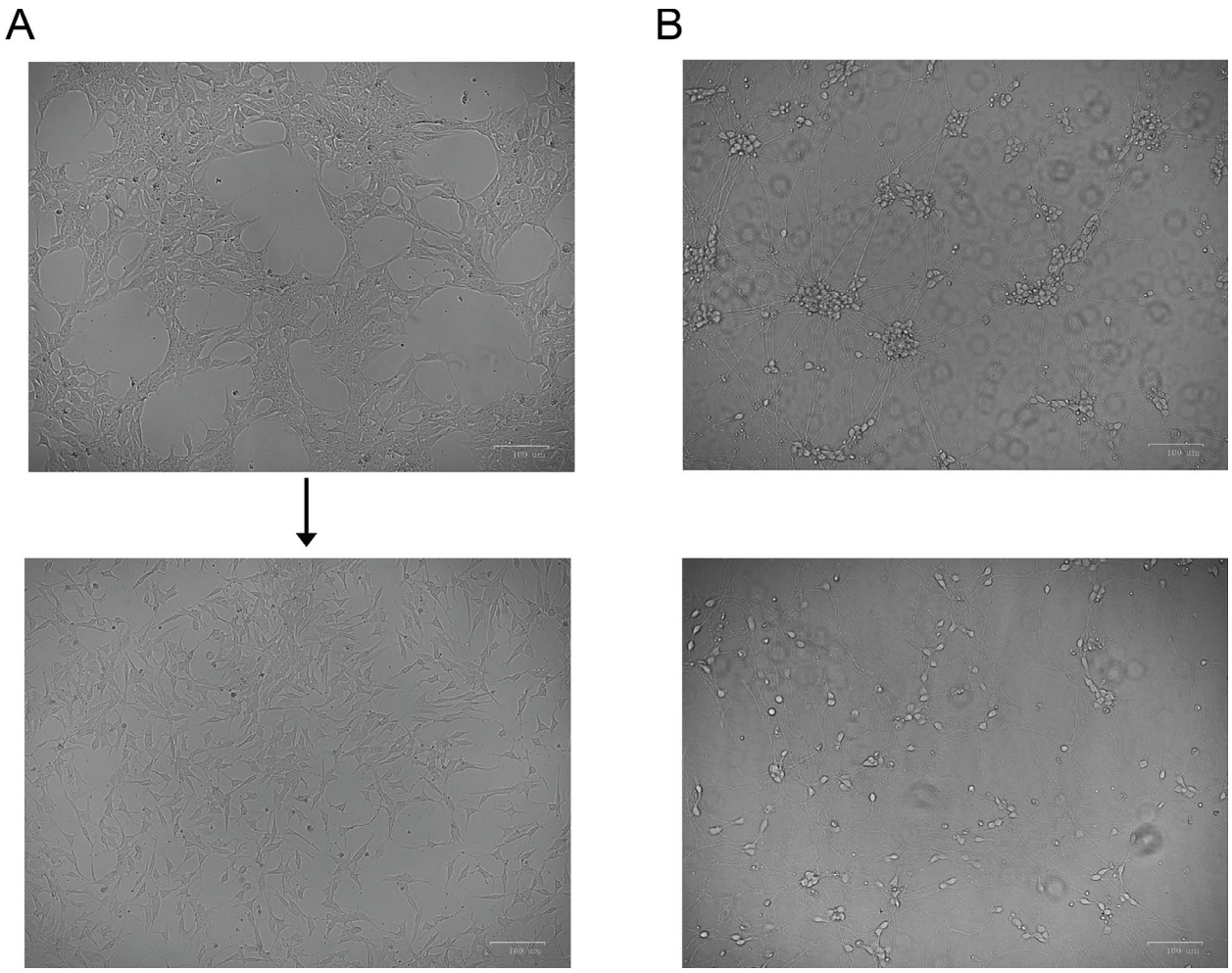

Figure 4.3. ZOE images of (A) Ngn2 iPSCs change in morphology upon pre-differentiation and (B) mature i^{3}Neurons.

4.8.3 Differentiating iPSCs into microglia

Table 4.3. Materials for microglia differentiation

Item	Catalog #
DMEM/F-12, HEPES, no phenol red	11039021
ReLesR™	50-206-9324
mTeSR™1	5850
Y-27632 (hydrochloride), ROCK inhibitor	10005583
StemDiff® Hematopoetic Kit	05310
GlutaMax	35050061
NEAA	11140050
Human Insulin	I2643-50MG
Insulin-Transferrin-Selenium (ITS-G) (1003)	41400045
B27	17504044
N2	17502048
Monothioglycerol	M1753-100ML11.5M
Human IL-34	200-34
Human TGFb1	100-21
Human MCSF	300-25
Human Fractalkine (CX3CL1)	300-31
Human CD200	C311-50ug

Aliquotting
Measurements are for 50 mL of media
Reconstituted and thawed cytokines are good at 4° for up to a week

Monothioglycerol 1M (Final 400 µM)
dilute in EtOH from 11.5 M to1 M by adding 1 mL to 10.5 mL EtOH aliquot to 20 µL (store at 4°)

Insulin 5 mg/mL (Final 5 ug/mL)
50mg in 10ml 0.01N HCl + 0.1%BSA, aliquot 50 µL/vial (store at -20°)

IL-34 100 µg/mL (final 100 ng/mL)
100ug in 1ml 0.1%BSA/DPBS aliquoted to 50 µL/vial (store at -20°)

TGF B1 100 µg/mL (final 50 ng/mL)
100ug in 1ml 0.1%BSA in Water, aliquoted to 25 µL/vial (store at -20°)

Human M-CSF 25 µg/mL (final 25 ng/mL)
50ug in 2ml 0.1%BSA in Water, aliquoted to 50 µL/vial (store at -20°)

Human Fractalkine (CX3CL1) 100 ug/ml (final 100 ng/mL)
100 µg in 1 mL 0.1%BSA in Water, aliquoted to 50 µL/vial (store at -20°)

Human CD200 100 µg/mL (final 100 ng/mL)
50 µg in 500 µL 0.1 % BSA in Water, aliquoted to 50 µL/vial (store at -20° for three months)

Media preparation
Medium A
store at 4 for three weeks (or -20° for 6 months)
45 mL Stemdiff™ Hematopooietic basal media
225 µL 200x Supplement A

Medium B
store at 4 for three weeks (or -20° for 6 months)
75 mL Stemdiff™ Hematopooietic basal media
375 µL 200x Supplement B

Microglia Basal Media (MBM)
50 mL DMEM/F12 phenol-free
500 µL 100x Glutamax™
500 µL 100x NEAA
50 µL Insulin (5 mg/mL stock)*
1 mL insulin-transferin-selenite or 250 µL of ITS dissolved
1 mL 50x B27
250 µL 100x N2
20 µL monothioglycerol (1M)*
IL-34 50 µL 100 µg/mL
TGBF-1 25µL 100 µg/mL
M-CSF 50 µL 25 µg/mL
* not sterile, requires filtration

Microglia Maturation Media (MMM)
50 mL DMEM/F12 phenol-free
500 µL 100x Glutamax™
500 µL 100x NEAA
50 µL Insulin (5 mg/mL stock)*
1 mL insulin-transferin-selenite or 250 µL of ITS dissolved
1 mL 50x B27
250 µL 100x N2
20 µL monothioglycerol (1M)*

IL-34 50ul 100 µg/mL
TGBF-1 25ul 100 µg/mL
M-CSF 50ul 25 µg/mL
CD200 50ul 100 µg/mL
CX3CL1 50ul 100 µg/mL
*not sterile, requires filtration

Note: cytokines should be added fresh to media (not done in bulk)

Forming HPCs from ADRC76 iPSCs
Grow ADRC76 iPSCs in mTeSR™ for >2 passages to 40-60% confluency
Day 0

1. Wash cells with DPBS (no Ca or Mg)
2. Add 1 mL ReLeSR™ for 1 min
3. Aspirate, let sit 4 min
4. Add 1 mL mTeSR™ + RI and tap plate to detach cell clumps
5. Check clump size –if too large, pipet once (want final clumps to be 100-200 µm in diameter)
6. Dilute 500 µL–1 mL into 5 mL mTeSR™ + RI, mix gently
7. Take three 50 µL aliquots of cells and put them in three wells of 96-well plate
8. Count clumps that are 100-200 µm in diameter
9. Seed 60 – 100 clumps per well of a 6-well plate in mTeSR™ + RI (want about 40 surviving clumps per well)

Day 1

10. (once colonies look good, wait an extra day if necessary - density and size must be good to continue on successfully)
11. Replace mTeSR™ with Medium A

Day 3

12. Add another 1ml of Medium A

Day 4 (make sure colonies look good before proceeding - if not, leave in A for another day)

13. Let plate sit in hood 5min
14. Aspirate media from top and replace with Medium B
15. Every two days, half medium change

HPC Collection (Day 11 -13)

1. Use 1000 µL pipet to withdraw media and gently flush semi-attached cells
2. Transfer to 15 mL conical
3. Centrifuge 10 min at 200 g
4. Transfer supernatant back to wells (1ml/well) grow for two more days and collect again

5. Resuspend pellet in Bambanker freezing medium at 1 million cells/ 1 mL (or resuspend in MBM and go directly to microglial differentiation)
6. Put in CoolCell® in -80 °C 48 hr
7. Put in liquid nitrogen

HPC differentiation to microglia
Note: HPCs should be CD43+
Day 1

1. Thaw HPCs in per-warmed DMEM/F12 phenol-free w/HEPES (or come straight from HPC differentiation)
2. Transfer to 15 mL conical tube
3. Centrifuge 8 min at 400 g
4. resuspend in MBM
5. Plate 200,000–600,000 cells per well of 6-well Matrigel™-coated plate in MBM
6. Every two days add another 1 mL of media per well

Day 13

1. Remove cells from plate, leave 1 mL media behind
2. Centrifuge 6 min at 300 g
3. Resuspend in 1 mL MBM
4. Add back to plate
5. Every two days add 1 mL media per well

Day 26 (or go to co-culture)

1. Remove cells, leave 1 mL behind
2. Centrifuge 5 min 300 g
3. Resuspend in 1 mL MMM
4. Add back to plate

Day 28

1. Add 1 mL/well MMM

Day 29
Cells can be gently flushed from plate and moved to assay plate (coated with Matrigel™) for experimentation

3.9.4 Co-Culture I³Neurons and iMGL
***This section requires trial and error regarding media contents, timing, and cell-density

Co-Culture Media (CCM)
half neuronal maturation Meda and half microglial maturation media

Preparation for Co-Culture

1. Culture I3 in neuronal maturation media for 4 days
2. Culture iMGL in microglia basal medium 25 days

Day 26

1. Collect immature microglia in 15 mL conical tube
2. Centrifuge 5 min 300 g
3. Resuspend in co-culture media and dilute so that the final ratio of microglia to neurons is 1:5
4. Remove neuronal maturation media from mature I3 neurons and replace with co-culture media containing microglia

Day 28

Add half amount of CCM per well

Day 29

Begin Experimentation (viable for ~1week)

4.9 References and Notes

1. Al Abbar, A.; Ngai, S. C.; Nograles, N.; Alhaji, S. Y.; Abdullah, S. Induced Pluripotent Stem Cells: Reprogramming Platforms and Applications in Cell Replacement Therapy. *BioResearch Open Access* 2020, *9* (1), 121–136. https://doi.org/10.1089/biores.2019.0046.
2. Bragança, J.; Lopes, J. A.; Mendes-Silva, L.; Santos, J. M. A. Induced Pluripotent Stem Cells, a Giant Leap for Mankind Therapeutic Applications. *World Journal of Stem Cells* 2019, *11* (7), 421–430. https://doi.org/10.4252/wjsc.v11.i7.421.
3. Grandy, R.; Tomaz, R. A.; Vallier, L. Modeling Disease with Human Inducible Pluripotent Stem Cells. *Annual Review of Pathology: Mechanisms of Disease* 2019, *14* (1), 449–468. https://doi.org/10.1146/annurev-pathol-020117-043634.
4. Huang, C.-Y.; Liu, C.-L.; Ting, C.-Y.; Chiu, Y.-T.; Cheng, Y.-C.; Nicholson, M. W.; Hsieh, P. C. H. Human IPSC Banking: Barriers and Opportunities. *Journal of Biomedical Science* 2019, *26* (1). https://doi.org/10.1186/s12929-019-0578-x.
5. Kim, C. IPSC Technology-Powerful Hand for Disease Modeling and Therapeutic Screen. *BMB Reports* 2015, *48* (5), 256–265. https://doi.org/10.5483/bmbrep.2015.48.5.100.
6. Singh, V. K.; Kalsan, M.; Kumar, N.; Saini, A.; Chandra, R. Induced Pluripotent Stem Cells: Applications in Regenerative Medicine, Disease Modeling, and Drug Discovery. *Frontiers in Cell and Developmental Biology* 2015, *3* (2). https://doi.org/10.3389/fcell.2015.00002.
7. Takahashi, K.; Yamanaka, S. A Decade of Transcription Factor-Mediated Reprogramming to Pluripotency. *Nature Reviews Molecular Cell Biology* 2016, *17* (3), 183–193. https://doi.org/10.1038/nrm.2016.8.
8. Teshigawara, R.; Cho, J.; Kameda, M.; Tada, T. Mechanism of Human Somatic Reprogramming to IPS Cell. *Laboratory Investigation* 2017, *97* (10), 1152–1157. https://doi.org/10.1038/labinvest.2017.56.
9. Dolmetsch, R.; Geschwind, Daniel H. The Human Brain in a Dish: The Promise of IPSC-Derived Neurons. *Cell* 2011, *145* (6), 831–834. https://doi.org/10.1016/j.cell.2011.05.034.

10. Marescal, O.; Cheeseman, I. M. Cellular Mechanisms and Regulation of Quiescence. *Developmental Cell* 2020, *55* (3), 259–271. https://doi.org/10.1016/j.devcel.2020.09.029.
11. Urbán, N.; Cheung, T. H. Stem Cell Quiescence: The Challenging Path to Activation. *Development* 2021, *148* (3), dev165084. https://doi.org/10.1242/dev.165084.
12. Oh, Y.; Jang, J. Directed Differentiation of Pluripotent Stem Cells by Transcription Factors. *Molecules and cells* 2019, *42* (3), 200–209. https://doi.org/10.14348/molcells.2019.2439.
13. Lin, S. S.; DeLaura, S.; Jones, E. M. The CIRM IPSC Repository. *Stem Cell Research* 2020, *44*, 101671. https://doi.org/10.1016/j.scr.2019.101671.
14. Ramos, D. M.; Skarnes, W. C.; Singleton, A. B.; Cookson, M. R.; Ward, M. E. Tackling Neurodegenerative Diseases with Genomic Engineering: A New Stem Cell Initiative from the NIH. *Neuron* 2021, *109* (7), 1080–1083. https://doi.org/10.1016/j.neuron.2021.03.022.
15. Fernandopulle, M. S.; Prestil, R.; Grunseich, C.; Wang, C.; Gan, L.; Ward, M. E. Transcription Factor-Mediated Differentiation of Human IPSCs into Neurons. *Current Protocols in Cell Biology* 2018, *79* (1), e51. https://doi.org/10.1002/cpcb.51.
16. Pawlowski, M.; Ortmann, D.; Bertero, A.; Tavares, J. M.; Pedersen, R. A.; Vallier, L.; Kotter, M. R. N. Inducible and Deterministic Forward Programming of Human Pluripotent Stem Cells into Neurons, Skeletal Myocytes, and Oligodendrocytes. *Stem Cell Reports* 2017, *8* (4), 803–812. https://doi.org/10.1016/j.stemcr.2017.02.016.
17. Otomo, J.; Woltjen, K.; Sakurai, H. Uniform Transgene Activation in Tet-on Systems Depends on Sustained RtTA Expression. *iScience* 2023, *26* (10), 107685–107685. https://doi.org/10.1016/j.isci.2023.107685.
18. Castro-Viñuelas, R.; Sanjurjo-Rodríguez, C.; Piñeiro-Ramil, M.; Rodríguez-Fernández, S.; López-Baltar, I.; Fuentes-Boquete, I.; Blanco, F. J.; Díaz-Prado, S. Tips and Tricks for Successfully Culturing and Adapting Human Induced Pluripotent Stem Cells. *Molecular Therapy - Methods & Clinical Development* 2021, *23*, 569–581. https://doi.org/10.1016/j.omtm.2021.10.013.
19. Yasui, R.; Sekine, K.; Taniguchi, H. Clever Experimental Designs: Shortcuts for Better IPSC Differentiation. *Cells* 2021, *10* (12), 3540. https://doi.org/10.3390/cells10123540.
20. Bonaventura, G.; Iemmolo, R.; Attaguile, G. A.; La Cognata, V.; Pistone, B. S.; Raudino, G.; D'Agata, V.; Cantarella, G.; Barcellona, M. L.; Cavallaro, S. IPSCs: A Preclinical Drug Research Tool for Neurological Disorders. *International Journal of Molecular Sciences* 2021, *22* (9), 4596. https://doi.org/10.3390/ijms22094596.
21. Engle, S. J.; Blaha, L.; Kleiman, R. J. Best Practices for Translational Disease Modeling Using Human IPSC-Derived Neurons. *Neuron* 2018, *100* (4), 783–797. https://doi.org/10.1016/j.neuron.2018.10.033.
22. Hong, Y. J.; Do, J. T. Neural Lineage Differentiation from Pluripotent Stem Cells to Mimic Human Brain Tissues. *Frontiers in Bioengineering and Biotechnology* 2019, *7*. https://doi.org/10.3389/fbioe.2019.00400.
23. Pandey, S.; Jirásko, M.; Lochman, J.; Chvátal, A.; Chottova Dvorakova, M.; Kučera, R. IPSCs in Neurodegenerative Disorders: A Unique Platform for Clinical Research and Personalized Medicine. *Journal of Personalized Medicine* 2022, *12* (9), 1485. https://doi.org/10.3390/jpm12091485.

24. Takahashi, K.; Tanabe, K.; Ohnuki, M.; Narita, M.; Ichisaka, T.; Tomoda, K.; Yamanaka, S. Induction of Pluripotent Stem Cells from Adult Human Fibroblasts by Defined Factors. *Cell* 2007, *131* (5), 861–872.https://doi.org/10.1016/j.cell.2007.11.019.
25. Yu, J.; Vodyanik, M. A.; Smuga-Otto, K.; Antosiewicz-Bourget, J.; Frane, J. L.; Tian, S.; Nie, J.; Jonsdottir, G. A.; Ruotti, V.; Stewart, R.; Slukvin, I. I.; Thomson, J. A. Induced Pluripotent Stem Cell Lines Derived from Human Somatic Cells. *Science* 2007, *318* (5858), 1917–1920. https://doi.org/10.1126/science.1151526.
26. Malik, N.; Rao, M. S. A Review of the Methods for Human IPSC Derivation. *Methods in Molecular Biology* 2013, *997*, 23–33. https://doi.org/10.1007/978-1-62703-348-0_3.
27. Estrada, V.; Ayse Tekinay; Hans Werner Müller. Neural ECM Mimetics. *Progress in brain research* 2014, 391–413. https://doi.org/10.1016/b978-0-444-63486-3.00016-5.
28. Hughes, C. S.; Postovit, L. M.; Lajoie, G. A. Matrigel: A Complex Protein Mixture Required for Optimal Growth of Cell Culture. *PROTEOMICS* 2010, *10* (9), 1886–1890. https://doi.org/10.1002/pmic.200900758.
29. Kim, H. Splitting HESC/HiPSC Lines on MEF Using Accutase. *StemBook* 2014. https://doi.org/10.3824/stembook.1.87.1.
30. Kantor, B.; Ornit Chiba-Falek. Lentiviral Vectors as the Delivery Vehicles for Transduction into IPSCs. *Elsevier eBooks* 2021, 79–100. https://doi.org/10.1016/b978-0-323-85766-6.00005-x.
31. Fajrial, A. K.; He, Q. Q.; Wirusanti, N. I.; Slansky, J. E.; Ding, X. A Review of Emerging Physical Transfection Methods for CRISPR/Cas9-Mediated Gene Editing. *Theranostics* 2020, *10* (12), 5532–5549. https://doi.org/10.7150/thno.43465.
32. Chong, Z. X.; Yeap, S. K.; Ho, W. Y. Transfection Types, Methods and Strategies: A Technical Review. *PeerJ* 2021, *9*. https://doi.org/10.7717/peerj.11165.
33. Geng, B.; Choi, K.-H.; Wang, S.; Chen, P.; Pan, X.; Dong, N.; Ko, J.-K.; Zhu, H. A Simple, Quick, and Efficient CRISPR/Cas9 Genome Editing Method for Human Induced Pluripotent Stem Cells. *Acta Pharmacologica Sinica* 2020, *41* (11), 1427–1432. https://doi.org/10.1038/s41401-020-0452-0.
34. Ng, A. H. M.; Khoshakhlagh, P.; Rojo Arias, J. E.; Pasquini, G.; Wang, K.; Swiersy, A.; Shipman, S. L.; Appleton, E.; Kiaee, K.; Kohman, R. E.; Vernet, A.; Dysart, M.; Leeper, K.; Saylor, W.; Huang, J. Y.; Graveline, A.; Taipale, J.; Hill, D. E.; Vidal, M.; Melero-Martin, J. M. A Comprehensive Library of Human Transcription Factors for Cell Fate Engineering. *Nature Biotechnology* 2020, *39* (4), 510–519. https://doi.org/10.1038/s41587-020-0742-6.
35. Telias, M. Neural Differentiation Protocols: How to Choose the Correct Approach. *Neural Regeneration Research* 2023, *18* (6), 1273. https://doi.org/10.4103/1673-5374.360171.
36. Earley, A. M.; Burbulla, L. F.; Krainc, D.; Awatramani, R. Identification of ASCL1 as a Determinant for Human IPSC-Derived Dopaminergic Neurons. *Scientific Reports* 2021, *11* (1). https://doi.org/10.1038/s41598-021-01366-4.
37. Ng, Y. H.; Chanda, S.; Janas, J. A.; Yang, N.; Kokubu, Y.; Südhof, T. C.; Wernig, M. Efficient Generation of Dopaminergic Induced Neuronal Cells with Midbrain Characteristics. *Stem Cell Reports* 2021, *16* (7), 1763–1776. https://doi.org/10.1016/j.stemcr.2021.05.017.

38. Bell, S.; Hettige, N.; Silveira, H.; Peng, H.; Wu, H.; Jefri, M.; Antonyan, L.; Zhang, Y.; Zhang, X.; Ernst, C. Differentiation of Human Induced Pluripotent Stem Cells (IPSCs) into an Effective Model of Forebrain Neural Progenitor Cells and Mature Neurons. *BIO-PROTOCOL* 2019, *9* (5). https://doi.org/10.21769/bioprotoc.3188.
39. Zink, A.; Lisowski, P.; Prigione, A. Generation of Human IPSC-Derived Neural Progenitor Cells (NPCs) as Drug Discovery Model for Neurological and Mitochondrial Disorders. *BIO-PROTOCOL* 2021, *11* (5). https://doi.org/10.21769/bioprotoc.3939.
40. Hofrichter, M.; Nimtz, L.; Tigges, J.; Kabiri, Y.; Friederike Schröter; Royer-Pokora, B.; Hildebrandt, B.; Schmuck, M.; Alexey Epanchintsev; Theiss, S.; Adjaye, J.; Egly, J.-M.; Krutmann, J.; Fritsche, E. Comparative Performance Analysis of Human IPSC-Derived and Primary Neural Progenitor Cells (NPC) Grown as Neurospheres in Vitro. *Stem Cell Research* 2017, *25*, 72–82. https://doi.org/10.1016/j.scr.2017.10.013.
41. Neaverson, A.; Andersson, M. H. L.; Arshad, O. A.; Foulser, L.; Goodwin-Trotman, M.; Hunter, A.; Newman, B.; Patel, M.; Roth, C.; Thwaites, T.; Kilpinen, H.; Hurles, M. E.; Day, A.; Gerety, S. S. Differentiation of Human Induced Pluripotent Stem Cells into Cortical Neural Stem Cells. *Frontiers in Cell and Developmental Biology* 2023, *10*, 1023340. https://doi.org/10.3389/fcell.2022.1023340.
42. Kang, S.; Chen, X.; Gong, S.; Yu, P.; Yau, S.; Su, Z.; Zhou, L.; Yu, J.; Pan, G.; Shi, L. Characteristic Analyses of a Neural Differentiation Model from IPSC-Derived Neuron according to Morphology, Physiology, and Global Gene Expression Pattern. *Scientific Reports* 2017, *7* (1), 12233. https://doi.org/10.1038/s41598-017-12452-x.
43. D'Aiuto, L.; Zhi, Y.; Kumar Das, D.; Wilcox, M. R.; Johnson, J. W.; McClain, L.; MacDonald, M. L.; Di Maio, R.; Schurdak, M. E.; Piazza, P.; Viggiano, L.; Sweet, R.; Kinchington, P. R.; Bhattacharjee, A. G.; Yolken, R.; Nimgaonka, V. L. Large-Scale Generation of Human IPSC-Derived Neural Stem Cells/Early Neural Progenitor Cells and Their Neuronal Differentiation. *Organogenesis* 2015, *10* (4), 365–377. https://doi.org/10.1080/15476278.2015.1011921.
44. Cao, S.-Y.; Hu, Y.; Chen, C.; Yuan, F.; Xu, M.; Li, Q.; Fang, K.-H.; Chen, Y.; Liu, Y. Enhanced Derivation of Human Pluripotent Stem Cell-Derived Cortical Glutamatergic Neurons by a Small Molecule. *Scientific Reports* 2017, *7* (1). https://doi.org/10.1038/s41598-017-03519-w.
45. Hansen, David V.; Rubenstein, John L. R.; Kriegstein, Arnold R. Deriving Excitatory Neurons of the Neocortex from Pluripotent Stem Cells. *Neuron* 2011, *70* (4), 645–660. https://doi.org/10.1016/j.neuron.2011.05.006.
46. Zhang, Y.; Pak, C.; Han, Y.; Ahlenius, H.; Zhang, Z.; Chanda, S.; Marro, S.; Patzke, C.; Acuna, C.; Covy, J.; Xu, W.; Yang, N.; Danko, T.; Chen, L.; Wernig, M.; Südhof, Thomas C. Rapid Single-Step Induction of Functional Neurons from Human Pluripotent Stem Cells. *Neuron* 2013, *78* (5), 785–798. https://doi.org/10.1016/j.neuron.2013.05.029.
47. Wang, C.; Ward, M. E.; Chen, R.; Liu, K.; Tracy, T. E.; Chen, X.; Xie, M.; Sohn, P. D.; Ludwig, C.; Meyer-Franke, A.; Karch, C. M.; Ding, S.; Gan, L. Scalable Production of IPSC-Derived Human Neurons to Identify Tau-Lowering Compounds by High-Content Screening. *Stem Cell Reports* 2017, *9* (4), 1221–1233. https://doi.org/10.1016/j.stemcr.2017.08.019.

48. Barretto, N.; Zhang, H.; Powell, S. K.; Fernando, M. B.; Zhang, S.; Flaherty, E. K.; Ho, S.-M.; Slesinger, P. A.; Duan, J.; Brennand, K. J. ASCL1- and DLX2-Induced GABAergic Neurons from HiPSC-Derived NPCs. *Journal of Neuroscience Methods* 2020, *334*, 108548. https://doi.org/10.1016/j.jneumeth.2019.108548.
49. Colasante, G.; Lignani, G.; Rubio, A.; Medrihan, L.; Yekhlef, L.; Sessa, A.; Massimino, L.; Giannelli, S. G.; Sacchetti, S.; Caiazzo, M.; Leo, D.; Alexopoulou, D.; Dell'Anno, M. T.; Ciabatti, E.; Orlando, M.; Studer, M.; Dahl, A.; Gainetdinov, R. R.; Taverna, S.; Benfenati, F. Rapid Conversion of Fibroblasts into Functional Forebrain GABAergic Interneurons by Direct Genetic Reprogramming. *Cell Stem Cell* 2015, *17* (6), 719–734. https://doi.org/10.1016/j.stem.2015.09.002.
50. Nicholas, C. R.; Chen, J.; Tang, Y.; Southwell, D. G.; Chalmers, N.; Vogt, D.; Arnold, C. M.; Chen, Y.-J. J.; Stanley, E. G.; Elefanty, A. G.; Sasai, Y.; Alvarez-Buylla, A.; Rubenstein, J. L. R.; Kriegstein, A. R. Functional Maturation of HPSC-Derived Forebrain Interneurons Requires an Extended Timeline and Mimics Human Neural Development. *Cell Stem Cell* 2013, *12* (5), 573–586. https://doi.org/10.1016/j.stem.2013.04.005.
51. Yang, N.; Chanda, S.; Marro, S.; Ng, Y.-H.; Janas, J. A.; Haag, D.; Ang, C. E.; Tang, Y.; Flores, Q.; Mall, M.; Wapinski, O.; Li, M.; Ahlenius, H.; Rubenstein, J. L.; Chang, H. Y.; Buylla, A. A.; Südhof, T. C.; Wernig, M. Generation of Pure GABAergic Neurons by Transcription Factor Programming. *Nature Methods* 2017, *14* (6), 621–628. https://doi.org/10.1038/nmeth.4291.
52. Grigor'eva, E. V.; Malankhanova, T. B.; Surumbayeva, A.; Pavlova, S. V.; Minina, J. M.; Kizilova, E. A.; Suldina, L. A.; Morozova, K. N.; Kiseleva, E.; Sorokoumov, E. D.; Lebedev, I. N.; Zakian, S. M.; Malakhova, A. A. Generation of GABAergic Striatal Neurons by a Novel IPSC Differentiation Protocol Enabling Scalability and Cryopreservation of Progenitor Cells. *Cytotechnology* 2020, *72* (5), 649–663. https://doi.org/10.1007/s10616-020-00406-7.
53. Kim, T.-G.; Yao, R.; Monnell, T.; Cho, J.-H.; Vasudevan, A.; Koh, A.; Peeyush, K. T.; Moon, M.; Datta, D.; Bolshakov, V. Y.; Kim, K.-S.; Chung, S. Efficient Specification of Interneurons from Human Pluripotent Stem Cells by Dorsoventral and Rostrocaudal Modulation. *STEM CELLS* 2014, *32* (7), 1789–1804. https://doi.org/10.1002/stem.1704.
54. Meneghello, G.; Verheyen, A.; Van Ingen, M.; Kuijlaars, J.; Tuefferd, M.; Van Den Wyngaert, I.; Nuydens, R. Evaluation of Established Human IPSC-Derived Neurons to Model Neurodegenerative Diseases. *Neuroscience* 2015, *301*, 204–212. https://doi.org/10.1016/j.neuroscience.2015.05.071.
55. Chinta, S. J.; Andersen, J. K. Dopaminergic Neurons. *The International Journal of Biochemistry & Cell Biology* 2005, *37* (5), 942–946. https://doi.org/10.1016/j.biocel.2004.09.009.
56. Razan Sheta; Teixeira, M.; Walid Idi; Pierre, M.; de, A.; Emond, V.; Zorca, C. E.; Benoît Vanderperre; Durcan, T. M.; Fon, E. A.; Calon, F.; Chahine, M.; Abid Oueslati. Combining NGN2 Programming and Dopaminergic Patterning for a Rapid and Efficient Generation of HiPSC-Derived Midbrain Neurons. 2022, *12* (1). https://doi.org/10.1038/s41598-022-22158-4.

57. de Rus Jacquet, A. Preparation and Co-Culture of IPSC-Derived Dopaminergic Neurons and Astrocytes. *Current Protocols in Cell Biology* 2019, *85* (1). https://doi.org/10.1002/cpcb.98.
58. Du, Z.-W.; Chen, H.; Liu, H.; Lu, J.; Qian, K.; Huang, C.-L.; Zhong, X.; Fan, F.; Zhang, S.-C. Generation and Expansion of Highly Pure Motor Neuron Progenitors from Human Pluripotent Stem Cells. *Nature Communications* 2015, *6* (1). https://doi.org/10.1038/ncomms7626.
59. Mazzoni, E. O.; Mahony, S.; Closser, M.; Morrison, C. A.; Nedelec, S.; Williams, D. J.; An, D.; Gifford, D. K.; Wichterle, H. Synergistic Binding of Transcription Factors to Cell-Specific Enhancers Programs Motor Neuron Identity. *Nature Neuroscience* 2013, *16* (9), 1219–1227. https://doi.org/10.1038/nn.3467.
60. Thiry, L.; Hamel, R.; Pluchino, S.; Durcan, T.; Stifani, S. Characterization of Human IPSC-Derived Spinal Motor Neurons by Single-Cell RNA Sequencing. *Neuroscience* 2020, *450*, 57–70. https://doi.org/10.1016/j.neuroscience.2020.04.041.
61. Bianchi, F.; Malboubi, M.; Li, Y.; George, J. H.; Jerusalem, A.; Szele, F.; Thompson, M. S.; Ye, H. Rapid and Efficient Differentiation of Functional Motor Neurons from Human IPSC for Neural Injury Modelling. *Stem Cell Research* 2018, *32*, 126–134. https://doi.org/10.1016/j.scr.2018.09.006.
62. Sances, S.; Bruijn, L.; Chandran, S.; Eggan, K.; Ho, R.; Klim, J.; Livesey, M.; Lowry, E.; Macklis, J.; Rushton, D.; Sadegh, C.; Sareen, D.; Wichterle, H.; Zhang, S.; Svendsen, C. Modeling ALS Using Motor Neurons Derived from Human Induced Pluripotent Stem Cells. *Nature neuroscience* 2016, *19* (4), 542–553. https://doi.org/10.1038/nn.4273.
63. Shi, Y.; Lin, S.; Staats, K. A.; Li, Y.; Chang, W.-H.; Hung, S.-T.; Hendricks, E.; Linares, G. R.; Wang, Y.; Son, E. Y.; Wen, X.; Kisler, K.; Wilkinson, B.; Menendez, L.; Sugawara, T.; Woolwine, P.; Huang, M.; Cowan, M. J.; Ge, B.; Koutsodendris, N. Haploinsufficiency Leads to Neurodegeneration in C9ORF72 ALS/FTD Human Induced Motor Neurons. *Nature Medicine* 2018, *24* (3), 313–325. https://doi.org/10.1038/nm.4490.
64. Dimos, J. T.; Rodolfa, K. T.; Niakan, K. K.; Weisenthal, L. M.; Mitsumoto, H.; Chung, W.; Croft, G. F.; Saphier, G.; Leibel, R.; Goland, R.; Wichterle, H.; Henderson, C. E.; Eggan, K. Induced Pluripotent Stem Cells Generated from Patients with ALS Can Be Differentiated into Motor Neurons. *Science (New York, N.Y.)* 2008, *321* (5893), 1218–1221. https://doi.org/10.1126/science.1158799.
65. Kumar, M.; Nguyen, N. T. P.; Milanese, M.; Bonanno, G. Insights into Human-Induced Pluripotent Stem Cell-Derived Astrocytes in Neurodegenerative Disorders. *Biomolecules* 2022, *12* (3), 344. https://doi.org/10.3390/biom12030344.
66. Stöberl, N.; Maguire, E.; Salis, E.; Shaw, B.; Hall-Roberts, H. Human IPSC-Derived Glia Models for the Study of Neuroinflammation. *Journal of Neuroinflammation* 2023, *20* (1). https://doi.org/10.1186/s12974-023-02919-2.
67. Pocock, J. M.; Piers, T. M. Modelling Microglial Function with Induced Pluripotent Stem Cells: An Update. *Nature Reviews Neuroscience* 2018, *19* (8), 445–452. https://doi.org/10.1038/s41583-018-0030-3.
68. Soubannier, V.; Maussion, G.; Chaineau, M.; Sigutova, V.; Rouleau, G.; Durcan, T. M.; Stifani, S. Characterization of Human IPSC-Derived Astrocytes with Potential for Disease Modeling and Drug Discovery. *Neuroscience Letters* 2020, *731*, 135028. https://doi.org/10.1016/j.neulet.2020.135028.

69. Dittlau, K. S.; Chandrasekaran, A.; Freude, K.; Den, V. Generation of Human Induced Pluripotent Stem Cell (HiPSC)-Derived Astrocytes for Amyotrophic Lateral Sclerosis and Other Neurodegenerative Disease Studies. *Bio-protocol* 2024, *14* (4). https://doi.org/10.21769/bioprotoc.4936.
70. Haenseler, W.; Rajendran, L. Concise Review: Modelling Neurodegenerative Diseases with Human Pluripotent Stem Cell Derived Microglia. *STEM CELLS* 2019. https://doi.org/10.1002/stem.2995.
71. Leventoux, N.; Morimoto, S.; Imaizumi, K.; Sato, Y.; Takahashi, S.; Mashima, K.; Ishikawa, M.; Sonn, I.; Kondo, T.; Watanabe, H.; Okano, H. Human Astrocytes Model Derived from Induced Pluripotent Stem Cells. *Cells* 2020, *9* (12), 2680. https://doi.org/10.3390/cells9122680.
72. Perriot, S.; Canales, M.; Mathias, A.; Du Pasquier, R. Differentiation of Functional Astrocytes from Human-Induced Pluripotent Stem Cells in Chemically Defined Media. *STAR Protocols* 2021, *2* (4), 100902. https://doi.org/10.1016/j.xpro.2021.100902.
73. Gunhanlar, N.; Shpak, G.; van der Kroeg, M.; Gouty-Colomer, L. A.; Munshi, S. T.; Lendemeijer, B.; Ghazvini, M.; Dupont, C.; Hoogendijk, W. J. G.; Gribnau, J.; de Vrij, F. M. S.; Kushner, S. A. A Simplified Protocol for Differentiation of Electrophysiologically Mature Neuronal Networks from Human Induced Pluripotent Stem Cells. *Molecular Psychiatry* 2017, *23* (5), 1336–1344. https://doi.org/10.1038/mp.2017.56.
74. Klapper, S. D.; Garg, P.; Dagar, S.; Lenk, K.; Gottmann, K.; Nieweg, K. Astrocyte Lineage Cells Are Essential for Functional Neuronal Differentiation and Synapse Maturation in Human IPSC-Derived Neural Networks. *Glia* 2019, *67* (10), 1893–1909. https://doi.org/10.1002/glia.23666.
75. Paşca, A. M.; Sloan, S. A.; Clarke, L. E.; Tian, Y.; Makinson, C. D.; Huber, N.; Kim, C. H.; Park, J.-Y.; O'Rourke, N. A.; Nguyen, K. D.; Smith, S. J.; Huguenard, J. R.; Geschwind, D. H.; Barres, B. A.; Paşca, S. P. Functional Cortical Neurons and Astrocytes from Human Pluripotent Stem Cells in 3D Culture. *Nature methods* 2015, *12* (7), 671–678. https://doi.org/10.1038/nmeth.3415.
76. Kim, Y. H.; Choi, S. H.; D'Avanzo, C.; Hebisch, M.; Sliwinski, C.; Bylykbashi, E.; Washicosky, K. J.; Klee, J. B.; Brüstle, O.; Tanzi, R. E.; Kim, D. Y. A 3D Human Neural Cell Culture System for Modeling Alzheimer's Disease. *Nature Protocols* 2015, *10* (7), 985–1006. https://doi.org/10.1038/nprot.2015.065.
77. Pelin Saglam-Metiner; Duran, E.; Sabour-Takanlou, L.; Cigir Biray-Avci; Ozlem Yesil-Celiktas. Differentiation of Neurons, Astrocytes, Oligodendrocytes and Microglia from Human Induced Pluripotent Stem Cells to Form Neural Tissue-On-Chip: A Neuroinflammation Model to Evaluate the Therapeutic Potential of Extracellular Vesicles Derived from Mesenchymal Stem Cells. *Stem cell reviews and reports (Online)* 2023, *20* (1), 413–436. https://doi.org/10.1007/s12015-023-10645-8.
78. McQuade, A.; Coburn, M.; Tu, C. H.; Hasselmann, J.; Davtyan, H.; Blurton-Jones, M. Development and Validation of a Simplified Method to Generate Human Microglia from Pluripotent Stem Cells. *Molecular Neurodegeneration* 2018, *13* (1). https://doi.org/10.1186/s13024-018-0297-x.

CHAPTER 5

A Side Quest: Quantifying Hydrolytic Enzymes in the Human Vitreous Humor using an LC-/MS/MS-based Targeted Proteomics Approach

5.1 Preface to chapter 5

Chapter 5 is adapted from a manuscript that will be submitted for publication this year. This chapter details the work I did as a bioanalytical intern in the department of translational sciences at AbbVie in the department of local delivery and translational sciences. I was in this position for three months over the summer of 2024 and was tasked with quantifying hydrolytic enzymes in the vitreous humor using primarily high-pressure liquid chromatography triple quadrupole tandem mass spectrometry. This research was of interest to AbbVie for informing the design of models of intravitreal implant degradation. I thank AbbVie, Executive Director of Local Delivery and Translational Sciences Joshua Rowe, and Dr. Alireza Abdolvahabi for giving me this opportunity, guiding me through this research, being co-authors on this chapter, and allowing me to include this chapter as part of my dissertation.

5.2 Introduction

The vitreous humor is a highly hydrated, viscoelastic, gelatinous fluid that occupies the posterior compartment of the eye between the lens and the retina.[1-3] This ocular fluid is avascular and generally considered to be connective tissue.[1] The make-up of the vitreous humor predominantly consists of collagen fibrils and glycosaminoglycans.[1,3-5] This matrix serves to maintain the shape and elasticity of the eye while protecting it from mechanical

trauma.[1,3,5] Additionally, the vitreous body serves to store and transport metabolites while acting as a barrier to biomolecules and cells.[1,4-6]

The eye has several natural barriers in addition to the vitreous humor including tears, the cornea, and the conjunctiva, among others.[1,2,4,7] While these ocular barriers are necessary to maintain vision and eye health, they make ocular drug delivery difficult.[2,4,7-9] Intravitreal injections have become a common route of administration for back of the eye diseases to overcome these barriers, even though they are relatively invasive procedures.[2,4,6-10] To avoid repeating these procedures, sustained drug delivery systems have been developed that slowly release a drug over several months.[2,6-12]

Biodegradable intravitreal implants have become a popular strategy for achieving sustained drug delivery to the back of the eye.[8,9,11,12] These implants are made of various biodegradable polymers that can be injected directly into the vitreous humor where they are hydrolyzed over time, allowing for the controlled release of a drug into the eye.[9,11,12] This method of drug delivery provides long-acting treatment where the rate of drug delivery is a function of implant degradation.[2,9,11-14] Because these implants are degraded through hydrolysis, hydrolytic enzymes have been hypothesized to play a role in their degradation.[6,7,9,11-14] Further investigation is needed to better understand the role of hydrolytic enzymes in the vitreous humor in implant degradation.[6] An important step in this investigation is to identify and quantify these enzymes in the vitreous humor.

Limited information is currently available regarding the abundance of hydrolytic enzymes in the vitreous humor.[6] Reports of absolute quantitation of any proteins in the vitreous humor are also limited.[3,5] Untargeted proteomic analyses of the human vitreous humor have been published for both “surrogate normal” samples and disease samples.[5,15-

[29] These studies report the identification of a variety of hydrolytic enzymes, often accompanied by a measure of relative abundance, but not absolute concentrations. To fill this gap, we report the identification and absolute quantification of selected hydrolytic enzymes in the human vitreous humor using liquid chromatography triple quadrupole tandem mass spectrometry.

Seven enzymes were selected for quantification based on data from five untargeted proteomics studies of the "surrogate normal" human vitreous humor: cathepsin D, carboxypeptidase E, ectonucleotide pyrophosphatase 2, β-hexosaminidase subunit α, serum paraoxonase 1, tripeptidyl peptidase 1, and ubiquitin carboxy-terminal hydrolase lysozyme 1 (**Table 5.1**). Cathepsin D (CTSD) is a lysosomal aspartic protease involved in the degradation of both intracellular and extracellular proteins, regulation of cell death, and activation of inflammatory cells (Benes).[30] Carboxypeptidase E (CPE) is an exopeptidase that removes C-terminal basic residues from prohormone and neuropeptide intermediates (Ji).[31] Ectonucleotide pyrophosphatase 2 (ENPP2), also known as autotaxin, is a secreted glycoprotein that mainly functions by hydrolyzing lysophosphatidylcholine to form lysophosphatidic acid.[32] β-hexosaminidase subunit α (HEXA) is a lysosomal glycoside hydrolase that removes terminal non-reducing GalNAc from the GM2 ganglioside.[33] Serum paraoxonase-1 (PON1) is a high-density lipoprotein-associated esterase that decreases lipid peroxide accumulation on low-density lipoprotein and protects against N-homocysteinylation.[34] Tripeptidyl peptidase 1 (TPP1) is a lysosomal serine protease that cleaves tripeptides from the amino terminus of small proteins.[35] Finally, ubiquitin carboxy-terminal hydrolase lysozyme 1 (UCHL1) is a deubiquitinating enzyme that is most abundant in the brain, where it is required for the maintenance of axonal integrity.[36]

Table 5.1. The most abundant hydrolytic enzymes in the human vitreous humor.

ENZYME (GENE)	ENZYME TYPE	PHYSIOLOGICAL PURPOSE
CTSD	Aspartic protease	Degrades intra- and extra-cellular proteins, regulates cell death, activates inflammatory responses
CPE	Exopeptidase	Cleaves prohormones and neuropeptide intermediates
ENPP2	Glycoprotein	Hydrolyzes lysophosphatidylcholine to form lysophosphatidic acid
HEXA	Lysosomal glycoside hydrolase	Removes terminal GalNAc from the GM2 ganglioside
PON1	High-density lipoprotein-associated esterase	Removes lipid peroxide from low-density lipoproteins, protects against N-homocysteinylation
TPP1	Serine protease	Cleaves N-terminal tripeptides in lysosomes
UCHL1	Deubiquinating	Maintains axonal integrity in neurons

5.3 Methods

5.3.1 Sample Preparation

Sample Preparation of Recombinant Proteins. Protein digestion was performed according to the literature.[37] Briefly, the enzymes were diluted to the desired concentration in 90 µL of 50 mM ammonium bicarbonate pH 8.4 with 5 mM DTT and 0.1 % Rapigest in a low protein-binding Eppendorf tube. The samples were then subjected to heating at 60 °C with orbital shaking for 30 min to reduce disulfide bond formation. Afterward, the samples were briefly centrifuged and 10 µL of trypsin was added to the samples at a ratio of 1:20 to the total protein concentration, bringing the total volume to 100 µL. The samples were heated to 37 °C overnight with orbital shaking. The following day the tubes were briefly centrifuged, and the reactions were quenched with 0.5 µL of formic acid. 1 µL of 1 µg/mL human repulsive

guidance molecular A (RGMa) was then added as an internal standard (~10 nM final concentration).

Sample Preparation of Vitreous Humors. Human VH samples were extracted from whole cadaver eyes that were purchased from San Diego Eye Bank (San Diego, CA). The average post-mortem interval for purchased eyes was 2 hours. The age, gender, and other underlying medical conditions for each subject were recorded. VH samples were frozen at -80 °C immediately after dissection and extraction and thawed at room temperature on the day of experiment.

The method of standard addition was implemented for quantification of the enzymes in vitreous humor samples. For this method, samples were made by transferring four 70 µl aliquots of a vitreous humor sample into low protein-binding Eppendorf tubes and adding 5 µl of varying concentrations of the recombinant enzymes diluted in 50 mM ammonium bicarbonate buffer pH 8.4. Initially, each enzyme was added at the same set of concentrations ranging from 0.2 to 5 µg/ml. Following preliminary results, relevant concentration ranges were chosen for each enzyme individually on the calculated abundance of the enzyme in the samples (**Table C1**). The unenriched sample had 5 µL of just buffer added. After enrichment, 5 µL of 100 mM DTT and 10 µL of 1% Rapigest (both in ammonium bicarbonate buffer) were added to each sample, bringing the volume to 90 µL. Proteasemax was substituted for Rapigest when it became temporarily unavailable. The two surfactants are both designed to enhance trypsin digestion.[38,39] Vitreous humor samples were subjected to the same method of digestion as previously described.

5.3.2 Method Development

Representative peptide fragments were chosen for each enzyme based on a simulated trypsin digestion, and three criteria: uniqueness, number of amino acids, and type of amino acids present.[40,41] The peptides needed to be exclusively present in the enzyme of interest and not contain the easily oxidizable amino acids cysteine and methionine.[40] Ideally, the peptides would have multiple charged residues to increase the number of potential ion transitions that could be detected by LC-MS. Uniqueness was determined using protein blast.[42] Any peptides between six and fourteen residues that fit these criteria were selected for method development. Once multiple peptides were chosen for each enzyme, protonated molecular ion and potential fragmented ion m/z values were determined using Skyline.[43] The resulting multiple reaction monitoring (MRM) ion pairs were monitored in LC-MS/MS experiments (**Table C2**).

5.3.3 Liquid Chromatography Tandem Mass Spectrometry

The samples were transferred to 200 µL glass HPLC vials and 30 µL was injected into the LC/MS-MS system for analysis. Samples were eluted off a C18 reverse phase column (Waters corp.) using 0.1% formic acid in water as solvent A and 0.1% formic acid in acetonitrile as solvent B. The total run time was 80 minutes. Peptides were detected using a Sciex triple quadrupole 7500 mass spectrometer operating in positive mode. MRM pairs are shown in **Table C2**. Peak areas for each MRM ion pair in the resulting chromatograms were calculated using Sciex OS software. These peak areas were plotted against the concentration of the added recombinant enzyme to make the standard addition calibration curve. To determine the initial concentration of enzyme in the sample, the equation for the

linear trendline was set equal to 0 and the x-intercept was calculated. The absolute value of the x-intercept was equivalent to the concentration in the VH sample.

5.4 Results

Five untargeted proteomic studies of the human vitreous humor were evaluated to determine the most abundant hydrolytic enzymes present in the human vitreous humor (**Table 5.2**).[16,17,23-25] Seven enzymes were chosen for the present study: cathepsin D (CTSD), carboxypeptidase E (CPE), ectonucleotide pyrophosphatase 2 (ENPP2), B-hexosaminidase subunit alpha (HEXA), serum paraoxonase 1 (PON1), tripeptidyl peptidase 1 (TPP1), and ubiquitin carboxy-terminal hydrolase lysozyme 1 (UCHL1). These enzymes varied in relative abundance from study to study (**Table C3**).

Table 5.2. Untargeted proteomic studies of the human vitreous humor.

Study	Study Purpose	Fractionation Method	Quantitation Method
Gao et al. 2008	Comparing vitreous proteome of Diabetes with and without diabetic retinopathy	SDS-PAGE	Nano-LC, ion trap MS/MS
Aretz et al. 2013	Mapping proteome of normal vitreous humor	Liquid phase isoelectric focusing and 1D SDS gel electrophoresis	UPLC, Orbitrap MS/MS
Murthy et al. 2014	Mapping proteome of normal vitreous humor	SDSPAGE, cation exchange chromatography, OFFGEL fractionator	Nano-LC, Orbitrap MS/MS
Naru et al. 2016	Comparing protein expression in normal and retinoblastoma vitreous humors	Basic reverse phase liquid chromatography	iTRAQ labelling, nano-LC, ESI-MS/MS (TOF)
Mohanty et al. 2020	Mapping proteome of normal vitreous humor	SDSPAGE, high-pH RPLC	Nano-UPLC, Orbitrap MS/MS

To identify the best peptides and ion transitions for quantitation, we first simulated digestion and fragmentation to determine all possible options.[40,41] Potential MRMs determined from Skyline calculations were inputted into the SCIEX system for detection (**Table C4**).[43] Trypsin digested samples of two representative human VH samples and recombinant forms of each enzyme were injected and analyzed by LC-MS/MS. Based on resulting peak intensities and consistencies we chose two MRM ion pairs for one representative peptide fragment for each of the seven enzymes for quantitation. The resulting LC-MS/MS method was used for sample analysis (**Figure 5.1)**.

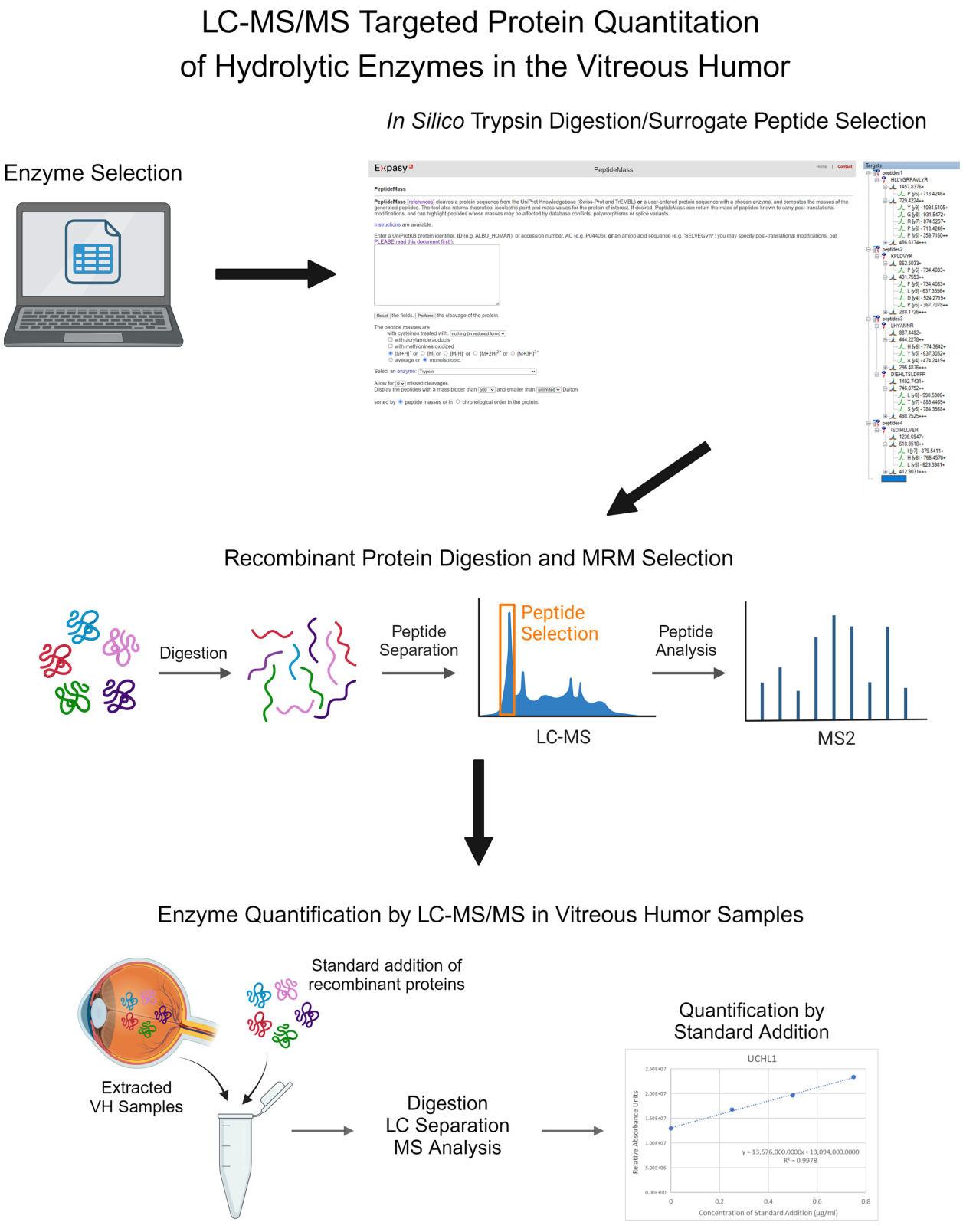

Figure 5.1. Schematic of the workflow for quantifying hydrolytic enzymes in the human vitreous humor using an LC-MS/MS-based targeted proteomics workflow.

Vitreous humor samples from eight human "surrogate normal" subjects (four male and four female) were digested. The enzyme concentrations varied minimally between replicate digestions for most of the enzymes and samples (**Figure 5.2**). Exceptions are likely due to a lack of homogeneity in the original vitreous humor sample or in the final samples. Some samples exhibited small amounts of precipitate before or after digestion, supporting this theory. Some digestions did not yield reliable or quantifiable data for all enzymes and these data points were excluded. Data was excluded for one of two reasons: either the results suggested that the concentration of that enzyme was below the limit of quantitation or the r-squared value for the line of best fit of the calibration curve was below 0.7. An enzyme was classified as below the limit of quantitation (LQ) if the peak for that enzyme in the unenriched sample exhibited a difference in retention time greater than a minute compared to the same peak in the samples with standard addition or if the line of best fit for the calibration curve had a negative y-intercept. CPE was below the limit of quantitation for all samples.

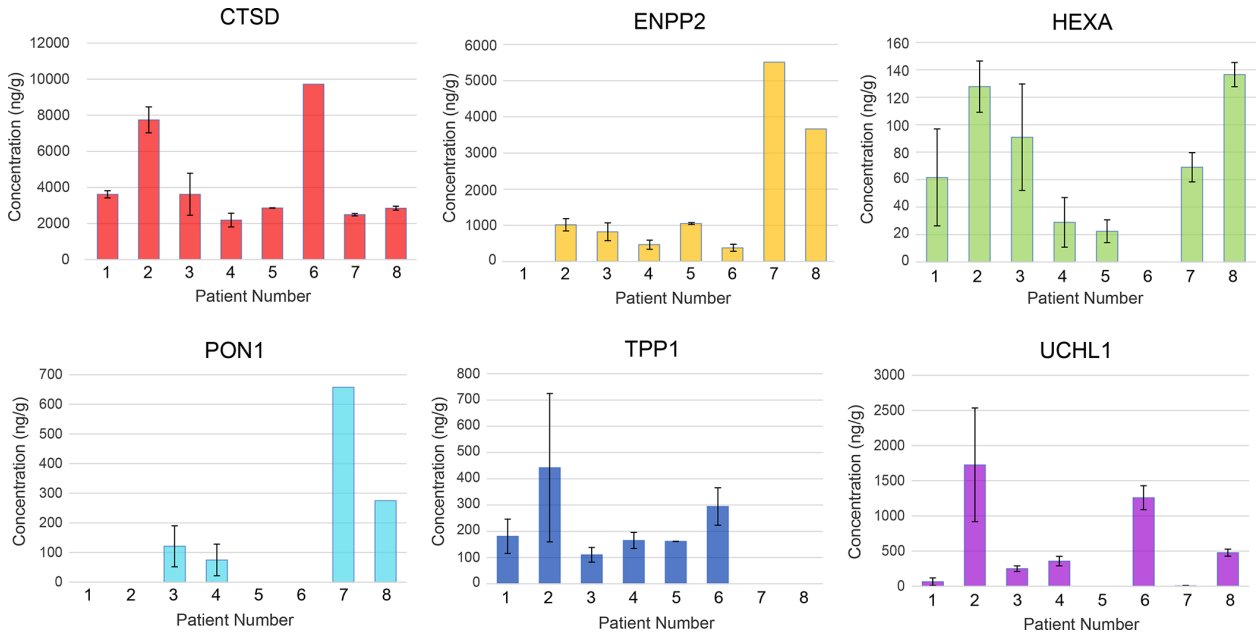

Figure 5.2. Levels of selected hydrolytic enzymes determined in human vitreous humors by LC-MS/MS.

Variation in enzyme concentration between different vitreous humor samples was significant, but there were a few notable trends (**Figure 5.2**) (**Table 5.3**). CTSD was the most abundance enzyme in most of the samples usually followed by either ENPP2 or UCHL1. Exceptions included subjects 1 and 5. Subject 1 had an abundance of ENPP2 below the limit of quantitation and an abundance of UCHL1 less than that of TPP1. Subject 5 had an abundance of UCHL1 below the limit of quantitation. The lowest abundance enzymes of the six, PON1 TPP1, and HEXA varied in order of abundance between samples.

On average, the order of abundance of each enzyme in the normal vitreous humor samples studied from most to least abundant was CTSD, ENPP2, UCHL1, TPP1, PON1, and HEXA (**Table 5.3**). However, there were two noticeable sex differences. The female averages followed the trend of the overall averages, but the male averages deviated slightly. Subjects 1, 3, 5, and 9 were male and subjects 2, 4, 6, and 8 were female. All the female subjects had higher abundances of UCHL1 than any of the male subjects and most of

the female subjects had higher abundances of TPP1 than the male subjects. For the males, on average, UCHL1 was less abundant than TPP1 and PON1 was more abundant than TPP1.

Table 5.3. Averages and ranges of concentrations for each enzyme from all samples. If an enzyme was below the limit of quantitation, it was reported as 0 for these calculations.

Enzyme	Average (ng/g)	Range (ng/g)	Female Average (ng/g)	Male Average (ng/g)
CTSD	4387.3	7537.6	5627.4	3147.2
ENPP2	1613.5	5514.1	1380.7	1846.4
HEXA	67.1	136.6	73.3	61.0
PON1	141.0	657.3	87.5	194.6
TPP1	169.4	442.5	225.6	113.2
UCHL1	517.4	1727.1	954.9	79.8

We also evaluated hydrolytic enzyme abundance in rabbits and non-human primates — animals commonly used to test ocular drugs.[44,45] Animal vitreous humors tested included two non-human primates, two New Zealand white rabbits, and two Dutch-belted rabbits (**Table 5.4**). CTSD and ENPP2 were the most abundant enzymes in all three species. Both rabbit species generally had higher concentrations of all the measurable enzymes than the non-human primates, but none of the compatible MRMs for human TPP1 were present in rabbits so we could not do a direct comparison. PON1 and UCHL1 were both below the limit of quantitation in both non-human primates. On average, all the animal vitreous humors tested had lower concentrations of all the enzymes than the human vitreous humors.

Table 5.4. Concentrations of each enzyme in all animal samples tested. "Below LQ" indicates that a value was below the limit of quantitation. "No compatible MRMs" indicates that there were no peptide sequences in the protein that matched the human peptide sequences that were suitable for quantitation.

Animal	CTSD ng/g	ENPP2 ng/g	HEXA ng/g	PON1 ng/g	TPP1 ng/g	UCHL1 ng/g
Non-human Primate 1	214.7	516.8	71.1	Below LQ	121.4	Below LQ
Non-human Primate 2	351.7	340.9	43.2	Below LQ	149.9	Below LQ
New Zealand White Rabbit 1	654.9	1426.8	567.6	Below LQ	no compatible MRMs	376.1
New Zealand White Rabbit 2	1145.5	Below LQ	74.1	40.2	no compatible MRMs	338.6
Dutch-Belted Rabbit 1	938.6	1256.4	106.8	Below LQ	no compatible MRMs	468.7
Dutch-Belted Rabbit 2	1678	1579.5	132.2	102.5	no compatible MRMs	551.8

5.5 Discussion

The five untargeted proteomics studies we used to select the enzymes of interest were chosen because they provided relative abundances for the largest number of proteins for control vitreous humor samples. Three out of five of these studies provided relative abundance in terms of percent sequence coverage (some in addition to other metrics).[16,24,25] Gao *et al*. provided spectral counts, the total number of spectra identified for each protein.[17,46] Mohanty *et al*. provided iBAQ (intensity-based absolute quantitation) values which represent the intensities of all peptides that map to a protein summed together and divided by the number of theoretically observable peptides.[23,47] This metric is thus similar in concept to percent sequence coverage. While these metrics are indicative of relative abundance, they are by no means totally quantitative.

The variation in average relative abundances between the untargeted studies can likely be explained by the small sample sizes used in each study. However, it should be

noted that while each of these studies used control vitreous humor samples, these samples did come from patients with various ocular conditions that led to vitrectomies or from dissected donor eyes. Aretz *et al*. used control samples from patients with epiretinal gliosis. Murthy *et al*. used control samples from five patients with macular holes, three patients with congenital cataracts, and two patients with traumatic cataract. Mohanty *et al*. and Naru *et al*. used samples dissected from healthy donor eyes. Vitreous humors obtained from live subjects were collected by pars plana vitrectomy.[16,17,24] Gao *et al*. did not specify why the control patients were undergoing this procedure. Every study performed LC-MS/MS and used nano-UPLC, and electrospray ionization. Three of the studies used orbitrap mass analyzers. Gao *et al*. used an ion trap, and Naru *et al*. used a qTOF mass analyzer.

We decided to use only one peptide per enzyme for quantification because some of the enzymes did not contain more than one peptide with sufficiently intense and consistent LC data for quantitation. If there had been multiple peptides suitable for quantitation for each enzyme, we likely would have performed quantification using multiple peptides to cross-check our results. While we did use multiple ion transitions for data verification, this served to verify the legitimacy of the data point as being representative of the intended protein, rather than verifying the abundance of that protein.

It is unsurprising that CTSD was the most abundant in our study since it has been reported in more proteomic studies of the vitreous humor than any other hydrolytic enzyme.[20,26,27] CTSD was either the most or second most abundant hydrolytic enzyme in the five untargeted studies we looked at. To our knowledge, of the seven enzymes we studied only ENPP2 has been absolutely quantified in human vitreous humor samples prior

to this study. In 2016, Dacheva *et al*. compared ENPP2 levels in 24 control vitreous humor samples (with idiopathic floaters) and 64 vitreous humor samples with retinal vein occlusion using Luminex technology. They reported that the average concentration of ENPP2 in control samples was 1.9 +/- 1.00 nM (roughly 0.2375 ng/g).[48] This value is almost three orders of magnitude less than our calculated average. This difference is likely due to differing methods of vitreous humor acquisition and quantitation. ELISAs like Luminex are typically less sensitive than LC/MS-MS analysis.

There have been a few studies that have focused on the abundances of some of these enzymes in the aqueous humor, but none were able to provide absolute concentrations.[49,50] Despite being below our limit of quantitation, CPE is reported to be highly abundant in the aqueous humor and other ocular tissue .[31,51] To our knowledge, the exact abundance of this enzyme in either the aqueous or vitreous humors has not been reported, but the relative abundances of CPE in studies of the vitreous and aqueous humors were high enough for the enzyme to be clearly identified.[16,17,23-25,31,51] CPE may have been undetectable in our study due to our method of quantitation, and further research using other methods may be able to absolutely quantify this enzyme.

To our knowledge, only one study has absolutely quantified hydrolytic enzymes in animal vitreous humors.[52] The study by Hammid *et al*. used NanoLC-MS/MS (Qtrap) analysis to quantify carboxylesterases in rabbit and pig ocular tissues. They reported that there were significant differences in the abundances of these enzymes between species and in different ocular regions. They also studied the hydrolytic activity of these enzymes with generic esterase substrates and ultimately concluded that additional esterases likely participate in the hydrolysis of these substrates in ocular tissue.[52] Untargeted proteomic

analyses of rabbit vitreous humors have also been reported,[53-55] but similar analyses of non-human primates have not been published.

Our results suggest that commonly used animal models have lower concentrations of hydrolytic enzymes in the vitreous humor compared to humans. While more in-depth analyses of the abundance of hydrolytic enzymes in model species should be done to confirm these results, the potential differences in concentrations of hydrolytic enzymes in animal vitreous humors should be taken into consideration when using animal models to study intravitreal implant degradation.[45] The methodology developed in this study may be used for this purpose, or to compare enzyme levels between patient populations and disease states. Studies have shown that these enzymes may be up or downregulated in certain diseases and that should be considered when designing *in vitro* models.[2,15,17,19,21,25,26,56,57]

5.6 Summary and Conclusions

The potential for hydrolytic enzymes to be involved in the degradation of intravitreal biodegradable implants, or metabolism of intravitreal drugs and prodrugs needs further research. The identity and concentrations of the most abundant hydrolytic enzymes in the vitreous humor enables future research to address this need. Current *in vitro* models of implant degradation do not mimic all the factors in the eye that can affect degradation and more realistic models are needed.[7,58] While there are several aspects of model design that have room for improvement, we anticipate that the knowledge gained from this research can aid in the development of better *in vitro* models of intravitreal implant degradation and help inform the design of said implants.

5.7 References and Notes

1. Chirila, T. V.; Hong, Y. Chapter C2 the Vitreous Humor. *Handbook of Biomaterial Properties* 2016, 125–134. https://doi.org/10.1007/978-1-4939-3305-1_12.
2. O'Brien Laramy, M. N.; Nagapudi, K. Long-Acting Ocular Drug Delivery Technologies with Clinical Precedent. *Expert Opinion on Drug Delivery* 2022, 1–17. https://doi.org/10.1080/17425247.2022.2108397.
3. Monteiro, J. P.; Santos, F. M.; Rocha, A. S.; Castro-de-Sousa, J. P.; Queiroz, J. A.; Passarinha, L. A.; Tomaz, C. T. Vitreous Humor in the Pathologic Scope: Insights from Proteomic Approaches. *Proteomics. Clinical Applications* 2015, *9* (1-2), 187–202. https://doi.org/10.1002/prca.201400133.
4. Käsdorf, B.; Arends, F.; Lieleg, O. Diffusion Regulation in the Vitreous Humor. *Biophysical Journal* 2015, *109* (10), 2171–2181. https://doi.org/10.1016/j.bpj.2015.10.002.
5. Fátima Milhano Santos; Ciordia, S.; Mesquita, J.; João Paulo Sousa; Paradela, A.; Tomaz, C. T.; Passarinha, L. A. Vitreous Humor Proteome: Unraveling the Molecular Mechanisms Underlying Proliferative and Neovascular Vitreoretinal Diseases. *Cellular and Molecular Life Sciences* 2022, *80* (1). https://doi.org/10.1007/s00018-022-04670-y.
6. del Amo, E. M.; Rimpelä, A.-K.; Heikkinen, E.; Kari, O. K.; Ramsay, E.; Lajunen, T.; Schmitt, M.; Pelkonen, L.; Bhattacharya, M.; Richardson, D.; Subrizi, A.; Turunen, T.; Reinisalo, M.; Itkonen, J.; Toropainen, E.; Casteleijn, M.; Kidron, H.; Antopolsky, M.; Vellonen, K.-S.; Ruponen, M. Pharmacokinetic Aspects of Retinal Drug Delivery. *Progress in Retinal and Eye Research* 2017, *57*, 134–185. https://doi.org/10.1016/j.preteyeres.2016.12.001.
7. Adrianto, M. F.; Annuryanti, F.; Wilson, C. G.; Sheshala, R.; Thakur, R. R. S. In Vitro Dissolution Testing Models of Ocular Implants for Posterior Segment Drug Delivery. *Drug Delivery and Translational Research* 2021. https://doi.org/10.1007/s13346-021-01043-z.
8. Al-Qaysi, Z. K.; Beadham, I. G.; Schwikkard, S. L.; Bear, J. C.; Al-Kinani, A. A.; Alany, R. G. Sustained Release Ocular Drug Delivery Systems for Glaucoma Therapy. *Expert Opinion on Drug Delivery* 2023, 1–15. https://doi.org/10.1080/17425247.2023.2219053.
9. García-Estrada, P.; García-Bon, M. A.; López-Naranjo, E. J.; Basaldúa-Pérez, D. N.; Santos, A.; Navarro-Partida, J. Polymeric Implants for the Treatment of Intraocular Eye Diseases: Trends in Biodegradable and Non-Biodegradable Materials. *Pharmaceutics* 2021, *13* (5), 701. https://doi.org/10.3390/pharmaceutics13050701.
10. Mishra, D.; Gade, S.; Glover, K.; Sheshala, R.; Singh, T. R. R. Vitreous Humor: Composition, Characteristics and Implication on Intravitreal Drug Delivery. *Current Eye Research* 2022, 1–11. https://doi.org/10.1080/02713683.2022.2119254.
11. Manna, S.; Augsburger, J. J.; Corrêa, Z. M.; Landero, J. A.; Banerjee, R. K. Development of Chitosan and Polylactic Acid Based Methotrexate Intravitreal Micro-Implants to Treat Primary Intraocular Lymphoma: An in Vitro Study. *Journal of biomechanical engineering* 2014, *136* (2). https://doi.org/10.1115/1.4026176.

12. Manna, S.; Donnell, A. M.; Kaval, N.; Al-Rjoub, M. F.; Augsburger, J. J.; Banerjee, R. K. Improved Design and Characterization of PLGA/PLA-Coated Chitosan Based Micro-Implants for Controlled Release of Hydrophilic Drugs. *International Journal of Pharmaceutics* 2018, *547* (1-2), 122–132. https://doi.org/10.1016/j.ijpharm.2018.05.066.
13. Azevedo, H.; Reis, R. *2 Understanding the Enzymatic Degradation of Biodegradable Polymers and Strategies to Control Their Degradation Rate*. https://repositorium.sdum.uminho.pt/bitstream/1822/14150/1/file.pdf.
14. Hegyesi, N.; Hodosi, E.; Polyák, P.; Faludi, G.; Balogh-Weiser, D.; Pukánszky, B. Controlled Degradation of Poly-ε-Caprolactone for Resorbable Scaffolds. *Colloids and Surfaces B: Biointerfaces* 2020, *186*, 110678. https://doi.org/10.1016/j.colsurfb.2019.110678.
15. Ahmad, M. T.; Zhang, P.; Dufresne, C.; Ferrucci, L.; Semba, R. D. The Human Eye Proteome Project: Updates on an Emerging Proteome. *PROTEOMICS* 2018, *18* (5-6), 1700394. https://doi.org/10.1002/pmic.201700394.
16. Aretz, S.; Krohne, T. U.; Kammerer, K.; Warnken, U.; Hotz-Wagenblatt, A.; Bergmann, M.; Stanzel, B. V.; Kempf, T.; Holz, F. G.; Schnölzer, M.; Kopitz, J. In-Depth Mass Spectrometric Mapping of the Human Vitreous Proteome. *Proteome Science* 2013, *11* (1), 22. https://doi.org/10.1186/1477-5956-11-22.
17. Gao, B.-B.; Chen, X.; Timothy, N.; Aiello, L. P.; Feener, E. P. Characterization of the Vitreous Proteome in Diabetes without Diabetic Retinopathy and Diabetes with Proliferative Diabetic Retinopathy. *Journal of Proteome Research* 2008, *7* (6), 2516–2525. https://doi.org/10.1021/pr800112g.
18. Kim, T.; Sang Jin Kim; Kim, K.; Kang, U.-B.; Lee, C.; Kyong Soo Park; Hyeong Gon Yu; Kim, Y. Profiling of Vitreous Proteomes from Proliferative Diabetic Retinopathy and Nondiabetic Patients. *Proteomics* 2007, *7* (22), 4203–4215. https://doi.org/10.1002/pmic.200700745.
19. Komatsu, H.; Usui, Y.; Tsubota, K.; Fujii, R.; Yamaguchi, T.; Maruyama, K.; Wakita, R.; Masaki Asakage; Shimizu, H.; Yamakawa, N.; Naoya Nezu; Ueda, K.; Hiroshi Gotô. Comprehensive Proteomic Profiling of Vitreous Humor in Ocular Sarcoidosis Compared with Other Vitreoretinal Diseases. *Journal of Clinical Medicine* 2022, *11* (13), 3606–3606. https://doi.org/10.3390/jcm11133606.
20. Koss, M. J.; Hoffmann, J.; Nguyen, N.; Pfister, M.; Mischak, H.; Mullen, W.; Husi, H.; Rejdak, R.; Koch, F.; Jankowski, J.; Krueger, K.; Bertelmann, T.; Klein, J.; Schanstra, J. P.; Siwy, J. Proteomics of Vitreous Humor of Patients with Exudative Age-Related Macular Degeneration. *PLoS ONE* 2014, *9* (5), e96895. https://doi.org/10.1371/journal.pone.0096895.
21. Loukovaara, S.; Nurkkala, H.; Tamene, F.; Gucciardo, E.; Liu, X.; Repo, P.; Lehti, K.; Varjosalo, M. Quantitative Proteomics Analysis of Vitreous Humor from Diabetic Retinopathy Patients. *Journal of Proteome Research* 2015, *14* (12), 5131–5143. https://doi.org/10.1021/acs.jproteome.5b00900.
22. Mirzaei, M.; Gupta, V. B.; Chick, J. M.; Greco, T. M.; Wu, Y.; Chitranshi, N.; Wall, R. V.; Hone, E.; Deng, L.; Dheer, Y.; Abbasi, M.; Rezaeian, M.; Braidy, N.; You, Y.; Salekdeh, G. H.; Haynes, P. A.; Molloy, M. P.; Martins, R.; Cristea, I. M.; Gygi, S. P. Age-Related Neurodegenerative Disease Associated Pathways Identified in Retinal and Vitreous

Proteome from Human Glaucoma Eyes. *Scientific Reports* 2017, *7*, 12685. https://doi.org/10.1038/s41598-017-12858-7.
23. Mohanty, V.; Pinto, S. M.; Yashwanth Subbannayya; Mohd Altaf Najar; Kalpana Babu Murthy; Prasad, K.; Murthy, K. R. Digging Deeper for the Eye Proteome in Vitreous Substructures: A High-Resolution Proteome Map of the Normal Human Vitreous Base. *Omics A Journal of Integrative Biology* 2020, *24* (6), 379–389. https://doi.org/10.1089/omi.2020.0020.
24. Murthy, K. R.; Goel, R.; Subbannayya, Y.; Jacob, H. K.; Murthy, P. R.; Manda, S. S.; Patil, A. H.; Sharma, R.; Sahasrabuddhe, N. A.; Parashar, A.; Nair, B. G.; Krishna, V.; Prasad, T. K.; Gowda, H.; Pandey, A. Proteomic Analysis of Human Vitreous Humor. *Clinical Proteomics* 2014, *11* (1). https://doi.org/10.1186/1559-0275-11-29.
25. Naru, J.; Aggarwal, R.; Singh, U.; Mohanty, A. K.; Bansal, D.; Mangat, N.; Kakkar, N.; Agnihotri, N. Proteomic Analysis of Differentially Expressed Proteins in Vitreous Humor of Patients with Retinoblastoma Using ITRAQ-Coupled ESI-MS/MS Approach. *Tumor Biology* 2016, *37* (10), 13915–13926. https://doi.org/10.1007/s13277-016-5162-3.
26. Reich, M.; Dacheva, I.; Nobl, M.; Siwy, J.; Schanstra, J. P.; Mullen, W.; Koch, F. H. J.; Kopitz, J.; Kretz, F. T. A.; Auffarth, G. U.; Koss, M. J. Proteomic Analysis of Vitreous Humor in Retinal Vein Occlusion. *PLOS ONE* 2016, *11* (6), e0158001. https://doi.org/10.1371/journal.pone.0158001.
27. Shitama, T.; Hayashi, H.; Noge, S.; Uchio, E.; Oshima, K.; Haniu, H.; Takemori, N.; Komori, N.; Matsumoto, H. Proteome Profiling of Vitreoretinal Diseases by Cluster Analysis. *PROTEOMICS - CLINICAL APPLICATIONS* 2008, *2* (9), 1265–1280. https://doi.org/10.1002/prca.200800017.
28. Skeie, J. M.; Roybal, C. N.; Mahajan, V. B. Proteomic Insight into the Molecular Function of the Vitreous. *PLOS ONE* 2015, *10* (5), e0127567. https://doi.org/10.1371/journal.pone.0127567.
29. Yee, K. M. P.; Feener, E. P.; Madigan, M.; Jackson, N. J.; Gao, B.-B.; Ross-Cisneros, F. N.; Provis, J.; Aiello, L. P.; Sadun, A. A.; Sebag, J. Proteomic Analysis of Embryonic and Young Human Vitreous. *Investigative Opthalmology & Visual Science* 2015, *56* (12), 7036. https://doi.org/10.1167/iovs.15-16809.
30. Benes, P.; Vetvicka, V.; Fusek, M. Cathepsin D—Many Functions of One Aspartic Protease. *Critical Reviews in Oncology/Hematology* 2008, *68* (1), 12–28. https://doi.org/10.1016/j.critrevonc.2008.02.008.
31. Ji, L.; Wu, H.-T.; Qin, X.-Y.; Lan, R. Dissecting Carboxypeptidase E: Properties, Functions and Pathophysiological Roles in Disease. *Endocrine Connections* 2017, *6* (4), R18–R38. https://doi.org/10.1530/EC-17-0020.
32. Perrakis, A.; Moolenaar, W. H. Autotaxin: Structure-Function and Signaling. *Journal of Lipid Research* 2014, *55* (6), 1010–1018. https://doi.org/10.1194/jlr.R046391.
33. Lemieux, M. J.; Mark, B. L.; Cherney, M. M.; Withers, S. G.; Mahuran, D. J.; James, M. N. G. Crystallographic Structure of Human β-Hexosaminidase A: Interpretation of Tay-Sachs Mutations and Loss of GM2 Ganglioside Hydrolysis. *Journal of Molecular Biology* 2006, *359* (4), 913–929. https://doi.org/10.1016/j.jmb.2006.04.004.
34. Shunmoogam, N.; Naidoo, P.; Chilton, R. Paraoxonase (PON)-1: A Brief Overview on Genetics, Structure, Polymorphisms and Clinical Relevance. *Vascular Health and Risk Management* 2018, *Volume 14*, 137–143. https://doi.org/10.2147/vhrm.s165173.

35. Kondo, M. Y.; Gouvêa, I. E.; Okamoto, D. N.; Jorge A.N. Santos; Caden Souccar; Oda, K.; Juliano, L.; Juliano, M. A. Analysis of Catalytic Properties of Tripeptidyl Peptidase I (TTP-I), a Serine Carboxyl Lysosomal Protease, and Its Detection in Tissue Extracts Using Selective FRET Peptide Substrate. *Peptides* 2016, *76*, 80–86. https://doi.org/10.1016/j.peptides.2016.01.009.
36. Bishop, P.; Rocca, D.; Henley, Jeremy M. Ubiquitin C-Terminal Hydrolase L1 (UCH-L1): Structure, Distribution and Roles in Brain Function and Dysfunction. *Biochemical Journal* 2016, *473* (16), 2453–2462. https://doi.org/10.1042/bcj20160082.
37. Switzar, L.; Giera, M.; Niessen, W. M. A. Protein Digestion: An Overview of the Available Techniques and Recent Developments. *Journal of Proteome Research* 2013, *12* (3), 1067–1077. https://doi.org/10.1021/pr301201x.
38. *RapiGest SF Surfactant for Enzymatic Protein Digestion | Waters*. Waters.com. https://www.waters.com/nextgen/us/en/products/standards-and-reagents/rapigest-sf-surfactant.html
39. *Improve Protein Analysis with the New, Mass Spectrometry-Compatible ProteaseMAX Surfactant*. www.promega.com. https://www.promega.com/resources/pubhub/promega-notes-2008/improve-protein-analysis-with-the-new-mass-spectrometry-compatible-proteasemax-surfactant/
40. Bollinger, J. G.; Stergachis, A. B.; Johnson, R. S.; Egertson, J. D.; MacCoss, M. J. Selecting Optimal Peptides for Targeted Proteomic Experiments in Human Plasma Using in Vitro Synthesized Proteins as Analytical Standards. *Methods in molecular biology* 2016, 207–221. https://doi.org/10.1007/978-1-4939-3524-6_12.
41. Wilkins, M. R.; Lindskog, I.; Gasteiger, E.; Bairoch, A.; Sanchez, J.-C.; Hochstrasser, D. F.; Appel, R. D. Detailed Peptide Characterization Using PEPTIDEMASS - a World-Wide-Web-Accessible Tool. *Electrophoresis* 1997, *18* (3-4), 403–408. https://doi.org/10.1002/elps.1150180314.
42. Altschul, S. F.; Gish, W.; Miller, W.; Myers, E. W.; Lipman, D. J. Basic Local Alignment Search Tool. *Journal of Molecular Biology* 1990, *215* (3), 403–410. https://doi.org/10.1016/s0022-2836(05)80360-2.
43. Pino, L. K.; Searle, B. C.; Bollinger, J. G.; Nunn, B.; MacLean, B.; MacCoss, M. J. The Skyline Ecosystem: Informatics for Quantitative Mass Spectrometry Proteomics. *Mass Spectrometry Reviews* 2020, *39* (3), 229–244. https://doi.org/10.1002/mas.21540.
44. Mains, J.; Lay Ean Tan; Zhang, W.; Young, L.; Shi, R.; Wilson, C. G. Species Variation in Small Molecule Components of Animal Vitreous. *Investigative Ophthalmology & Visual Science* 2012, *53* (8), 4778–4778. https://doi.org/10.1167/iovs.12-9998.
45. del Amo, E. M.; Urtti, A. Rabbit as an Animal Model for Intravitreal Pharmacokinetics: Clinical Predictability and Quality of the Published Data. *Experimental Eye Research* 2015, *137*, 111–124. https://doi.org/10.1016/j.exer.2015.05.003.
46. Lundgren, D. H.; Hwang, S.-I.; Wu, L.; Han, D. K. Role of Spectral Counting in Quantitative Proteomics. *Expert Review of Proteomics* 2010, *7* (1), 39–53. https://doi.org/10.1586/epr.09.69.

47. Krey, J. F.; Wilmarth, P. A.; Jung Bum Shin; Klimek, J.; Sherman, N. E.; Jeffery, E.; Choi, D.; David, L. L.; Barr-Gillespie, P. G. Accurate Label-Free Protein Quantitation with High- and Low-Resolution Mass Spectrometers. *Journal of Proteome Research* 2013, *13* (2), 1034–1044. https://doi.org/10.1021/pr401017h.
48. Dacheva, I.; Ullmer, C.; Ceglowska, K.; Nogoceke, E.; Hartmann, G.; Müller, S.; Rejdak, R.; Nowomiejska, K.; Reich, M.; Nobl, M.; Tandogan, T.; Kretz, F. T. A.; Auffarth, G. U.; Koss, M. J. LYSOPHOSPHATIDIC ACIDS and AUTOTAXIN in RETINAL VEIN OCCLUSION. *Retina* 2016, *36* (12), 2311–2318. https://doi.org/10.1097/iae.0000000000001112.
49. Ptaszyńska-Sarosiek, I.; Chojnowska, S.; Szajda, S. D.; Szeremeta, M.; Wardaszka, Z.; Cwalina, U.; Niemcunowicz-Janica, A.; Waszkiewicz, N. The Activity of N-Acetyl-β-Hexosaminidase in the Blood, Urine, Cerebrospinal Fluid and Vitreous Humor Died People due to Alcohol Intoxication. *Journal of Clinical Medicine* 2020, *9* (11), 3636. https://doi.org/10.3390/jcm9113636.
50. Soler, N.; García-Heredia, A.; Judit Marsillach; Bharti Mackness; Mackness, M. I.; Joven, J.; Romero, P.; Camps, J. Paraoxonase-1 Is Associated with Corneal Endothelial Cell Alterations in Patients with Chronic Obstructive Pulmonary Disease. *Investigative Ophthalmology & Visual Science* 2013, *54* (8), 5852–5852. https://doi.org/10.1167/iovs.13-11951.
51. Ortego, J.; Escribano, J.; Crabb, J. W.; Coca-Prados, M. Identification of a Neuropeptide and Neuropeptide-Processing Enzymes in Aqueous Humor Confers Neuroendocrine Features to the Human Ocular Ciliary Epithelium. *Journal of Neurochemistry* 2002, *66* (2), 787–796. https://doi.org/10.1046/j.1471-4159.1996.66020787.x.
52. Anam Hammid; Fallon, J. K.; Lassila, T.; Giulia Salluce; Smith, P. C.; Tolonen, A.; Sauer, A.; Arto Urtti; Paavo Honkakoski. Carboxylesterase Activities and Protein Expression in Rabbit and Pig Ocular Tissues. *Molecular Pharmaceutics* 2021, *18* (3), 1305–1316. https://doi.org/10.1021/acs.molpharmaceut.0c01154.
53. Liu, Y.; Bouhenni, R. A.; Dufresne, C. P.; Semba, R. D.; Edward, D. P. Differential Expression of Vitreous Proteins in Young and Mature New Zealand White Rabbits. *PLOS ONE* 2016, *11* (4), e0153560. https://doi.org/10.1371/journal.pone.0153560.
54. Mandal, N.; Lewis, G. P.; Fisher, S. K.; Steffen Heegaard; Jan Ulrik Prause; Morten la Cour; Henrik Vorum; Bent Honoré. Proteomic Analysis of the Vitreous Following Experimental Retinal Detachment in Rabbits. *Journal of Ophthalmology* 2015, *2015*, 1–9. https://doi.org/10.1155/2015/583040.
55. Qin, G.; Zhang, P.; Sun, M.; Fu, W.; Cai, C. Comprehensive Spectral Libraries for Various Rabbit Eye Tissue Proteomes. *Scientific Data* 2022, *9* (1). https://doi.org/10.1038/s41597-022-01241-5.
56. Li, J.; Lu, Q.; Lu, P. Quantitative Proteomics Analysis of Vitreous Body from Type 2 Diabetic Patients with Proliferative Diabetic Retinopathy. *BMC Ophthalmology* 2018, *18* (1). https://doi.org/10.1186/s12886-018-0821-3.
57. Sen, S.; Prithviraj Udaya; Jeya Maheshwari Jayapal; Ramasamy, K.; Naresh Babu Kannan; Kuppamuthu Dharmalingam. Profiling of Idiopathic Macular Hole Vitreous Proteome Identifies the Role of Extracellular Matrix Remodelling, Epithelial–Mesenchymal Transformation and Unfolded Protein-Response Pathways. *Indian*

Journal of Ophthalmology 2023, *71* (5), 2027–2040. https://doi.org/10.4103/ijo.ijo_2068_22.
58. Stein, S. L.; Auel, T.; Kempin, W.; Malte Bogdahn; Weitschies, W.; Seidlitz, A. Influence of the Test Method on in Vitro Drug Release from Intravitreal Model Implants Containing Dexamethasone or Fluorescein Sodium in Poly (D,L-Lactide-Co-Glycolide) or Polycaprolactone. 2018, *127*, 270–278. https://doi.org/10.1016/j.ejpb.2018.02.034.

Appendix A

Supporting Information for Chapter 2

A1. Materials and Methods[1]

A1.1 General information

All chemicals were used as received unless otherwise noted. All Fmoc-protected amino acids, coupling agents, triisopropylsilane (TIPS), and 2-chlorotrityl chloride resin was purchased from Chem-Impex. HPLC grad acetonitrile (MeCN) was purchased from Fischer Scientific. Methylene chloride (DCM) was passed through alumina under nitrogen prior to use. Anhydrous, amine-free *N,N*-dimethylformamide (DMF), DIPEA, 2,4,6-collidine, and piperidine were purchased from Alfa Aesar. Trifluoroacetic acid (TFA) and hexafluoroisopropanol (HFIP) were purchased from Oakwood Chemical. Deionized water (18 MΩ) was obtained from a Barnstead NANOpure Diamond water purification system. Analytical reverse-phase HPLC was performed on an Agilent 1260 instrument equipped with a Phenomonex Aeris PEPTIDE 2.6 μm XB-C18 150 mm x 4.6 mm column. Preparative reverse-phase HPLC was performed on a Rainin Dynamax instrument equipped with an Agilent Zorbax 300SB-C18 21.2 mm x 250 mm (7 μm) column. Peptides were first purified on a Biotage® Isolera™ One system equipped with a 25 g Biotage® Sfär Bio C18 – Duo 300 Å 20 μm column, before repurification on the Rainin Dynamax. UV detection (214 nm) was used for analytical and preparative HPLC. HPLC grade acetonitrile and deionized water, each containing 0.1% trifluoroacetic acid (TFA), were used for analytical and preparative reverse-phase HPLC. Matrix-assisted laser desorption/ionization time-of-flight (MALDI-TOF) mass spectrometry was performed on an AB SCIEX TOF/TOF 5800 system with α-cyano-4-hydroxycinnamic acid as the sample matrix. All peptides were prepared and used as the trifluoroacetate salts and were assumed to have one trifluoroacetic acid molecule per amine group on each peptide.

A1.2 Synthesis of Aβm$_{17–36}$ and Aβm$_{17–35}$

Loading of the resin. 2-Chlorotrityl chloride resin (300 mg, 1.6 mmol/g) was added to a Bio-Rad Poly-Prep chromatography column. The resin was suspended in dry DCM (8

mL) and allowed to swell for 30 min. The solution was drained from the resin and a solution of Boc-Orn(Fmoc)-OH (0.6 equiv, 100 mg, 0.22 mmol) in 6% (v/v) 2,4,6-collidine in dry DCM (8 mL) was added immediately and the suspension was gently agitated for 12 h. The solution was then drained and a mixture of DCM/MeOH/*N*,*N*-diisopropylethylamine (DIPEA) (17:2:1, 6 mL) was added immediately. The mixture was gently agitated for 1 h to cap the unreacted 2-chlorotrityl chloride resin sites. The resin was then washed with dry DCM (2x) and dried by passing nitrogen through the vessel. This procedure typically yields 0.12–0.18 mmol of loaded resin (0.4–0.6 mmol/g loading).

Peptide coupling. The Boc-Orn(Fmoc)-2-chlorotrityl resin generated from the previous step was transferred to a solid phase reaction vessel and washed with DMF (5x). The linear peptide was synthesized from the C-terminus to the N-terminus. Each coupling cycle consisted of i. Fmoc-deprotection with 20% (v/v) piperidine in DMF for 5 min, ii. washing with DMF (5x), iii. coupling of the amino acid (0.75 mmol, 5 equiv) in the presence of HCTU (0.675 mmol, 4.5 equiv) and 20% (v/v) 2,4,6-collidine in DMF for 20 min iv. washing with DMF (5x). Special coupling conditions were used for the isoleucine that followed the *N*-methyl-glycine in $A\beta m_{17-36}$ and for the isoleucine that followed the *N*-methyl-isoleucine in $A\beta m_{17-35}$: The isoleucine was double coupled (0.75 mmol, 5 equiv.) and allowed to react for 1 h per coupling with HATU (5 equiv) and HOAt (5 equiv) in 20% (v/v) 2,4,6-collidine in DMF. After coupling of the last amino acid, the terminal Fmoc group was removed with 20% (v/v) piperidine in DMF (5 min). The resin was transferred from the reaction vessel to a Bio-Rad Poly-Prep chromatography column.

Cleavage of the peptide from the resin. The linear peptide was cleaved from the resin by agitating the resin for 45 min with a solution of 1,1,1,3,3,3-hexafluoroisopropanol (HFIP) in DCM (1:4, 8 mL). The suspension was filtered and the filtrate was collected in a 250-mL round-bottomed flask. An additional 8 ml of the HFIP cleavage cocktail was added to the resin and agitated for 30 min. The solution was then filtered into the same flask. The combined filtrates were concentrated by rotary evaporation to give a white solid, which was cyclized without further purification.

Cyclization of the linear peptide. The crude protected linear peptide was dissolved in dry DMF (150 mL). HOBt (114 mg, 0.75 mmol, 5 equiv) and HBTU (317 mg, 0.75 mmol, 5 equiv) were added to the solution. DIPEA (0.33 mL, 1.8 mmol, 12 equiv) was added to the solution and the mixture was stirred under nitrogen for 48 h. The mixture was dried by rotary evaporation to afford the crude protected cyclic peptide. Cyclized peptides were further dried by vacuum pump.

Global deprotection and Ether Precipitations. The protected cyclic peptide was dissolved in TFA/triisopropylsilane (TIPS)/H_2O (18:1:1, 20 mL) in a 250-mL round-bottomed flask equipped with a nitrogen-inlet adaptor. The solution was stirred for 1.5 h. The reaction mixture was then separated evenly into two 50 ml conical tubes. 30 ml of ice-cold diethyl ether was added to each tube and left to sit on ice for 15 minutes. The 50-ml conical tubes were centrifuged (2000 x g) for 10 min to pellet the crude peptide. The supernatant was removed, and the pellets were redissolved in 5 ml of MeCN. The MeCN peptide solutions were combined in a 250 ml round-bottom flask concentrated by rotary evaporation to afford the crude cyclic peptide. The crude cyclic peptide was immediately subjected to purification by reverse-phase HPLC (RP-HPLC), as described below.

Reverse-phase HPLC purification. The peptide was dissolved in H_2O and MeCN (4:1, 10 mL), and purified on a Biotage® Isolera™ One system equipped with a 25 g Biotage® Sfär Bio C18 – Duo 300 Å 20 µm column using a MeCN (15%-45%) gradient in H_2O. Fractions were analyzed by MALDI-TOF and analytical HPLC. Fractions containing the desired peptide were combined in a 250 ml round-bottom flask and concentrated by rotary evaporation. The peptide was then redissolved in H_2O and MeCN (4:1, 10 mL), filtered through a 0.2 µm syringe filter, and purified by RP-HPLC on a Rainin Dynamax instrument equipped with an Agilent Zorbax 300SB-C18 21.2 mm x 250 mm (7 µm) column (gradient elution with 20–45% MeCN in H_2O over 70 min). Fractions were analyzed by MALDI-TOF and analytical HPLC. Pure fractions were concentrated by rotary evaporation and lyophilized. Typical syntheses yielded ~30 mg of the peptide as the TFA salt.

A1.3. SDS-PAGE and silver staining

Solutions of $A\beta m_{17-36}$ and $A\beta m_{17-35}$ were prepared gravimetrically by dissolving lyophilized peptide in the appropriate amount of 18 MΩ deionized water to achieve a 10 mg/ml stock. Stock solutions of all peptides were diluted with 18 MΩ deionized water to create 400 μM, 200 μM, and 100 μM sample solutions. 1 μl of 6X SDS-PAGE sample loading buffer (G Biosciences) and 2 μl 18 MΩ deionized water was added per 3 μl of sample solution to create working solutions. 5 μl aliquots of each working solution were run on a 16.5% polyacrylamide Mini-PROTEAN® Tris/Tricine Precast Gel from Bio-Rad Laboratories.[2] Reagents for Tricine SDS-PAGE were prepared and used according to recipes and procedures detailed in the Mini-PROTEAN Precast Gels Instruction Manual and Application Guide (2011) from Bio-Rad Laboratories.[2] The gel was run at a constant 100 V for approximately 2 hours. The migration of $A\beta m_{17-36}$ and $A\beta m_{17-35}$ was compared with a molecular weight protein ladder (SpectraTM Multicolor Low Range Protein Ladder, ThermoFisher Scientific, catalog #: 26628).

Staining with silver nitrate was used to visualize $A\beta m_{17-36}$ and $A\beta m_{17-35}$ in the SDS-PAGE gel. Reagents for silver staining were prepared according to procedures detailed in Simpson, R. J. CSH Protoc. 2007.[3] [The sodium thiosulfate solution, silver nitrate solution, and developing solution were prepared fresh each time silver staining was performed]. Briefly, the gel was removed from the casting glass and rocked in fixing solution (50% (v/v) MeOH and 5% (v/v) acetic acid in deionized water) for 20 min. Next, the fixing solution was discarded and the gel was rocked in 50% (v/v) aqueous MeOH for 10 min. Next, the 50% methanol was discarded and the gel was rocked in deionized water for 10 min. Next, the water was discarded and the gel was rocked in 0.02% (w/v) sodium thiosulfate in deionized water for 1 min. The sodium thiosulfate was discarded and the gel was rinsed with deionized water for 1 min (2X). After the last rinse, the gel was submerged in chilled 0.1% (w/v) silver nitrate in deionized water and rocked at 4 °C for 20 min. Next, the silver nitrate solution was discarded and the gel was rinsed with deionized water for 1 min (2X). To develop the gel, the gel was incubated in developing solution (2% (w/v) sodium carbonate, 0.04% (w/v) formaldehyde until the desired intensity of staining was reached (~1–3 min). When the desired intensity of staining was reached, the development

was stopped by discarding the developing solution and submerging the gel in 5% aqueous acetic acid.

A1.4. Crystallization conditions for Aβm$_{17–36}$ and Aβm$_{17–35}$

Crystallization conditions for Aβm$_{17–36}$ were determined using a 4x6 matrix Hampton VDX 24-well plate. The conditions mimicked the optimization screen previously used for a homologue of Aβm$_{17–36}$ that contained ornithine in place of Met$_{35}$ (PDB 4NTR) which previously crystallized in HEPES with Jeffamine M-600.[4] The HEPES buffer pH was varied in each row in increments of 0.5 pH units (6.5, 7.0, 7.5, and 8.0) and the Jeffamine concentration in each column in increments of 2% (24%, 26%, 28%, 30%, 32%, 34%). The first well in the 4x6 matrix for Aβm$_{17–36}$ was prepared by combined 100 μL of 1 M HEPES buffer at pH 6.5, 480 μL of 50% v/v aqueous Jeffamine M-600 pH 7.0, and 420 μL of deionized water. The other wells were prepared in analogous fashion, by combining 100 μL of HEPES buffer of varying pH, Jeffamine in varying amounts, and deionized water for a total volume of 1 mL in each well. Three hanging-drops were prepared per borosilicate glass slide by combining a solution of peptide 2 or peptide 4 (10 mg/mL in deionized water) and the well solution in the following amounts: 1 μL:1 μL, 2 μL:1 μL, and 1 μL:2 μL. Crystallization conditions for Aβm$_{17–36}$ were further optimized using the same method. The HEPES buffer pH was varied in each row in increments of 0.2 pH units (6.1, 6.3, 6.5, and 6.7) and the Jeffamine concentration in each column in increments of 1% (21%, 22%, 23%, 24%, 25%, 26%). Crystals suitable for diffraction grew in most of the pH increments and most of the Jeffamine concentrations.

Initial crystallization conditions for Aβm$_{17–35}$ were determined using the hanging nanodrop vapor-diffusion method. Crystallization conditions were screened using six crystallization kits in a 96-well plate format (Hampton Index, PEG/Ion, and Crystal Screen; Molecular Dynamics Morpheus, MemPlus/MemSys, PGA). Three 150 nL hanging drops that differed in the ratio of peptide to well solution were made per condition in each 96-well plate for a total of 1728 experiments. Hanging drops were made by combining an appropriate volume of Aβm$_{17–36}$ or Aβm$_{17–35}$ (10 mg/mL in deionized water) with an appropriate volume of well solution to create three 150 nL hanging drops with 1:1, 1:2, and 2:1 peptide:well solution. The hanging drops were made using a TTP LabTech Mosquito

nanodisperse instrument. Crystals of Aβm$_{17–35}$ suitable for diffraction grew in a Molecular Dynamics' Morpheus solution containing 0.12M ethylene glycols mix, 0.1M Buffer System 3 pH 8.5, and 37.5% v/v precipitant mix 4. Molecular Dynamics' ethylene glycols mix consists of 0.3 M diethylene glycol, 0.3 M triethylene glycol, 0.3 M tetraethylene glycol, 0.3 M penta(ethylene glycol). Molecular Dynamic's Buffer System 3 consists of 1 M BICINE and 1 M Trisma Base. Molecular Dynamics precipitant mix 4 consists of 25 % w/v hexaethylene glycol, 25 % w/v poly(ethylene glycol) 1000, and 25 % w/v poly(ethylene glycol) 3350.[5]

A1.5. X-ray diffraction data collection, data processing, and structure determination for peptides Aβm$_{17–36}$ and Aβm$_{17–35}$

Crystals were harvested with a nylon loop attached to a copper or steel pin and flash frozen in liquid nitrogen prior to data collection. Aβm$_{17–36}$ was soaked in a 1:1 mixture of well solution and 1 M potassium iodide for approximately 5 minutes prior to flash freezing to incorporate iodide ions into the crystal lattice.

Diffraction data for Aβm$_{17–36}$was collected on a Rigaku Micromax-007HF X-ray diffractometer with a rotating copper anode at 1.54 Å wavelength with 0.5° oscillation. Diffraction data were collected using CrystalClear. Diffraction data were scaled and merged using XDS.[6] Coordinates for the anomalous signals were determined by HySS in the Phenix software suite 1.10.1.7.[7] Electron density maps were generated using single-wavelength anomalous diffraction (SAD) using the anomalous signal from iodine ions incorporated into the crystal lattice from soaking the crystals in KI prior to data collection. The electron density map for Aβm$_{17–36}$ was generated using anomalous coordinates determined by HySS as initial positions in Autosol.

Diffraction data for Aβm$_{17–35}$ was collected at the Advanced Light Source at Lawrence Berkeley National Laboratory with a synchrotron source at 0.998-Å wavelength. Data for Aβm$_{17–35}$ suitable for refinement at 1.431 Å were obtained from the synchrotron. Diffraction data were scaled and merged using XDS.[6] The electron density map for Aβm$_{17–35}$ was generated by molecular replacement using the coordinates from an all-alanine model of a monomeric peptide from the structure with PDB accession ID 5W4H.[1,8] Molecular

manipulation of the Aβm$_{17–36}$ and Aβm$_{17–35}$ models was performed with Coot.[6] Coordinates for Aβm$_{17–36}$ and Aβm$_{17–35}$ were refined with phenix.refine.

A2. Tables

Table A1. Crystallography data for Aβm$_{17–36}$ and Aβm$_{17–35}$

Peptide	Aβm$_{17–36}$	Aβm$_{17–35}$
PDB ID	8GJD	8GJC
Space Group	R 3 :H	P 32 2 1
a, b, c (Å)	68.1848, 68.1848, 168.564	36.164, 38.164, 32.054
A, β, λ (°)	90, 90, 120	90, 90, 120
Peptides per Asymmetric Unit	16	2
Wavelength (Å)	1.54	0.998
Resolution (Å)	34.09 - 2.03 (2.103 - 2.03)	23.01 - 1.431 (1.482 - 1.431)
Total Reflections	399917 (18431)	81086 (1686)
Unique Reflections	18832 (1806)	5078 (384)
Multiplicity	21.2 (10.2)	16.0 (4.4)
Completeness (%)	99.49 (96.27)	97.02 (74.46)
Mean I/σ	35.86 (4.81)	24.44 (0.71)
Wilson B factor	23.85	15.0
R_{merge}	0.2206 (0.57)	0.09013 (1.775)
$R_{measure}$	0.2253 (0.5992)	0.09285 (2.026)
$CC_{1/2}$	0.981 (0.899)	0.999 (0.25)
CC^*	0.995 (0.973)	1 (0.633)
R_{work}	0.2465 (0.2797)	0.1545 (0.5371)
R_{free}	0.2901 (0.3380)	0.1789 (0.5666)
Number of Non-Hydrogen Atoms	2180	301
RMS_{bonds}	0.020	0.009
RMS_{angles}	0.81	1.20
Ramachandran Favored (%)	100	100
Outliers (%)	0	0
Clashscore	1.83	12.10
Average B-Factor	26.19	21.14

A3 Peptide Characterization Data

A2.1 Characterization of Aβm$_{17-36}$

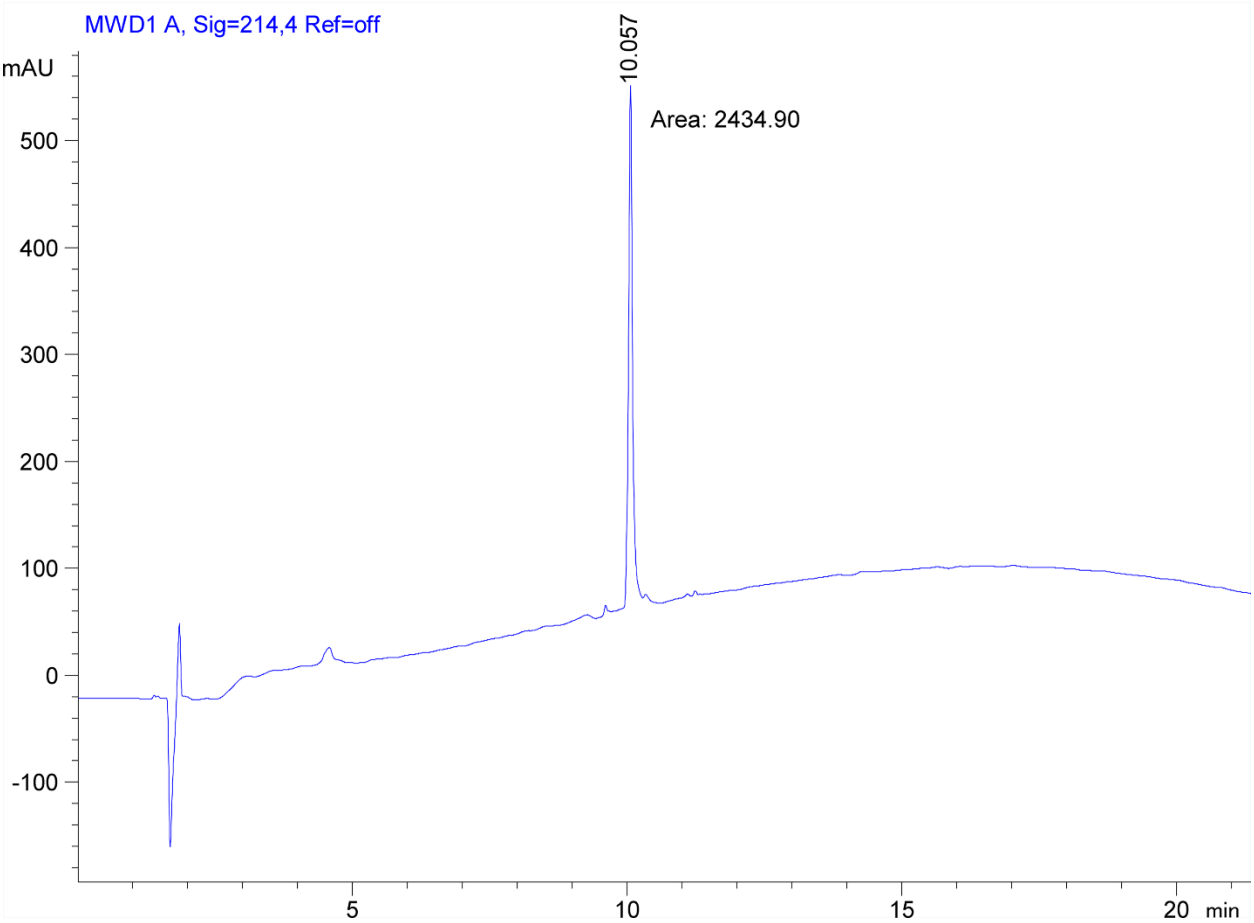

Figure A1. Analytical HPLC trace of Aβm$_{17-36}$

Table A2. Mass spectrometry ions of Aβm$_{17-36}$

Calculated Mass for Aβm$_{17-36}$: 1760.99 g/mol
$[M+1H^+]^+$ = 1762.03
$[M+2H^+]^{2+}$ = 881.42

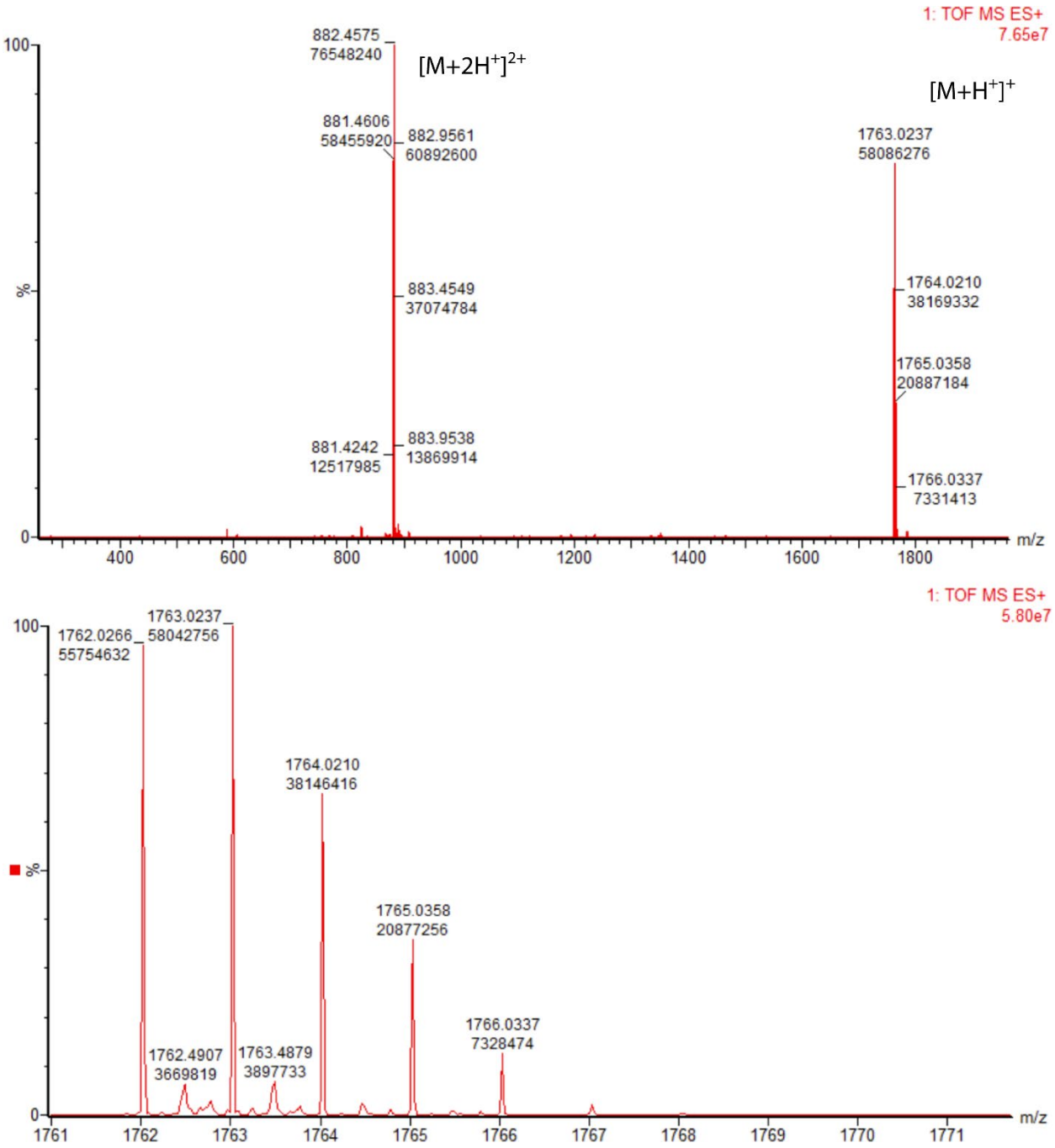

Figure A2. High-resolution mass spectrometry of Aβm$_{17-36}$ obtained via Xevo

A2.2. Characterization of Aβm$_{17-35}$

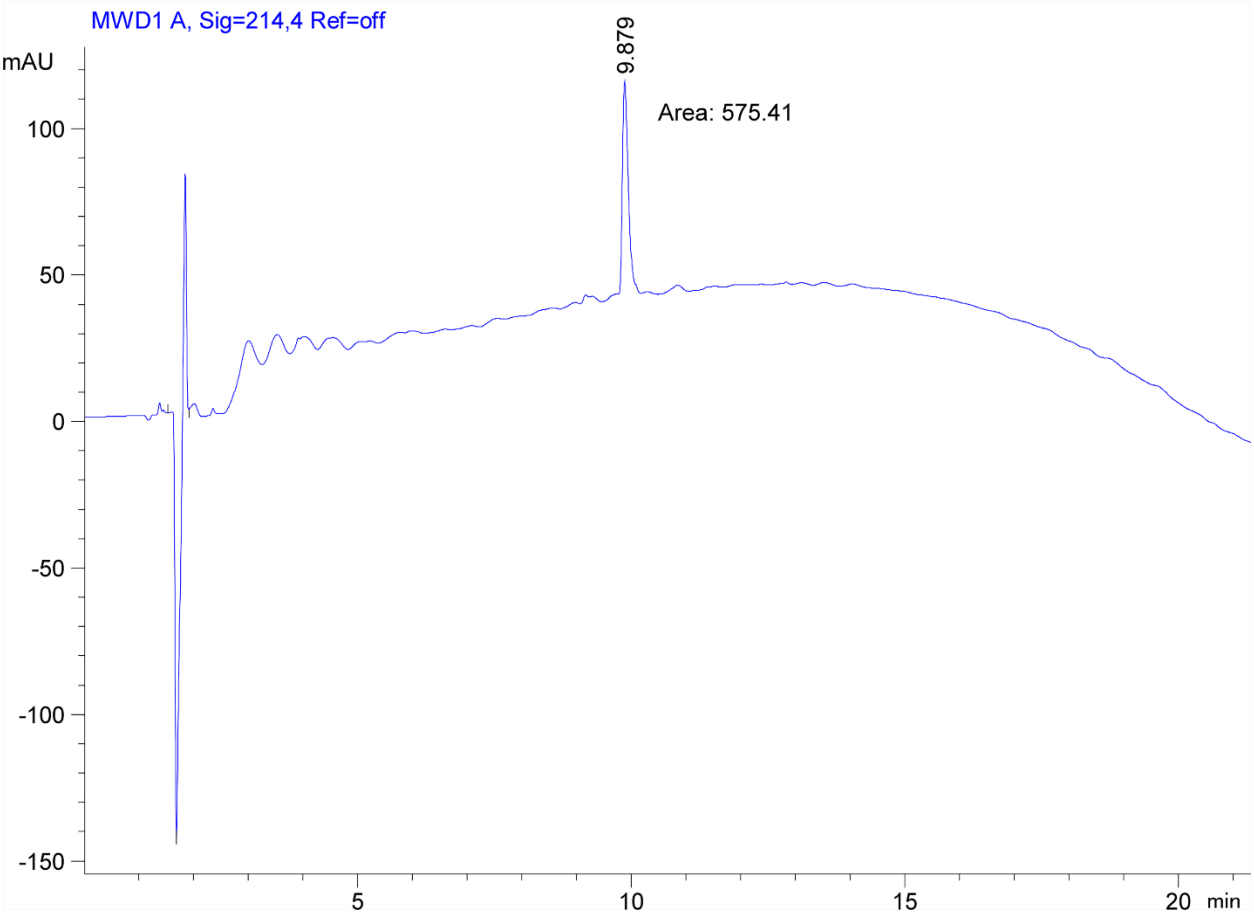

Figure A3. Analytical HPLC trace of Aβm$_{17-35}$

Table A3. Mass spectrometry ions of Aβm$_{17-35}$

Calculated Mass for Aβm$_{17-36}$: 1718.94 g/mol
$[M+1H^+]^+$ = 1719.96
$[M+2H^+]^{2+}$ = 860.43
$[M+3H^+]3^+$ = 574.31

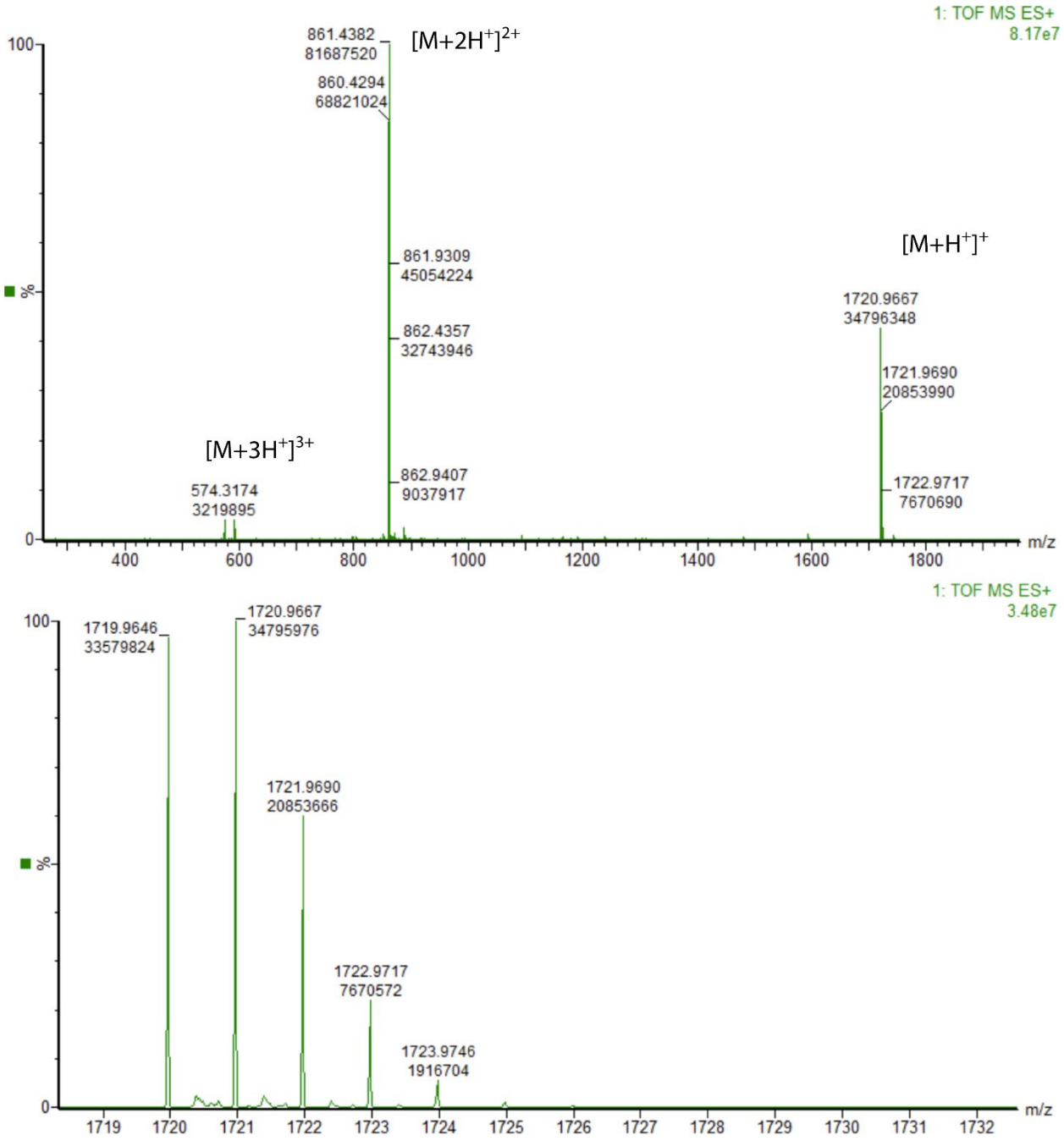

Figure A4. High-resolution mass spectrometry of Aβm$_{17-35}$ obtained via Xevo

A3. References and Notes

1. These procedures follow closely those that our laboratory has previously published. The procedures in this section are adapted from and in some cases taken verbatim from Kreutzer, A. G., Spencer, R. K., McKnelly, K. J., Yoo, S., Hamza, I. L., Salveson, P. J., Nowick, J. S. (2017). A hexamer of a peptide derived from $A\beta_{16-36}$. *Biochemistry*, *56*(45), 6061–6071. 10.1021/acs.biochem.7b00831
2. BioRad. (n.d.). *Mini-PROTEAN® tris/tricine precast gels*. BioRad. Retrieved March 7, 2023, from https://www.bio-rad.com/en-us/product/mini-protean-tris-tricine-precast-gels?ID=N3GRYEKG4
3. Simpson, R. J. (2007). Staining proteins in gels with silver nitrate. *Cold Spring Harbor Protocols*, *2007*(7). https://doi.org/10.1101/pdb.prot4727
4. Kreutzer, A. G., Yoo, S., Spencer, R. K., Nowick, J. S. (2017). Stabilization, Assembly, and Toxicity of Trimers Derived from Aβ. *Journal of the American Chemical Society*. *139* (2), 966–975. 10.1021/jacs.6b11748.
5. Calibre Scientific. (n.d.). Moleculardimensions.com. Retrieved March 7, 2023, from https://www.moleculardimensions.com/products/morpheus-mixes
6. Emsley, P., Lohkamp, B., Scott, W. G., & Cowtan, K. (2010). Features and development of *coot*. *Acta Crystallographica Section D Biological Crystallography*, *66*(4), 486–501. https://doi.org/10.1107/s0907444910007493
7. Kabsch, W. (2010). *xds*. *Acta Crystallographica Section D Biological Crystallography*, *66*(2), 125–132. https://doi.org/10.1107/s0907444909047337
8. Adams, P. D., Afonine, P. V., Bunkóczi, G., Chen, V. B., Davis, I. W., Echols, N., Headd, J. J., Hung, L.-W., Kapral, G. J., Grosse-Kunstleve, R. W., McCoy, A. J., Moriarty, N. W., Oeffner, R., Read, R. J., Richardson, D. C., Richardson, J. S., Terwilliger, T. C., & Zwart, P. H. (2010). *phenix*: A comprehensive python-based system for Macromolecular Structure Solution. *Acta Crystallographica Section D Biological Crystallography*, *66*(2), 213–221. https://doi.org/10.1107/s0907444909052925

Appendix B

Supporting Information for Chapter 3

B1. Figures

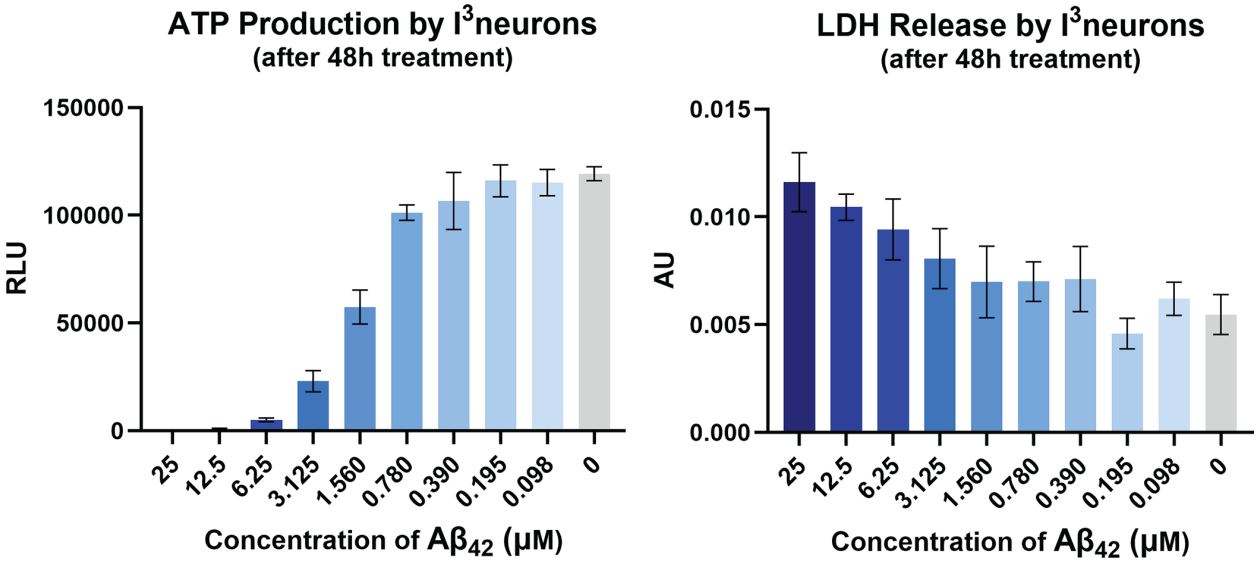

Figure B1. Graphs of (A) ATP production and (B) LDH release by i^{3}Neurons in the presence of varying concentrations of Aβ$_{42}$.

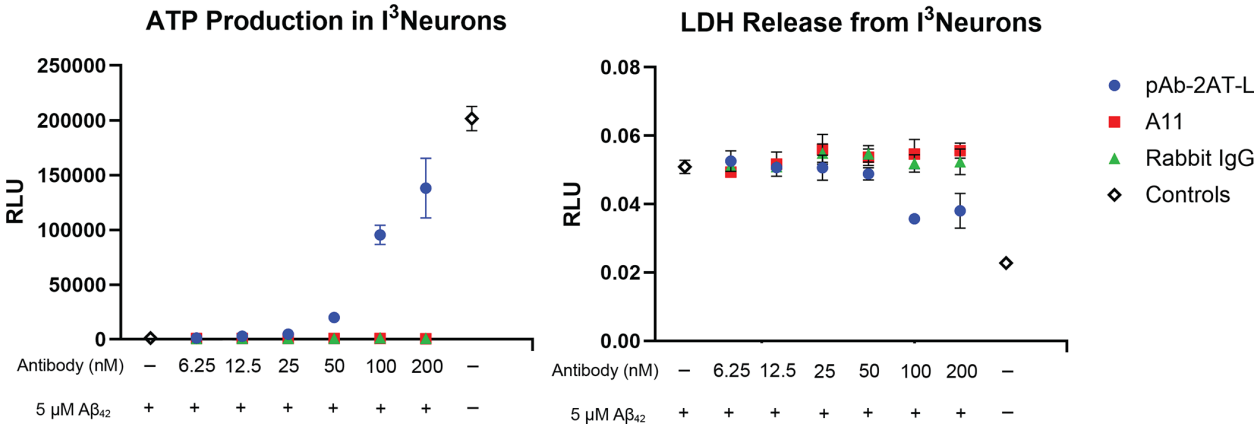

Figure B2. Graph of ATP production (left) and LDH release (right) by i^{3}Neurons in the presence of 5 μM Aβ$_{42}$ and varying concentrations of pAb$_{2AT-L}$, A11 (Fisher catalog #AHB0052), or a generic rabbit IgG.

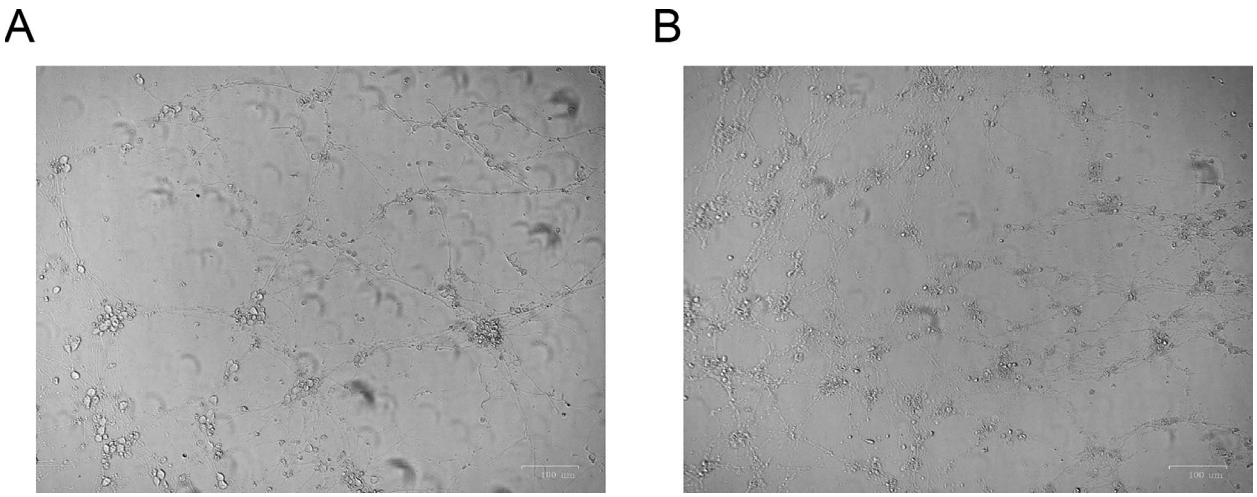

Figure B3. ZOE images of i^{3}Neurons treated with 5 µM Aβ$_{42}$ and 200 nM (A) pAb$_{2AT\text{-}L}$ or (B) generic rabbit IgG.

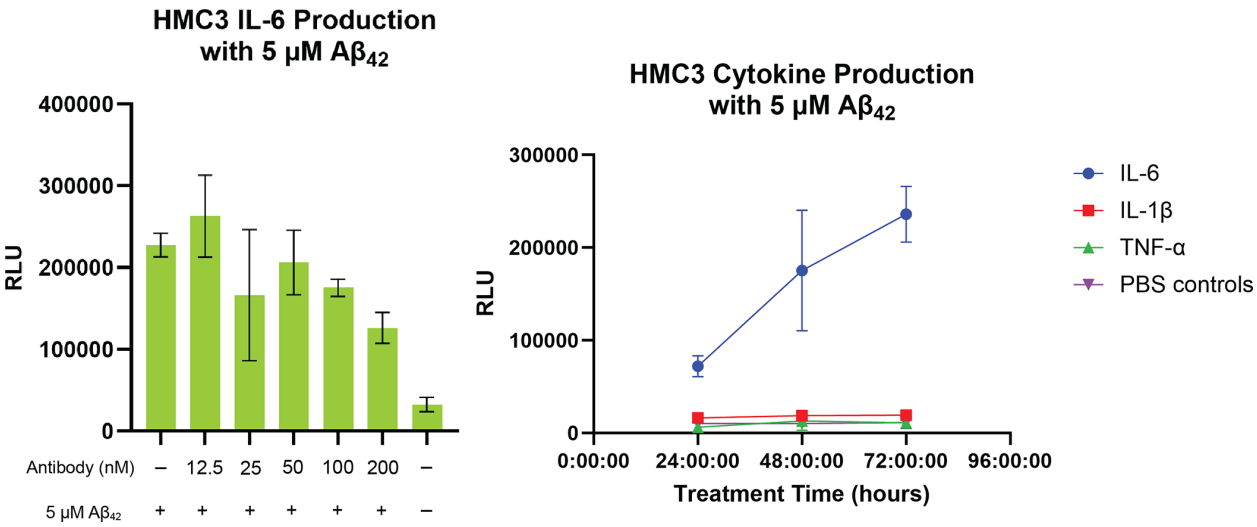

Figure B4. (A) Graph of IL-6 production by HMC3 microglia cells in the presence of 5 µM Aβ$_{42}$ and varying concentrations of pAb$_{2AT\text{-}L}$ as measured by the Promega™ Lumit™ IL-6 Human Immunoassay on the Promega™ GloMax® Discover plate reader. (B) Graph of IL-6, IL-1β, and TNFα production by HMC3 microglia cells at different time points in the presence of 5 µM Aβ$_{42}$ as measured by the Promega Lumit™ IL-6, Lumit™ IL-1β, and Lumit™ TNF-α human immunoassays.

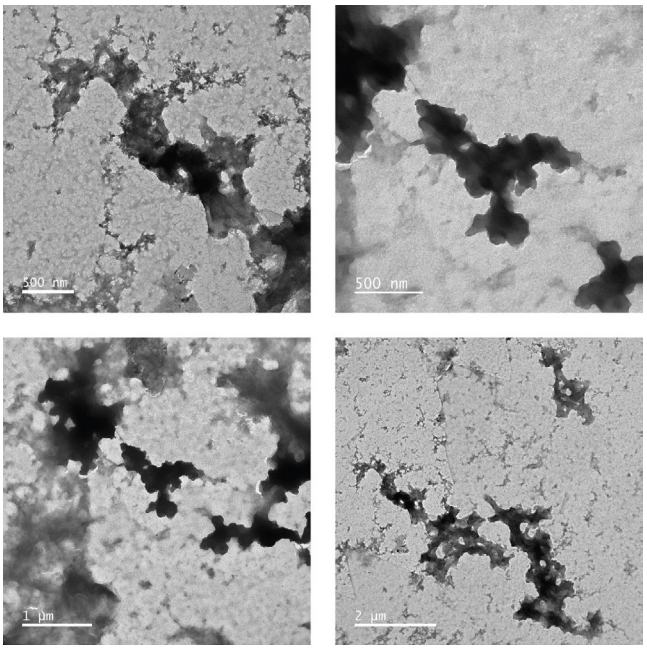

Figure B5. Representative TEM images of 800nM generic rabbit IgG antibody in PBS prepared in the same manner as the $pAb_{2AT\text{-}L}$ sample.

A

Antibody	A280
$pAb_{2AT\text{-}L}$	0.17
6E10	0.37
4G8	0.45

B

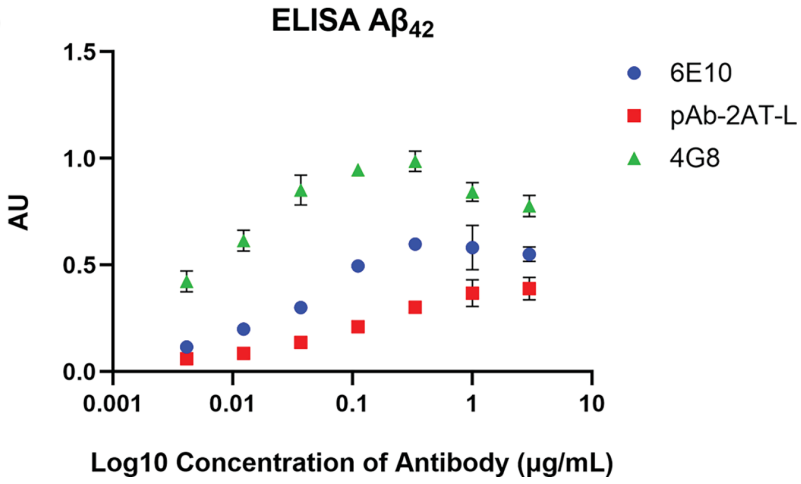

Figure B6. (A) Absorbance at 280 nm of stock 2 µM solutions of antibodies used for assays. (B) ELISA of $pAb_{2AT\text{-}L}$, 6E10, and 4G8 against $A\beta_{42}$.

B2. Materials and Methods

B2.1 General Information

All chemicals were used as received unless otherwise noted. Deionized water (18 MΩ) was obtained from a Barnstead NANOpure Diamond water purification system. 6E10 and 4G8 were purchased from Biolegend (cataolog #803016 and #800702, respectively). The generic IgG rabbit antibody was purchased from ThermoFisher Scientific (catalog #31235).

B2.2. Design of $pAb_{2AT\text{-}L}$

2AT-L consists of three cyclic β-hairpin peptides covalently linked by three disulfide bonds to form a triangular trimer. The individual peptides that form this trimer were designed based on crystal structures of peptides that mimic the 17–36 Aβ β-hairpin originally reported by Hard and coworkers in 2007.[1] These peptides all have a propensity to assemble into trimers which further assemble into higher-order oligomers.[2-5] The monomers that comprise 2AT-L, are each composed of Aβ residues 17 through 36 connected at the C and N termini by a δ-linked ornithine turn unit. This linkage conformationally constrains the peptide in a β-hairpin conformation. Each peptide also contains an N-methyl on the backbone of the peptide at Phe20 to prevent fibrillization, a mutation at Met35 to α-linked ornithine to aid in structural elucidation, and two cysteine mutations at positions 17 and 21 to allow for disulfide bond formation. Upon oxidation, this peptide readily forms triangular trimers (2AT-L).[6]

The structure of 2AT-L was elucidated at atomic resolution by X-ray crystallography, and further characterized by SDS-PAGE, size-exclusion chromatography, and dynamic light scattering, revealing a propensity to form higher-order assemblies in solution.[6] Cell assays showed that 2AT-L elicits LDH release, decreases ATP production, and activates caspase-3/7 mediated apoptosis in SH-SY5Y neuroblastoma cells[6] and iPSC-derived neurons (,unpublished results).

B2.3. Generation of $pAb_{2AT\text{-}L}$

Rabbit immunization. $pAb_{2AT\text{-}L}$ was generated by Pacific Immunology (Ramona, CA, www.pacificimmunology.com) using standard custom antibody production procedures. Briefly, 2AT-L was conjugated to the carrier protein keyhole limpet hemocyanin (KLH) using standard EDC conjugation chemistry. The EDC was obtained from Thermo Scientific (catalog # 22980) and the conjugation was performed according to manufacturer's instructions in MES buffer at an acidic pH of 5. We have previously found that at acidic pH, a related covalently stabilized trimer does not assemble to form higher-order assemblies [*JACS*, **2020**, *142*, 20708].[#] It is thus likely that 2AT-L does not assemble to form higher-order structures under the conditions of the conjugation reaction to KLH. Two New Zealand white rabbits, 9–10 weeks of age, were used to generate $pAb_{2AT\text{-}L}$. Rabbits were primed with 200 μg of the 2AT-L-KLH conjugate in AdjuLite Complete Freund's Adjuvant (CFA) (Cat. #A5001), by subcutaneous injection using a 19-gauge needle in the neck/shoulder region. On days 21, 42, and 70 the rabbits received booster injections of 100 μg of the 2AT-L-KLH conjugate in AdjuLite Incomplete Freund's Adjuvant (IFA) (Cat. #A5002). Blood was drawn from the central ear artery using a 19-gauge needle on days 0, 49, 63, 77, and 91.

As whole blood was collected, it was diluted in Anticoagulant Citrate Dextrose Solution USP (ACD) Solution A (0.80 g citric acid monohydrate, 2.45 g dextrose monohydrate, and 2.20 g of sodium citrate dihydrate in 100 mL) in a 1:10 ratio. The blood-ACD solution was diluted 1:1 with sterile PBS containing 2.5 mM EDTA and 0.5% BSA. 20 mL of StemCell Lymphoprep

was added to a 50-mL StemCell SepMate-50 separation tube, then 30 mL of the blood and ACD solution was added over the Lymphoprep, then centrifuged for 30 minutes at 3,000 RPM. The supernatant (plasma) was retrieved and decanted once the PBMCs have been spun down to form a pellet. The plasma was then used in the affinity purification as described below.

Affinity purification of $pAb_{2AT\text{-}L}$. $pAb_{2AT\text{-}L}$ was purified from the plasma using affinity chromatography. To create the affinity chromatography column, 10 mg of the 2AT-L TFA salt was dissolved in 2 mL DMSO. The 2AT-L/DMSO solution was then added to 10 mL PBS (pH 7.4) to create a 1 mg/mL 2AT-L solution in PBS with 20% DMSO. The 1 mg/mL 2AT-L solution was then added to 750 mg dry NHS-activated agarose resin (Thermo Scientific, catalog # 26197) in a 15 mL polypropylene conical tube. The 2AT-L/agarose suspension was then continuously inverted using a tube rotator for two hours at room temperature. After the two-hour incubation, the agarose was transferred to a Bio-Rad Poly-Prep chromatography column (10 mL) and washed 3x with PBS. The agarose was then incubated in 5 mL 1 M Tris buffer (pH 8.5) for 1 hour at room temperature on a tube rotator to cap unreacted NHS-ester groups, and then washed 3x with PBS.

For the affinity purification of $pAb_{2AT\text{-}L}$ from the plasma, the 2AT-L-agarose was transferred to a 50 mL CrystalCruz® glass chromatography column. The plasmas from a single production bleed from both rabbits were combined and then filtered through 0.45 μm syringe filters. The filtered plasma was then added to the column containing the 2AT-L-agarose and rocked on a rocker for ~3 hours at room temperature or overnight at 4 ºC. Next, the plasma was drained from the column into a 50 mL polypropylene conical tube, and the 2AT-L-agarose was washed with ice-cold PBS. Washing was performed with 50 mL portions of ice-cold PBS until the absorbance at 214 nm of the wash buffer eluent measured less than 0.05 on a NanoDrop One/One^{c} Microvolume UV-Vis Spectrophotometer.

$pAb_{2AT\text{-}L}$ was then eluted from the 2AT-L-agarose using ice-cold 0.2 M glycine buffer (pH 1.85). The $pAb_{2AT\text{-}L}$ elution was performed by adding the glycine buffer in 1 mL portions and then collecting the eluent into 1.7 mL microcentrifuge tubes containing 0.5 mL 1 M Tris buffer (pH 8.5). Typically, 10–15 1-mL portions of the glycine buffer were sufficient to elute all of $pAb_{2AT\text{-}L}$ from the 2AT-L-agarose. The eluents were then combined and transferred to a 30 kDa molecular weight cutoff filter (30K MWCOF) (Thermo Scientific catalog # 88531) and buffer exchange with PBS was performed. The 30K MWCOF was centrifuged in a swinging bucket centrifuge at 3800 x g until the volume fell below 1 mL, after which the buffer was replenished with ice-cold PBS up to the 20 mL marker on the 30K MWCOF. This process was repeated at least six times. For the final centrifugation step, the $pAb_{2AT\text{-}L}$ volume was allowed to reach ~0.5 mL in the 30K MWCOF and was then transferred to a 1.7 mL microcentrifuge tube. The $pAb_{2AT\text{-}L}$ concentration was determined using a BCA assay and then adjusted to 1 mg/mL with PBS. Typical affinity purifications yielded 1–3 mg of $pAb_{2AT\text{-}L}$ from 50 mL of antisera. The affinity purified $pAb_{2AT\text{-}L}$ was then portioned into 50 μL aliquots, which were stored at -80 ºC and thawed as needed. Once thawed, the aliquot was stored at 4 ºC.

B2.4. Preparation of $A\beta_{42}$.

A 1 mg portion of recombinantly expressed $A\beta_{42}$ as the ammonium salt was purchased from rPeptide (catalog# A-1167-2) and received as a fluffy lyophilized solid in a glass amber vial. The 1 mg $A\beta_{42}$ portion was dissolved with 1 mL of 2 mM NaOH to create a 1 mg/mL $A\beta_{42}$ solution. The 1 mg/mL $A\beta_{42}$ solution was then sonicated in a water bath sonicator for 5 minutes. After sonication, 0.02 μmol aliquots of $A\beta_{42}$ were prepared by transferring 92.6 μL portions of the 1 mg/mL $A\beta_{42}$ solution to low-binding microcentrifuge tubes (Axygen, catalog# MCT-175-L-C) containing a hole in the lid of the tube created by puncturing the lid with a 22-gauge needle. The aliquots were then frozen on dry ice for 1 hour, transferred to a lyophilization vessel, and lyophilized overnight. The next day, the aliquots were removed from the lyophilizer and each microcentrifuge tube was immediately transferred to its own 50 mL conical tube. The 50 mL conical tubes were sealed by tightening the lid and stored at -80 °C until use.

B2.5. Indirect ELISAs

Indirect ELISA was used to verify the binding of $pAb_{2AT\text{-}L}$, 4G8, and 6E10 to $A\beta_{42}$. Three technical replicates were performed for each experiment. Each aspiration and washing step in the ELISA procedure was performed using a Fisherbrand™ accuWash™ Microplate Washer (catalog # 14-377-577).

Coating the wells of the ELISA plates. A 0.02 μmol aliquot of $A\beta_{42}$ (prepared as described above) was removed from the -80 °C freezer and allowed to equilibrate to room temperature. The aliquot was then dissolved in 92.6 μL of deionized water to create a 216 μM solution of $A\beta_{42}$. A 1 μM solution of $A\beta_{42}$ in carbonate buffer (15 mM Na_2CO_3, 35 mM $NaHCO_3$, 0.02% (w/v) sodium azide, pH 9.5) was then prepared from the 216 μM solution. The 1 μM $A\beta_{42}$ solution was then poured into a reagent reservoir and a multichannel pipette was used to transfer 50 μL to the appropriate wells of a Thermo Scientific™ Maxisorp 96-well plate (catalog# 12-565-135). The 96-well plate was then sealed with an adhesive 96-well plate seal (Axygen, catalog# PCR-SP) and incubated overnight (~16 hours) at room temperature on a rotating shaker set to 90 RPM.

Treating the ELISA plates with $pAb_{2AT\text{-}L}$, 4G8, or 6E10. The next day, 20 mL of 1% BSA was prepared by adding 200 mg of BSA (Fraction V) (Fisher BioReagents™, catalog # BP1600-100) to 20 mL PBS. The solution of $A\beta_{42}$ was aspirated from the wells of the 96-well plate and then washed 1x with PBST (10 mM Na_2HPO_4, 1.8 mM KH_2PO_4, 137 mM NaCl, 2.7 mM KCl, 0.5% Tween-20). A multichannel pipette was then used to transfer 75 μL of 1% BSA to each well, the plate was sealed, and incubated for at least 1 hour at room temperature on a rotating shaker set to 90 RPM to block uncoated sites in the wells. During the last 15 minutes of the blocking step, a 3 μg/mL $pAb_{2AT\text{-}L}$ solution, 3 μg/mL 6E10 solution, and 3 μg/mL 4G8 solution were prepared by diluting a 636 nL of a 1.18 mg/ml ($pAb_{2AT\text{-}L}$) or 750 nL 1.0 mg/ml (6E10 and 4G8) stock solution into 250 μL of 1% BSA in PBS. After the blocking step, the wells were aspirated and washed 3x with PBST. Using a multi-channel pipette, 50 μL of 1% BSA was then added to the wells in the bottom seven rows of the 96-well plate (rows B–H). 75 μL of the 3 μg/mL

$pAb_{2AT\text{-}L}$, 6E10, and 4G8 solutions were added to their respective wells in the top row (row A). A multi-channel pipette was then used to create a three-fold dilution series of the antibodies by transferring 25 μL of the solutions from row A to row B and then mixing up and down 8 times. 25 μL was then transferred from row B to row C, and so on, until the last 25 μL had been transferred to row H. The 96-well plates were then sealed with an adhesive plate seal and incubated for 2 hours at room temperature on a rotating shaker set to 90 RPM.

Treating the ELISA plate with the secondary antibodies. After the 2-hour incubation, the primary antibody solutions were aspirated and the wells were washed 3x with PBST. A 50 μL portion of AffiniPure Goat Anti-Rabbit IgG (H+L) conjugated to horse radish peroxidase (GαR-HRP; Jackson ImmunoResearch, catalog # 111-035-144) diluted 1:10,000 in 1% BSA was then added to the wells that received $pAb_{2AT\text{-}L}$; a 50 μL portion of AffiniPure Goat Anti-Mouse IgG (H+L) conjugated to horse radish peroxidase (GαM-HRP; Jackson ImmunoResearch, catalog # 115-035-146) diluted 1:10,000 in 1% BSA was added to the wells that received 6E10 and 4G8. The 96-well plate was then sealed with an adhesive plate seal and incubated for 1 hour at room temperature on a rotating shaker set to 90 RPM.

Developing the ELISA plates. After the 1-hour incubation, the secondary antibody solutions were aspirated and the wells were washed 3x with PBST. A 50 μL portion of 3,3',5,5'-tetramethybenzidine (TMB) (Millipore Sigma, catalog # ES001-500ML) was then added to each well and allowed to react until the blue color reached a sufficient hue. A 50 μL portion of 1 M aqueous HCl was then added to each well to quench the reaction and the absorbance was measured at 450 nm using a MultiSkan GO plate reader. The absorbance readings for the three replicates were averaged and the standard deviations were calculated using GraphPad Prism. The data were then plotted and fit using GraphPad Prism to estimate the EC_{50} values.

B2.6. Cell-based assays of antibodies in iPSC-derived neurons

Differentiation of NGN2 iPSCs into cortical neurons. Ngn2 iPSCs were obtained from the UCI Sue and Bill Gross Stem Cell Research Center, courtesy of the Blurton-Jones laboratory and differentiated according to the protocols published by Gan and coworkers.[7] An aliquot of Ngn2 iPSCs were thawed in 10 mL pre-warmed mTeSR media treated with 10 μL of 10 mM rock inhibitor (final concentration 10 μM) and centrifuged at 200g for 4 minutes. The media was aspirated and replaced with fresh mTesR with rock inhibitor and plated at a density of about 500,000 cells per ml on a Matrigel coated 6-well plate (2 ml per well). Cells were incubated at 37C with 5% CO2 and cell media was aspirated and replaced daily with mTesR (without rock inhibitor) until the cell density reached 80% confluency. Cells were then passaged by aspirating the media, treating with accutase, centrifuging, and replating in fresh mTesR with rock inhibitor.

Once the cell density again reached 80 % confluency, cells were passaged and resuspended in neuronal predifferentiation media (Knockout DMEM:F12, 1x N2, 1x non-

essential amino acids, 10 ng/ml BDNF, 10 ng/ml NT3, 1 ug/ml mouse laminin, 2 ug/ml doxyclyine) with rock inhibitor (10 uM), plated in a new Matrigel coated 6-well plate at the same density in 2ml of media per well, and incubated at 37C. The following two days media was aspirated and replaced. Cells were then either frozen in Knockout DMEM with 10% DMSO for later maturation or passaged and resuspended in neuronal maturation media (1:1 neurobasal A media and DMEM f:12, 1x B27 0.5x N2, 1x non-essential amino acids, 0.5x glutamax 10 ng/ml BDNF, 10 ng/ml NT3, 1 ug/ml mouse laminin, 2 ug/ml doxyclyine).

96-well black, clear bottom, tissue culture treated plates were coated in 0.5 mg/ml poly-D-lysine solution in Dubeccos Phosphate buffered saline. After one hour, the solution was removed and the plates were washed twice with DPBS and left to dry for two hours. Cells were plated for maturation on the inner 60 wells of the plate at a density of 200000 cells per ml. Media was added to the outer wells of the plate to saturate the environment. After one week of maturation, media was gently removed and replaced with maturation media containing the compounds of interest, but lacking doxycycline. The neurons were incubated for 72 hours before assaying.

Preparation of reagents for cell assays. Antibodies were diluted in PBS to 10X of the desired final concentration and spin filtered. In a replica 96-well plate antibodies were diluted in a series of two-fold dilutions with PBS in triplicate to get final volumes of 10 µL per well. The positive and negative controls contained just 10 µL of PBS. For cell assays, two aliquots of 0.02 µmoles of Aβ42 were dissolved in 7.2 mL of maturation media to obtain a concentration of 5.56 µM. 90 µL of 5.56 µM Aβ42 in maturation media was added to each well of the replica plate, except the negative control which had media without Aβ42. Upon receipt, CellTiter-Glo® 2.0 cell viability reagent as thawed, aliquoted, and stored at -80C. For the assay, one 4 µL aliquot was thawed to room temperature before use. The CyQuant™ LDH substrate and buffer were stored at -20C. For the assay, the LDH buffer was equilibrated to room temperature, dissolved in 11.4 ml of nanopure water, and vortexed. 600 µL of LDH substrate was equilibrated to room temperature and then added to the reconstituted LDH buffer and vortexed before use.

CellTiter-Glo® 2.0 Cell Viability Assay and CyQuant™ LDH Cytotoxicity Assay. Cell assays were performed according to manufacturers' instructions. After 72 hours of incubation, the cells were removed from the incubator and allowed to equilibrate to room temperature for 30 minutes. 50 µL of media per well was removed and transferred to a clear 96-well plate. 50 µL of LDH reagent was added to the clear plate, briefly mixed, and incubated in the dark for 1 hour. The absorbance of each well was measured at 490 nm on a Thermo Scientific MultiSkan GO plate reader. The remaining 50 µL of media containing the cells was treated with 50 µL per well of CellTiter-Glo® 2.0 viability reagent. The plate was incubated at room temperature with orbital shaking for 15 minutes at 80 RPM. The luminescence from each well was then measured on a Promega™ GloMax® Discover Microplate Reader. The absorbance and luminescence measurements for the three replicates of each treatment

group were averaged and the standard deviations were calculated using GraphPad Prism for each assay. The data were then plotted using GraphPad Prism.

B2.7. ThT assay on Aβ42

Assay notes: The ThT assay was performed on 3 μM Aβ42 in PBS at pH 7.4 (10 mM Na_2HPO_4, 1.8 mM KH_2PO_4, 137 mM NaCl, 2.7 mM KCl) containing 10 μM ThT in the presence of a dilutions series of $pAb_{2AT\text{-}L}$ (800–210 nM, 0nM). The assay was performed in triplicate in Corning® 96-well Half Area Black/Clear Flat Bottom Polystyrene NBS Microplates (product# 3881) at 25 °C under quiescent conditions.

A 0.02 μmol aliquot of Aβ42 was removed from the -80 °C freezer and allowed to equilibrate to room temperature. During this equilibration time, an 11 μM solution of thioflavin T (ThT) was prepared in PBS at pH 7.4 (10 mM Na_2HPO_4, 1.8 mM KH_2PO_4, 137 mM NaCl, 2.7 mM KCl) and a serial dilution series of 10x concentrations of 2AT and KLT were prepared in deionized water.

Preparation of 11 μM ThT in PBS. To prepare the 11 μM ThT solution in PBS, a concentrated solution of ThT (1–3 mM) was prepared in a 15 mL polypropylene conical tube by adding ~5–7 mg of ThT (TCI Chemicals, catalog# T0558) to 7–10 mL PBS. The concentrated ThT solution was sonicated in a water bath sonicator for ~5 minutes and then passed through a 0.2 μm nylon syringe filter into a new 15 mL conical tube. The concentration of the concentrated ThT solution was determined photospectrometrically by first preparing 2 mL of a 1:200 diluted ThT solution (0.010 mL of the concentrated ThT solution into 1.990 mL PBS). The absorbance of the diluted ThT solution was then measured at 412 nm in a 1 cm quartz cuvette and the concentration was calculated using an estimated extinction coefficient (ε) of 36,000 M^{-1} cm^{-1}. The concentration of the diluted ThT solution was multiplied by 200 to calculate the concentration of the concentrated ThT solution. A 10 mL portion of 11 μM ThT in PBS was prepared by diluting an appropriate volume of the concentrated ThT solution with PBS. The 11 μM ThT solution was then kept on ice until used.

A 1.25-fold dilution series containing 10x concentrations of $pAb_{2AT\text{-}L}$ (8–2.1 μM, 0 μM) was prepared in row A. The serial dilution was then performed by transferring 15 μL from well A1 to well A2 and then mixing by pipetting up and down 8–12 times, and so on, stopping on well A11. Well A12 did not receive $pAb_{2AT\text{-}L}$ and only contained 15 μL of deionized water. A 12-channel pipette was then used to transfer 4 μL portions of the $pAb_{2AT\text{-}L}$ solutions from all 12 wells of row A to all 12 wells in rows B,C, and D. After the dilution series was prepared and aliquoted to the respective rows, the 96-well assay plate was kept on ice for the remainder of the experimental setup.

Adding Aβ42 to the ThT assay plate. After the 11 μM ThT solution was prepared and the $pAb_{2AT\text{-}L}$ dilution series was completed, a 3.33 μM solution of Aβ42 was prepared in 11 μM ThT. To prepare the 3.33 μM solution of Aβ42, the equilibrated 0.02 μmol Aβ42 aliquot was first dissolved in 500 μL deionized water to yield a 40 μM solution and sonicated in a water bath sonicator for 5 minutes. During the sonication time, 2 mL of ice-cold 11 μM ThT was transferred to a 15 mL conical tube and kept on ice. After sonication, 166.5 μL was removed

from the 2 mL of 11 μM ThT and 166.5 μL of the 40 μM solution of $A\beta_{42}$ was added and mixed by inverting the tube 4 times to create the 3.33 μM $A\beta_{42}$ solution. The $A\beta_{42}$ solution was then dumped into a sterile 25 mL reagent reservoir (ThermoFisher, catalog# 8093-11) and a 12-channel pipette was used to transfer 36 μL of the $A\beta_{42}$ solution to rows C–H.

Reading the ThT assay plate. The ThT assay plate was sealed with a clear adhesive plate seal (Axygen, catalog# PCR-SP) and was immediately inserted into a ThermoFisher Scientific Varioskan Lux plate reader. Fluorescence measurements of each well in rows C–H were acquired every 2 minutes over a 5 hour period with the following parameters:

excitation: 440 nm emission: 485 nm

measurement time: 1000 ms optics: bottom read

excitation bandwidth: 12 nm

The data were plotted in GraphPad Prism.

B2.8. Transmission Electron Microscopy

A 0.02 μmol aliquot of $A\beta_{42}$ was removed from the -80 °C freezer and allowed to equilibrate to room temperature. During this time, 6.78 μL of a 1.18 mg/ml stock solution of $pAb_{2AT\text{-}L}$ was diluted into 60 μL of PBS at pH 7.4 (10 mM Na_2HPO_4, 1.8 mM KH_2PO_4, 137 mM NaCl, 2.7 mM KCl) to yield a 888.89 nM solution of $pAb_{2AT\text{-}L}$. 27 μL of the 888.89 nM solution of $pAb_{2AT\text{-}L}$ was added to two low-binding microcentrifuge tubes. A third tube was treated with 27 μL of just PBS. The 0.02 μmol aliquot of $A\beta_{42}$ was then dissolved in 666.7 μL of PBS to yield a 30 μM solution. 3 μL of this solution was added to the microcentrifuge tube containing 27 μL of just PBS to yield a 3 μM solution. Another 3 μL of 30 μM $A\beta_{42}$ was added to one of the microcentrifuge tubes containing 27 μL of an 888.89 nM solution of $pAb_{2AT\text{-}L}$ to yield an 800 nM solution of $pAb_{2AT\text{-}L}$ in 3 μM $A\beta_{42}$. 3 μL of just PBS was added to the other tube containing 27 μL of an 888.89 nM solution of $pAb_{2AT\text{-}L}$ to yield an 800 nM solution of $pAb_{2AT\text{-}L}$.

Samples were incubated for three hours at room temperature without shaking to elicit fibril formation. After incubation, 5 μL of sample was deposited on a carbon-copper mesh grid and left to dry for 15 minutes. The grids were then gently wicked and treated with 5 μL of two percent uranyl acetate for 2 minutes for negative staining. The grids were then gently wicked and washed with 5 μL of nanopure water. After a minute, the water was wicked, and the grids were left to dry for 10 minutes before imaging. Samples were transferred to a TEM-JEOL JEM-2100F instrument for imaging.

B3. References and Notes

1. Hoyer, W.; Grönwall, C.; Jonsson, A.; Ståhl, S.; Härd, T. Stabilization of a β-Hairpin in Monomeric Alzheimer's Amyloid-β Peptide Inhibits Amyloid Formation. *Proceedings of the National Academy of Sciences* **2008**, *105* (13), 5099–5104. https://doi.org/10.1073/pnas.0711731105.

2. https://doi.org/10.1021/ja5017409
3. Kreutzer, A. G.; Hamza, I. L.; Spencer, R. K.; Nowick, J. S. X-Ray Crystallographic Structures of a Trimer, Dodecamer, and Annular Pore Formed by an $A\beta_{17-36}$ β-Hairpin. *Journal of the American Chemical Society* **2016**, *138* (13), 4634–4642. https://doi.org/10.1021/jacs.6b01332.
4. Sepehr Haerianardakani; Kreutzer, A. G.; Salveson, P. J.; Samdin, T. D.; Guaglianone, G. E.; Nowick, J. S. Phenylalanine Mutation to Cyclohexylalanine Facilitates Triangular Trimer Formation by β-Hairpins Derived from Aβ. *Journal of the American Chemical Society* 2020, *142* (49), 20708–20716. https://doi.org/10.1021/jacs.0c09281.
5. Ruttenberg, S. M.; Kreutzer, A. G.; Truex, N. L.; Nowick, J. S. β-Hairpin Alignment Alters Oligomer Formation in Aβ-Derived Peptides. *Biochemistry* 2024. https://doi.org/10.1021/acs.biochem.3c00526.
6. Wang, C.; Ward, M. E.; Chen, R.; Liu, K.; Tracy, T. E.; Chen, X.; Xie, M.; Sohn, P. D.; Ludwig, C.; Meyer-Franke, A.; Karch, C. M.; Ding, S.; Gan, L. Scalable Production of IPSC-Derived Human Neurons to Identify Tau-Lowering Compounds by High-Content Screening. *Stem Cell Reports* **2017**, *9* (4), 1221–1233. https://doi.org/10.1016/j.stemcr.2017.08.019.
7. Fernandopulle, M. S.; Prestil, R.; Grunseich, C.; Wang, C.; Gan, L.; Ward, M. E. Transcription Factor-Mediated Differentiation of Human IPSCs into Neurons. *Current Protocols in Cell Biology* **2018**, *79* (1), e51. https://doi.org/10.1002/cpcb.51.

Appendix C

Supporting Information for Chapter 5

C1. Supplementary Tables

Table C1. Standard addition concentrations for each enzyme.

Enzyme (Gene)	Concentrations of standard additions (µg/mL)
CTSD	0, 1, 2, 3
CPE	0, 1, 2, 3
ENPP2	0, 1, 2, 3
HEXA	0, 0.25, 0.5, 0.75
PON1	0, 0.25, 0.5, 0.75
TPP1	0, 0.25, 0.5, 0.75
UCHL1	0, 0.25, 0.5, 0.75

Table C2. Selected multiple reaction monitoring ion pairs for LC-MS/MS quantification of seven enzymes in the human vitreous humor determined by Skyline.[1]

Enzyme (Gene)	Peptide	Parent Ion m/z	Fragmented Ion m/z	Avg. Retention Time (minutes)	Quantitation (Q) or Confirmation (C)
CTSD	YYTVFDR	482.2322^{++}	637.33^{+}	23.6	Q
CTSD	YYTVFDR	482.2322^{++}	800.394^{+}	23.6	C
CPE	IVDQNTK	409.2243^{++}	605.289^{+}	5.6	Q
CPE	IVDQNTK	409.2243^{++}	704.357^{+}	5.6	C
ENPP2	KPLDVYK	431.7553^{++}	734.408^{+}	12.2	Q
ENPP2	KPLDVYK	431.7553^{++}	637.356^{+}	12.2	C
HEXA	GLLLDTSR	437.7533^{++}	591.31^{+}	24.8	Q
HEXA	GLLLDTSR	437.7533^{++}	704.394^{+}	24.8	C
PON1	STVELFK	412.2316^{++}	536.308^{+}	24.4	Q
PON1	STVELFK	412.2316^{++}	635.376^{+}	24.4	C
TPP1	TLPPGWVSLGR	591.8351^{++}	871.479^{+}	34.4	Q
TPP1	TLPPGWVSLGR	591.8351^{++}	968.531^{+}	34.4	C
UCHL1	QFLSETEK	491.2480^{++}	593.278^{+}	15.9	Q
UCHL1	QFLSETEK	491.2480^{++}	706.362^{+}	15.9	C

Table C3. Relative abundances of each enzyme of interest in four untargeted proteomic analyses of the "normal" human vitreous humor reported as average percent sequence coverage or average iBAQ values.[2-6] The n value indicates the number of donor samples analyzed.

Enzyme (Gene)	Gao et al. 2008 Mean Spectral Count n = 6	Aretz et al. 2013 Avg % Sequence Coverage n = 3	Murthy et al. 2014 Avg % Sequence Coverage n = 5	Naru et al. 2016 Avg % Sequence Coverage n = 4	Mohanty et al. 2020 iBAQ Relative Abundance n = 3
CTSD	19.08	33.6	64.1	36.2	1.84E8
CPE	6.00	5.2	50.0	Not detected	2.96E6
ENPP2	3.33	21.8	26.1	19.7	2.02E6
HEXA	Not detected	not detected	16.8	5.5	2.33E6
PON1	0.75	12.4	34.9	37.5	1.34E6
TPP1	0.67	7	46.0	12.6	8.13E6
UCHL1	Not detected	64.4	49.8	6.3	7.27E7

Table C4. Peptides tested for quantitation for each enzyme determined by simulated trypsin digestion and Protein Blast.[7-9]

CTSD	CPE	ENPP2	HEXA	PON1	TPP1	UCHL1
SSTYVK	EGGPNNHLLK	HLLYGRPAVLYR	AGAVAER	IHVYEK	TLPPGWVSLGR	GQEVSPK
YYTVFDR	IVDQNTK	KPLDVYK	GLLLDTSR	HANWTLTPLK	FPPTSSLR	QFLSETEK
QPGITFIAAK	FPPEETLK	LHYANNR	EVIEYAR	STVELFK		

C2. References

1. Pino, L. K.; Searle, B. C.; Bollinger, J. G.; Nunn, B.; MacLean, B.; MacCoss, M. J. The Skyline Ecosystem: Informatics for Quantitative Mass Spectrometry Proteomics. *Mass Spectrometry Reviews* 2020, *39* (3), 229–244. https://doi.org/10.1002/mas.21540
2. Aretz, S.; Krohne, T. U.; Kammerer, K.; Warnken, U.; Hotz-Wagenblatt, A.; Bergmann, M.; Stanzel, B. V.; Kempf, T.; Holz, F. G.; Schnölzer, M.; Kopitz, J. In-Depth Mass Spectrometric Mapping of the Human Vitreous Proteome. *Proteome Science* 2013, *11* (1), 22. https://doi.org/10.1186/1477-5956-11-22.
3. Gao, B.-B.; Chen, X.; Timothy, N.; Aiello, L. P.; Feener, E. P. Characterization of the Vitreous Proteome in Diabetes without Diabetic Retinopathy and Diabetes with Proliferative Diabetic Retinopathy. *Journal of Proteome Research* 2008, *7* (6), 2516–2525. https://doi.org/10.1021/pr800112g.
4. Mohanty, V.; Pinto, S. M.; Yashwanth Subbannayya; Mohd Altaf Najar; Kalpana Babu Murthy; Prasad, K.; Murthy, K. R. Digging Deeper for the Eye Proteome in Vitreous

Substructures: A High-Resolution Proteome Map of the Normal Human Vitreous Base. *Omics A Journal of Integrative Biology* 2020, *24* (6), 379–389. https://doi.org/10.1089/omi.2020.0020.
5. Murthy, K. R.; Goel, R.; Subbannayya, Y.; Jacob, H. K.; Murthy, P. R.; Manda, S. S.; Patil, A. H.; Sharma, R.; Sahasrabuddhe, N. A.; Parashar, A.; Nair, B. G.; Krishna, V.; Prasad, T. K.; Gowda, H.; Pandey, A. Proteomic Analysis of Human Vitreous Humor. *Clinical Proteomics* 2014, *11* (1). https://doi.org/10.1186/1559-0275-11-29.
6. Naru, J.; Aggarwal, R.; Singh, U.; Mohanty, A. K.; Bansal, D.; Mangat, N.; Kakkar, N.; Agnihotri, N. Proteomic Analysis of Differentially Expressed Proteins in Vitreous Humor of Patients with Retinoblastoma Using ITRAQ-Coupled ESI-MS/MS Approach. *Tumor Biology* 2016, *37* (10), 13915–13926. https://doi.org/10.1007/s13277-016-5162-3.
7. Bollinger, J. G.; Stergachis, A. B.; Johnson, R. S.; Egertson, J. D.; MacCoss, M. J. Selecting Optimal Peptides for Targeted Proteomic Experiments in Human Plasma Using in Vitro Synthesized Proteins as Analytical Standards. *Methods in molecular biology* 2016, 207–221. https://doi.org/10.1007/978-1-4939-3524-6_12.
8. Wilkins, M. R.; Lindskog, I.; Gasteiger, E.; Bairoch, A.; Sanchez, J.-C.; Hochstrasser, D. F.; Appel, R. D. Detailed Peptide Characterization Using PEPTIDEMASS - a World-Wide-Web-Accessible Tool. *Electrophoresis* 1997, *18* (3-4), 403–408. https://doi.org/10.1002/elps.1150180314.
9. Altschul, S. F.; Gish, W.; Miller, W.; Myers, E. W.; Lipman, D. J. Basic Local Alignment Search Tool. *Journal of Molecular Biology* 1990, *215* (3), 403–410. https://doi.org/10.1016/s0022-2836(05)80360-2.